The University of Nottingham

UNITED KINGDOM · CHINA · MALAYSIA

Understanding Microwave Pyrolysis of Biomass Materials

Mohamed Adam, MSc

Thesis submitted to the University of Nottingham

for the degree of Doctor of Philosophy

March 2017

ABSTRACT

Global challenges related to energy security, resource sustainability and the environmental impacts of burning fossil fuels have led to an increasing need for switching to the use of clean and sustainable resources. Bio-oil produced through pyrolysis has been suggested as one of the sustainable alternatives to fossil resources for power generation as well as chemicals and biofuels production. Pyrolysis is a thermochemical process during which the biomass feedstock is heated in an inert atmosphere to produce gas, liquid (bio-oil) and solid (char) products. Microwave heating has been considered a promising technique for providing the energy required for biomass pyrolysis due to its volumetric and selective heating nature which allows for rapid heating in a cold environment. This helps to preserve the product quality by limiting secondary reactions.

The aim of this research was to study the interactions between biomass materials and microwave energy during pyrolysis, and to develop a reliable and scalable microwave pyrolysis process.

The dielectric properties of selected biomass materials were studied and found to vary significantly with temperature due to the physical and structural changes happening during pyrolysis. The loss factor of the biomass materials was found to reach a minimum value in the range between 300 ^{o}C and 400 ^{o}C followed by a sharp increase caused by the char formation.

A microwave fluidised bed process was introduced as an attempt to overcome the challenges facing the scaling-up of microwave pyrolysis. The concept of microwave pyrolysis in a fluidised bed process was examined for the first time in this thesis. A systematic approach was followed for the process design taking into account the pyrolysis reaction requirements, the microwave-material interactions and the fluidisation behaviour of the biomass particles. The steps of the process design involved studying the fluidisation behaviour of selected biomass materials,

theoretical analysis of the heat transfer in the fluidised bed, and electromagnetic simulations to support the cavity design.

The developed process was built, and batch pyrolysis experiments were carried out to assess the yield and quality of the product as well as the energy requirement. Around 60 % to 70 % solid pyrolysed was achieved with 3.5 $kJ \cdot g^{-1}$ to 4.2 $kJ \cdot g^{-1}$ energy input. The developed microwave fluidised bed process has shown an ability to overcome many of the challenges associated with microwave pyrolysis of biomass including improvement in heating uniformity and ability to control the solid deposition in the process, placing it as a viable candidate for scaling-up. However, it was found to have some weaknesses including its limitations with regards to the size and shape of the biomass feed.

Microwave pyrolysis of biomass submerged in a hydrocarbon liquid was introduced for the first time in this thesis as a potential alternative to overcome some of the limitations of the gas-based fluidised bed process. Batch pyrolysis experiments of wood blocks submerged in different hydrocarbon liquids showed that up 50 % solid pyrolysis could be achieved with only 1.9 $kJ \cdot g^{-1}$ energy input. It was found that the overall degree of pyrolysis obtained in the liquid system is lower than that obtained from the fluidised bed system. This was attributed to the large temperature gradient between the centre of the biomass particle/block and its surface in the liquid system leaving a considerable fraction of the outer layer of the block unpyrolysed. It was shown that the proposed liquid system was able to overcome many of the limitations of the gas-based systems.

ACKNOWLEDGEMENTS

I would like first to thank Professor Sam Kingman for giving me the opportunity to do my PhD research at the Microwave Process Engineering Research Group, University of Nottingham. I would like also to thank the Faculty of Engineering, University of Nottingham for providing the funding which allowed me to undertake this research.

I would like to express my deepest gratitude to my PhD supervisors Professor Sam Kingman, Dr John Robinson and Dr Juliano Katrib for their continuous support, patience, motivation, and immense knowledge. Their guidance helped me in all the time of research and writing of this thesis. Many thanks to my assessors for their constructive comments and valuable feedback.

My appreciation also extends to the researchers, technicians, and fellow postgraduate research students at the Microwave Process Engineering Research Group for all of their help and support during my PhD research.

Special thanks to my amazing family for the love, support, and constant encouragement I have gotten over the years. I would also like to thank all my friends in Nottingham who have been very supportive all the time during my PhD research.

TABLE OF CONTENTS

LIST OF FIGURES

LIST OF ABBREVIATIONS AND NOMENCLATURE

Abbreviations

HR	Heating rate
RT	Residence time
CHP	Combined heat and power
CFB	Circulating fluidised bed
RF	Radio frequency
MW	Microwave
Q-factor	Quality factor
DC	Direct current
TE	Transvers electric
TM	Transverse magnetic
TGA	Thermogravimetric analysis
DSC	Differential scanning calorimetry
SDT	Simultaneous DSC-TGA
DTG	Derivative weight loss
IR	Infrared
VNA	Vector network analyser
ID	Inner diameter
OD	Outer diameter
PTFE	Polytetrafluoroethylene
CRI	Complex refractive index
CVD	Chemical vapour disposition

Nomenclature

ε	Complex permittivity
ε_0	Free space permittivity = $8.854 \times 10^{-12}\ F \cdot m^{-1}$
ε'	Real part of the complex permittivity (dielectric constant)
ε''	Imaginary part of the complex permittivity (dielectric loss factor)
$\tan\delta$	Loss tangent (dissipation factor)
P	Power, W.
f	Frequency, Hz
V	Volume, m^3
E	Electric field intensity, $V \cdot m^{-3}$
α	Attenuation factor
β	Phase factor
D_p	Penetration depth, m
λ	Wavelength, m
λ_0	Free-space wavelength, m
τ	Relaxation time, s
ω	Angular frequency, radians per second.
T	Temperature, ^oC (or K)
m_c	Critical moisture content
Q	Cavity quality factor
η	Efficiency of the heating cavity
Q_{py}	Specific enthalpy for pyrolysis, $J \cdot kg^{-1}$
H	Heat flow, $W \cdot kg^{-1}$
C_p	Specific heat capacity, $J \cdot kg^{-1} \cdot K^{-1}$
t	Time, s
ρ	Density , $kg \cdot m^{-3}$
S'	Surface area per unit volume, $m^2 \cdot m^{-3}$
h	Convective heat transfer coefficient, $W \cdot m^{-2} \cdot K^{-1}$

k	Conductive heat transfer coefficient (thermal conductivity), $W \cdot m^{-1} \cdot K^{-1}$
Nu	Nusselt's number
W	Weight, g
e	Bed porosity
r	Radius, m
v	Volume fraction
ΔP	Pressure drop, bar
u	Velocity, $m \cdot s^{-1}$
u_{mf}	Minimum fluidisation velocity, $m \cdot s^{-1}$
d_p	Particle diameter, m
Ga	Galileo's number
μ	Viscosity, Pa·s
μ_r	Complex relative permeability
k_0	Wave number
c_o	Speed of light in vacuum = 3×10^8 $m \cdot s^{-1}$
σ	Electric conductivity, $S \cdot m^{-1}$
S_{11}	Reflection parameter, dB
q	Heat flux, $W \cdot m^{-2}$

1 INTRODUCTION

Global challenges related to energy security, resource sustainability and the environmental impacts of burning fossil fuels have led to an increasing need for switching to the use of clean and sustainable resources.

Oil and natural gas are considered the main raw materials for about 95 % of chemicals produced worldwide (Koutinas et al., 2008), and according to the International Energy Agency (IEA), 81 % of the world energy supply comes from fossil fuels (IEA, 2015). Burning fossil fuels releases carbon dioxide which is one of the greenhouse gases believed to have the major contribution towards global warming and climate change (IPCC, 2013).

Demand for resources including energy are expected to increase with the increase in world population which is currently estimated at 7.3 Billion and predicted to reach 9.7 in 2050 (UN, 2015). Resources consumption per individual is also expected to increase due the foreseeable increase in humans wealth (Clark and Deswarte, 2008). This predicted rapid increase in demand for resources including energy, has raised many questions regarding resource security and the need for sustainable development.

Sustainable development requires replacing current sources of materials and energy with sustainable sources and increasing the utilisation efficiency of such resources (Clark and Deswarte, 2008). Renewable resources such as solar radiation, wind, tides and biomass have been considered as strong alternatives to replace fossil resources due to their inexhaustible availability and the environmental benefits related to the reduction of the carbon dioxide emissions (van Dam et al., 2005; Clark and Deswarte, 2008). Currently, renewable resources contribution towards total world's energy supply is estimated at about 14 % as can be seen in Figure 1-1.

Among the available renewable resources, biomass has a unique advantage in that it can be used to produce chemicals as well as fuel products. Moreover, biomass is

considered the only available renewable resource to replace fossil resources for liquid transportation fuels production (Cherubini, 2010).

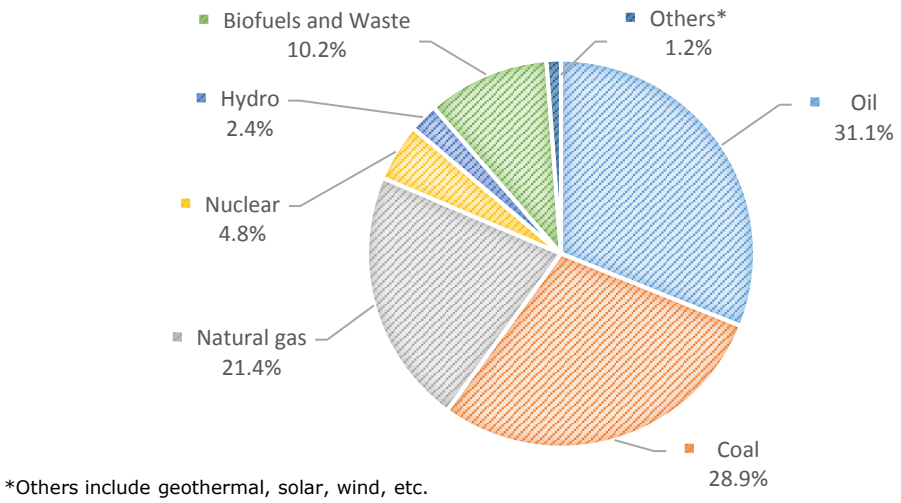

Figure 1-1: World total energy supply shares in 2013 (IEA, 2015)

In general, biomass refers to any organic matter available on a renewable basis (Clark and Deswarte, 2008). Biomass is the largest renewable source of carbon on earth (Foust et al., 2009). It is formed through the photosynthesis process during which atmospheric carbon dioxide and water are converted into sugars. These sugars are considered the base compounds from which more complex materials are synthesised forming the biomass (Cherubini, 2010). When it comes to fuels and their environmental implications, biomass and its fuel products are considered CO_2 neutral as biomass releases when burnt, approximately the same amount of CO_2 absorbed during its syntheses; i.e. it forms a closed CO_2 loop (Clark et al., 2012).

For commercial-scale applications, biomass can be obtained from four main sectors: agriculture, forestry, aquaculture (micro- and macro-algae) and wastes from industries and households (Cherubini, 2010).

Raw biomass materials have a low energy density compared to fossil resources. This is because of their low calorific value and low density. Wood chips, for example,

have a calorific value of around 18 $MJ \cdot kg^{-1}$ and a typical density of 200 $kg \cdot m^{-3}$ (McKendry, 2002) providing an energy density of around 3.6 $GJ \cdot m^{-3}$. In contrast, heavy fuel oil has a typical calorific value of 40 $MJ \cdot kg^{-1}$ and a density 990 $kg \cdot m^{-3}$ (Lehto et al., 2014) providing an energy density of 39.6 $GJ \cdot m^{-3}$ which is more than ten times that of the wood chips. Therefore, instead of using them directly as fuels, it might be preferable to process the feedstocks to produce higher energy density fuels and/or more valuable material products. It is to be noted here that there could be considerable amount of energy consumed in the conversion process depending on the technology used. This processing energy needs to be taken into consideration when evaluating the economic feasibility for converting biomass feedstocks into more valuable products rather than using them directly as fuels.

Biomass conversion processes can be classified into chemical, thermochemical and biochemical processes. Chemical processes, by definition, refer to those processes involving changes in the material chemical structure. The most common biomass chemical conversion processes are hydrolysis and transesterification (Cherubini, 2010). Hydrolysis uses a catalyst to depolymerise the polysaccharides in the biomass material to produce sugars or derivative chemicals (Sun and Cheng, 2002; Cherubini, 2010). Transesterification is the process during which fatty acids extracted from appropriate biomass feedstocks are reacted with methanol or ethanol in the presence of a catalyst to produce bio-diesel (Gude et al., 2013).

Biochemical (or biological) processes are those involve adding micro-organisms or enzymes to assist in achieving the required chemical reactions. The most common biochemical conversion processes are fermentation for ethanol production and anaerobic digestion for the production of biogas which is a mixture of mainly methane and carbon dioxide (Cherubini, 2010). One the drawbacks of the biochemical processes is that among the whole feedstock, only the simple sugars are used in the reaction and that the conversion process takes relatively long time of hours to days (Mettler et al., 2012).

Thermochemical processes involve heat-assisted structural changes. The major thermochemical processes are combustion, gasification and pyrolysis. Combustion is the 100 % oxidation of all the organic matter using oxygen (air) while gasification is a partial combustion of the biomass material to produces heat and syngas which could be used for chemicals and/or energy production. Pyrolysis is heating the biomass feedstock in the absence of oxygen to produce gases, oil and char (Arshadi and Sellstedt, 2008; Luque et al., 2012). Thermochemical processes have the advantage of that the entire feed is involved in the products formation. Also, the conversion process occurs in a shorter time compared to the chemical and biochemical processes (Mettler et al., 2012). The residence time of the solid biomass during the thermochemical processes can be as short as few seconds as the case in fast pyrolysis (Bridgwater, 2012).

Among the thermochemical processes, pyrolysis have received great attention with hundreds of papers have been published over the last decade. The target product from pyrolysis is usually the liquid fraction which is called bio-oil or pyrolysis oil. Bio-oil has a typical energy density of around 20 $GJ \cdot m^{-3}$ (Bridgwater, 2012) compared to around 3.6 $GJ \cdot m^{-3}$ for the biomass feed if wood chips is used. It can be used directly for heat and power generation, or upgraded to be used for chemicals and biofuels production as will be discussed later in Section 2.1. High bio-oil yield requires high heat transfer rates. Bridgwater (2012) have identified five pyrolysis modes among which fast pyrolysis provides the highest bio-oil yield. However, this requires a residence time of an order of seconds for both the solid and the vapour. A number of technologies have been developed for bio-oil production through fast pyrolysis as will be discussed in Section 2.2. However, providing the energy required to achieve the biomass reaction (around 2.7 $kJ \cdot g^{-1}$*) with high heating rate without degrading the product quality has been of the major

* Bridgwater (2012) estimated that the pyrolysis process requires about 15 % of the energy in the biomass feed. Woods have a typical gross calorific value of about 18 $MJ \cdot kg^{-1}$ (Günther et al., 2012). Based on the 15 % figure, around 2.7 $kJ \cdot g^{-1}$ would be needed for the pyrolysis of wood.

challenges facing the development of fast pyrolysis technologies (Bridgwater, 2012).

Microwave heating has been considered as a promising technique for providing the energy required for biomass pyrolysis due to its volumetric and selective heating nature which allows for rapid heating in a cold environment. This helps to preserve the product quality by limiting secondary reactions. It can also help to reduce the energy consumption as the energy is used to directly heat the biomass material with no need to heat its environment (Robinson et al., 2015). The focus of this thesis is on the processing aspects of microwave pyrolysis of biomass material.

1.1 Aim and Objectives

The aim of this research is to study the interaction between biomass materials and microwave energy during pyrolysis, and to develop a reliable and scalable microwave pyrolysis process. Number of objectives have been set to achieve this goal:

- To identify different types of biomass materials for characterisation based on their abundance, economic value and suitability for pyrolysis.
- To study the dielectric properties of the selected biomass materials over the pyrolysis temperature range, and to relate their variations with temperature to the physical and structural changes during pyrolysis.
- To develop a microwave pyrolysis process based on the understanding of the dielectric properties of the biomass material, the pyrolysis reaction requirements, the heat transfer characteristics, and the bulk solid flow behaviour.
- To assess the yield and quality of the products obtained from the developed process as well as the energy requirement.

The thesis is structured into eight chapters including the current introductory chapter. Chapter 2 gives a general overview of the fundamentals of biomass

pyrolysis including its reaction mechanisms and conditions as well as the energy requirement. It includes also a review of the existing fast pyrolysis technologies.

Chapter 3 focuses on the fundamentals of microwave heating technique. It details the microwave heating mechanisms and the microwave-material interactions. The recent developments in the microwave pyrolysis of biomass materials are also reviewed. The details of the experimental methodologies involved in this thesis are presented in Chapter 4.

Chapter 5 is dedicated for characterising selected biomass material as candidates for microwave pyrolysis. Characterisation includes studying the dielectric properties of the selected biomass materials and their temperature dependency, and relating them to the physical and structural changes in the biomass materials during pyrolysis.

Chapter 6 and 7 investigate the microwave pyrolysis in a fluidised bed process as an attempt to overcome the challenges associated with the heterogeneity of microwave heating, and to provide a reliable and scalable microwave pyrolysis process. Chapter 6 covers the steps of the process design including studying the fluidisation behaviour of the biomass particles, estimating the energy and power density requirements for pyrolysis, and the microwave cavity design. Chapter 7 focuses on operating the developed microwave fluidised bed process and running batch pyrolysis experiments to investigate the product yield and quality and the energy consumption.

Chapter 8 investigates the microwave pyrolysis of biomass in a hydrocarbon liquid instead of using an inert gas as a way to overcome some of the limitations in the gas-based fluidised bed system. The conclusions of the thesis are presented in Chapter 9 together with recommendations for future studies.

2 BIOMASS PYROLYSIS: PRINCIPLES AND TECHNOLOGIES

2.1 Reaction Conditions and Mechanisms

Pyrolysis is a thermochemical process during which the biomass feedstock is heated in an inert atmosphere at around 500 °C to produce gas, liquid and solid products. The liquid product which is also called bio-oil is usually the target product because of its eligibility to be used in applications similar to those of petroleum oil such as heat and power generation. It could be also used as a feedstock for chemicals and transportation fuels production. The gas product is a mixture of mainly CO, H_2, CO_2, and some low molecular weight hydrocarbons. The solid product is a carbonaceous material or char.

Figure 2-1 shows the pyrolysis products and their typical applications. The fraction and quality of each of the three products are functions of the type of the biomass material used and the processing conditions which include the temperature, the heating rate and the solid and vapour residence time (Bridgwater, 2012).

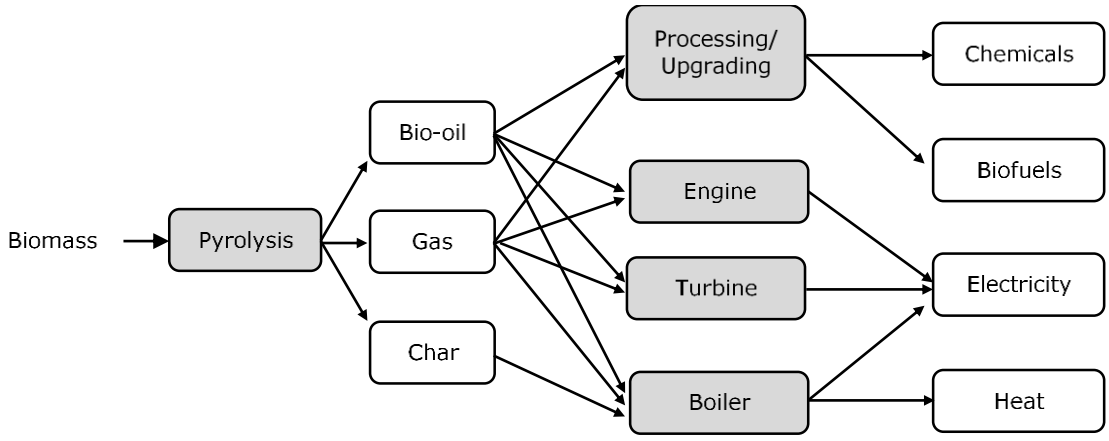

Figure 2-1: Pyrolysis products and their applications. Adopted from (Bridgwater, 2012).

Different kinds of lignocellulosic biomass from forestry and agricultural wastes can be used as a feedstock for bio-oil production. This includes, but not limited to, wood, straws, switchgrass, corn stover and bagasse. Number of studies have used algae as well (Mohan et al., 2006).

Lignocellulosic biomass have been considered the most suitable type of biomass to be used for commercial scale production of chemicals and biofuels because of their abundance, low cost, and that they do not interfere with food supply (Cherubini, 2010; Isikgor and Becer, 2015). Lignocellulosic biomass is made up of three main constituents: cellulose, hemicellulose and lignin. Both cellulose and hemicellulose are carbohydrate polymers. Cellulose is a linear polymer of β-glucose while hemicellulose is a branched polymer that can contain different monosaccharides of which xylose is the most common especially in hardwoods (Wang et al., 2015). Lignin is a complex highly aromatic non-carbohydrate polymer consisting of three primary monomers as shown in Figure 2-2 which also shows the chemical structure of the cellulose and hemicellulose (Turley, 2008; Alonso et al., 2012).

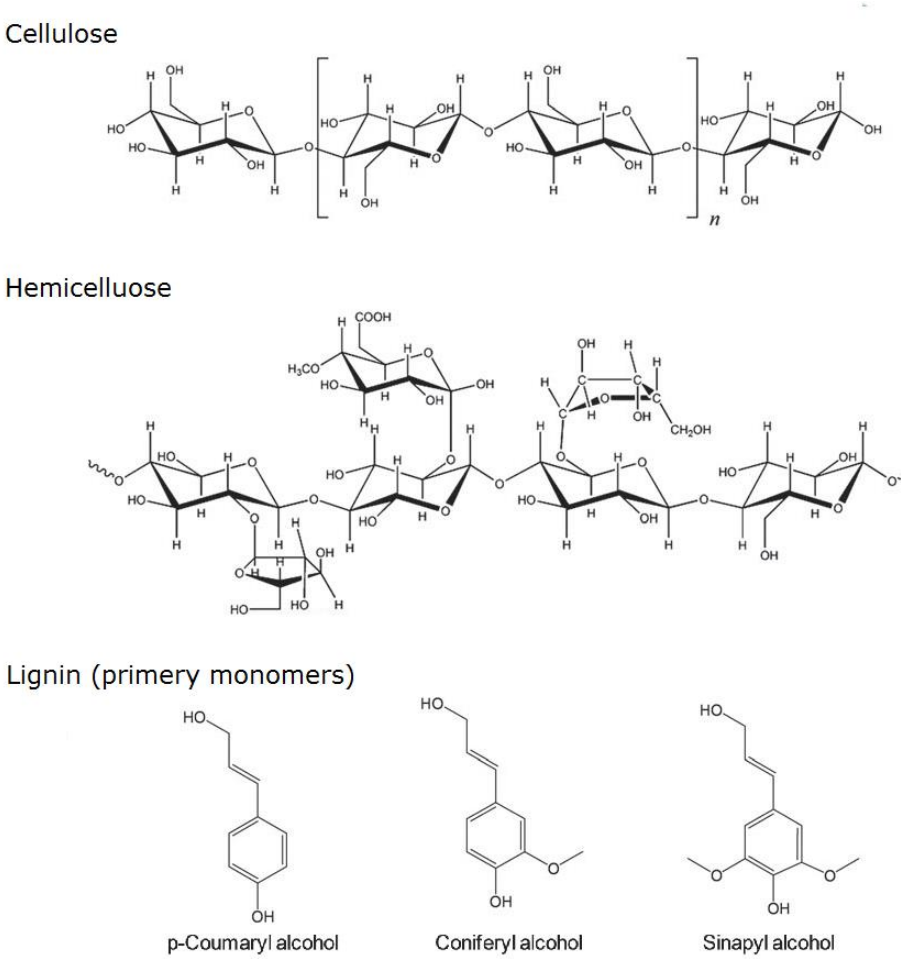

Figure 2-2: Chemical structure of the main biomass constituents (Alonso et al., 2012)

The kinetics of biomass pyrolysis is still considered a complex subject (Van de Velden et al., 2010; Collard and Blin, 2014). Many authors have tried to understand the mechanism of biomass pyrolysis through the study of the decomposition mechanisms of its individual constituents; cellulose, hemicellulose and lignin (Yang et al., 2006; Yang et al., 2007; Giudicianni et al., 2013). Yang et al. (2007) studied the decomposition temperature of the three constituents using thermogravimetric analysis (TGA). They found that hemicellulose decomposition happens first at around 220–315 °C while cellulose decomposes in the range 315–400 °C. Lignin was found to decompose slowly over a wide temperature range starting from 150 °C and continues up to 900 °C (Yang et al., 2007).

Regarding the product distribution and quality, it has been strongly believed that the pyrolysis of biomass constituents is a superposition of three primary mechanisms and secondary mechanisms (Van de Velden et al., 2010; Collard and Blin, 2014). The primary mechanisms which are explained by Figure 2-3 are:

- Char formation: this pathway is favoured at low reaction temperatures, below 500 °C, and low heating rates (Collard and Blin, 2014). It is characterised by rearrangement reactions leading to the formation of a thermally stable solid product called char which has a polycyclic aromatic structure. Water and incondensable gases are formed as a result of these rearrangement reactions (Van de Velden et al., 2010; Collard and Blin, 2014).
- Depolymerisation: this pathway involves the breakage of the bonds between the monomer units leading to the formation of shorter chains. Depolymerisation continues until the produced molecules become volatile at the operating conditions (Collard and Blin, 2014). Cellulose depolymerisation leads to the formation of levoglucosan as the primary product with concentration up to nearly 60 % (Demirbaş, 2000; Patwardhan et al., 2011). Hemicellulose depolarisation products depend on the type of

monosaccharides involved. Xylose-rich hemicellulose depolymerises into mainly five-carbon compounds such as furfural while hexoses-rich hemicellulose depolymerises into products rich in six-carbon compounds such as Hydroxymethylfurfural (HMF) (Wang et al., 2015). Lignin depolymerisation leads to the formation phenolic compounds which could be monophenols or oligomers (Bai et al., 2014).

- Fragmentation: this involves the breakage of covalent bonds including those within the monomer units leading to the formation of low MW molecules and incondensable gases (Collard and Blin, 2014). This pathway is favoured at high temperatures of 600°C and more (Van de Velden et al., 2010).

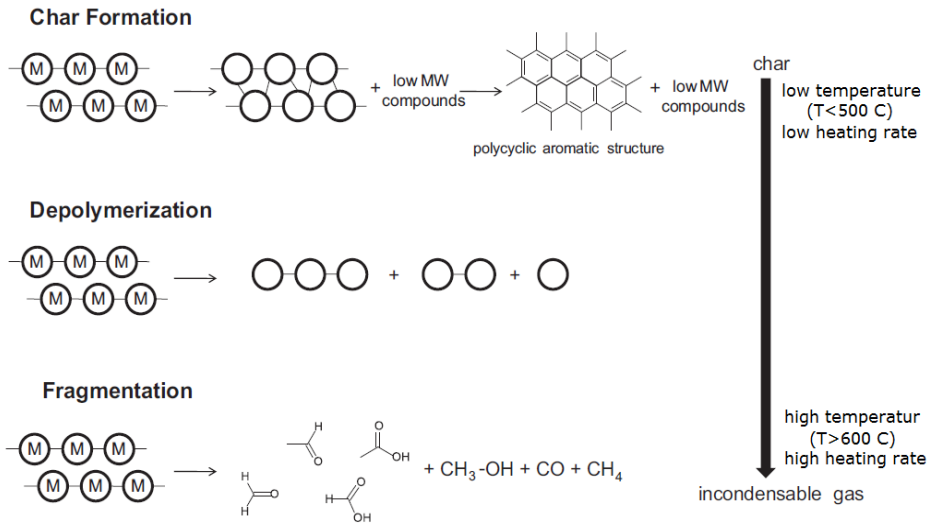

Figure 2-3: Primary mechanisms of biomass pyrolysis (Collard and Blin, 2014).

Secondary mechanisms take place when the volatile products are not stable at the reactor conditions. These conditions catalysis the secondary cracking and/or recombination reactions leading to the formation of low MW compounds and incondensable gases which could be similar to those usually formed under the fragmentation mechanism (Van de Velden et al., 2010; Collard and Blin, 2014). Some of the secondary reactions are catalysed by the minerals present in the solid (Lin et al., 2015).

In addition to the pyrolysis mechanisms of the individual biomass constituents, product distribution and quality is also affected by the interactions between the individual constituents. Zhang et al. (2015) studied these interactions and found a reduction in the levoglucosan yield in native cellulose-lignin mixture. No significant change in the product distribution was found when a native cellulose−hemicellulose mixture was used (Zhang et al., 2015)*.

Understanding the above discussed mechanisms and pathways helps to predict the conditions required to maximise or minimise the yield of each of the three pyrolysis products. Low reaction temperature with slow heating rate tends to maximise the char yield. On the other hand, high reaction temperature with fast heating rate tends to maximise the gas fraction as it stimulates fragmentation reactions. High liquid (bio-oil) yield requires the conditions that favour the depolymerisation pathway to be imposed which are a high heating rate and an intermediate temperature. High bio-oil yield requires also short vapours residence time and rapid cooling in order to avoid secondary cracking and recombination reactions. Bridgwater (2012) have identified five pyrolysis modes based on the operating conditions and the products fractions as shown in Table 2-1. Among these modes, fast pyrolysis has received great attention as it gives the highest bio-oil yield.

Table 2-1: Typical product distribution on dry wood basis obtained at different modes of pyrolysis (Bridgwater, 2012).

Mode	Conditions	Product fractions (%)		
		Liquid	Solid	gas
Fast pyrolysis	~500 °C, fast HR, vapour RT ~1 s	75	12	13
Intermediate	~500 °C, vapour RT ~10-30 s	50	25	25
Carbonisation	~400 °C, slow HR, vapour RT hours to days	30	35	35
Gasification	~750-900°C	5	10	85
Torrefaction	~290 °C, slow HR, solid RT ~10-60 min	0-5	80	20

HR = heating rate, RT = residence time

* The native cellulose−lignin mixture was obtained by selectively removing hemicellulose from the original biomass, and the binary native mixture of cellulose−hemicellulose was obtained after delignification of corn stover (Zhang, 2015).

The minimum energy required for pyrolysis is called the enthalpy for pyrolysis. The enthalpy for pyrolysis is the sum of the sensible enthalpy and the enthalpy for reactions. The former is the energy required to heat the biomass material up to the pyrolysis reaction temperature while the latter is the energy required to drive the pyrolysis reaction (Daugaard and Brown, 2003). This definition of the enthalpy for pyrolysis does not include any energy losses which depends on the technology used and the reactor design which are discussed in Section 2.2.

Table 2-2 shows values of enthalpy for pyrolysis for various biomass materials obtained from previous studies. It can be seen from Table 2-2 that there is a large variations in the enthalpy for pyrolysis ranging from 0.049 to 1.64 $MJ \cdot kg^{-1}$. This large variations can be regarded to different reasons including the use of different types of biomass material, employing different measurement techniques and the variations in the temperature range.

Table 2-2: Enthalpy for pyrolysis for various biomass materials from previous studies.

Study	Material	Enthalpy for pyrolysis ($MJ \cdot kg^{-1}$)	Method
Daugaard and Brown (2003)	Oak wood	1.46 ± 0.28	Energy balance in a fluidised bed at 500 °C
	Pine wood	1.64 ± 0.33	
	Oat hulls	0.78 ± 0.20	
	Corn Stover	1.35 ± 0.28	
He et al. (2006)	Wheat straw	0.558	Differential Scanning Calorimetry (DSC), at 500 °C
	Cotton stalk	0.465	
	Pine wood	0.600	
	Peanut shell	0.389	
Van de Velden et al. (2010)	Poplar	0.207	Differential Scanning Calorimetry (DSC), at 600 °C
	Sawdust	0.434	
	Straw	0.375	
Yang et al. (2013)	Cedar	1.30	Energy balance in a screw-conveyer at 600 °C
	Pine	1.50	
	Willow	1.50	
	Bamboo	1.50	
Chen et al. (2014)	Poplar wood	0.114	Differential Scanning Calorimetry (DSC), at 500 °C
	Pine bark	1.135	
	Corn stalk	0.049	
	Rice straw	0.880	
Atsonios et al. (2015)	Beech wood	1.12 ± 0.17	Energy balance in a fluidised bed at 500 °C

2.2 Technologies and Reactor Design for Fast Pyrolysis

Bio-oil production through pyrolysis is usually achieved in four main steps as explained by Figure 2-4: (a) feed preparation which includes drying and grinding; (b) reactor system where the pyrolysis reaction takes place; (c) solid separation where the solid is separated from the volatiles; and (d) condensation system in which bio-oil is condensed and separated from the other incondensable gases.

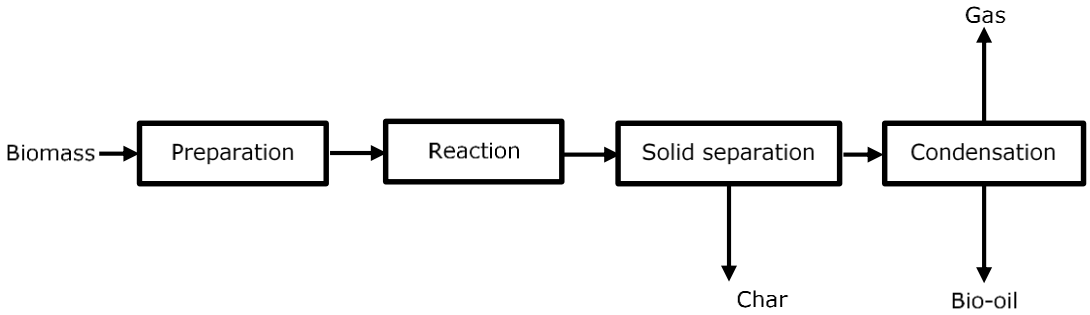

Figure 2-4: Biomass pyrolysis – main processing steps

The reaction conditions required to achieve high bio-oil yield as discussed in Section 2.1, limit the choices for the reactor design and the overall process. A number of technologies have been introduced as candidates to meet these reactor requirements, each has its advantages and limitations. The main existing pyrolysis technologies include bubbling fluidised bed, circulating fluidised bed, rotating cone, ablative pyrolysis, and the auger (screw) system.

2.2.1 Bubbling Fluidised Bed

Bubbling fluidised bed (also known as fluidised bed) reactors have been used for decades in petroleum and chemical processes. One of the main advantages of the fluidised bed process is its ability to provide high heat transfer rate due to the large contact area between the fluid and the solid particles (Ringer et al., 2006; Fouilland et al., 2010; Bridgwater, 2012).

Figure 2-5 shows a flow diagram for a typical bubbling fluidised bed process for biomass pyrolysis. The biomass material, after preparation, is fed to the fluidised

bed column where the pyrolysis reaction takes place. The fluidising gas, which is fed at the bottom of the column, controls the vapour and solid residence time. The pyrolysis products are carried with the fluidising gas and exit at the top of the reactor. This mixture is passed through a series of cyclones where char is separated. The vapours are then fed to a quench cooler where bio-oil is condensed. Bio-oil yield from a fluidised bed reactor could be as high as 75 % (Bridgwater, 2012). The incondensable gases from the condenser could be recycled and used as a fluidising gas.

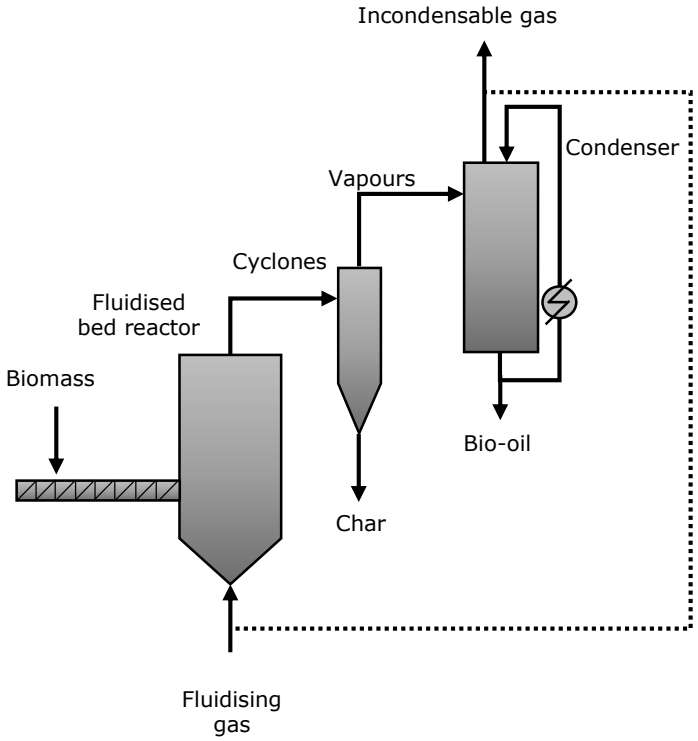

Figure 2-5: Typical bubbling fluidised bed technology for bio-oil production through fast pyrolysis. Adopted from (Robson, 2000)

The operating temperature for bubbling fluidised bed reactors is around 500 – 550 ^{o}C which can be controlled through the temperature and flowrate of the fluidising gas (Ringer et al., 2006). The heat required to achieve the pyrolysis reaction could be provided through one or a combination of the following methods (Ringer et al., 2006; Bridgwater, 2012):

- Hot fluidising gas
- Heating through the reactor walls
- Immersed heating tubes
- Recycled hot sand

One of the limitations of this technology is that it requires the use of small particle sizes of less than 3 mm in order to achieve high heat transfer (Bridgwater, 2012). Also, the high gas flow required for fluidisation decreases the vapour pressure of the pyrolysis vapours, making oil condensation and recovery more difficult (Bridgwater and Peacocke, 2000).

Early research on biomass pyrolysis in fluidised beds was pioneered by the researchers at the University of Waterloo in Canada (Scott and Piskorz, 1982; Scott and Piskorz, 1984; Scott et al., 1985) which led to the development of RTI process (Scott et al., 1999). Based on the RTI process, Dynamotive built a 100 tonne per day and 200 tonne per day plants in Canada (Bridgwater, 2012). Recently, Fortum has built and commissioned a commercial-scale 10 tonne per day plant in Finland employing the fluidised bed technology. The bio-oil plant is integrated with a combined heat and power (CHP) plant (Oasmaa et al., 2015).

2.2.2 Circulating Fluidised Bed

Circulating fluidised bed (CFB) is similar to bubbling fluidised bed in many aspects. The main difference is that CFB technology uses higher gas velocity which results in a shorter particle and vapour residence times (Fouilland et al., 2010; Bridgwater, 2012). Hot sand is usually used in CFB to provide the process with most of the heat required to achieve the pyrolysis reaction. It also assists lifting the biomass and char particles in the reactor. Figure 2-6 shows a typical CFB process in which the biomass material, after preparation, is fed to the column where it is heated rapidly as soon as it comes into contact with the hot fluidising gas and sand at its entrance. The produced vapours together with the char and sand are carried up with the gas

which is fed at the bottom of the column. The char and sand are separated from the hot vapours in cyclones and fed to a combustor where the char is burned. The combustion heat it transferred to the sand which is then recycled to the reactor. The hot vapours from the cyclones are fed to a quench cooler to condense and collect the bio-oil. The incondensable gases are recycled to the column to be used as a carrier.

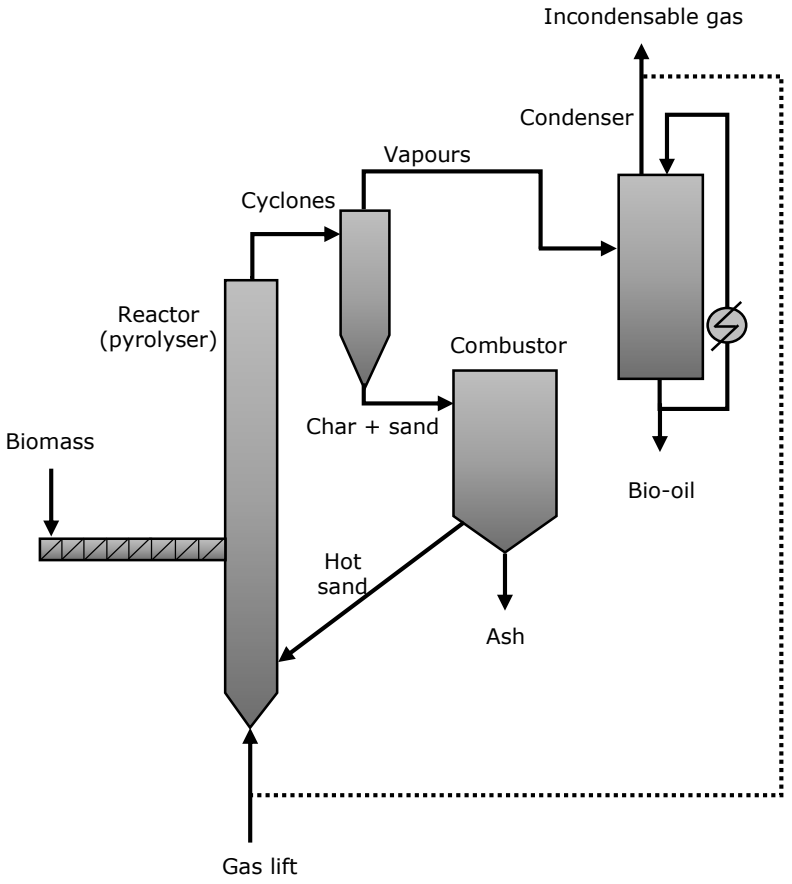

Figure 2-6: Simplified flow diagram of the circulating fluidised bed process developed by (Ensyn)

One of the main advantages of CFB technology is its short vapour and solid residence times which limits the secondary cracking reactions. The solid residence time is usually less than 2 seconds (Fouilland et al., 2010). Also, CFB technology has the advantage of its suitability for high throughputs which favours this technology for commercial scale operation (Bridgwater, 2012). However, the design and operation of the CFB process are more complicated compared to the bubbling

fluidised bed process due to the high gas velocity and the presence of the recirculated sand (Ringer et al., 2006; Bridgwater, 2012). The sand flowrate is usually 10 to 20 times greater than the biomass feed rate which adds high energy cost for moving this sand around the process (Ringer et al., 2006).

The developments and commercialisation of the CFB technology have been led by Ensyn who, with partners, have designed and constructed several commercial-scale bio-oil plants in USA, Canada and Brazil (Oasmaa et al., 2015).

2.2.3 Rotating Cone

This technology, which was developed by the Biomass Technology Group (BTG), involves mixing the biomass material with hot sand in rotating cone inside a vessel (BTG-BTL, 2015). It does not require using an inert gas which substantially reduces the size of the reactor and the condenser (Ringer et al., 2006). As in the CFB technology, the sand and the produced char from the reactor are fed into a combustor where the char is burned and the heat is transferred to the sand which is then recycled to the reactor. Typical flow diagram of the process developed by BTG-BTL is shown in Figure 2-7.

The main disadvantage of the rotating cone process is its complexity involving a rotating cone (moving parts), a fluidised bed combustor for burning the char and a pneumatic transport of the sand. EMPYRO has recently constructed and opened a 5 tonne per hour demonstration plant in Netherlands. Employing BTG's rotating cone technology, the plant simultaneously produces process steam, electricity and pyrolysis oil (Meulenbroek and Beld, 2015).

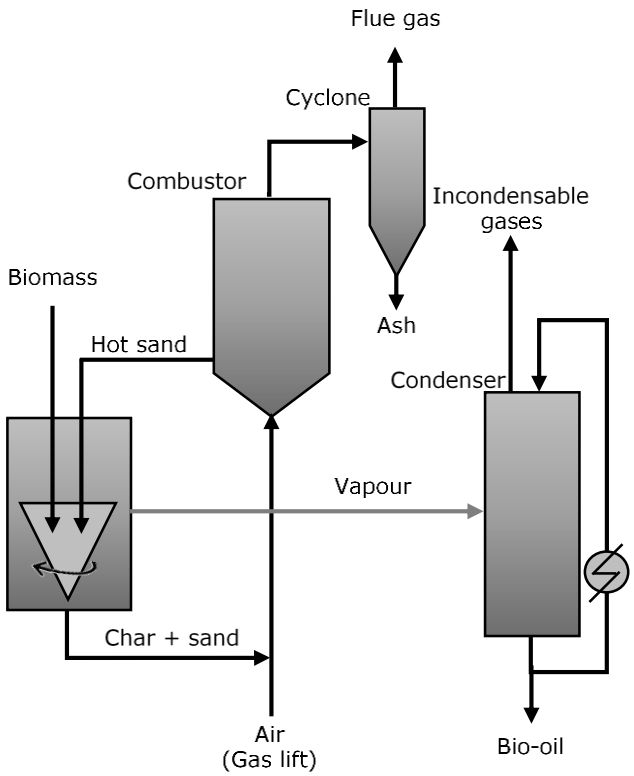

Figure 2-7: Process flow diagram of the rotating cone technology developed by BTG-BTL (BTG-BTL, 2015)

2.2.4 Ablative Pyrolysis

The concept of this technology is different than the others in that instead of using a heat carrier, the biomass particles are contacted with a hot metal surface (Oasmaa et al., 2015). The char layer formed on the particle's surface during the reaction is continuously removed as a result of an ablative force applied on the particle through either high gas velocity flowing tangentially to the reactor walls (gas ablation) or mechanically using a rotary disc/blade (Ringer et al., 2006; Bridgwater, 2012). The reactor wall temperature is usually kept around 600 °C. The main advantage of this technique is that it can process particles as large as 20mm (Ringer et al., 2006).

Research on this technology was led by SERI (then NREL)* between 1980 and 1996 who employed the gas ablation method (Ringer et al., 2006). However, NREL's work

* The Solar Energy Research Institute (SERI) which became the National Renewable Energy Laboratory (NREL) in 1991.

on this technology was abandoned in 1997 due to technical issues related to the high gas and particle velocities which resulted in excessive erosion, and also because of uncertainties regarding the scalability of the technology (Ringer et al., 2006). Recent activities on this technology have been focused more on the mechanical ablation such as the 250 $kg \cdot h^{-1}$ plant constructed by Pytec and the 100 $kg \cdot h^{-1}$ plant operated by Fraunhofer UMSICHT, both in Germany (Oasmaa et al., 2015).

2.2.5 Auger Reactor

The main feature of this technology is that the biomass material is fed to the reactor and moved inside it mechanically through auger or screw. The heat for the reaction is usually provided through hot sand which is mixed with the feed at the entrance. The sand is then separated from the product, reheated and recycled again (Dahmen et al., 2012). The heat could also be provided externally through the wall (Bridgwater, 2012). The main advantages of the auger reactor are its simplicity and flexibility in terms of feed particle size and shape (Bridgwater, 2012). However, the solid and vapours residence time inside the reactor for this technology are long compared to the fluid-transported technologies leading to high char and low liquid yields (Bridgwater, 2012).

2.2.6 Other Technologies

There are other types of reactor design which have not received as much attention and development towards scaling up as the earlier discussed technologies. One of these is the vacuum reactor which does not require a carrier gas to sweep the vapours out of the reactor. This makes the condensation easier and results in a clean oil with little or no char particles (Ringer et al., 2006). Although the vapour residence time is short, vacuum pyrolysis is still considered a slow pyrolysis process with a liquid yield of 35 – 50 % (Bridgwater, 2012).

Another technology is the fixed bed reactor which has been used widely in laboratory scale studies but there is no evidence that it could be used in larger scale applications (Bridgwater, 2012).

2.3 Conclusions

A number of technologies have been introduced as possible candidates to meet the requirements for high bio-oil yield through fast pyrolysis. These requirements include a high heating rate, intermediate temperature and a short vapour residence time.

The differences in the reactor design between these technologies can be found in mainly two areas: the method of solid flow/movement and the method of heat transfer to the biomass material. These are actually the main focus of most of the research and development in fast pyrolysis technologies.

Biomass materials, in general, are known for their complex flow behaviour and in the above-discussed technologies, there are essentially two methods for feeding and moving the biomass materials inside the reactor. One is using a gas carrier such as in the bubbling and circulating fluid bed reactors and the gas ablative reactors. The other is mechanical such as in the auger reactor and the mechanical ablative reactors. Although the rotating cone reactor uses the gravity force for feeding the solid into the reactor, it could be considered as a mechanical flow method because the reaction takes place in the rotating cone and the char and sand are transported out of the reaction area using the centrifugal force supplied by the rotating cone.

The gas carrier systems have the advantage of their ability to provide shorter vapour residence time which is required for high liquid yield. They can also improve the heat transfer if the gas is preheated. However, a large condenser is required to cope with the high gas flowrate.

The heat required to achieve the pyrolysis reaction can be provided to the biomass material through either a heating medium (hot gas or hot sand) which is the most common method or through a hot surface such as in the ablative reactor. Using hot gas alone is usually not sufficient to provide the heat of reaction unless the gas temperature is excessively raised which would degrade the liquid yield and quality (Bridgwater, 2012). This is why it is usually used in a combination with hot sand or hot surface. Adding hot sand to the process adds high energy cost for moving the sand around the process (Ringer et al., 2006).

Providing the energy required to achieve the biomass reaction with high heating rate has been of the major challenges facing the development of fast pyrolysis technologies (Bridgwater, 2012).

One of the promising heating methods which has been considered to replace the conventional heating techniques is the microwave heating technique. Microwave is a volumetric heating technique meaning that the workload molecules are heated instantaneously as a result of their interaction with the microwave electromagnetic field. It is therefore an energy transfer rather than heat transfer. Microwave is also a selective heating technique meaning that it could be targeted to heat any good microwave absorbent material such as water without heating its environment. Air and free space are transparent to microwaves (Meredith, 1998). With its selective and volumetric heating features, microwaves can provide a rapid heating in a cold environment. In biomass pyrolysis, this helps to preserve the product quality by limiting secondary reactions. It can also help to reduce the energy consumption as the energy is used to directly heat the biomass material with no need to heat its environment (Robinson et al., 2015).

Many studied have been published on biomass pyrolysis employing the microwave heating technique. However, before reviewing these studies, some fundamentals of microwave heating will be discussed.

3 MICROWAVE HEATING FUNDAMENTALS

3.1 Background

Microwave heating technique is one of the electrical volumetric heating family which includes also conduction and induction heating (resistive heating), Ohmic heating and, radio frequency (RF) heating (Meredith, 1998). The frequency and wavelength ranges for each of these heating techniques are indicated in Figure 3-1.

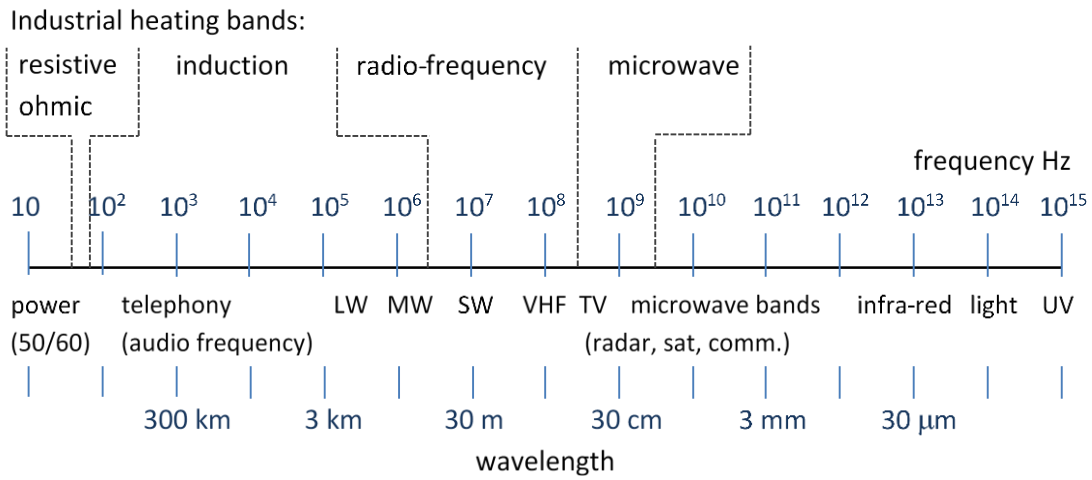

Figure 3-1: Volumetric heating methods in the electromagnetic spectrum. Adopted from (Meredith, 1998)

Certain frequencies have been specified for domestic, industrial, and medical uses as an international agreement to avoid interference with communication signals (Meredith, 1998). However, the most commonly used microwave frequencies for these applications are 2.45 GHz and near 900 MHz (896 MHz in the United Kingdom and 915 MHz in the United States). In the RF region, 6.78 MHz, 13.56 MHz, 27.12 MHz and 40.68 MHz are commonly used (Reader, 2006).

3.2 Microwave Heating Mechanisms

Materials could be classified according to their interaction with the electromagnetic fields into conductors, insulators and absorbers. In the case of microwave frequencies (0.3 to 300 GHz) conductors reflect the radiation and they are used as waveguides and walls in microwave cavities, insulators behave as transparent

mediums and they are used as supports and holders in microwave heating applications, and absorbers (also called dielectric materials) absorb the radiation and can be heated by the microwave energy (Jones et al., 2002).

Dielectric materials can be heated electromagnetically due to polarisation (also referred to as relaxation) or conduction loss effects (Clark and Sutton, 1996).

Polarisation loss occurs as a result of the charges displacement from their equilibrium position when the alternating electromagnetic field is applied to them. This is accompanied by a motion in the charge carriers leading to heat dissipation (Metaxas and Meredith, 1983; Yu et al., 2001). There are, in general, four polarisation loss mechanisms: dipolar, electronic, atomic and interfacial polarisation. Electronic and atomic polarisation mechanisms have a negligible effect within the microwave and RF frequency ranges and they are effective only in the infrared and visible parts of the electromagnetic spectrum (Metaxas and Meredith, 1983).

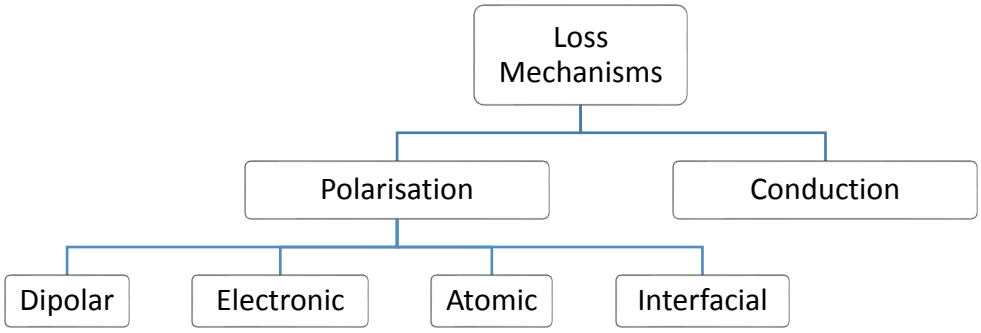

Figure 3-2: Electromagnetic loss mechanisms.

The dipolar loss is associated with materials with permanent dipoles such as water. When the electromagnetic field is applied, the dipoles try to align themselves responding to the oscillating electromagnetic field as explained in Figure 3-3. Energy is then dissipated as heat as a result of this motion (Meredith, 1998). Dipolar loss is more significant in liquids (Kitchen et al., 2014).

Figure 3-3: Dipolar molecules trying to align themselves according to the applied field (Lidström et al., 2001)

Interfacial loss, which is also called Maxwell-Wager mechanism, is related to heterogeneous materials containing free charged particles confined within a non-conducting medium structure. Polarisation, in this case, occurs at the interface as a result of charges build-up at the interface when the electromagnetic field is applied (Metaxas and Meredith, 1983).

Conductive loss (also called ionic conduction) is related to poor electric conductors which contain charge carriers free to move under the influence of the electric field (Meredith, 1998; NPL, 2003). The applied electric field redistributes the charge carriers forming a conducting path and the material, in this case, is heated due to the electrical resistance (charged particles collision) resulted from the conduction (Metaxas and Meredith, 1983; Remya and Lin, 2011). Conductive loss is the dominant loss mechanism in solids (Kitchen et al., 2014). Figure 3-4 explains how the charged particles in a solution follow the applied field.

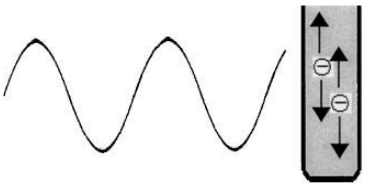

Figure 3-4: Conduction mechanism: charged particles move following the applied field (Lidström et al., 2001)

For biomass materials, their moisture content make the dipolar loss the dominant loss mechanism at room temperature. However, during biomass pyrolysis when char starts to form at high temperature, the conductive loss becomes the dominant loss mechanism (Robinson et al., 2010b). More details about the loss mechanisms in biomass materials are discussed in Section 3.3.

3.3 Dielectric Properties

3.3.1 Definition and Mathematical Representation

Dielectric properties define the interaction of materials with the electromagnetic field. Biomass materials are considered nonmagnetic materials and, therefore, their interaction is limited to the electric field (Nelson, 2010). The mathematical representation of dielectric properties is commonly explained through the polarisation loss. When an electric field is applied to a dielectric material, some energy is stored as a result of charges polarisation. The dielectric permittivity, ε, is used to quantitatively describe this stored energy. If the electric field is alternating, as in the case of microwave field where part of the energy is dissipated into heat, the dielectric permittivity is, then, expressed as a complex quantity as shown in Equation 3-1 (Meredith, 1998; Yu et al., 2001):

$$\varepsilon = \varepsilon' - j\varepsilon'' \qquad 3\text{-}1$$

The real part of the complex permittivity, ε', is called the dielectric constant and it determines the amount of the stored energy while the imaginary part, ε'', is the dielectric loss factor and it determines the amount of power dissipation into heat. It is to be noted here that the real part of the complex permittivity has been traditionally called the dielectric constant. However, it is not constant as it does change with frequency and temperature as will be shown later in this section. The ratio of the dielectric constant to the loss factor is called the loss tangent or dissipation factor, tan δ. The loss tangent is commonly used to assess the general ability of a material to heat in an electric field (Robinson et al., 2010a). If two materials have the same loss factor, then the material with lower dielectric constant would heat better as it would have higher loss tangent.

The dielectric properties of biomass materials at room temperature are affected significantly by their moisture content. Robinson et al. (2009) investigated the loss factor of dried and undried (6.3 % water content) pine pellets at 2.45 GHz. They

found that at room temperature the loss factor is 0.05 and 0.81 for the dried and undried samples respectively. This study showed clearly the significant contribution of the water content in the dielectric properties of biomass materials as only 6.3 % moisture increases the loss factor with an order of magnitude.

There are other factor that affects the dielectric properties of biomass materials including the frequency, temperature and the packing density. Table 3-1 shows the dielectric properties of different biomass materials at room temperature together with water which is a good microwave absorbent.

Table 3-1: Dielectric properties of different biomass materials together with water at room temperature (~25°C), no errors were defined in these papers other than in the case of the pine pellet report

Material	Moisture (%, d.b)	Density ($g \cdot cm^{-3}$)	Frequency (MHz)	ε'	ε''	tan δ	Reference
Pine pellets	6.3±0.2	-	2450	-	0.81	-	(Robinson et al., 2010b)
	dry	-	2450	-	0.05	-	
Palm Kernel Shell	8.5	-	2450	2.76	0.35	0.13	(Salema et al., 2013)
Palm Fibre	10	-	2450	1.99	0.16	0.08	
Switchgrass pellets	2.23	0.94	915	2.63	0.17	0.06	(Motasemi et al., 2014)
	2.23	0.94	2450	2.55	0.16	0.06	
Municipal solid waste	2.9	0.166	2450	2	<0.05	<0.03	(Beneroso et al., 2016)
Distilled water	-	1	2450	77	13	0.17	(Meredith, 1998):

It can be seen from Table 3-1 that there are significant variations in the dielectric properties of biomass materials, especially the loss factor. These variations are regarded to many reasons of which the most important are the type of the biomass materials used and the measurement conditions i.e. the material's moisture content and density and the frequency used. It is, therefore, important to present the dielectric properties of biomass with their moisture content, density, temperature and the frequency as these factors significantly affect the dielectric properties. The factors influencing the dielectric properties will be discussed in more details later in this section.

When an electromagnetic field is applied on a dielectric nonmagnetic material, the power dissipation (P) could be estimated from the following equation (Meredith, 1998):

$$p = 2\pi f \varepsilon_0 \, \varepsilon'' \, E_i^2 \qquad 3\text{-}2$$

Where p is the power dissipation density ($p = P/V$); v is the volume of the dielectric material (m^3); E_i is the internal electric field intensity or voltage stress ($V \cdot m^{-3}$); f is the frequency of the applied field (Hz); ε'' is the loss factor of the dielectric material; and ε_0 is the free space permittivity ($\varepsilon_0 = 8.854 \times 10^{-12} \, F \cdot m^{-1}$).

Substituting the constant values, Equation 3-2 could be written as:

$$p = 55.63 \times 10^{-12} \, f \, {E_i}^2 \, \varepsilon'' \;\; (W \cdot m^{-3}) \qquad 3\text{-}3$$

Equation 3-3 shows that the power dissipation is a function of the material's loss factor, frequency and the square of the electric field intensity. The loss factor varies with the frequency which makes the relationship between the power dissipation density and frequency not linear.

Although, the dielectric constant does not appear in Equation 3-3 it affects the power dissipation through the electric field intensity, E_i (Nelson, 1999).

Electric field intensity propagation through the material could be represented graphically as displayed in Figure 3-5 and mathematically as follows (Metaxas and Meredith, 1983; Nelson, 1999):

$$E(z) = E_0 e^{-\alpha z} e^{-j(\omega t - \beta z)} \qquad 3\text{-}4$$

Where α and β are called the attenuation factor and phase factor respectively and both of them are functions of the dielectric constant and loss factor of the medium (Metaxas and Meredith, 1983; Nelson, 1999).

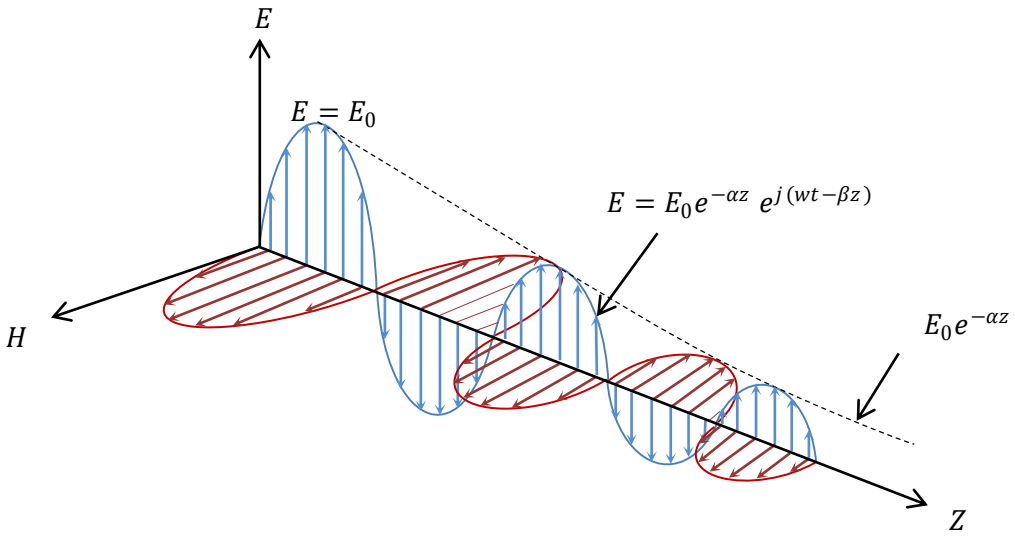

Figure 3-5: Electromagnetic field propagation in a dielectric medium. Redrawn from (Metaxas and Meredith, 1983)

The maximum electric-field stress should be less than a critical value at which voltage breakdown (or electric breakdown) occurs. This high electric field stress can ionise gases forming a conducting path at which considerable power dissipation takes place (arcing). This high local power dissipation density can damage the workload and some parts of the microwave heating system as well. The electric breakdown voltage of air at the standard conditions is about 30 kV·cm^{-1} (Meredith, 1998). The electric breakdown voltage of a gas is proportional to its density which decreases with increasing temperature at a constant pressure (Meredith, 1998).

As mentioned in Section 2.1, the biomass pyrolysis reaction happens at high temperature of around 500 °C. Operating at such temperature increases the possibility of electric breakdown by reducing the breakdown voltage to around 11 kV·cm^{-1}*.

Another important parameter in material interaction with electromagnetic energy is the penetration depth which is a measure of how deep the electric field can penetrate into a material. The penetration depth (D_p) is defined as the distance from

* The change in the voltage breakdown is inversely proportional to the change in the absolute temperature at constant pressure (Meredith, 1998). Therefore, the voltage breakdown at 500 °C (773 K) could be estimated as 30×(288/773) = 11.2 kv·cm^{-1}.

the surface at which the power flux drops to 1/e (≈0.368) of its surface value (Meredith, 1998). This definition comes from the fact that as the wave progresses inside a dielectric material, the electric field intensity and its associated power density fall exponentially with the distance from the surface as explained by Figure 3-5. The penetration depth can be estimated from the following equation (Metaxas and Meredith, 1983):

$$D_p = \frac{\lambda_0}{2\pi\sqrt{(2\varepsilon')}} \frac{1}{\sqrt{\left[\left(1+\left(\frac{\varepsilon''}{\varepsilon'}\right)^2\right)^{0.5}-1\right]}} \qquad 3\text{-}5$$

It is important to note here that this definition does not suggest that no heating at distance exceeding D_p as about 37 % of the power is dissipated in the material at depth greater than D_p. From Equation 3-5, it is clear that the penetration depth is a function of the dielectric constant, loss factor and the free-space wavelength, λ_0. lossy materials will have a short penetration depth. Water for example has a penetration depth of 1.3 cm at room temperature and 2.45 GHz. A materials with a complex permittivity of 2 - 0.1j, which is a typical value for a biomass material at room temperature, would have a penetration depth of 27.5 cm. However, the dielectric properties of biomass materials change with temperature and it becomes lossy when char starts to form at high temperature leading to reduction in the penetration depth.

3.3.2 Factors Influencing Dielectric Properties

Many factors affect the dielectric properties of materials: frequency; temperature; density; and the moisture content in the case of wet materials such as biomass (Nelson and Trabelsi, 2012).

3.3.2.1 Frequency

With the exception of transparent and extremely low-loss materials, dielectric constant and loss factor vary significantly with frequency (Nelson and Trabelsi,

2012). The relationship between the frequency and dielectric properties depends on the loss mechanism(s) involved.

One of the well-known equations used to mathematically represent the relationship between the permittivity of polar materials such as water and frequency is Debye equation which is as follows (Metaxas and Meredith, 1983):

$$\varepsilon = \varepsilon_{\infty} + \frac{\varepsilon_s - \varepsilon_{\infty}}{1 + j\omega\tau} \qquad 3\text{-}6$$

Where ε_s and ε_{∞} represent the dielectric constant at d.c (static) and very high frequency respectively, while τ is called the relaxation time (in seconds) which is the time required for the dipole to revert to a random orientation when the applied field is removed (Nelson and Trabelsi, 2012). The relaxation time is strongly related to the intermolecular forces which are affected by temperature (Gabriel et al., 1998).

Equation 4-15 could be separated into real and imaginary parts to give the dielectric constant and the loss factor as follows (Metaxas and Meredith, 1983):

$$\varepsilon' = \varepsilon_{\infty} + \frac{\varepsilon_s - \varepsilon_{\infty}}{1 + (\omega\tau)^2} \qquad 3\text{-}7$$

$$\varepsilon'' = \frac{(\varepsilon_s - \varepsilon_{\infty})\omega\tau}{1 + (\omega\tau)^2} \qquad 3\text{-}8$$

Debye equation could be represented graphically as displayed in Figure 3-6 which shows that the dielectric constant has a constant high value, ε_s, at static and very low frequencies and a constant low value, ε_{∞}, at very high frequencies. The drop in the dielectric constant at high frequency is because that the molecules become no longer able to rotate with a significant amount before the field is reversed. The loss factor has zero values at very low and very high frequencies. There is a peak at an intermediate frequency called the relaxation frequency, ω_o, and it is equal to the reverse of the relaxation time ($\omega_o = 1/\tau$).

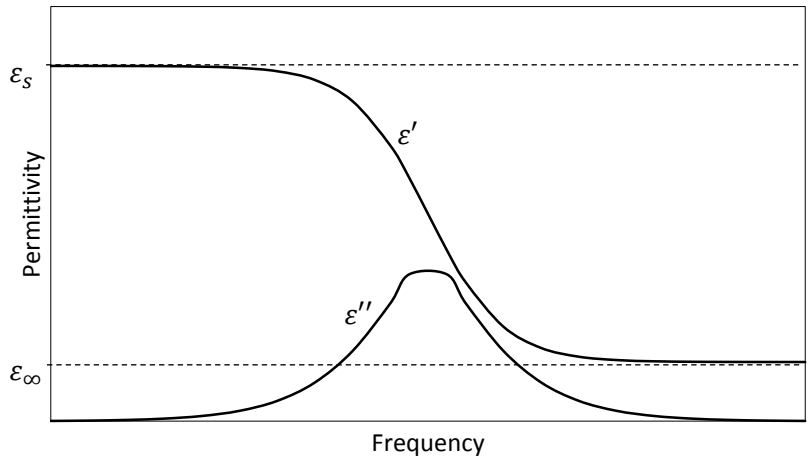

Figure 3-6: Dielectric permittivity for a material following Debye's equation. Adopted from (Metaxas and Meredith, 1983)

The frequency dependency of dielectric properties is more complex in heterogeneous materials when more than one loss mechanism is involved at the same time. Figure 3-7 is a typical representation of the relationship between the loss factor and the frequency for a heterogeneous material exhibiting dipolar and conductive losses. It shows how the conductive loss is the dominant at lower frequencies while at higher frequencies the dominant mechanism is the dipolar loss.

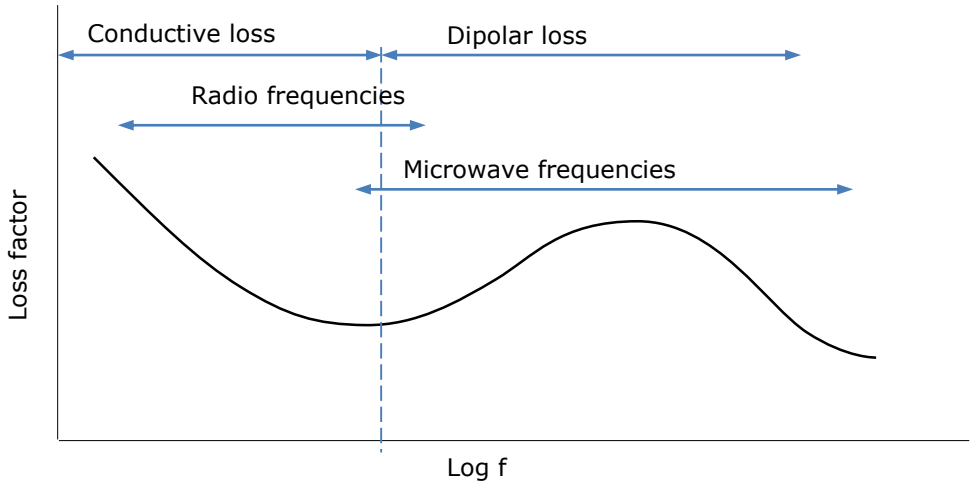

Figure 3-7: The loss factor for a homogeneous dielectric material exhibiting dipolar and conductive losses

3.3.2.2 *Temperature and moisture content*

The importance of studying the effect of temperature on the dielectric properties is coming from the fact that under electromagnetic heating the material's temperature does change. Temperature has an effect on the intermolecular forces and the molecules mobility (Gabriel et al., 1998; Nelson and Trabelsi, 2012) which affects the molecules ability to store and dissipate energy. The influence of the temperature on the dielectric properties depends on the loss mechanism involved and the applied frequency (Nelson and Trabelsi, 2012).

For polar materials exhibiting polarisation loss, increasing the temperature decreases the relaxation time. This is because increasing the temperate increases the ability of the molecules to rotate by freeing them from the intermolecular forces such the hydrogen bond in water (Gabriel et al., 1998). Decreasing the relaxation time increases the relaxation frequency and shifts the loss factor peak in Debye's formula towards a higher frequency as explained by Figure 3-8.

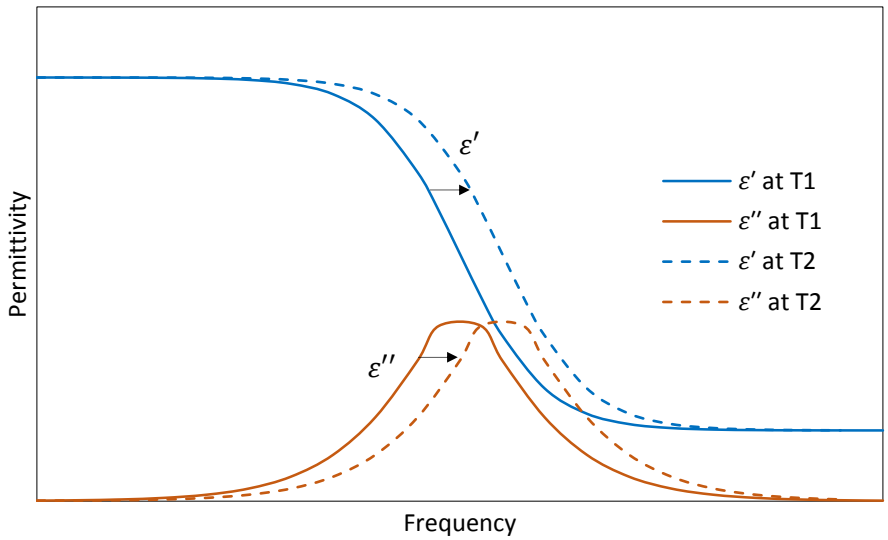

Figure 3-8: Permittivity at two different temperatures, T1 and T2; where T2 > T1.

The reduction in the relaxation time with increasing temperature leads to an increase in the dielectric constant for polar materials as explained by Figure 3-8. For the loss factor, the behaviour depends on the position of the measurement

frequency relative to the relaxation frequency. If the frequency is less than the relaxation frequency, then increasing the temperature will decrease the loss factor. On the other hand, increasing the temperature will increase the loss factor if the measurement frequency in higher than the relaxation frequency. Pure water has a relaxation frequency of about 20 GHz at 25 ^{o}C (Kaatze, 1989). Therefore, at 2.45 GHz the loss factor of pure water will decrease when the temperature is increased.

As mentioned earlier, the water content of biomass materials significantly affects their dielectric properties at room temperature. Therefore, the discussed influence of temperature on the dielectric properties of polar materials can be used to understand the dielectric behaviour of biomass materials at low temperatures. However, the water content of biomass materials is not purely free water.

The water content of wet materials, in general, could either be free water or bound water. Free water is found in capillaries and cavities while bound water could be physically attached to the dry surface or chemically combined with other molecules such as that of $MgCl_2 \cdot 6H_2O$ (Metaxas and Meredith, 1983; Shrestha et al., 2011).

Because of their restricted movement, bound water has less ability to polarise under the alternating electric field resulting in a lower dielectric constant and loss factor values compared to free water (Metaxas and Meredith, 1983; Bergo et al., 2012). Figure 3-9 explains a typical dielectric-moisture relation for a wet material. Both, the dielectric constant and loss factor, increase apparently above a critical point called the critical moisture content, m_c, above which the free water dictates the behaviour of the dielectric properties (Metaxas and Meredith, 1983; Shrestha et al., 2011; Bergo et al., 2012).

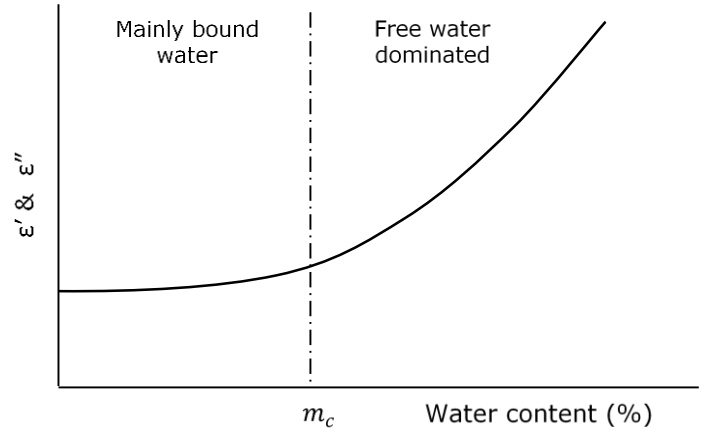

Figure 3-9: Relationship between loss factor and moisture content for moist solid; adopted from (Metaxas and Meredith, 1983), (Shrestha et al., 2011), and (Bergo et al., 2012)

Tinga (1969) studied the relationship between the loss factor of Douglas fir at 2.45 GHz and the temperature up to 90 °C at differed initial moisture contents. They found that the loss factor decreases with temperature when high initial moisture contents were used. At low initial moisture contents, the loss factor was found to increase with temperature and reaches a peak before it starts decreasing. This was regarded to that at low moisture content (probably lower than the critical moisture content), the dielectric behaviour is dictated by the bound water. Increasing the temperature makes the bound water molecules freer to polarise and rotate under the alternating electromagnetic field which results in an increase in the loss factor.

The presence of soluble ions could have a significant effect on the dielectric properties of wet materials, especially above the critical moisture content. Shrestha et al. (2011) studied the dielectric properties of alfalfa leaves and their moisture and frequency dependencies. They found that above the critical moisture content, the loss factor increases more rapidly at lower frequencies which was regarded to the increased ionic loss caused by the presence of larger number of dissolved ions.

During pyrolysis, the biomass material experiences several physical and structure changes starting by drying until the formation of char which has different chemical

structure to the raw biomass as discussed in Section 2.1. These transformations have significant effect on the dielectric properties of biomass materials.

Robinson et al. (2015) studied the influence of temperature on the loss tangent of Larch (wood) at 2.45 GHz over the pyrolysis temperature. They showed that the loss tangent drops while increasing the temperature up to around 120 ^{o}C which was regarded to the moisture evaporation. A second reduction in the loss tangent was seen above 200 ^{o}C leading to the formation of a very low loss material between 250 to 480 ^{o}C. A sharp increase in the loss tangent was observed above 500 ^{o}C which was regarded to the carbonisation of the woody material and the formation of char which is a good microwave absorber.

3.3.2.3 Density

Packing density is a very important parameter that influence the dielectric properties of granular and pulverised solids as higher packing density results in higher permittivity. This is because that at higher packing density, the air fraction (or void fraction) in the mixture is smaller, and as the permittivity of air is lower than that of the solid material, then the overall permittivity of the mixture will be greater.

Biomass materials are found in different forms, and their density varies depending on their shape and size. Wood, for example, could be found in the form of logs, chips, pellets, shavings, or sawdust. In addition, shape and size of the feedstock for processing are decided based on many factors such as the form at which the material feedstock is available, processing requirements and the economic considerations.

Many authors have suggested using dielectric mixing models for studying the relationship between the permittivity and the packing density (Nelson, 2005; Nelson and Trabelsi, 2012; Tuhkala et al., 2013). Dielectric mixing models are used, in general, to estimate the effective permittivity of a mixture of more than one

component. Porous and granular materials can be considered as binary mixtures of air and a solid material, and their effective permittivity could then be determined by substituting the permittivity of air with $1 - 0j$.

3.3.3 Dielectric Measurement Techniques

Many techniques are used to measure the dielectric properties of materials. Each of these techniques has its advantages and limitations. The choice of the appropriate dielectric measurement technique for specific application depends on many factors. Nelson (1999) highlighted the most important factors: the frequency range of interest, the nature of the material to be measured and its physical and electrical properties, and the required accuracy (Nelson, 1999). Dielectric measuring techniques could be classified into two broad classes: Lumped impedance methods and Wave methods (NPL, 2003). Lumped-impedance methods are only suitable for measuring dielectric properties at low frequencies up to 1 GHz (NPL, 2003) and high loss materials* (Venkatesh and Raghavan, 2005). Wave methods measure the interaction of the dielectric material with travelling or standing electromagnetic waves. The most common wave methods used for measuring dielectric properties in the microwave and RF frequencies are: the cavity perturbation technique, the open-ended probe technique, waveguide and coaxial transmission line method, and the free-space transmission technique.

3.3.3.1 The cavity perturbation technique

This technique measures the shift in the resonant frequency and the quality factor (Q-factor) caused by the insertion of the sample inside a resonant cavity. The Q-factor is a measure for the ratio of the energy stored in the cavity to that dissipated. The change in the cavity Q-factor is used to calculate the loss factor while the frequency shift is used to calculate the dielectric constant (Metaxas and Meredith, 1983). One of the advantages of this technique is that it can measure the dielectric

* This is based on NPL (2003) classification of dielectric materials: low loss ($\tan\delta < 3\times10^{-4}$), medium loss ($3\times10^{-4} \leq \tan\delta < 3\times10^{-2}$), and high loss dielectrics ($\tan\delta \geq 3\times10^{-2}$)

properties of low-loss materials with high accuracy compared to the other wave techniques (Sheen, 2005; Lester et al., 2006). It can be used to measure the dielectric properties of different types of materials including liquids, solids and powders. However, the sample volume in this technique needs to be relatively small depending on how lossy the material is (Sheen, 2005). One of the limitations of the cavity perturbation technique is that it measures the dielectric properties at only few frequencies depending on the cavity size (Bois et al., 1999b).

The cavity perturbation technique has been used previously to measure the dielectric properties of different biomass materials in the form of pellets over the pyrolysis temperature (Robinson et al., 2010b; Motasemi et al., 2015; Sait and Salema, 2015).

3.3.3.2 The open-ended probe technique

This technique is used to determine the dielectric properties of materials by measuring the amplitude and phase of the signal reflected from the sample using an open-ended coaxial probe touching the sample (Venkatesh and Raghavan, 2005). It is capable of measuring dielectric properties of high loss materials (Nelson, 1999). The probe technique is a broadband that covers a broad range of RF and microwave frequencies (Nelson and Bartley, 1998). However, the probe technique has a poor accuracy for low loss materials compared to the cavity perturbation technique (Nelson and Bartley, 1998, Bois et al., 1999). Although it works well with liquids and semisolids, the accuracy of the probe technique is questioned for solids and pulverised materials. This is mainly because of the difficulty to get a smooth surface with no air gaps in solids and particles which is a requirement for accurate probe measurement (Nelson and Bartley, 1998).

The open-ended probe is not a favourable technique for measuring the dielectric properties of biomass materials mainly because of its poor accuracy for measuring the dielectric low-loss materials and its surface finishing requirements.

3.3.3.3 *Waveguide and coaxial transmission line*

This technique measures the reflected and/or transmitted signals from a workload placed inside a waveguide or transmission line (Bois et al., 1999b; Venkatesh and Raghavan, 2005). It is one of the best techniques to measure the permittivity of bulk samples with high and medium loss over the microwave range (NPL, 2003). It can be used for measuring the dielectric properties of inhomogeneous materials including biomass wastes as it allows for using a large sample which is more representative to the bulk material. It has some limitations for the high temperature measurements which may cause some measurement errors including: the difference in the thermal expansion between the sample and the waveguide; the temperature gradient caused by using large sample; and the difficulty in isolating the measurement apparatus (Varadan et al., 1991a).

3.3.3.4 *Free-space transmission technique*

In this technique, the attenuation and phase shift of a signal is measured after placing the sample in a free space between a transmission antenna and a receiving antenna facing each other (Trabelsi and Nelson, 2003; Venkatesh and Raghavan, 2005). The main advantage of this technique is its flexibility in terms of sample shape. However the free-space technique requires a relatively large sample size as transversal dimensions must be large to avoid diffraction effects at the sample edges (Dhondt et al., 1996). Similar to the waveguide technique, it can be used to measure the dielectric properties of inhomogeneous materials because of the large sample size it can accommodate (Ghodgaonkar et al., 1989). Another advantage is that it can be used for high temperature measurements and the sample could be thermally isolated from the measuring apparatus (Varadan et al., 1991a).

3.4 Microwave Heating Equipment

Microwave heating systems consist of three main components and some accessories for measurement and control. The main components are the microwave power source (generator), the waveguide, and the applicator.

3.4.1 Generators

The types of microwave generators could be classified into microwave power tubes, which include magnetrons and klystrons, and solid-state generators. Solid-state generators are essentially transistor-based amplifiers that increase the power in steps. They are not commonly used for heating applications because of their low efficiency, high cost and limited output power (Meredith, 1998; Brace, 2009). Both, magnetrons and klystrons can provide high microwave output power. The magnetron is a high vacuum electronic valve that generates the microwave power from a high-voltage source of DC power while the klystron is an electronic valve that amplifies the microwave signals into high microwave power using an electron beam (Meredith, 1998). Magnetrons are the most commonly used type of generators for heating applications because of their high efficiency and low cost (Meredith, 1998; Brace, 2009). Commercially, microwave generators of up to 100 kW at 915 MHz are currently provided (Sairem, 2015).

3.4.2 Waveguides

Waveguides are hollow metal pipes (usually rectangular) used for transmitting the microwave power. The distribution pattern of the electric and magnetic fields inside the waveguide is defined by the propagation mode. Rectangular waveguides can support two types of mode: transverse electric ($TE_{m,n}$ or $H_{m,n}$ modes) in which the electric field in the direction of propagation is zero, and transverse magnetic ($TM_{m,n}$ or $E_{m,n}$ modes) in which the magnetic field in the direction of propagation is zero. The suffixes m & n represent the number of half-cycles along the coordinate directions normal to the propagation direction. Rectangular waveguides are usually designed to support a TE_{10} mode which is the lowest order mode for rectangular waveguides (Metaxas and Meredith, 1983; Meredith, 1998). Figure 3-10 shows the electric field patterns for a TE_{10} mode in a rectangular waveguide.

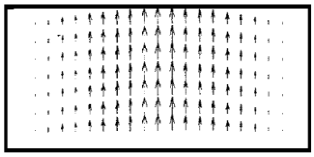

Transverse section across waveguide. The electric field is maximum at the centre of the waveguide

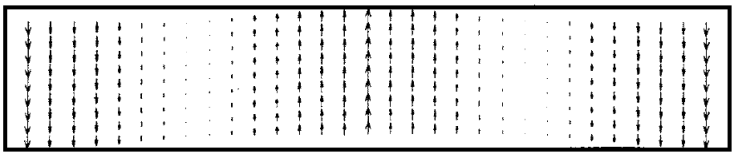

Longitudinal view along axis of propagation

Figure 3-10: electric field pattern in a TE_{10} mode rectangular waveguide (Meredith, 1998)

For free propagation, the dimensions of the waveguide has to be chosen so that the frequency is larger than a minimum value called the cut-off frequency, or the wavelength is smaller than the cut-off wavelength. For example, for the TE_{10} mode to propagate in a rectangular waveguide without attenuation the width must be at least half the free-space wavelength (Meredith, 1998). The microwave power passing through the waveguide is another factor that affects the choice of the dimensions of the waveguide as higher power at certain frequency requires larger waveguide to avoid arcing. Some standard waveguide dimensions and their corresponding frequency ranges are listed in Table 3-2.

Table 3-2: Some standard waveguide dimensions and their corresponding frequencies (Metaxas and Meredith, 1983).

Official designation			Frequency range (GHz)	Dimensions	
EIA	RCSC	IEC		inches	mm (approx.)
WR975	WG4	-	0.75 - 1.12	9.75 x 4.875	248.0 x 124.0
WR770	WG5	-	0.96 - 1.45	7.7 x 3.85	196.0 x 98.0
WR430	WG8	R22	1.7 - 2.6	4.3 x 2.15	109.0 x 55.0
WR340	WG9A	R26	2.2 - 3.3	3.4 x 1.7	86.0 x 43.0

EIA: The Electronic Industries Alliance; RCSC: The Radio Components Standardization Committee;
IEC: International Electrotechnical Commission.

3.4.3 Applicators

There are three main classes of applicators: travelling waves, near-field and resonant applicators (Reader, 2006). Travelling wave applicators are simply waveguides connected to a microwave generator on one side and a terminating load on the other side. The power fed by the generator is essentially absorbed by the

workload and the rest is absorbed by the terminating load (Metaxas and Meredith, 1983). Near-field applicators are usually defined as those which have a small distance between the material and the applicator compared to the wavelength. They can be open-ended waveguides, antennas, or slotted feed waveguide (Reader, 2006).

Resonant applicators (or cavities) are the most commonly used types of applicators (Mehdizadeh, 2015). Resonant cavities can be single-mode or multimode. Multimode cavities are designed to support many TE_{mn} and TM_{mn} modes simultaneously. Their dimensions are several half-wavelengths long in at least two directions (Meredith, 1998). Domestic microwave ovens are an example of multimode cavities.

Besides their simple construction, multimode applicators have the advantage of being able to process a wide range of workloads with different sizes and properties (Meredith, 1998). The main disadvantage of multimode applicators is their complexity in terms of theoretical analysis, so they are usually subjected to experimental studies for design purposes (Metaxas and Meredith, 1983). However, with the developments of the computer modelling and simulation programmes, the field distribution could now be predicted with reasonable accuracy (Salema and Afzal, 2015). Multimode ovens also have the disadvantage of the non-uniform field strength distribution which results in the formation of hot and cold spots (Lidström et al., 2001; Salema and Afzal, 2015).

Single mode cavities, as the name implies, are designed to allow only one mode to be exited inside the cavity (Meredith, 1998; Lidström et al., 2001). They have the ability to establish high electric field intensity (Metaxas and Meredith, 1983; Reader, 2006). Better heating homogeneity could be achieved in single mode cavities. However this homogeneity comes at the expense of the sample size which is limited by the half-wavelength of the applied microwave field (Reader, 2006). When the

parameters are well controlled, single mode cavities are able to achieve reproducible and predictable results (Lidström et al., 2001).

The power dissipation efficiency inside resonant cavities is commonly expressed through their quality factor (Q factor) which is given by (Metaxas and Meredith, 1983; Meredith, 1998):

$$Q = 2\pi \frac{energy\ stored}{energy\ dissipated/cycle} \qquad 3\text{-}9$$

The efficiency of the heating cavity (η) can be related to the Q factor and the resonant frequency as follows (Mehdizadeh, 2015):

$$\eta = 1 - \sqrt{\frac{f_0}{f_1}\frac{Q_1}{Q_0}} \qquad 3\text{-}10$$

Where f_0 and f_1 are the resonant frequencies of the empty and loaded cavity respectively while Q_0 and Q_1 are the quality factors of the empty and loaded cavity respectively.

3.5 Microwave Pyrolysis: Features and Recent Developments

Microwave heating has been considered as a promising technique for providing the energy input to biomass pyrolysis due to its volumetric and selective nature which allows for rapid heating in a cold environment. These features can help to preserve the product quality by limiting the unwanted secondary reactions (Miura et al., 2004; Robinson et al., 2015). They can also help to reduce the energy consumption as the energy is used to directly heat the biomass material with no need to heat its environment (Robinson et al., 2015).

Many studies have been conducted and there are already several review papers published on microwave pyrolysis of biomass materials (Luque et al., 2012; Macquarrie et al., 2012; Yin, 2012; Motasemi and Afzal, 2013; Huang et al., 2016). Different factors have been found to effect the product yield and quality. These

include the type and size of the biomass material, the microwave energy input (power and time), the type of the microwave cavity and the reactor design (Motasemi and Afzal, 2013). Liquid yields as high as 60 % have been reported (Robinson et al., 2015).

One of the early studies that discussed in some details the benefits of the *heating in a cold environment* during microwave pyrolysis is the work reported by Miura et al. (2004). They looked at the temperature gradient and the mass transfer for both conventional and microwave heating as explained by Figure 3-11. In conventional heating, the direction of mass transfer is opposite to the direction of heat transfer which results in that the volatile products pass through areas of higher temperature where secondary reactions can be activated. This is not the case in microwave heating where the centre has usually higher temperature than the outer surface.

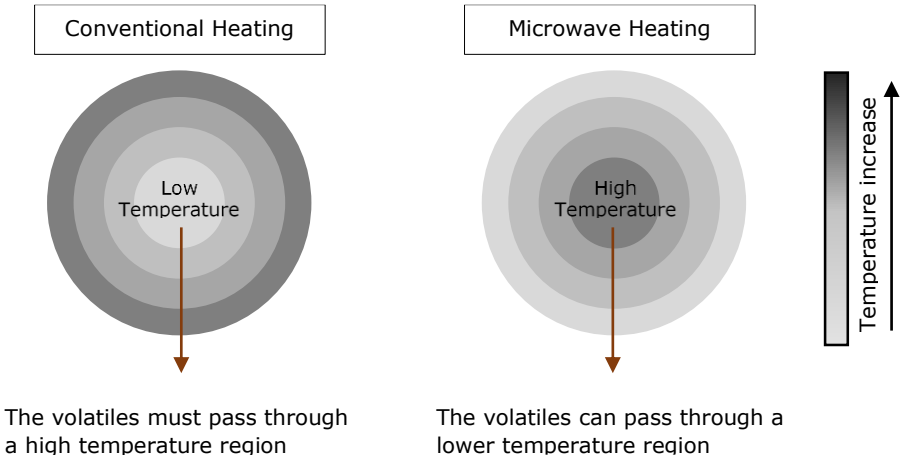

Figure 3-11: Temperature gradient and mass transfer in conventional and microwave heating. Adopted from (Miura et al., 2004)

Robinson et al. (2015) studied the effect of microwave pyrolysis on the quality of the produced bio-oil and compared the results to those obtained using conventional pyrolysis. They found that the composition of the high molecular weight primary compounds such as levoglucosan in the bio-oil obtained after microwave pyrolysis was significantly higher than that from conventional pyrolysis. This was regarded to

the *heating in cold environment* advantage that microwave provides which limits the secondary degradations.

Microwave can provide an added advantage over conventional techniques which is that it requires less pre-treatment in terms of drying, crushing and grinding (Luque et al., 2012). Because of that water is a good microwave absorbent, its presence in the form of moisture within the biomass feedstock increases the heating rate at the start of the process. Also, the time and energy consumed for crushing and grinding the feedstock could be substantially decreased under microwave treatment. This is because that, unlike conventional heating techniques, achieving high heating rate does not require using a very small particle size (Luque et al., 2012).

Biomass materials, in general, have low loss values which may limit their heating rate and the final achievable temperature at certain power density. Many studies have suggested mixing the biomass material with a microwave susceptor (good microwave absorbent) in order to improve the heating rate and reach the pyrolysis temperature. The most commonly used susceptors are the carbon based material and metal oxides (Li et al., 2013; Borges et al., 2014; Mushtaq et al., 2014). Many studies have shown improvements in terms of heating rate and the final temperature of the bulk material when these microwave susceptors are used (Hu et al., 2012; Salema and Ani, 2012; Li et al., 2013; Borges et al., 2014; Mohamed et al., 2016; Pianroj et al., 2016).

However, there is an ongoing debate about the feasibility of mixing biomass with a susceptor during microwave pyrolysis. Susceptors would result in localised heating and generation of hotspots with temperatures>1000 ^{o}C while the bulk temperature reads much less than that leading to significant gasification (Robinson et al., 2015). In fact, the use of susceptors eliminate the specific benefits of microwave heating which are the selective and volumetric heating. The biomass material, when a susceptor is used, is heated by conduction from the surface of the susceptor which is similar to what happens in conventional heating techniques.

The majority of the published studies on microwave pyrolysis were conducted on poorly designed cavities or modified domestic ovens. These cavities can not provide high electric field intensity to heat the low-loss biomass materials up to the pyrolysis temperature without using a suscueptor. Number of studies have demonstrated that by applying high enough electric field intensity, microwave pyrolysis of biomass could be achieved with no need for adding any microwave susceptor. Robinson et al. (2010b) estimated the minimum power density required to achieve the pyrolysis of wood pellets at around 5.0×10^{8} $W\cdot m^{-3}$.

Robinson et al. (2015) were able to get 60 % to 70 % of wood chips to pyrolyse in a single-mode applicator (TM_{01n}) operated at 2.45 GHz with no need for any additives. The cavity was designed to create power densities on the order of 10^{8} $W\cdot m^{-3}$ in the heated phase.

Shang et al. (2015) investigated the effect of various additives on the microwave pyrolysis of sawdust in a 3 kW single-mode system, operated at 2.45 GHz. They were able to obtain up to 27 % bio-oil without using any additive. They then studied the bio-oil yield after mixing the biomass materials with different susceptors including silica carbon (SiC), activated carbon, pyrolysis char, potassium carbonate (K_2CO_3), and sodium hydroxide (NaOH). They showed that, with the exception of the activated carbon, mixing the biomass with 5 % additive results in a reduction in the bio-oil yield. The silica carbon (SiC) resulted in a significant reduction in the gas and bio-oil yields. This was attributed to the non-uniform mixing caused by the large density difference between the sawdust and SiC particles. The pyrolysis char, the potassium carbonate and the sodium hydrate was found to increase the gas yield and reduce the oil yield. This increase in the gas yield at the expense of the oil yield could be attributed to the high-temperature hot-spots created by the microwave susceptor leading to significant gasification.

One of the major challenges facing microwave pyrolysis and many other high-temperature microwave heating applications is the heating non-uniformity. The

nature of the standing waves results in the formation of areas of high and low electric field intensity inside the microwave cavity leading to non-uniform heating. The implications of the heating heterogeneity of microwave heating are more significant in the processes where the loss factor of the material involved increases significantly with temperature such as in biomass pyrolysis where the loss factor of the formed char is significantly greater than that of the raw biomass. In such processes, the heating heterogeneity could lead to a rapid increase in the temperature at the areas of the high electric field intensity relative to the bulk material leading to, possibly, thermal runaway.

Thermal runaway is a condition which arises when the power dissipation in a small element within the heated material exceeds the rate of heat transfer to its surroundings. This results in a local acceleration of heating and a rapid increase of temperature. The unstable nature of thermal runaway could cause severe degradation of the heated material and may damage the processing equipment (Meredith, 1998; Mehdizadeh, 2015). In the case of biomass pyrolysis, thermal runaway can happen when char starts to form as char is a good microwave absorber and has a high loss factor compared to the raw biomass (Robinson et al., 2015).

Salema and Afzal (2015) studied the heating uniformity in the microwave pyrolysis of empty fruit bunch (EFB) pellets in a modified domestic microwave oven operated at 2.45 GHz frequency. The pellets were placed inside a quartz reactor with 100mm ID which was positioned at the centre of the cavity. They showed that this setup leads to significant heating heterogeneity and the formation of hot and cold spots as displayed in Figure 3-12.

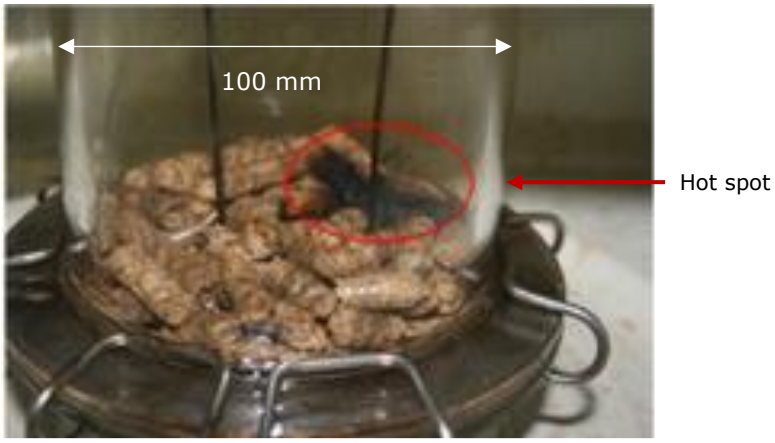

Figure 3-12: Heating heterogeneity in a multimode cavity (Salema and Afzal, 2015)

Single-mode cavities could provide better uniformity as the system could be set to have the sample placed at the area of a high field intensity, meaning that there will be only one hot-spot. However, the sample size in single-mode cavities is limited by the half-wavelength of the supplied microwave power. This make single-mode cavities not a practical choice for scaling-up.

Robinson et al. (2015) discussed the relationship between the sample size and the heating homogeneity when they studied the microwave pyrolysis of wood chips. They applied 2.45 GHz microwave power at a fixed bed of the biomass material placed in a single-mode applicator (TM_{01n}). They observed significant heating heterogeneity with thermal runaway at the centre of the sample when samples size of the order of 50 mm were used as shown in Figure 3-13. They concluded that for better heating uniformity and to avoid thermal runaway, the sample size needs to be kept within 15 mm. However, such size is far from what would be practical for large-scale operation. There is a need, therefore, to develop microwave pyrolysis systems that can provide homogenous heating while being able to process large feed sizes.

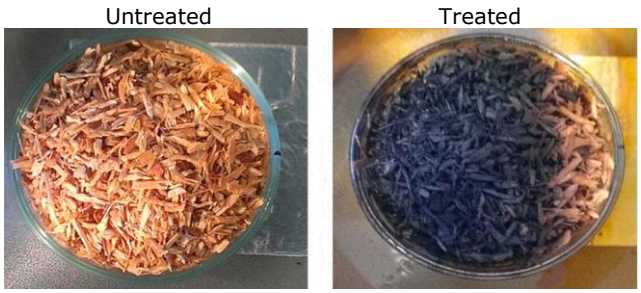

Figure 3-13: Heating heterogeneity in a single-mode cavity (TM_{01n}) (Robinson et al., 2015)

There have been several attempts to improve the heating homogeneity during microwave pyrolysis in multimode cavities to allow for larger sample to be processed. One of the early attempts on this area was the work reported by Salema and Ani (2012) who employed an overhead stainless steel stirrer to agitate the biomass material during the microwave pyrolysis. The study was carried out in a modified domestic microwave oven at 2.45 GHz with 150 g of the biomass material (oil palm shell) placed inside a 100 mm ID quartz reactor. They could not obtain bio-oil with the available power without using a microwave susceptor. When the biomass material was mixed with activated carbon, bio-oil yield of up to 18 % was obtained. This was achieved after heating the mixture for 20 minutes at 450 W, a biomass to activated carbon mixing ratio of 1:05, and a stirrer speed of 200 rpm.

In another study Abubakar et al. (2013) also employed an overhead stainless stirrer to agitate the biomass material during pyrolysis in a 100 mm quartz reactor placed in modified domestic microwave oven at 2.45 GHz. They used a setup in which the inert gas (nitrogen) was introduced at the top of the reactor and the pyrolysis vapours were condensed and collected at the bottom of the reactor. This was to avoid bio-oil deposition on the reactor wall above the bed. The biomass material (oil palm shell with 1.4 mm particle size) was mixed with activated carbon as a microwave susceptor. They studied the effect of the stirrer speed and the percentage of the microwave susceptor. They reported a maximum bio-oil yield of 28 % at a stirrer speed of 50 rpm and 25 % activated carbon after applying 450 W microwave power for 30 minutes. They found that increasing the stirrer speed above

50 rpm results in a reduction in the bio-oil yield. It was also shown that increasing the fraction of the activated carbon above 25 % leads to a reduction in the bio-oil yield and an increase in the gas yield. This increase in the gas yield at the expense of the oil yield can be attributed to the increase in the high-temperature hot-spots formed around the activated carbon particles enhancing the secondary cracking reactions, leading to more gasification.

Pianroj et al. (2016) studied the microwave pyrolysis of oil palm shell in 107 mm ID fixed-bed quartz reactor placed in a multimode cavity. The cavity was designed and built based on numerical simulations. Two waveguide feeds were used with two 2.45 GHz magnetrons taken from domestic ovens with 800 W maximum power each. Employing two magnetrons was an attempt to provide higher microwave power, and based on the numerical simulations it improves the heating uniformity. As in most of the other microwave pyrolysis studies, they used activated carbon as a microwave susceptor. They reported a maximum bio-oil yield of 30 % which was obtained at a biomass to activated carbon ratio of 3:1 when a total power of 800 W was applied on 400 g biomass for 30 minutes. They found that decreasing the biomass to activated carbon ratio leads to a reduction in the bio-oil yield and increase in the char yield. This is probably because of the reduction in the microwave penetration depth with the increase in the fraction of activated carbon, meaning that most of the microwave energy is absorbed at the surface of the biomass bed leaving significant part of the biomass bed (fixed bed) at low temperature. It is to be noted here that there are no details about the parameters used for the numerical simulation in Pianroj et al. (2016) work, and it was not mentioned if the simulation was based on constant dielectric properties. The dielectric properties of biomass materials change significantly with temperature during pyrolysis. This change in the dielectric properties can alter the electromagnetic field distribution in the space inside the cavity and within the load. The heating uniformity in the case of a fixed

and unmixed bed cannot be guaranteed when the electromagnetic distribution is altered.

3.6 Discussion and Conclusions on Previous Microwave Pyrolysis Studies

Microwave heating has been considered as a promising technique for providing the energy input to biomass pyrolysis due to its volumetric and selective nature which allows for rapid heating in a cold environment. These features can help to preserve the product quality by limiting the unwanted secondary reactions (Robinson et al., 2015). The following remarks could be made on the previous studies on microwave pyrolysis of biomass material.

- All the published work on microwave pyrolysis of biomass materials is based on lab-scale batch pyrolysis experiments. The majority of the experiments were conducted in modified domestic microwave ovens which provide low powers and limited electric field intensity inside the cavity.
- In the majority of the previous studies, the biomass material was mixed with a microwave susceptor to increase the heating rate and to reach the the pyrolysis temperature. The use of susceptors eliminate the specific benefits of microwave heating which are the selective and volumetric heating. The biomass material is therefore heated by conduction from the surface of the susceptor which is similar to the conventional heating techniques.
- There is, in general, a lack of understanding about the impact of using microwave susceptors on the product yield and quality. There are number of studies which showed that increasing the fraction of the microwave susceptor increases the gas yield at the expense of the liquid yield (Abubakar et al., 2013; Shang et al., 2015) indicating an increase in the secondary cracking reactions.
- There is also a lack of understanding about the impact of the cavity design and the applied electric field intensity on the performance during microwave

heating. The proper design of the microwave heating cavity to provide high electric field intensity can eliminate the need for a microwave susceptor.

- One of the major challenges facing the microwave pyrolysis of biomass is the heating heterogeneity caused by the nature of the standing waves which creates hot- and cold-spots inside the heating cavity. Due to the high loss factor of the char formed during pyrolysis compared to the raw biomass, the heating heterogeneity can lead to thermal runaway in the hot-spots. In single mode cavities, the heating homogeneity can be controlled by processing a small sample size placed at the area of the high electric field intensity. Robinson et al. (2015) showed that for homogeneous heating and to avoid thermal runaway in a single mode cavity operating at 2.45 GHz, the sample needs to be not more than 15 mm. However, such size is too small for large scale processing.
- One of the ways which have been suggested to improve the heating homogeneity during the microwave pyrolysis in multimode cavities is employing an overhead stirrer to mix the biomass material during pyrolysis such as the studies reported by Salema and Ani (2012) and Abubakar et al. (2013). However, these studies are not fundamentally scalable, mainly because they do not provide an approach to control the char deposition in the system for continuous and large-scale processing.
- Apart from the work reported by Robinson et al. (2015), there is a lack in the analysis of the absorbed microwave power during the microwave pyrolysis in oreder to estimte the energy comsumption. This is mainly becasue that most of the studies were run in a modified domestic microwave ovens which do not provide information about the absorbed and reflected power.

Developing a reliable and scalable microwave pyrolysis process would require an understanding of the interactions between biomass materials and microwave energy

over the pyrolysis temperature. It would also require an understanding of the impact of the changes in the dielectric properties during pyrolysis on the process and the cavity design. Any process to be scalable needs to provide a way for controlling the char deposition in the system during processing.

4 EXPERIMENTAL METHODOLOGIES

4.1 Biomass Materials Involved in this Study

Different types of biomass materials were identified as candidates for microwave pyrolysis in this study incuding wheat straw, softwood, hardwood, wood bark, and seaweed. Apart from the seaweed, all the other biomass materials could be classified as lignocellulosic biomass.

Typical fractions of the main constituents of the lignocellulosic biomass materials involved in this study are listed in Table 4-1 which shows that softwood and hardwood have close compositions. Wood bark, in general, has a high lignin fraction (Mohan et al., 2006).

Table 4-1: Typical composition of the lignocellulosic biomass materials involved in this study.

Material	Cellulose [a]	Hemicellulose [a]	Lignin [a]
Softwood [b]	35-40	25-30	27-30
Hardwood [b]	45-50	20-25	20-25
Wood bark [c]	25	15	45
Wheat straw [b]	33-40	20-25	15-20

[a] The compositions are on the dry basis. The remaining fraction is mainly extractives and ash;
[b] (McKendry, 2002); [c] (Valentín et al., 2010)

It can be noted that seaweed is not included in Table 4-1. This is because it does not have a lignocellulosic structure as do the other biomass materials in this study. Seaweeds are usually characterised by their carbohydrates, proteins and lipids content depending on the type of the seaweed as will be discussed later in this section.

These biomass materials chosen for this study were selected mainly because of their abundance, relatively low economic value and suitability for pyrolysis. A brief discussion on the social and economic considerations for using these materials for the production of biofuels and chemicals is presented first.

4.1.1 Wood

Wood is one the oldest fuel sources known to humans. Before the 19th century, wood was the predominant fuel for cooking, heating, and lighting (Guo et al., 2015). Since the emergence of fossil resources, the use of wood as a fuel has declined and its applications were directed more towards construction, furniture, and packaging industries. Wastes from these global industries together with the forestry residues and municipal waste generate large quantities of wood waste. In the UK alone the total amount of wood waste arising was estimated in 2012 at around 4.3 million tonnes per year (DEFRA, 2012). The main markets for these wastes are panelboard industry, animal bedding and biomass for heat and power generation. The price of wood waste, in general, varies depending on its grade and cleanness. The price of the forestry wood used for heating depends on its form (chips, pellets, or logs) and moisture content. A typical price for wood chips with 20 % moisture content is about £150 per tonne (Forest-Fuels, 2016).

Wood is one of the most extensively studied type of biomass materials for pyrolysis due to its ability to produce more consistent and repeatable results compared to the other biomass materials (Gómez-Monedero et al., 2015). The bio-oil yield from wood could be as high as 75 % depending on the type of wood and the processing conditions (Mohan et al., 2006).

In this study two types of wood were used; pine which is a softwood and sycamore which is a hardwood. Both type of wood were provided by Eco-Fuels which is a biomass supplier local to the Nottingham area.

The bark removed from pine was also characterised as part of this study. Wood bark, in general, yields less bio-oil compared to wood mainly because of its high lignin content (Mohan et al., 2006). However, the bark is produced as waste with large quantities in various wood industries. Its poor physical structure makes it not suitable to be used in construction and furniture applications. It represents about 10-22 % of the log volume depending on the tree species and size (Parikka, 2004).

4.1.2 Wheat Straw

Straws are agricultural by-products from cereal crops such as wheat, barley and oats which are planted globally. In the UK alone, around 9 to 10 million tonnes of cereal straw is produced each year of which around 6 to 7 million tonnes comes from the wheat industry (DEFRA, 2015). The main uses of straws include bedding, animal feed, and heat and electricity generation in power stations and combined heat and power (CHP) units. However, there is a surplus of around 19 % in the cereal straws produced in the UK (DEFRA, 2015). This difference between the supply and demand keeps the economic value of the straws low, putting them as potential candidates for biofuels production. The farm price of wheat straw is estimated at around £50 to £60 per tonne (DEFRA, 2013).

Many studies have been published on the pyrolysis of wheat straw. The bio-oil yield from wheat straw, in general, is low compared to the woody biomass due to the high ash content and the lower volatile matter in the wheat straw (Mohan et al., 2006). Bio-oil yields of up to around 50 % have been reported (Henrich et al., 2016).

The wheat straw for the current study was obtained from the University of Nottingham farm in Sutton Bonington. It was harvested in August 2013.

4.1.3 Seaweed

Seaweeds or macroalgae include a wide range of multicellular marine algae found in seas and oceans. They are one of the biomass resources which have been considered as potential candidates for biofuels and chemicals production (Ross et al., 2008; FAO, 2009).

Seaweed was considered in this study because of its unique economic and social advantages. Seaweeds have larger productivity per unit area than terrestrial biomass (Subhadra and Edwards, 2010) with 6 – 8% photosynthesis efficiency compared to only 1.8 – 2.2% for terrestrial biomass (Anastasakis et al., 2011).

Their competition in land and fresh water with other human activities is less compared to terrestrial biomass as they grow in seas and oceans.

There are over 10,000 different kinds of seaweed all over the world (Wang et al., 2013a). However, they are often classified into four groups: blue algae (Cyanophyta), green algae (Chlorophyta), brown algae (Phaeophyta) and red algae (Rhodophyta) (Ross et al., 2008). Seaweeds have a different chemical structure to that of lignocellulosic biomass. They are usually characterised by their carbohydrates, proteins and lipids content depending on the type of the seaweed (Ross et al., 2008). Brown algae, which is the kind of seaweed used in this study, have a high carbohydrates fraction dominated by alginates (10 – 40 %), laminarin (2 – 34 %), mannitol (5 – 25 %) and fucoidan (5 – 20 %) (Ross et al., 2009). Seaweeds have, in general, lower volatile matter and higher ash content than lignocellulosic biomass. The seaweed ash contains high fractions of Ca, K, Na and Mg (Ross et al., 2008; Ross et al., 2009). Seaweeds have also high nitrogen content which is associated with their protein content (Ross et al., 2008).

Many studies have been published on the pyrolysis of seaweed, and bio-oil yields of up to around 40 % to 50 % have been reported (Bae et al., 2011; Ly et al., 2015; Ly et al., 2016).

The type of seaweed used in this study is Laminaria Digitata which is brown algae and it is one of the most abundant types of seaweed in Britain and Ireland (Hardy and Guiry, 2003). The seaweed was supplied by the Cornish Seaweed Company Ltd. It was harvested in Lizard Peninsula, Southern England, in March 2014.

4.2 Materials Characterisation

The aim of the of the experiments described in this section was to study the dielectric properties of the biomass materials involved in this study and link their variations with temperature to the physical and structural changes happening

during pyrolysis. Materials characterisation involved mainly thermogravimetric analysis and dielectric properties measurement.

4.2.1 Sample Preparation for Characterisation

The five biomass materials involved in this study were included in the dielectric and thermogravemitric characterisation. After receiving them from the suppliers, the biomass materials were left open for air drying for at least 48 hours. The sample from the woods were taken by cutting approximately 10 mm-thick cross-section discs after removing the bark. These discs allow for obtaining representative samples for the whole cross-section excluding the bark. For thermogravimetric analysis and dielectric properties measurement, the biomass materials were ground to less than 212 μm in two stages; first, the samples were shredded then pulverised in a disc mill. The aim of using a small particle size was to obtain representative samples that can fit in the 3 mm tube employed for the dielectric properties measurement. Sampling in all the stages after shredding was done using riffle splitters to ensure obtaining representative samples. All the samples were then stored in a fridge below 5 ^{o}C in plastic bags prior to further analysis.

4.2.2 Thermogravimetric Analysis

Thermogravimetric analysis (TGA) is one of the thermal analysis methods used to observe and study the different physical and chemical transformations through the changes in the material's weight with time and temperature. It has been used widely to study the decomposition of biomass and its constituents during pyrolysis (Collard and Blin, 2014). TGA has been also used to perform proximate analysis for biomass materials which involves determining the moisture content, volatile matter, fixed carbon, and the ash content (García et al., 2013).

In this study, thermogravimetric analysis was performed to determine the proximate analysis and to study the decomposition of the biomass materials as a function of temperature during pyrolysis. In both analyses, the sample size was

kept around 10 to 20 g. The TGA apparatus used in the analysis was Q5000 IR manufactured by TA Instruments.

Proximate analysis for the lignocellulosic biomass was performed following García et al. (2013) method which was developed specifically for biomass materials. Figure 4-1 shows the heating profile which was applied. The heating rate was 50 $^{o}C \cdot min^{-1}$ in step 1, 100 $^{o}C \cdot min^{-1}$ in step 3 and 5, and -100 $^{o}C \cdot min^{-1}$ in step 4 (cooling). Nitrogen at 40 $mL \cdot min^{-1}$ was introduced from the start of step 1 until the end of step 4 to act as a sweep gas and to ensure inert atmosphere. At the start of step 5, the gas was switched to air at 40 $mL \cdot min^{-1}$ to burn the fixed carbon and allow for the ash content calculation.

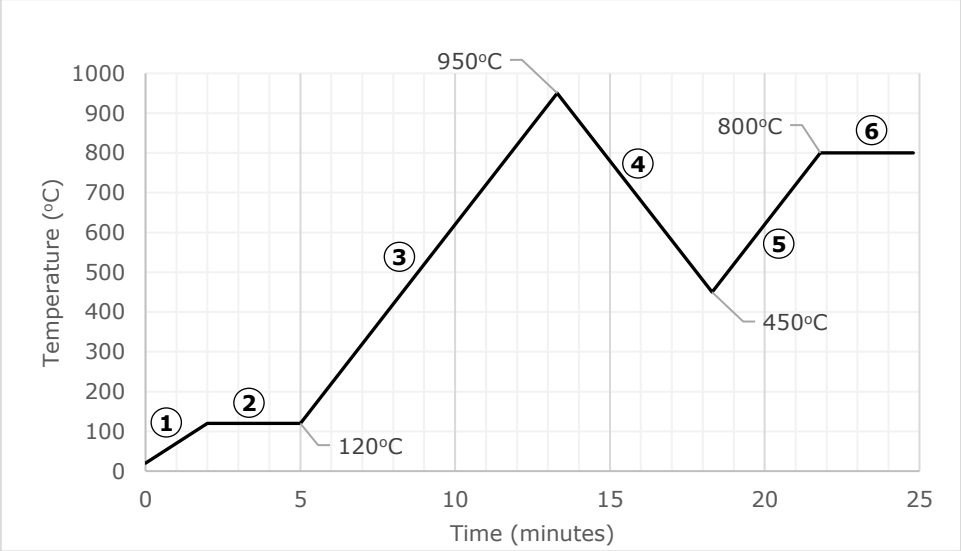

Figure 4-1: Heating profile for the proximate analysis based on the method reported by García et al. (2013).

The mass loss during step 1 and 2 was used to determine the moisture content. The volatile matter was calculated from the weight loss during step (3). The mass left at the end of step 6 was the ash content. The fixed carbon was calculated by difference.

The method reported by García et al. (2013) applies to only the lignocellulosic biomass and not to the seaweed. The reason for this is that seaweeds contain

significant amounts of volatile inorganics which start decomposition at around 600 ^{o}C (Ross et al., 2008; Ross et al., 2009). Therfore, the García et al. (2013) method would give inaccurate estimates of the volatile matter and the ash content as it involves heating the material up to 950 ^{o}C for the volatile matter. Instead, the method reported by Ross et al. (2008) was employed where the volatile matter is determined from the mass loss between 110 ^{o}C and 550 ^{o}C, the fixed carbon is determined by the mass loss after switching to air at 550 ^{o}C, and the remaining mass is the ash content.

The decomposition profile during the pyrolysis of the biomass materials was studied by heating the samples in the TGA from the room temperature up to 600 ^{o}C with a constant heating rate of 10 $^{o}C \cdot min^{-1}$ under an inert atmosphere of nitrogen.

4.2.3 Dielectric Properties Measurement

The most commonly used techniques to measure the dielectric properties of materials over the microwave and RF frequencies were discussed in Section 3.3.3. The advantages and limitations of each of these techniques were discussed. Among the dielectric measuring technique the cavity perturbation technique was highlighted as the most suitable technique for measuring the dielectric properties of biomass materials over the pyrolysis temperature. One the main advantages of the cavity perturbation technique is its high accuracy compared to the other techniques for measuring the dielectric properties of low loss materials such biomass materials (Varadan et al., 1991b; Bois et al., 1999a; Rattanadecho and Makul, 2016). Another advantage is its simplicity regarding sample preparation, and a broad range of sample states and shapes can be measured including powders and granular solids as the case for the biomass materials in the present study. Further, the cavity perturbation technique allows for high-temperature measurements by moving the sample, between the cavity and a furnace as will be described later in this section. The cavity perturbation technique requires relatively small sample leading to small temperature gradient within the sample compared to the other

techniques such as the waveguide and free space transmission techniques which require large sample.

The cavity perturbation technique measures the cavity's resonant frequency and quality factor before and after inserting the sample inside the cavity. The frequency change is then used to calculate the dielectric constant while the change in the cavity's quality factor is used to calculate the loss factor as follows (Nakamura and Furuichi, 1960; Smith et al., 2010):

$$\varepsilon' = 1 + 2\,J_1^2(x_{1,m})\,\frac{(f_0 - f_1)}{f_0}\,\frac{V_c}{V_s} \qquad 4\text{-}1$$

$$\varepsilon'' = J_1^2(x_{1,m})\left(\frac{1}{Q_1} - \frac{1}{Q_0}\right)\frac{V_c}{V_s} \qquad 4\text{-}2$$

Where f_0 and f_1 are the resonant frequencies of the empty and loaded cavity respectively; Q_0 and Q_1 are the quality factors of the empty and loaded cavity respectively; V_c and V_s are the volumes of the cavity and the sample respectively; and $J_1(x_{1,m})$ is the second order of the first kind root of the Bessel function (Smith et al., 2010).

In this study, the dielectric properties of the biomass samples were measured in a coaxial cylindrical cavity employing the cavity perturbation technique. A schematic diagram of the measurement setup is shown in Figure 4-2. The system included a TM_{0n0} cylindrical cavity, a vector network analyser (VNA), a tube furnace, a sample holder connected to a motor, and a computer with software to control the system and record the results.

The cylindrical cavity was designed to support six modes (n from 1 to 6) enabling measurement at frequencies ranging from about 400 MHz to 3 GHz. However, in the present study measurements were taken at only two frequencies: 912 MHz and 2.47 GHz corresponding to TM_{020} and TM_{050} modes respectively. These two frequencies are close to the frequencies allocated for Industrial, Scientific and Medical (ISM) heating applications which are 896 MHz and 2.45 GHz in UK.

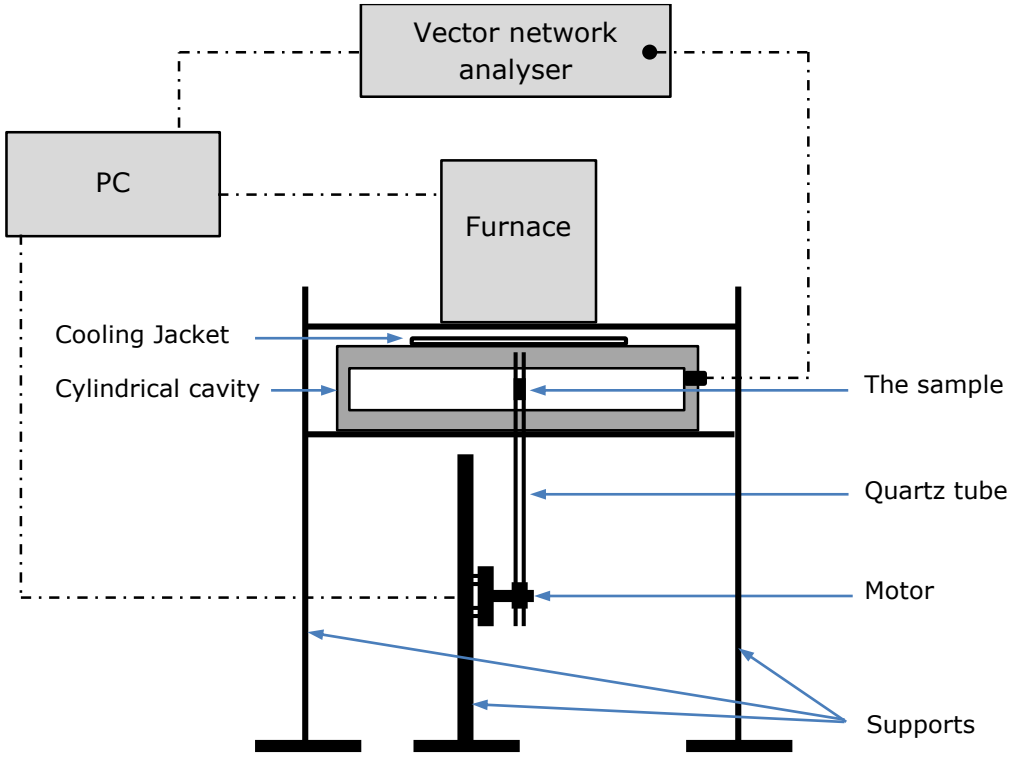

Figure 4-2: A schematic diagram of the dielectric properties measurement facility

A cooling jacket was attached to the top surface of the cavity to absorb any heat coming from the furnace and keep the cavity at the room temperature* during the high-temperature measurements. The role of the VNA (Hewlett Packard 8753C) was to generate and transmit the microwave signals to the cavity and then to measure the resonant frequency and the Q-factor of the cavity.

A 3 mm (ID) quartz tube was used as a sample holder. Quartz was chosen mainly because of its extremely low loss and its high thermal resistance. It has a loss factor less than 0.001 and an operating temperature greater than 1000 ^{o}C. Further, it is transparent to light which allows for controlling and measuring the dimensions of the sample inside the tube. Silica (quartz) wool was used to hold/support the sample inside the quartz tube. During the high temperature measurement, a piece of the silica wool was also placed on top of the sample inside the quartz tube to stop air from flowing to the sample and, therefore, avoid oxygenation reactions

* The temperature in the room where the measurements took place was controlled and set at 20^{o}C.

(combustion). Due to its porous nature, the silica wool allows the vapours formed during pyrolysis to escape from the sample. The positive pressure generated by the vapours within the sample and between the two silica wools (top and bottom), prevents air from entering to the sample during the high temperature measurements.

The quartz tube was connected to a motor which transports the sample between the cavity and the furnace during the high-temperature measurements.

Measurements were taken for the tube with and without the sample, and the differences in the resonance frequency and the Q-factor between the two measurements were then used to calculate the dielectric constant and the loss factor.

4.2.4 Study of the Factors Influencing Dielectric Properties

As discussed in Section 3.3, many factors affect the dielectric properties of materials including the applied frequency, temperature, the material composition and the packing density.

In this study, five different biomass materials were investigated representing different compositions. Typical fractions of the main constituents of the lignocellulosic biomass materials involved in this study are listed in Table 4-1. As mentioned earlier in Section 4.1, seaweed does not have a lignocellulosic structure as do the other biomass materials in this study. Instead, its carbohydrate fraction is dominated by other polysaccharides including alginic acid, laminarin, manntitol and fucoidan. It also has a high ash content compared to the lignocellulosic biomass (Ross et al., 2008).

The effect of the packing density on the dielectric properties of the biomass materials was studied. The importance of studying the density dependency comes from the fact that biomass materials, especially wastes, are found in different forms, and their density varies depending on their shape and size. Wood, for example,

could be found in the form of logs, chips, pellets, shavings, or sawdust. In addition, shape and size of the feedstock for processing are decided based on many factors such as the form at which the material feedstock is available, processing requirements and the economic considerations.

For the dielectric properties measurement, the packing density of the biomass samples was changed by using a metallic rod to press the sample inside the tube and change the volume of a certain mass. This allows for establishing relationships between the dielectric properties of the biomass materials and their packing density. These relationships could be used later to determine the dielectric properties at the processing density.

Temperature is one of the important factors affecting the dielectric properties of materials especially for those materials experiencing physical and chemical transformations during heating. One of the major challenges of the microwave pyrolysis is occurrence of thermal runaway when char starts to form at high temperature as discussed in Section 3.5. It was, therefore, important to study the dielectric properties of the biomass materials over the temperature range of pyrolysis. This would allow for identifying the char formation temperature where the loss factor starts to increase rapidly with temperature, and would help controlling the temperature during microwave pyrolysis to avoid thermal runaway.

Using the setup described in Figure 4-2, the dielectric constant and loss factor of the biomass materials involved in this study were measured starting from room temperature (20 ^{o}C) up to 600 ^{o}C with steps of 20 ^{o}C. The sample temperature was assumed to be the same as the temperature inside the furnace. During each step of the high-temperature measurements, the sample was kept inside the furnace for 10 minutes at the target temperature before taking it down to the cavity for measurement. This 10 minute holding time was to minimise the difference between the sample temperature and the temperature inside the furnace. The dielectric measurements inside the cavity were achieved in less than 10 seconds at each step

of the high-temperature measurements to minimise the difference in the sample temperature between the furnace and cavity positions.

During the high-temperature measurements, a significant shrinkage in the sample volume was observed at the end of each experiment as shown in Figure 4-3. This is due to the decomposition and evaporation of the volatile matter from the biomass material.

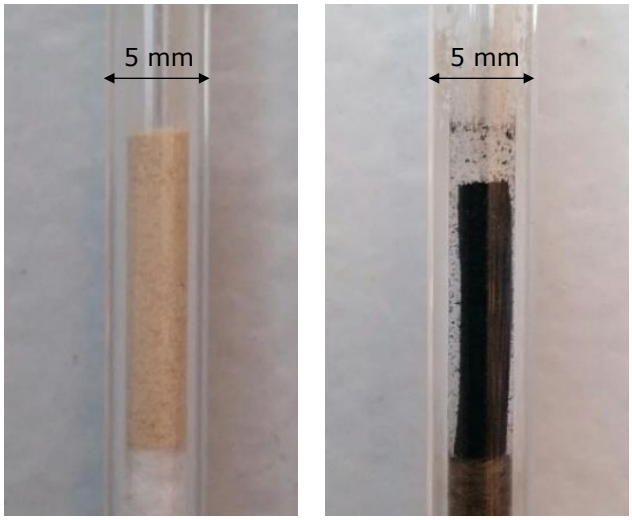

Figure 4-3: Reduction in the sample volume during the high-temperature dielectric measurements. These pictures are for sycamore (a) before heating (b) after heated to 600°C.

The sample volume is a parameter in calculating the dielectric constant and loss factor as shown in Equations 4-1 and 4-2. It was, therefore, necessary to determine the volume of the sample not just at the start of the measurement but also throughout the experiment. A volume-temperature relationship was established for each of the studied biomass material by heating samples of the same initial volume and density to those used in the actual dielectric-temperature measurements in the furnace to different temperatures (20 °C, 100 °C, 200 °C, 300 °C, 400 °C, 500 °C, and 600 °C). The height and diameter of the sample inside the quartz tube were measured at each temperature. The average diameter after each heating step was determined after tacking photos such as that shown in Figure 4-3. The photos were exported to a computer software (ImageJ) which measures the lengths in pixels.

The diameter of the sample at different heights was determined relative to the tube outer diameter which was measured using an electronic digital calliper*.

Figure 4-4 shows the volume reduction as a function of temperature for the five biomass materials. The new volumes were then used to correct the measured dielectric constant and loss factor by substituting in Equation 4-1 and 4-2 as follows:

$$\varepsilon'_{(T)} = 1 + 2\,J_1^2(x_{1,m})\,\frac{(f_0 - f_1)}{f_0}\,\frac{V_c}{V_{s(T)}} \qquad 4\text{-}3$$

$$\varepsilon''_{(T)} = J_1^2(x_{1,m})\left(\frac{1}{Q_1} - \frac{1}{Q_0}\right)\frac{V_c}{V_{s(T)}} \qquad 4\text{-}4$$

Where $\varepsilon'_{(T)}$ and $\varepsilon''_{(T)}$ are the corrected dielectric constant and the loss factor at a temperature, T, and a sample volume, $V_{s(T)}$. Substituting Equation 4-1 and 4-2 into Equation 4-3 and 4-4 leads to the following equations which were used to correct the dielectric constant and the loss factor:

$$\varepsilon'_{(T)} = \left[(\varepsilon' - 1)\frac{V_s}{V_{s(T)}}\right] + 1 \qquad 4\text{-}5$$

$$\varepsilon''_{(T)} = \varepsilon'' \times \frac{V_s}{V_{s(T)}} \qquad 4\text{-}6$$

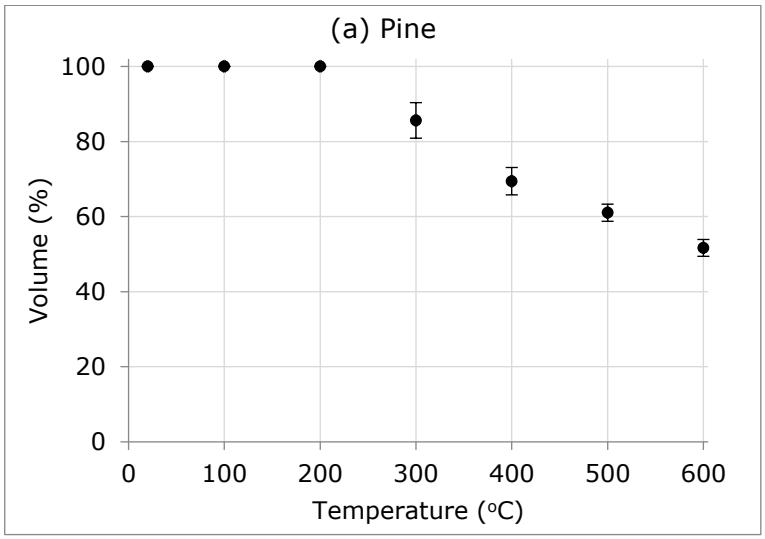

Figure 4-4 (a): Change in the volume of the pine samples with temperature.

* Swiss Precision Instruments (SPI® 13-610-1) which has a resolution of 0.01mm. This calliper was also used to measure the height of the sample from outside the tube before and during the high temperature measurements.

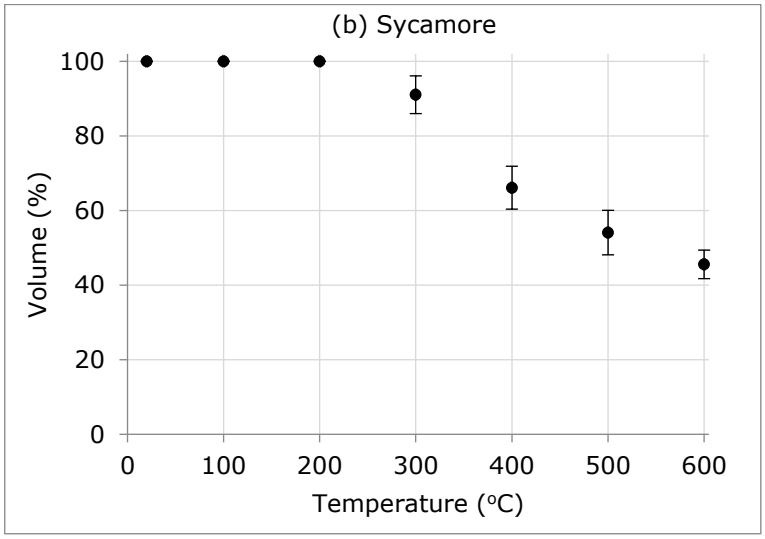

Figure 4-4 (b): Change in the volume of the sycamore samples with temperature.

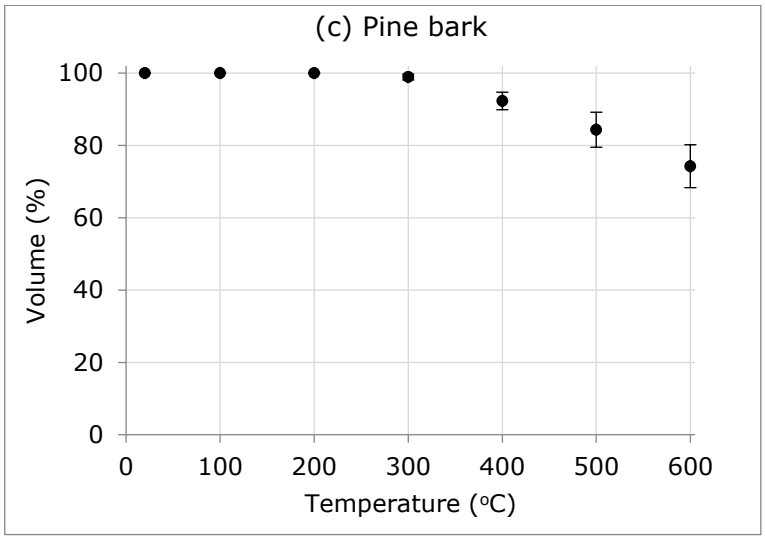

Figure 4-4 (c): Change in the volume of the pine bark samples with temperature.

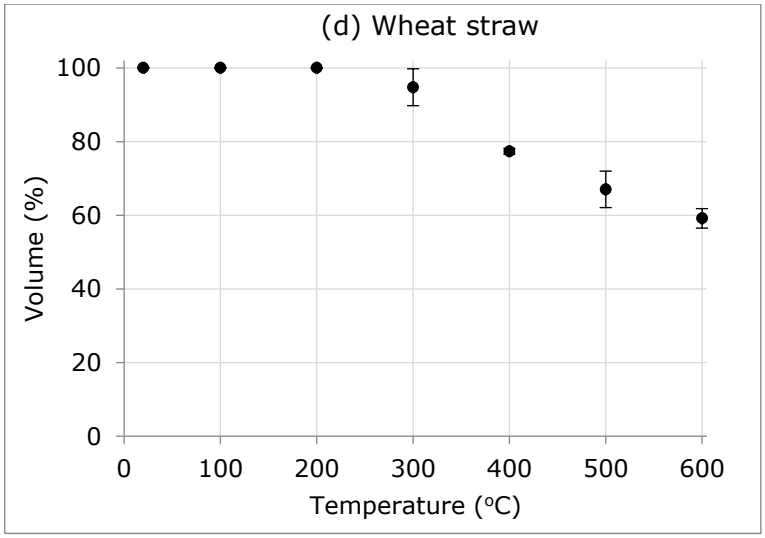

Figure 4-4 (d): Change in the volume of the wheat straw samples with temperature.

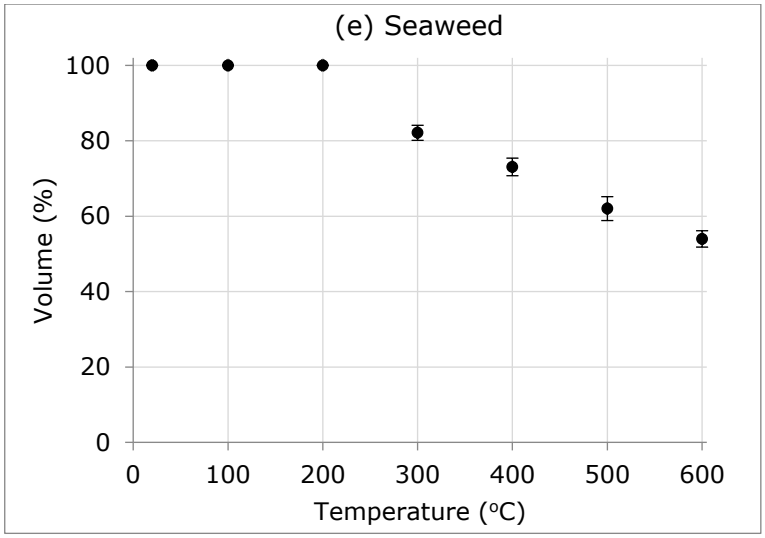

Figure 4-4 (e): Change in the volume of the seaweed samples with temperature.

4.3 Cold Fluidisation Experiments

The aim of the cold fluidisation experiments was to study the fluidisation behaviour of different particle sizes of the biomass materials, and to determine their minimum fluidisation velocity as one of the steps towards designing a microwave-heated fluidised bed process. The justifications for using a fluidised bed system are discussed in Sections 5.5 and 5.6. The steps of the process design are discussed in details in Chapter 6.

The fluidisation behaviour of the different biomass particles was studied in a 5 cm ID fluidised-bed column which was built solely to run the cold fluidisation tests. A schematic diagram of the experimental facility used for the cold fluidisation experiments is shown in Figure 4-5. The column was made of acrylic tube with 5 cm ID and 70 cm height. Acrylic (polyacrylonitrile) was chosed because it is transparent to light which allows for observing the particles behaviour inside the column. It is also easy to machine and has a lightwegiht compared to glass which is another light-transparent material that is commonly used in the design of experimental fluidised bed columns.

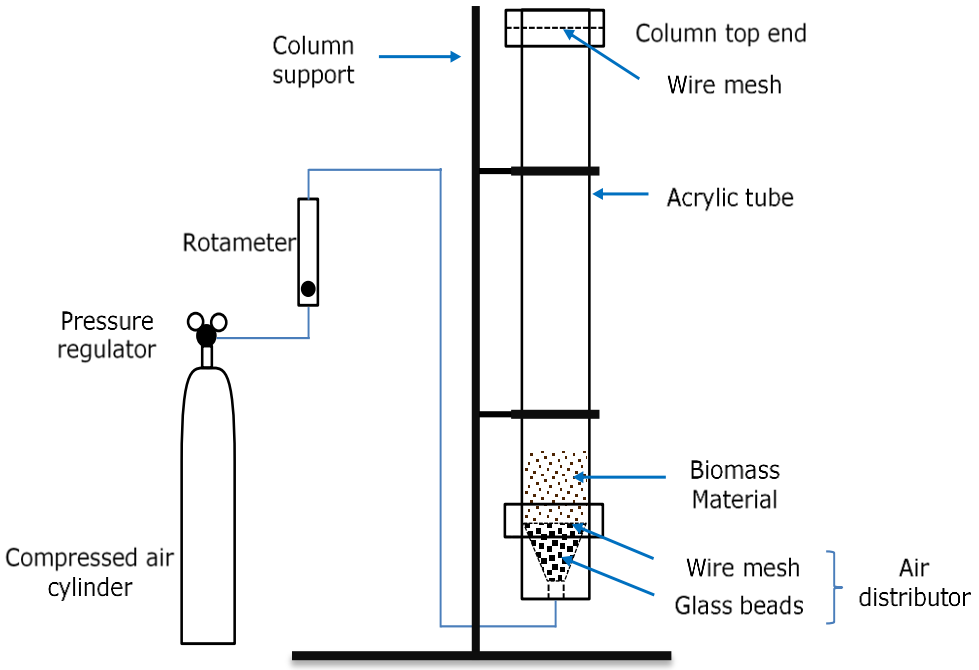

Figure 4-5: A schematic diagram of the fluidisation experiment facility

The choise of the column diameter was in line with many of the previous lab-scale studies on the fluidisation behaviour of biomass material (Reina et al., 2000; Abdullah et al., 2003; Liu et al., 2014). Di Felice and Gibilaro (2004) reported that to avoid a significant wall effect on the fluidisation behaviour and the minimum fludisation velocity, the ratio of the column diameter to the particle size (D/d_p) needs to be greater than 15. The maximum particle size used in the present study was 2.36 mm. Using a column diameter of 5 cm results in a column to particle diameter ratio of 21.2 which is greater than the minimum ratio specified by Di Felice and Gibilaro (2004).

The gas distributor consisted of 2 mm glass beads and a 37 µm wire mesh as shown in Figure 4-5. The pupose of the glass beads was to provide uniform gas distribution across the entire colmn. The wire mesh acted as physical barrier to separate the glass beads from the biomass particles. There was another 37 µm wire mesh at the top of the column as indicated in Figure 4-5 to retain any entrained particles. The minimum particle size used in the experiments was 45 µm which is larger than the

openning size of the wire mesh at both ends of the column. The fluidising gas was supplied to the system by a compressed gas cylinder with a maximum pessure of 200 bar, connected to a pressure regulator to keep the delivary pressure at a constant low value (2 bar). The gas flowrate is controlled by a rotameter as shown in Figure 4-5.

The fluidisation experiments were conducted for pine, sycamore and seaweed of different particle size groups ranging from 45 μm to 2360 μm. Air was used as the fluidising gas. Air has very close density and viscosity to nitrogen which will be later used in the actual pyrolysis experiments. During all the cold fluidisation experiments, the initial bed high was 50 mm.

The biomass materials were crushed in a shredder (Retsch SM 2000). Three different shredder sieve sizes were used to produce enough quantities of each particle size group for the fluidisation experiments. The sieve sizes used in the shredder were 0.75 mm, 2.0 mm, and 4.0 mm. The particles were sieved in wire meshes using an electric sieve shaker. The sieving mesh sizes were 45 μm, 212 μm, 425 μm, 600 μm, 850 μm, 1.18 mm, 1.70 mm, 2.36 mm, and 3.35 mm.

For the theoretical calculations of the minimum fluidisation velocity, the particle densities were determined using the Mercury Porosimetry technique (Micromeritics' AutoPore IV 9500 Series) following the method reported by Mukaida (1981). The mercury porosimetry technique is used, in general, for measuring the pore size distribution of porous materials through the intrusion of mercury, which is a non-wetting liquid, into the pores of the material. The pore size is determined based on the external pressure needed to force the mercury into the pores against the opposing force of the mercury's surface tension. Mukaida (1981) defined the types of density that can be determined from the porosimetry measurement as: (a) the bed bulk density which is determined at low pressure with the mercury surrounding the particle bed without entering the pores between the particles; (b) the particle

density which is determined when the mercury fills the pores between the particle; and (c) the true density when the inner pores on the individual particles are filled at high pressure. The particle density (numbered "b" in the above classification) is the one which is used for calculating the theoretical minimum fluidisation velocity (Mukaida, 1981). The porosimetry experiments in the current study were performed by a technical staff at the Microwave Process Engineering Group at the University of Nottingham. The mercury intrusion results could be found in Appendix B.

The fluidisation behaviour of char particles were also studied. This was an attempt to understand and predict the bed behaviour throughout the pyrolysis process including when char starts to form. The studied char particles were obtained by heating raw biomass particles in an electric furnace at 400 ^{o}C for 30 minutes.

4.4 Energy Requirement for Microwave Pyrolysis in a Fluidised Bed

4.4.1 Differential Scanning Calorimetry (DSC)

As discussed earlier in Section 2.1, the minimum energy required for pyrolysis is called the enthalpy for pyrolysis. It is the sum of the energy required to heat the biomass material up to the pyrolysis reaction temperature and that needed to drive the pyrolysis reaction.

The enthalpy for pyrolysis of the sycamore was determined using Deferential Scanning Calorimetry (DSC). The measurements were made in an SDT-Q600 apparatus which is a simultaneous DSC-TGA device that measures the heat flow and weight change as functions of temperature. The samples were prepared as described in Section 4.2.14.3 and a particle size of 212 – 850 μm was used. Before the analysis, the samples were dried in an electric oven at 105 ^{o}C for one hour. The aim of drying was to produce values of enthalpy for pyrolysis independent of the moisture content. The enthalpy for pyrolysis is commonly reported on a dry basis (Daugaard and Brown, 2003; He et al., 2006; Chen et al., 2014) because the moisture content is a variable when it comes to processing. The enthalpy for heating

and evapotating the moisture content of the biomass material can be added to the enthalpy for pyrolysis later depending on the moisture content of the biomass material. This can be acheived by calculating the sensible enthalpy for heating the water content form the ambient temperature up to 100 °C and the latent heat for evaporation of water, then multiplying the sum by the water fraction in the biomass material.

During the DSC-TGA measurements, the samples were heated from 30 °C to 550 °C at a constant heating rate of 10 °C·min^{-1}. Nitrogen at 100 mL·min^{-1} was used as a purging gas. Samples of approximately 10 mg were used, and three repeats were made. The main outputs from the DSC-TGA measurements were the heat flow and the weight change as a function of temperature. The enthalpy for pyrolysis was calculated by integrating the heat flow curve over the pyrolysis temperature range as follows:

$$Q_{py} = \int_{T_0}^{T_{py}} \frac{H(T)}{dT/dt} dT = \frac{1}{dT/dt} \sum_{T_0}^{T_{py}} H(T).\Delta T \qquad 4\text{-}7$$

Where:

Q_{py} is the specific enthalpy for pyrolysis, J·g^{-1};

T_0 and T_{py} are the starting and final temperature respectively, °C;

$H(T)$ is the specific heat flow to the sample at temperature T, W·g^{-1};

dT/dt is the heating rate which was constant at 10 °C·s^{-1};

The heat flow values were also used to calculate the specific heat capacity, $C_p(T)$, of the biomass material as a function of temperature as follows:

$$C_p(T) = \frac{-H(T)}{dT/dt} \qquad 4\text{-}8$$

4.4.2 Energy Balance and Mathematical Models

The enthalpy for pyrolysis gives the thermodynamic energy required to achieve the pyrolysis without taking into account any heat losses. As the fluidising gas is to be fed to the process at room temperature, there will be a considerable amount of heat loss from the biomass particles to the fluidising gas. Therefore, energy balance calculations were performed to estimate the minimum power density required to achieve the pyrolysis in the fluidised bed system. It should be highlighted here that these energy balance calculations will be useful for understanding the effect of the different parameters such as the particle size, gas velocity and temperature on the energy consumption and the performance of the process in general. This understanding will be used for troubleshooting and adjusting the processing parameters during the experimental investigations as will be shown later.

For the energy balance calculations, several assumptions were made as follows:

- The microwave power is absorbed only by the biomass particles, and the term power density refers to the absorbed microwave power by the biomass particles.
- A homogeneous heating throughout the bed volume, meaning that the power density is constant throughout the bed.
- Spherical biomass particles.
- The particle size is constant during heating. The reduction in the particle weight is accounted for in the specific heat capacity calculated from the DSC measurements which were based on the initial weight.
- The only heat loss is to the fluidising gas, and the heat losses to and through the reactor wall are ignored.
- The temperature around the particles inside the bed is an average of the gas inlet and outlet temperature. The gas is assumed to enter at 20^{o}C and leave at the particle temperature.

The energy balance equation per unit volume can then be written as follows:

$$\int_0^t P_{ab}.dt = \rho_b \int_0^t C_p \frac{dT}{dt}.dt + \int_0^t hS.(T - T_a).dt \qquad 4\text{-}9$$

Where:

P_{ab} is the absorbed microwave power per unit volume, W·m^{-3};

ρ_b is the bed density, g·m^{-3};

C_p the specific heat capacity of the biomass particle, J·g^{-1}·^{o}C $^{-1}$;

h is the particle-to-fluid heat transfer coefficient, W·m^{-2}.^{o}C;

S' is the surface area of the particles per unit volume, m^{2}·m^{-3};

T and T_a are the temperature of the particle and its surrounding fluid respectively at any time (t), ^{o}C.

The left-hand side of Equation 4-9 refers to the absorbed microwave energy. The first term on the right-hand side refers to the increase in the particle's thermal state while the second term accounts for the heat losses to the fluidising gas.

The specific heat capacity, C_p , was determined from the DSC measurements and it accounts for both, the sensible enthalpy and the reaction enthalpy. The convective heat transfer coefficient, h, was estimated using Ayers correlation which is one of the most widely used correlations for studying the heat transfer in fluidised bed processes (Richardson et al., 2002):

$$Nu = \frac{hd_p}{k_f} = 0.054\left(\frac{\rho_f d_p u}{e\mu_f}\right)^{1.28} \qquad 4\text{-}10$$

Where Nu is Nusselt's number; k_f is the conductive heat transfer coefficient of the fluid (W·m^{-1}·K^{-1}); and e is the bed porosity.

To estimate the particle temperature at any time, t, Equation 4-9 was rearranged and solved numerically as follows:

$$m.C_p\frac{(T-T^0)}{\Delta t} = P - h.S'(T^0 - T_a) \qquad 4\text{-}11$$

T and T^0 are the particles temperature at time t and $(t-\Delta t)$ respectively.

The temperature gradient within the particle was also studied. Equation 4-9 and 4-11 assume a constant temperature within the particle. To study the tempearure gradient inside the particle, the particle volume was divided into 20 control volumes (elements); a core and 19 shells with equal thicknesses as explained in Figure 4-6. The temperature within each of these elements is assumed constant.

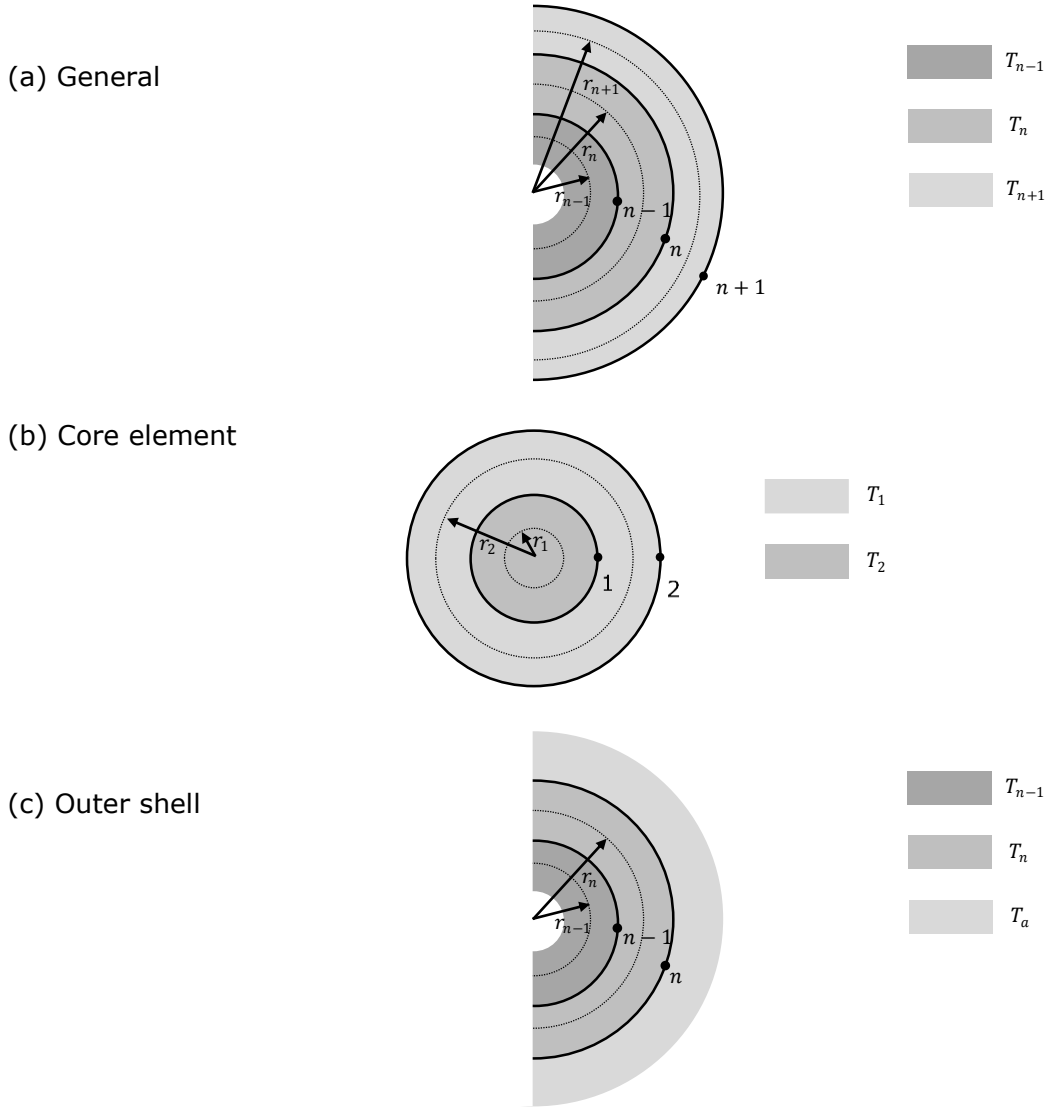

Figure 4-6: Control volumes (elements) used for estimating the temperature gradient within a particle during the microwave pyrolysis in a fluidised bed process.

The heat transfer equations were solved at each element iteratively in both space and time. At each time step, the increase in the element's thermal state is the sum of the absorbed microwave power by the element and the heat transferred from the previous element minus the heat transferred to the next element. Adopting the explicit finite difference method reported by Versteeg and Malalasekera (2007), a general equation for calculating the temperature at each element can be written as follows:

$$T_n = T_n^0 + \frac{\Delta t}{m.C_p}\left[P + \frac{4\pi k(T_n^0 - T_{n-1}^0)}{\frac{1}{r'_n} - \frac{1}{r'_{n-1}}} - \frac{4\pi k(T_{n+1}^0 - T_n^0)}{\frac{1}{r'_{n+1}} - \frac{1}{r'_n}}\right] \qquad 4\text{-}12$$

For the core element:

$$T_1 = T_1^0 + \frac{\Delta t}{m.C_p}\left[P - \frac{4\pi k(T_2^0 - T_1^0)}{\frac{1}{r'_2} - \frac{1}{r'_1}}\right] \qquad 4\text{-}13$$

For the outer shell:

$$T_n = T_n^0 + \frac{\Delta t}{m.C_p}\left[P + \frac{4\pi k(T_n^0 - T_{n-1}^0)}{\frac{1}{r'_n} - \frac{1}{r'_{n-1}}} - h.S(T_n^0 - T_a)\right] \qquad 4\text{-}14$$

Where T_n is the temperature of the n^{th} element and r'_n is the average of the inner and the outer radius of the n^{th} element. Equations 4-12, 4-13 and 4-14 were solved iteratively with time steps of 0.5 ms. The calculations were carried out using Microsoft Excel® 2013 spreadsheets. More details about the derivation of Equations 4-12, 4-13 and 4-14 and their use are discussed in Appendix C.

Sycamore of particle size range 212-850 μm was used as the basis for the design. The justification for using this particle size range is discussed in Section 6.2.3. The corresponding parameters which were used for the energy balance and temperature gradient calculations are listed in Table 4-2.

Table 4-2: Values used in the energy balance and temperature gradient calculations

Parameter	Value
Particles diameter (m)	0.6×10^{-3}
Particle density ($kg\cdot m^{-3}$)	900
Gas (N_2) velocity ($m\cdot s^{-1}$)	0.38
Gas inlet temperature (^oC)	20
Gas density ($kg\cdot m^{-3}$)	1.16[a]
Gas viscosity ($Pa\cdot s$)	1.85×10^{-5} [a]
Bed porosity at the minimum fluidisation	0.73
Bed bulk density at the minimum fluidisation (g/cm^3)	0.24
Specific heat capacity of the gas ($J\cdot kg^{-1}\cdot K^{-1}$)	1000[a]
Thermal conductivity of the gas ($W\cdot m^{-1}\cdot K^{-1}$)	0.026[a]
Thermal conductivity of the particles ($W\cdot m^{-1}\cdot K^{-1}$)	0.155[b]

[a] *Green and Perry (2007);* [b] *Guo et al. (2013)*

4.5 Microwave Pyrolysis Experiments in a Fluidised Bed

4.5.1 Materials

The aim of the experiments described in this section was to operate the microwave fluidised bed process which was developed following the steps discussed in Chapter 6, and run batch pyrolysis experiments to investigate the effect of different processing parameters on the product yield.

The biomass materials involved in the batch pyrolysis experiments were sycamore, pine and seaweed. Different particle size groups were studied. The samples for the pyrolysis experiments were prepared following the same procedure described in Section 4.3. The moisture content of the raw biomass particles was determined by measuring the weight loss after heating around 1 g samples in an electric oven at 105 ^oC for one hour. The moisture content measurement results are listed in Table 4-3.

Table 4-3: Initial moisture content of the biomass materials involved in the batch pyrolysis experiments

Biomass material	Sycamore	Pine	Seaweed
Moisture content (%) [a]	10.6 ± 2.0	11.0 ± 1.4	13.0 ± 2.6

[a] The moisture content was measured for different particle size groups ranging from 0.212 mm to 2.36 mm. At least 10 repeats were made for each biomass material. The average was taken for each material, and the standard uncertainty is indicated.

4.5.2 Experimental Setup

Figure 4-7 shows the experimental setup which was used to operate the developed microwave fluidised bed process. The microwave power was provided by a ~2.45 GHz generator with a maximum incident power of around 5 kW. The microwave power was transmitted to the multimode cavity through standard WR430 waveguides together with H- and E-bends.

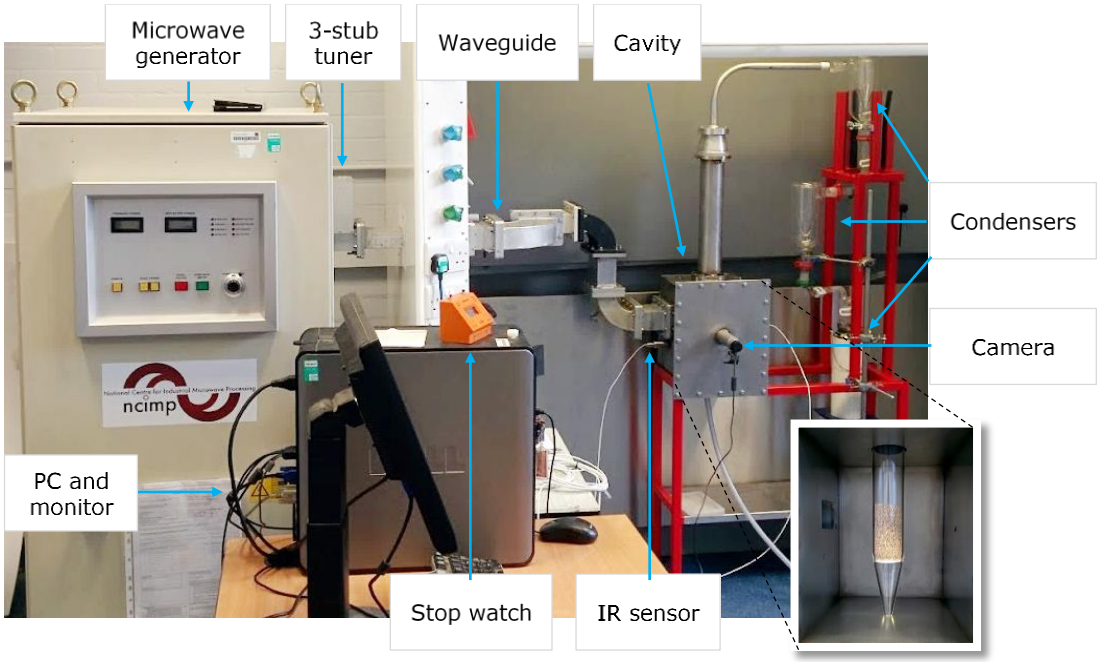

Figure 4-7: The experimental setup for biomass pyrolysis in the developed microwave fluidised bed process.

An automatic three-stub tuner (S-TEAM STHD v1.5) was attached to the waveguide for power analysis and impedance matching. The aim of the impedance matching was to minimise the reflected power. The tuner measures the phase and magnitude of the reflection coefficient as well as the power and frequency and uses these data to adjust the position of the stubs for matching. The automatic tuner was connected to a computer with software to control the tuner and record the results.

The pyrolysis reaction took place in a quartz column which was placed inside the multimode cavity. A sintered quartz disc was attached to the column to act as a gas distributor. Nitrogen, which was used as the fluidising gas, was supplied from a

compressed gas cylinder with a maximum pressure of 230 bar. A pressure regulator was connected to the cylinder to control the delivery pressure (2 bar). The gas flowrate was controlled by a flowmeter which can provide a maximum flowrate of 100 $L \cdot min^{-1}$ (0.85 $m \cdot s^{-1}$ superficial velocity through the bed).

During the pyrolysis experiments, the nitrogen and the evolved vapours exit at the top of the column and pass through a series of condensers as indicated in Figure 4-7 to recover the bio-oil. The condensation system consisted of 3 cold-traps filled with a mixture of water, ice and sodium chloride salt with which a temperature as low as -18 ^{o}C could be reached. The non-condensable gases were allowed to leave the system and extracted by the fumehood.

A camera (Microsoft® LifeCam Studio) was connected to the front cover of the cavity, as shown in Figure 4-7, directed towards the quartz column bed (the spot axis passes 60 mm above the distributor). The aim of using the camera was to monitor and record the process during pyrolysis and to allow for stopping the microwave power immediately in the cases of failure due to electric breakdown or thermal runaway. Both forms of failure are accompanied with light, arcing/plasma in the case of electric breakdown and thermal radiation in the case of thermal runaway.

Two infrared (IR) temperature sensors (Optris® CT LT15) were connected to the walls on either sides of the cavity and directed towards the quartz column. The IR sensors were used to monitor the temperature at the outer wall of the quartz column. It is to be noted here that the temperature readings from the IR sensors was not used in the results analysis. They were just used as a safety feature to stop the process in the case of overheating to avoid melting the reactor.

Before the microwave heating experiments, matching at room temperature (cold matching) was performed to set the stubs at a position to minimise the reflected power. The cold matching was performed using a vector network analyser

(ROHDE&SCHWARZ ZVL). The vector network analyser (VNA) sends signals to the cavity through a port connected to the waveguide, and measures the phase and magnitude of the reflected signal. More details about the cold matching are discussed in Section 7.2.

4.5.3 Pyrolysis Experiments Procedure

During each of the pyrolysis experiments, a weighed quantity of the biomass particles was added to the column. The cavity cover was then replaced, and the condensers were connected. The nitrogen flow was then switched on and allowed to flow for at least 10 seconds before turning on the microwave power to purge/inert the system before heating. The minimum nitrogen flowrate applied during the pyrolysis experiments was 40 $L{\cdot}min^{-1}$ which allowed to reducing the oxygen content inside the column to less than 0.1 % before the start of the heating. More details about the calculations pefrormed to estimate the purging time can be found in Appendix D. The microwave power was then turned on after setting the required power level. A stopwatch was used to measure the heating time. After reaching the required heating time, the microwave power was turned off.

At the end of each experiment, the solid left in the column was collected. All the glassware was then flushed with acetone to recover the bio-oil and any remaining solid particles. The mixture was first passed through a 37 µm wire mesh to filter the solid particles. The filtered solids were left for air drying before being added to the solids collected from the column at the end of the experiment. The total solid collected after the experiment was used to calculate the fraction of solid pyrolysed as follows:

$$Solid\ pyrolysed\ (\%) = \frac{W_i - W_p}{W_i} \times 100\% \qquad 4\text{-}15$$

Where W_i and W_p are the initial and the final weight collected respectively.

After filtering the solids, the pyrolysis oil was recovered by separating the acetone in a rotary vacuum evaporator (Büchi® R-200) at 48 °C for one hour. It is to be

noted here that the collected liquid was not used for calculating the product yield. This is because of the losses through entrainment during processing due to the high fluidising gas velocity and also losses while flushing the glassware with the solvent to recover the condensed liquid. The collected bio-oil was stored in glass vials in a fridge at 5 ^{o}C for further analysis.

4.5.4 Product Characterisation

The quality of the produced bio-oil was investigated by measuring its bulk properties including the density, viscosity, water content and calorific value. The density and viscosity are important flow properties as they affect the pressure drop and, therefore, the pumping costs. The calorific value is a measure of the energy stored in the fuel, and it is determined by the amount of energy released when a certain quantity of the fuel is completely combusted. The water content affects the calorific value and bio-oil is known to have high water content compared to petroleum fuels.

The density of the produced bio-oil was determined by measuring the weight of the sample in a 10 mL graduated cylinder. The viscosity was measured using an automatic viscometer (Brookfield DV-II+Pro) at room temperature (20 ^{o}C) with spinning speed of 50 rpm. The calorific value was measured by a technical staff at the Cleaner Fossil Energy and Carbon Capture Technologies Research Group using an IKA® C5000 Calorimeter.

The water content of the bio-oil was measured using the Dean-Stark method which involves mixing the oil with a water-immiscible solvent such as toluene. The mixture is heated in a glass still where the solvent co-evaporates with the water present in the oil. The solvent and the water are continuously condensed and separated in a trap with the water settling at the bottom of the trap and the solvent returning to the heated container. The Dean-Stark method was originally developed to measure the water content of petroleum oil (Dean and Stark, 1920). Several studies used the Dean-stark technique for measuring the water content of pyrolysis oil (Özbay

et al., 2001; Ateş et al., 2006; Onay, 2007; Cornelissen et al., 2008; Smets et al., 2011).

In the present study, the procedure reported by Smets et al. (2011) was followed. During each measurement, 100 mL toluene was mixed with 10 g bio-oil in a 250 mL beaker. The experiment setup was then assembled as shown in Figure 4-8. The heater was adjusted to give a distillation rate of 2 to 4 drops per second. After 2 hours of distillation, the heater was turned off, and the volume of the water was measured and used to calculate the water content.

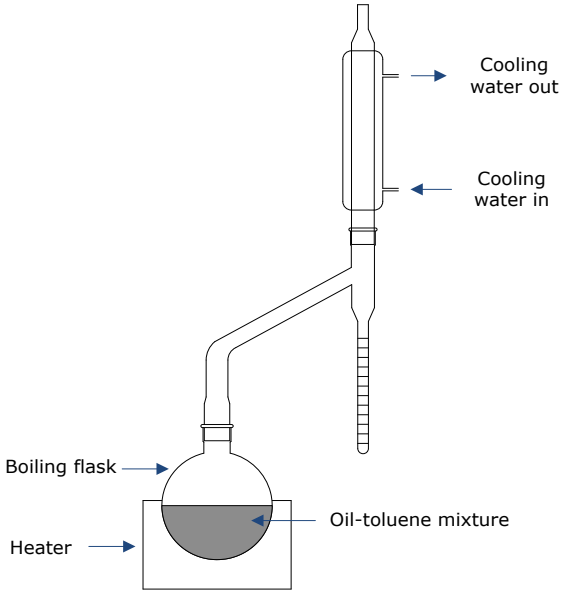

Figure 4-8: Schematic diagram of the Dean-Stark setup for the water content measurement.

4.6 Microwave Pyrolysis in a Liquid System

The aim of the experiments described in this section was to investigate the pyrolysis of biomass particles submerged in a hydrocarbon liquid as a potential alternative to overcome some of the limitations associated with the gas-based systems. These limitations are discussed in Section 7.8.

4.6.1 Materials

The biomass material used for the pyrolysis experiments in the liquid system was sycamore. The samples were prepared by cutting small blocks using an electric saw. More details on the particle sizes used in the pyrolysis experiments will be discussed later in Section**Error! Reference source not found.**

Three hydrocarbon solvents with different boiling points were used including hexane, iso-octane and kerosene. Table 8-1 shows the chemical formula, molecular weight and the boiling point of the three solvents.

Table 4-4: Properties of the hydrocarbon solvents involved in the batch pyrolysis experiments.

	Hexane [a]	Iso-octane [a]	Kerosene [b]
Formula	$CH_3(CH_2)_4CH_3$	$(CH_3)_3CCH_2CH(CH_3)_2$	A mixture of C10-C14 naphthenes, iso- and n-paraffins [c]
Molecular weight	86.18	114.23	
Boiling point (°C)	69	99.3	200 – 250

Source: [a] (Green and Perry, 2007); [b] obtained from the safety data sheet provided by the supplier (AlfaAesar, 2016); [c] (NIOSH, 2014)

4.6.2 Dielectric Properties Measurement of the Solvents

The dielectric properties of the solvents involved in the pyrolysis experiments were measured using the same setup described in Section 4.2.3. The measurement procedure was similar to that described in Section 4.2.3 with some differences in the sample preparation. Around 0.2 mL samples were taken from the solvents using a syringe, and transferred to a 4.0 mm ID quartz tube. The quartz tube was used to hold the samples to be moved between the furnace and the cavity for heating and measurement as illustrated by Figure 4.2 in Section 4.2.3. The measurements were made starting from 20 °C with steps of 10 °C up to just below the boiling point of the solvent. The mass and volume of the sample were measured before and directly after the end of the measurements.

4.6.3 Batch Pyrolysis Experiments in Hydrocarbon Solvents

The experimental setup for the microwave pyrolysis experiments is shown in Figure 4-9. The setup involves heating the biomass material while it is submerged in a hydrocarbon solvent.

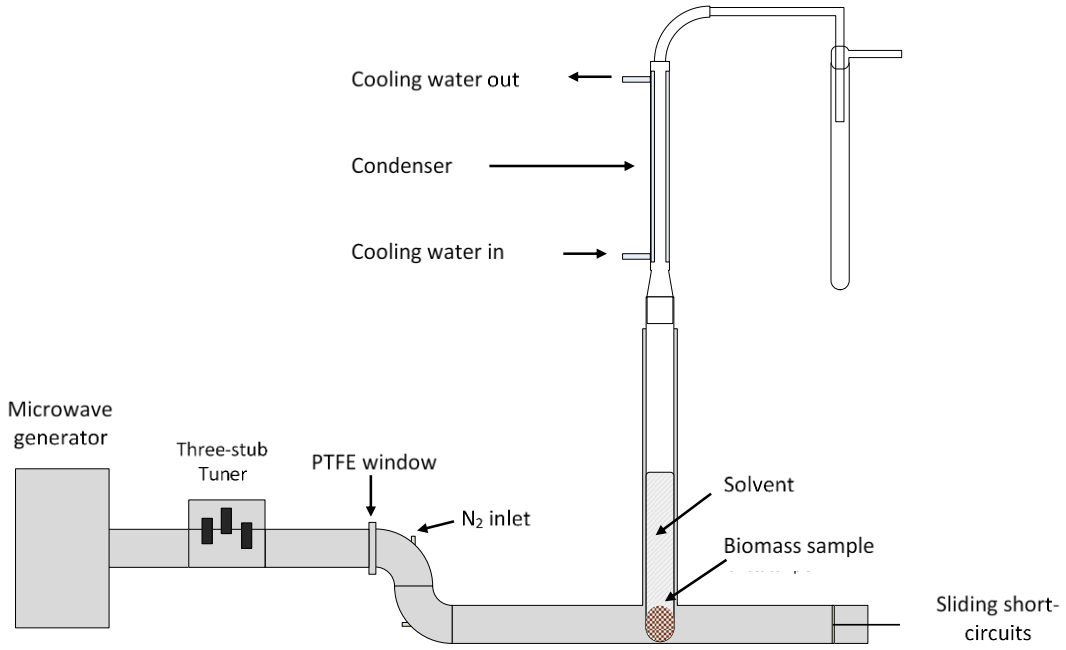

Figure 4-9: Experimental setup for biomass pyrolysis in an inert liquid.

The heating and the pyrolysis reaction took place inside a 3.2 cm borosilicate glass tube (the reactor). The glass tube was placed inside a single-mode cavity surrounded with a 40 cm long metallic tube with an internal diameter of 5.0 cm acting as a choke for the electromagnetic power. The microwave power was supplied by a 2.0 kW generator (~2.45 GHz) and transported to the cavity through WR340 aluminium waveguide together with E-bends as shown in Figure 4-9. An automatic three-stub tuner was attached to the waveguide for power analysis and impedance matching. More details on the role and use of the automatic tuner can be found in Section 4.5.2.

A water-cooled condenser was connected to the top of the reactor for condensing and recycling the evaporated solvent. The non-condensable gases were allowed to leave the system to be extracted by an extraction arm.

During the pyrolysis experiments, the cavity was inerted using nitrogen as a safety feature to avoid fire in cases of failure such as electric breakdown and/or any breaks in the glass tube. A PTFE window is attached to the waveguide as indicated in Figure 4-9 to stop the nitrogen and any vapours from flowing towards the generator.

For each of the pyrolysis experiments, a weighed quantity of the biomass material (5±1 g) was placed in the reactor, and 100 mL of the solvent was added. The condenser was then connected to the reactor and the cooling water was turned on. The nitrogen flow was turned on at 10 $L \cdot min^{-1}$ and allowed to flow for at least one minute before starting the microwave heating. This was to ensure reducing the oxygen content inside the cavity to less than 5 % as explained by the inerting calculations shown in Appendix D. The microwave power was then turned on after setting the required power value. A stopwatch was used to measure the heating time. At the end of the experiment the microwave power was turned off.

After each experiment, the solid left in the reactor was separated from the solvent-oil mixture. The collected solid was first washed with acetone to remove any oil sticking on its surface, then dried in an electric oven at 105 ^{o}C for an hour. The solid was then weighed to calculate the solid pyrolysed using Equation 6.1.

5 MATERIALS CHARACTERISATION

5.1 Introduction

This chapter focuses on the characterisation of selected biomass materials which are considered possible candidates for microwave pyrolysis. The characterisation includes studying the dielectric properties of the biomass materials and their temperature dependencies over the pyrolysis temperature range.

Thermogravimetric Analysis (TGA) was performed to link the variations in the dielectric properties with temperature to the physical and structural changes in the biomass materials during pyrolysis. This was an attempt to identify the char formation temperature for the different biomass materials where the loss factor starts to increase rapidly with temperature. This enables the experimental programme to be designed such that the temperature of the biomass material can be controlled sufficiently well during microwave pyrolysis to avoid thermal runaway.

The knowledge of dielectric properties is also essential for a proper design of the microwave heating cavity which will be discussed in Chapter 6.

5.2 Thermogravimetric Analysis

The experimental methods for the thermogravimetric analysis (TGA) are detailed in Section 4.2.2. Table 5-1 shows the proximate analysis for the biomass materials involved in this study obtained from the TGA analysis. It can be seen that among the studied biomass materials, the woods have the highest volatile matter content. The pine bark has a high carbon content compared to the other biomass materials involved in this study which can be attributed to its high lignin fraction. Lignin has a high carbon content compared to cellulose and hemicellulose (Stefanidis et al., 2014). As can be seen in Table 5-1, seaweed has the highest ash content which reflects the presence of high minerals content in the material. The wheat straw has a higher ash content than the other lignocellulosic biomass, but lower than that of the seaweed.

Table 5-1: Proximate analysis for the studied biomass materials. For each material, four repeats were made and the standard uncertainty is indicated.

Materials	Moisture content [a]	Volatile matter [b]	Fixed carbon [b]	Ash Content [b]
Pine	8.20 ± 0.46	83.22 ± 0.19	15.94 ± 0.25	0.84 ± 0.06
Sycamore	6.40 ± 0.08	86.35 ± 0.36	12.79 ± 0.41	0.86 ± 0.09
Pine Bark	11.32 ± 1.77	67.00 ± 0.43	31.58 ± 0.31	1.42 ± 0.22
Wheat Straw	7.26 ± 0.36	77.12 ± 0.54	16.63 ± 0.31	6.25 ± 0.24
Seaweed	9.30 ± 0.36	50.88 ± 0.19	10.80 ± 0.32	38.31 ± 0.27

All values are weight percentages; [a] wet basis, [b] dry basis.

It can also be seen from Table 5-1 that the pine bark has a moisture content greater than that of wood, eventhough, they were all left for air drying in the same environment. This can be attributed to the high equilibrium moisture content of the bark compared to the wood (Björk and Rasmuson, 1995) meaning that it can keep higher moisture content than wood even when they are both exposed to the same environment. The reason for the lower equilibrium moisture content in the bark compared to wood is the lower degree of crystallisation of the cellulose present in the bark compared to that in the wood leaving more primary sorption sites available for water molecules (Björk and Rasmuson, 1995).

The decomposition of the biomass materials during pyrolysis was studied using thermogravimetric analysis. Figure 5-1 shows the weight loss (TG curve) and derivative weight loss (DTG curve) of the biomass materials involved in this study as functions of temperature from room temperature up to 600 ^{o}C. The weight loss in the biomass materials over the studied temperature range could be divided into three main stages: drying, decomposition/depolymerisation, and char formation. The drying stage is similar for all the biomass materials, and it is represented by the first peak in the DTG curves. It includes the range from room temperature up to 120 ^{o}C.

The char formation (or charring) stage is also similar in all the biomass materials in that there is no significant mass loss as most of the reactions involved are

rearrangement reactions releasing only gases such as H_2, CO, CO_2, and CH_4 (Collard and Blin, 2014). The main difference between the biomass materials in the char formation stage is the starting temperature which is related to the end of the decomposition/depolymerisation stage.

As discussed in Section 2.1, the decomposition of biomass materials can be understood through the depolymerisation of their main building constituents. In the case of lignocellulosic biomass, hemicellulose decomposition starts first at around 220–315 °C while cellulose decomposes in the range 315–400 °C. Lignin decomposes slowly over a wide temperature range starting from 150 °C and continues up to 900 °C (Yang et al., 2007).

Figure 5-1 (a) and (b) show that pine and sycamore have similar decomposition behaviour with most of the mass loss happening in the range between 200 ^{o}C and 400 ^{o}C. This takes place in two stages as can be seen in the DTG curves which show different rates of weight loss before and after 300 ^{o}C. The first stage represents the hemicellulose decomposition while the second stage represents the cellulose decomposition. It can be noted that the rate of weight loss in the second stage for sycamore is greater than that of pine which can be attributed to the relatively high cellulose content in hardwoods compared to softwoods as indicated in Table 4-1. Lignin decomposes over a wide range of temperature including the hemicellulose and cellulose decomposition ranges. The small weight loss between 400 ^{o}C and 450 ^{o}C could be attributed to the decomposition of what left of the lignin.

Wheat straw, as can be seen in Figure 5-1 (d), has a decomposition behaviour close to the woods, and its decomposition/polymerisation happens over a similar temperature range. However, it does not have a clear two-stage decomposition in the range between 200 ^{o}C and 400 ^{o}C as in the pine and sycamore. Also, it has a DTG peak at lower temperature than that of the woody biomass as can be seen in Figure 5-1. This can be regarded to the high minerals content of the wheat straw, such as Na, Mg, Ca and K minerals (Mohan et al., 2006), which is reflected in its

high ash content compared to the woody biomass. The minerals presence is known to have a catalytic effect in cracking biomass constituents leading to decomposition at a lower temperature (Ding et al., 2012).

The decomposition of the pine bark, as can be seen in Figure 5-1 (c), happens more slowly over a wider range of temperature compared to the other lignocellulosic biomass materials. This can be attributed to its high lignin content which dominates its decomposition. However, the two-stage decomposition in the temperature range from 200 ^{o}C to 400 ^{o}C could still be clearly seen representing the depolymerisation of the hemicellulose and cellulose respectively.

The decomposition of seaweed is largely different from that of the other biomass materials in that it happens at a lower range of temperature starting from around 175 ^{o}C, and that it has two separate DTG peaks as shown in Figure 5-1 (e). This can be regarded to two main reasons. The first is that seaweed does not have the same lignocellulosic structure as in the other biomass materials leading to different decomposition behaviour. The first peak in the decomposition region at around 225 ^{o}C corresponds to the depolymerisation of the poly(alginic acid) while the second peak at around 280 ^{o}C represents the depolymerisation of the laminarin and mannitol (Anastasakis et al., 2011). The second reason is the high minerals content of the seaweed which is reflected in its significantly high ash content compared to the other biomass materials as shown in Table 5-1. The minerals content, as mentioned in the case of wheat straw, catalyses the cracking reactions leading to the pyrolysis to happen at lower temperatures. The decomposition of the seaweed continues up to around 320 ^{o}C above which char formation starts taking place with no significant weight loss.

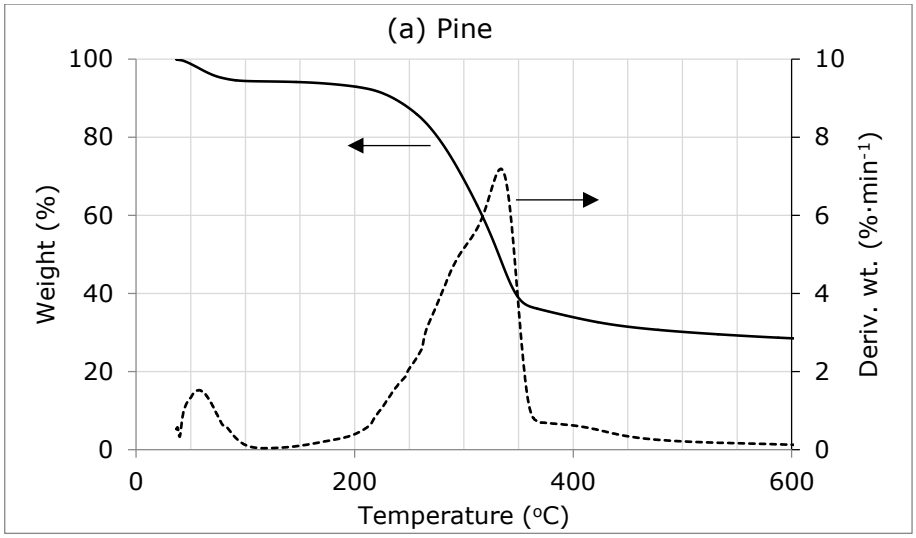

Figure 5-1 (a): Weight loss and derivative weight change during pyrolysis of pine.

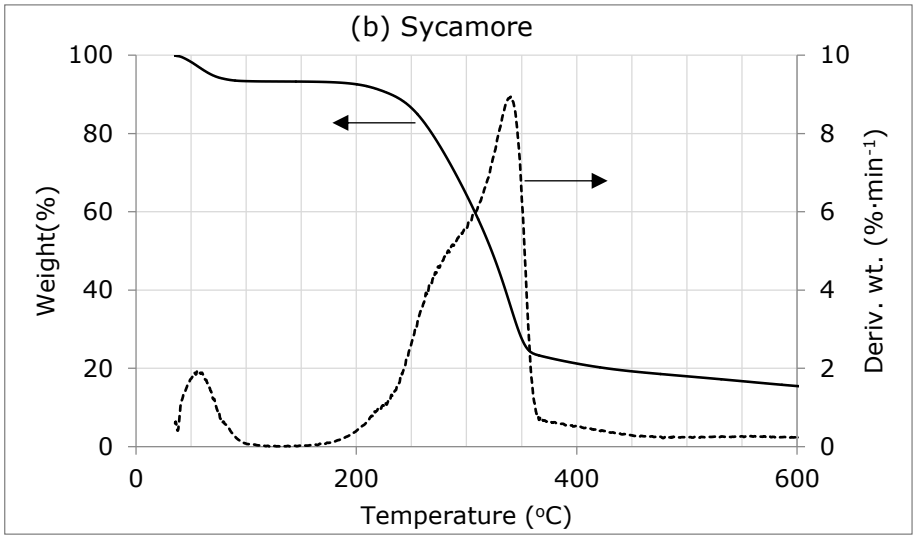

Figure 5-1 (b): Weight loss and derivative weight change during pyrolysis of sycamore.

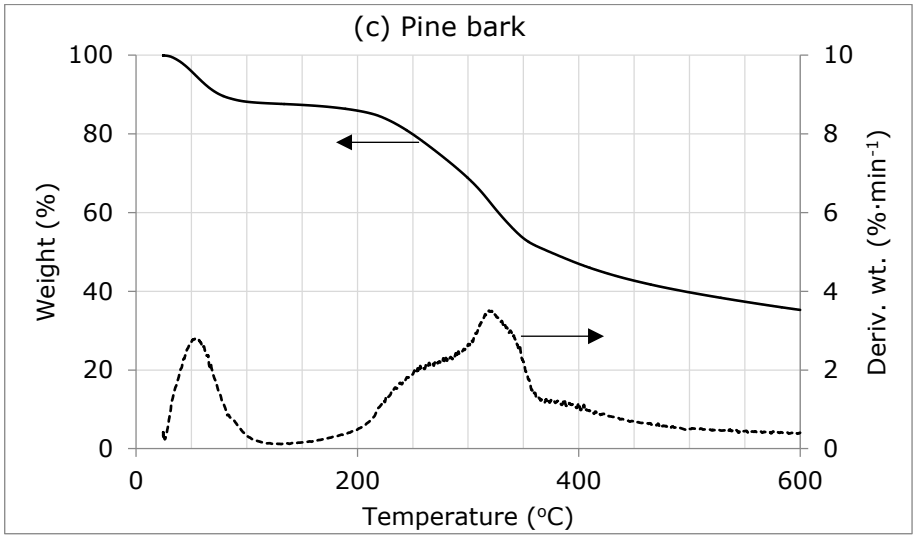

Figure 5-1 (c): Weight loss and derivative weight change during pyrolysis of pine bark.

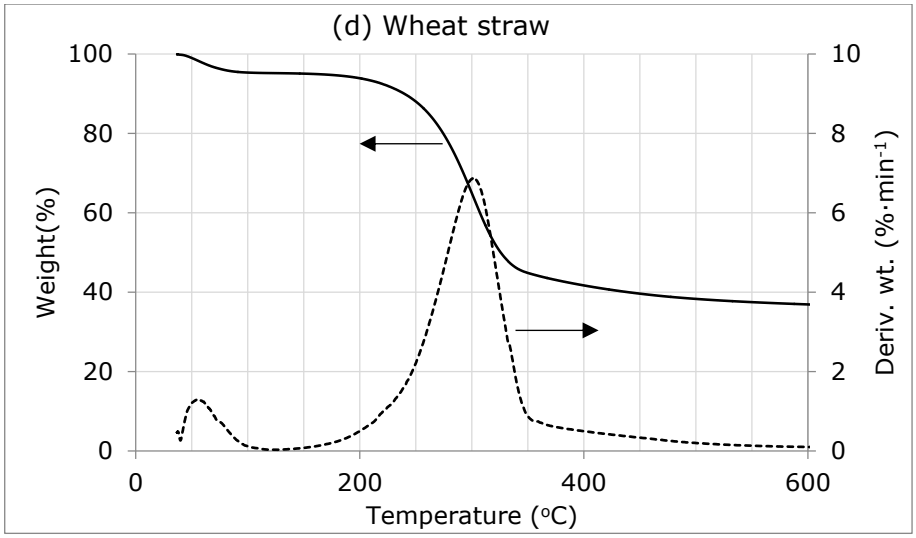

Figure 5-1 (d): Weight loss and derivative weight change during pyrolysis of straw.

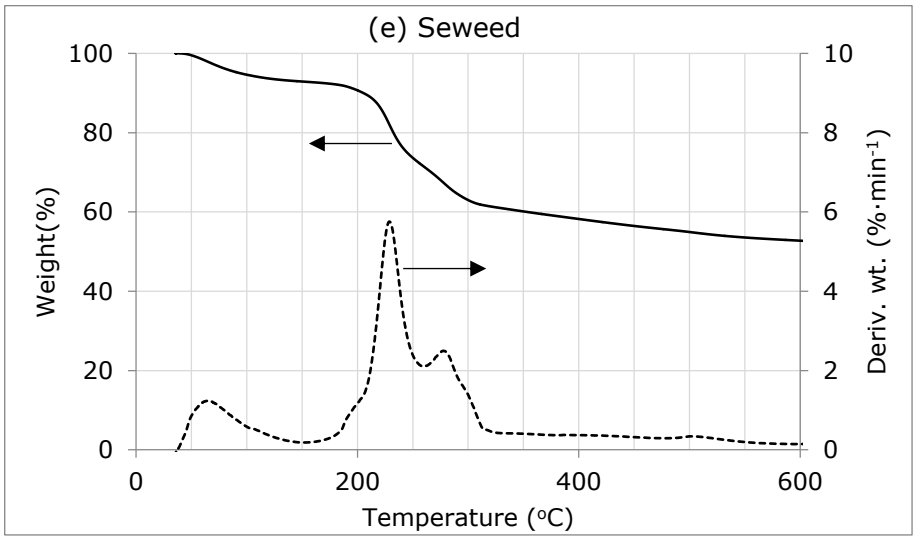

Figure 5-1 (e): Weight loss and derivative weight change during pyrolysis of seaweed.

5.3 Dielectric Properties and their Density Dependency

The experimental methods for the dielectric properties measurement are detailed in Section 4.2.3. Figure 5-2 shows the dielectric constant and loss factor of the biomass materials involved in this study at room temperature, 2.47 GHz frequency, and 0.5 g·cm^{-3} packing density. The same diagram also includes values for other materials obtained from (Meredith, 1998). It can be seen from Figure 5-2 that the studied biomass materials, in general, have a low dielectric loss when compared to materials such as water, alcohols and silicon carbide which are considered good microwave absorbers. However, the biomass materials have dielectric loss much

higher than that of other materials such as alumina ceramic and fused quartz which are considered transparent and therefore used as supports in microwave heating cavities. It is, therefore, possible to selectively heat these biomass materials by applying an appropriate electric field intensity as will be discussed in more details in the next chapter. Among the studied biomass materials, pine bark has the highest dielectric constant and loss factor values which is related to its high moisture content compared to the other biomass materials as shown in Table 5-1.

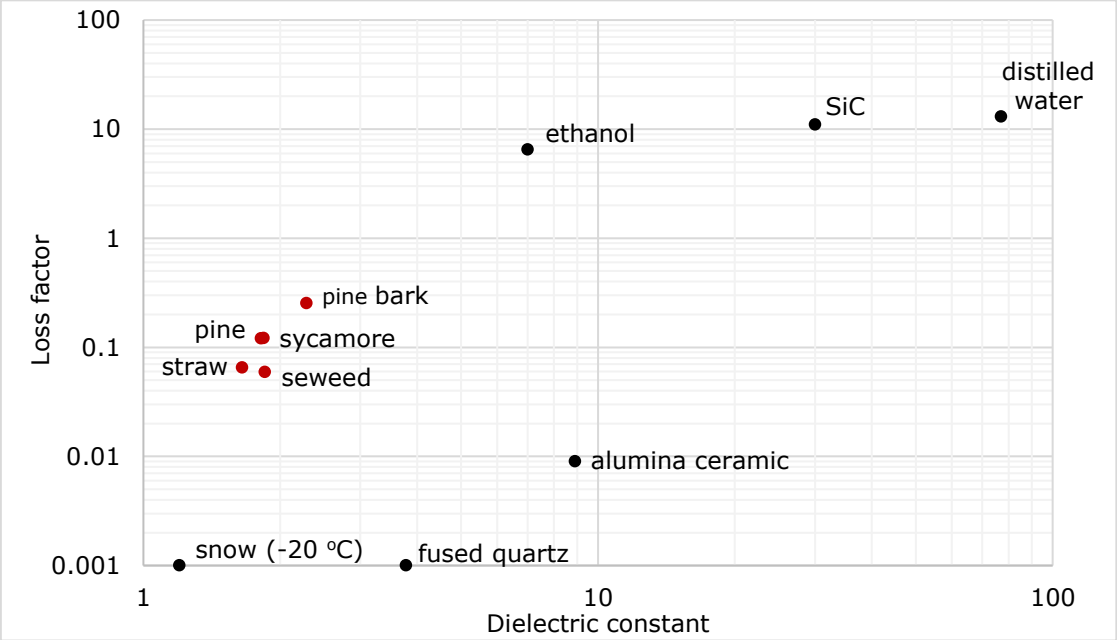

Figure 5-2: Dielectric properties of the studied biomass materials at room temperature, 2.47 GHz frequency, and 0.5 g·cm^{-3} packing density together with other materials which were obtained from (Meredith, 1998). For the measured biomass material, the presented values are the average of four repeats.

Figure 5-3 and Figure 5-4 show the change in the dielectric constant and loss factor respectively with the packing density of the biomass materials involved in this study. It can be seen that both parts of the permittivity could be related to the packing density through quadratic functions with a coefficient of determination, R^2, greater than 99% for all the biomass materials indicating strong correlations. The correlations, which are listed in Figure 5-3 and Figure 5-4, were obtained after imposing the constraints that the dielectric constant and loss factor curves must

intercept the y-axis at 1 and 0 respectively which are the corresponding values for the free space or at zero packing density.

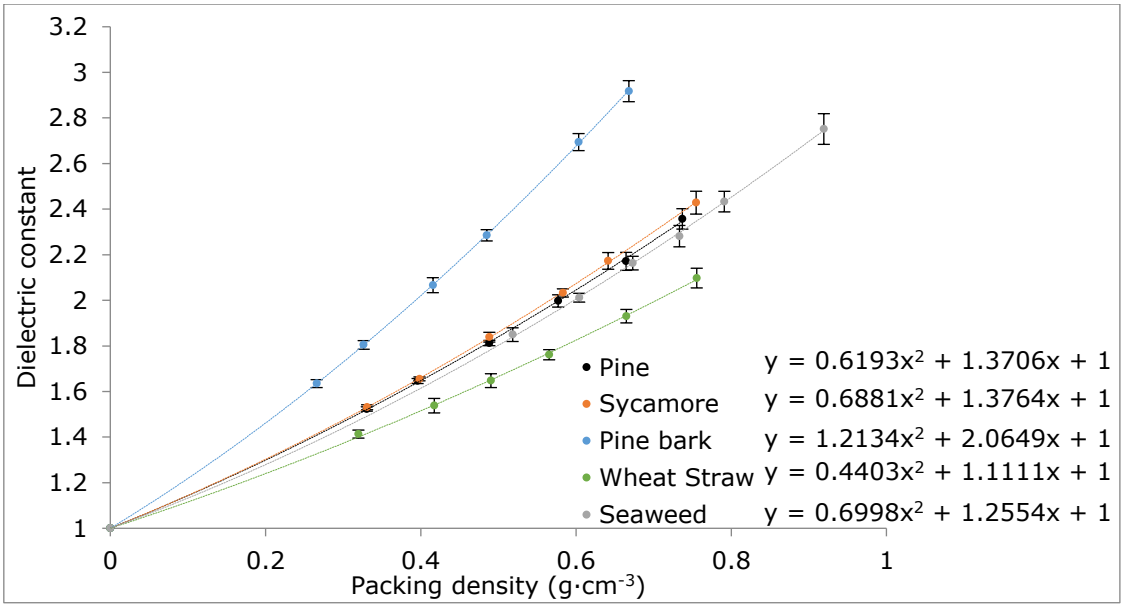

Figure 5-3: Dielectric constant of different biomass materials as a function of the packing density at 2.47 GHz. In the quadratic functions, x and y refer to the packing density in g·cm^{-3} and the dielectric constant respectively. The results are based on four repeats and the error bars reflect the standard uncertainty.

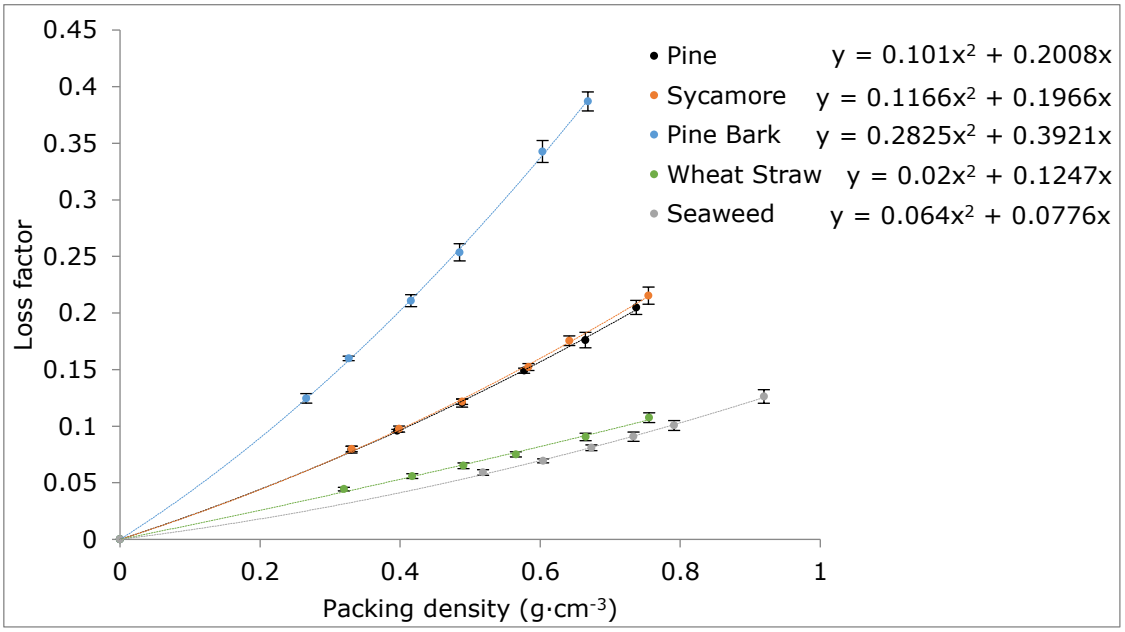

Figure 5-4: The loss factor of different biomass materials as a function of the packing density at 2.47 GHz. In the quadratic functions, x and y refer to the packing density in g·cm^{-3} and the loss factor respectively. The results are based on four repeats and the error bars reflect the standard uncertainty.

Many authors previously suggested using dielectric mixing models for studying the relationship between the permittivity and the packing density (Nelson, 2005; Nelson and Trabelsi, 2012; Tuhkala et al., 2013; Katrib et al., 2015). Dielectric mixing models are used, in general, to estimate the effective permittivity of a mixture of more than one component. Porous and granular materials can be considered as binary mixtures of air and a solid material, and their effective permittivity could then be determined by substituting the permittivity of air with $1 - 0j$.

Among the available dielectric mixing models, the Complex Refractive Index (CRI) model and Looyenga model are the most popular models, and they have been previously found to give a good dielectric-density representation for biomass type materials (Nelson and Trabelsi, 2012). Both, CRI and Looyenga, are based on the power-low approximation which averages the permittivity by the components volume fraction (Sihvola, 1999). They can be written as follows:

CRI:
$$(\varepsilon)^{\frac{1}{2}} = v_1(\varepsilon_1)^{\frac{1}{2}} + v_2(\varepsilon_2)^{\frac{1}{2}} \quad \text{5-1}$$

Looyenga:
$$(\varepsilon)^{\frac{1}{3}} = v_1(\varepsilon_1)^{\frac{1}{3}} + v_2(\varepsilon_2)^{\frac{1}{3}} \quad \text{5-2}$$

Where ε is the effective permittivity of the mixture, ε_1 and ε_2 are the permittivity of the individual components, and v_1 and v_2 are the volume fractions of the individual components.

The CRI and Looyenga models were used to estimate the permittivity of the biomass materials involved in this study at their solid density using the experimental data of the dielectric properties at different packing densities. This was achieved by substituting the air permittivity with $\varepsilon_1 = 1 + 0j$ and rearranging. Equations 5-1 and 5-2 could then be written as:

CRI:
$$\varepsilon_2 = \left(\frac{\varepsilon^{\frac{1}{2}} + v_2 - 1}{v_2} \right)^2 \quad \text{5-3}$$

Looyenga:

$$\varepsilon_2 = \left(\frac{\varepsilon^{\frac{1}{3}} + v_2 - 1}{v_2} \right)^3 \qquad 5\text{-}4$$

Equation 5-3 and 5-4 were used to estimate the dielectric constant (the real part) and loss factor (negative of the imaginary part) of the biomass materials at their solid density. The solid density of the biomass particles was determined using in a helium pycnometer (Micromeritics AccuPyc 1330). The pycnommeter employes the gas displacement technique which consists of two calibrated chambers of known volumes connected with a valve pathway. The sample is placed in one of the chamber where the pressure of the gas (helium) is increased to a maximum value (19.5 psig) keeping the pathway valve closed. The solid volume is then calculated from the pressure difference when the valve is opened allowing the gas to expand into the second chamber. The preperation and sampling of the biomass materials for the helium pycnometer was the same as discribed in Section 4.2.1. Approximately 1.0 g biomass was placed in the measuement chamber each run.

Table 5-2 shows the solid density obtained using the heluim pecnometer together with the dielectric constant and the loss factor at the solid density estimated using the CRI model, Looyenga model, and the quadratic functions obtained in Figure 5-3 and Figure 5-4.

Table 5-2: dielectric constant and loss factor of various biomass materials at their solid density, room temperature, and 2.47 GHz frequency estimated using different models.

Material	Solid density ($g \cdot cm^{-3}$)[a]	CRI				Looyenga				Quadratic function	
		ε'	u_r[b]	ε''	u_r[b]	ε'	u_r[b]	ε''	u_r[b]	ε'	ε''
Pine	1.53	4.37	0.02	0.04	1.50	4.80	0.03	0.73	0.07	4.55	0.54
Sycamore	1.51	4.41	0.03	0.03	1.31	4.85	0.03	0.73	0.06	4.65	0.56
Pine bark	1.60	7.20	0.03	0.04	1.46	8.54	0.04	2.10	0.09	7.41	1.35
Straw	1.82	4.26	0.04	0.08	2.98	4.71	0.05	0.49	0.11	4.48	0.29
seaweed	1.73	4.89	0.03	0.05	1.83	5.38	0.04	0.38	0.06	5.27	0.33

[a] Average of four measurements and the uncertainty was less than 0.06 $g \cdot cm^{-3}$ for all the samples.

[b] u_r is the relative standard uncertainty which was calculated by dividing the standard uncertainty by the average value as explained in Appendix E.

It can be seen from Table 5-2 that the CRI model gives closer results to those obtained using the quadratic functions compared to Looyenga model. Table 5-2 also shows that the dielectric constant and the loss factor at the solid density are estimated with lower relative uncertainty using the CRI model compared to the Looyenga model which suggests that the CRI model represents the dielectric-density relationship for the biomass materials better than the Looyenga model.

5.4 Dielectric Properties Variation with Temperature

The dielectric properties of the biomass materials were studied against temperature from 20 °C and up to 600 °C with steps of 20 °C. Figure 5-5 shows both the dielectric constant and the loss factor as functions of temperature at 2.47 GHz frequency with initial moisture contents as listed in Table 5-1. It can be seen from Figure 5-5 that the loss factor of biomass materials varied considerably with temperature with up to two orders of magnitude. These variations are caused by the physical and chemical changes during the pyrolysis and could be linked to the thermogravimetric behaviour of these materials as shown in Figure 5-1. As in the thermogravimetric analysis, the dielectric-temperature behaviour of the biomass materials in the studied range could be divided into three main stages: drying, decomposition and char formation.

The dielectric behaviour of the biomass materials during the drying stage, which covers the range from room temperature up to 120 °C, is influenced to a large extent by the moisture content. As can be seen in Figure 5-5 the loss factor of the biomass materials increases initially with temperature and reaches a peak at around 60 °C before it drops down. This contradicts the normal dielectric behaviour of free water in which the loss factor at this range of frequency (lower than the relaxation frequency) decreases continuously with temperature as discussed in Section 3.3.2. This behaviour suggests that most of the moisture content of the biomass materials is a physically bound water.

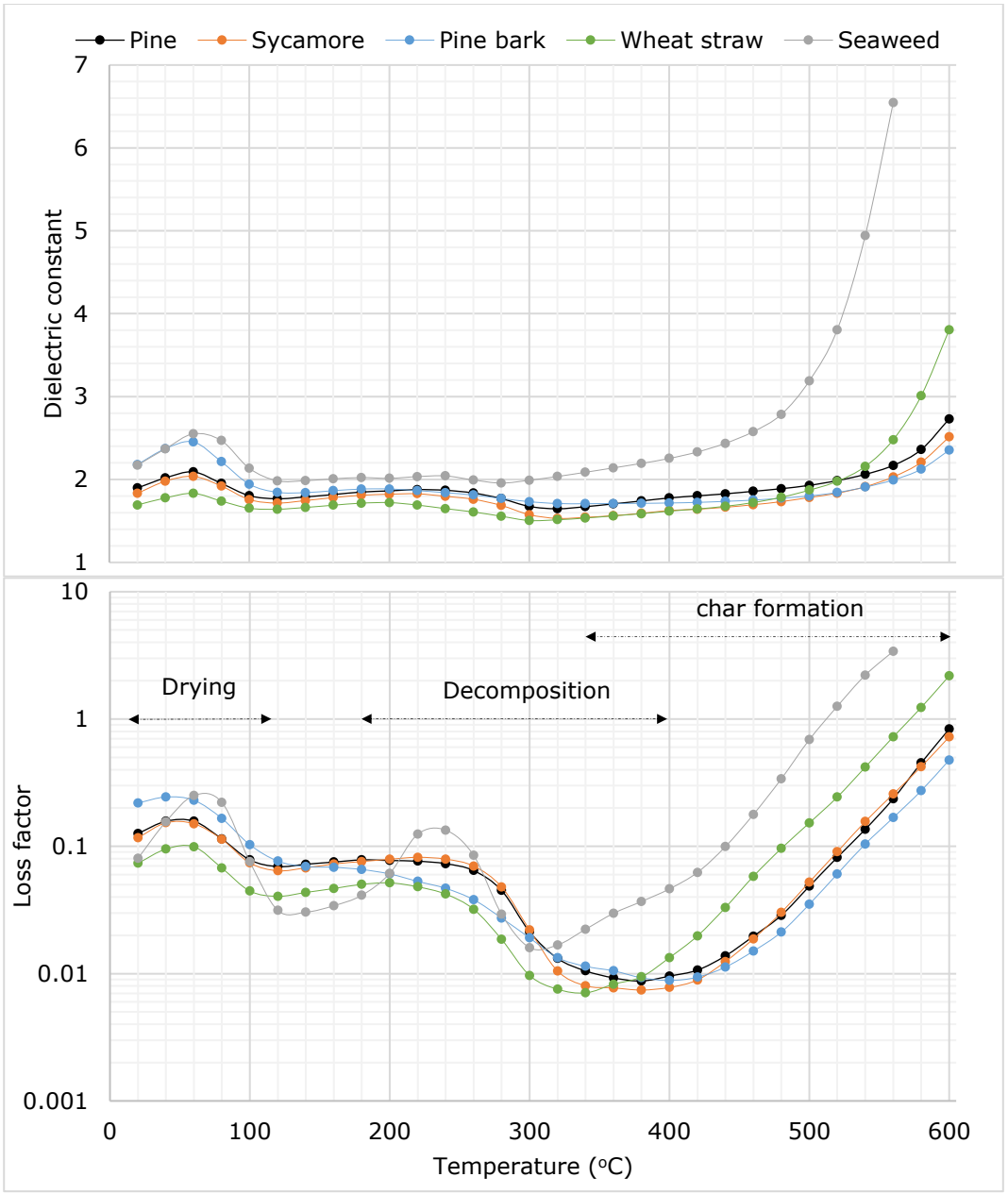

Figure 5-5: Variations in the dielectric constant and the loss factor of the different biomass materials with temperature at 2.47 GHz and 0.5 g·cm^{-3} initial packing density. The values of the initial moisture content are listed in Table 5-1. These results are average of four repeats. The standard uncertainty at temperature ≤400 °C is less than 0.2 and 0.02 for ε' and ε'' respectively, and less than 0.35 and 0.032 for ε' and ε'' respectively above 400 °C.

As discussed in Section 3.3.2, bound water has less ability to polarise and rotate under the alternating electric field compared to free water because of the binding forces between the water molecules and the solid surface. This leads to a lower dielectric constant and loss factor for the bound water compared to free water (Metaxas and Meredith, 1983; Bergo et al., 2012). The initial increase in the loss factor with temperature up to 60 °C can, therefore, be explained by that increasing

the temperature reduces the binding forces of the water molecules allowing them to rotate more freely resulting in an increase in their loss factor.

The reduction in the loss factor between 60 °C and 120 °C could then be due to the fact that enough water molecules have been freed to dominate the dielectric behaviour, and therefore, the loss factor decreases with temperature following the usual behaviour of the free water. The moisture evaporation in this range also contributes towards the reduction in the loss factor with temperature above 60 °C.

As shown in Figure 5-5, the loss factor for seaweed increases with a higher rate of change with temperature between 20 °C to 60 °C compared to the other biomass materials, and also decreases with a higher rate between 60 °C and 120 °C. These higher rates of change can be attributed to the high minerals content of seaweed which is reflected in its high ash content compared to the other biomass materials as shown in Table 5-1. The seaweed ash contains high fractions of Ca, K, Na and Mg which exist as salts of alginic acid (Ross et al., 2008; Ross et al., 2009) in addition to the solid salt deposited from the seawater on the surface of the seaweed blade. The hypothesis is that when the physically bound water molecules are freed as a result of the heating, part of the mineral ions starts to dissolve in these water molecules increasing its ionic conduction, and therefore, the overall loss factor. It is to be highlighted here that an aqueous solution of a mineral salt has a higher loss factor than that of both distilled water and the solid salt separately (Meredith, 1998). This hypothesis can be examined by looking at the dielectric-temperature behaviour at different frequencies. Figure 5-6 shows the dielectric loss of the studied biomass materials as a function of temperature at two different frequencies. It can be seen that the loss factor of the seaweed at 912 MHz frequency at around 60 °C is higher than that at 2.47 GHz which suggests that the more dominant loss mechanism at this point is the ionic conduction. This is not the case for the other biomass materials where the loss factor at 2.47 GHz is slightly higher than that of

912 MHz suggesting that the dominant loss mechanism is the dipolar loss which is associated with polar liquids, water in the present case.

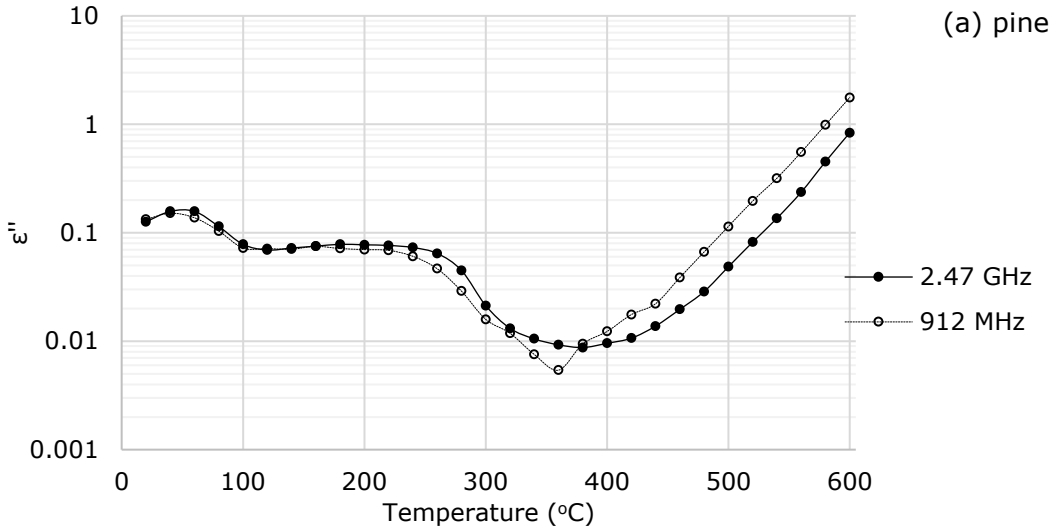

Figure 5-6 (a): Variations in the loss factor of pine with temperature

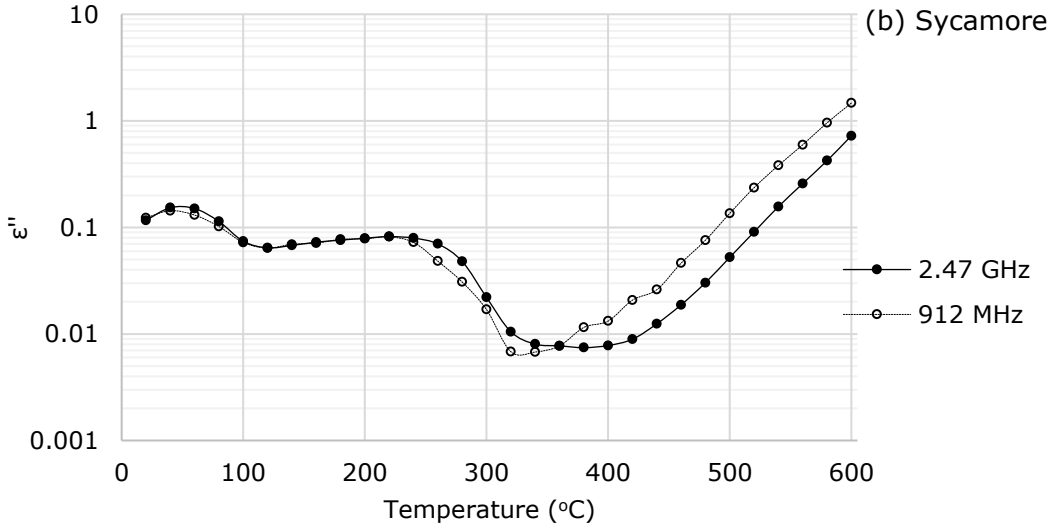

Figure 5-6 (b): Variations in the loss factor of sycamore with temperature

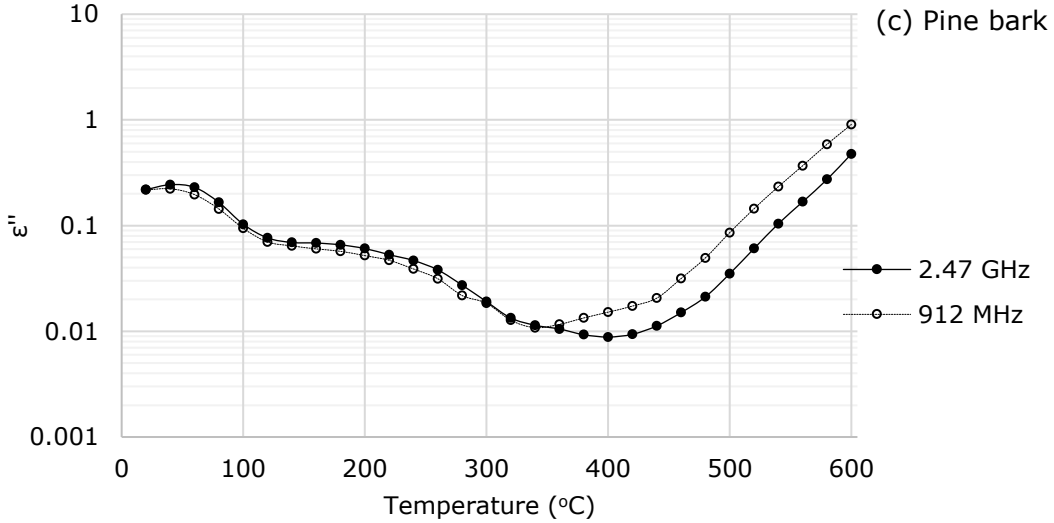

Figure 5-6 (c): Variations in the loss factor of pine bark with temperature

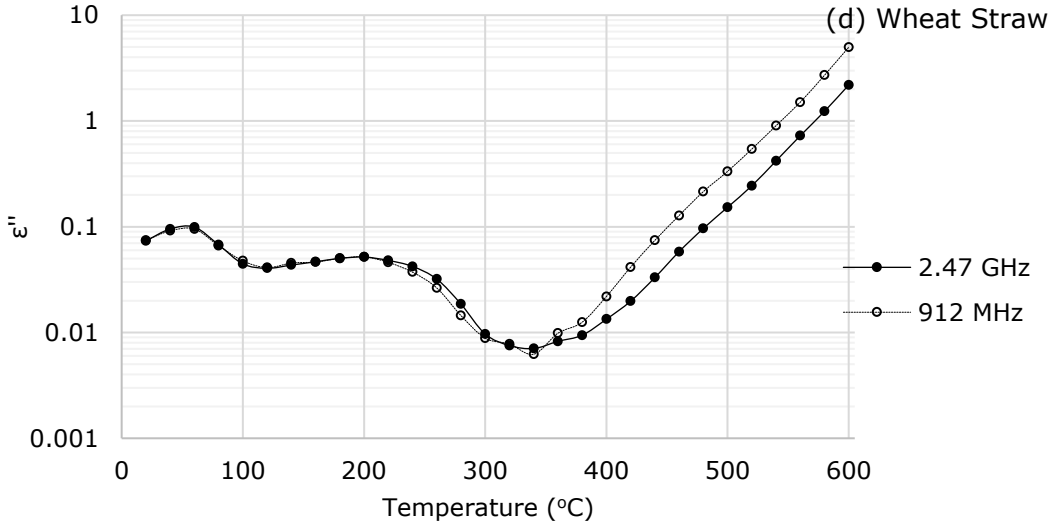

Figure 5-6 (d): Variations in the loss factor of wheat straw with temperature

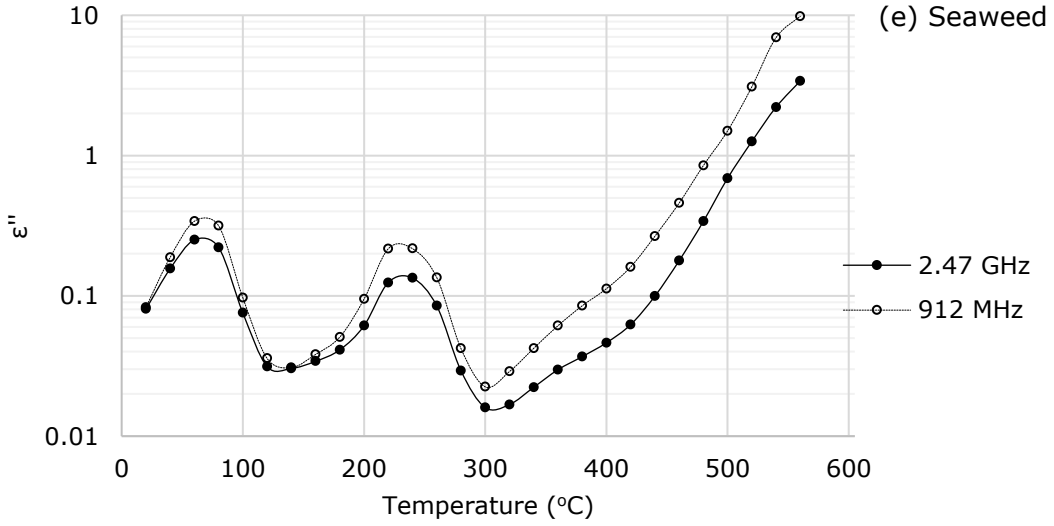

Figure 5-6 (e): Variations in the loss factor of seaweed with temperature. The initial packing density of all the biomass materials was 0.5 g·cm^{-3}. The values of the initial moisture content are listed in Table 5-1.

Apart from seaweed, there is no significant change in either the dielectric constant or the loss factor of the studied biomass materials in the range between 120 °C and 220 °C. The dielectric-temperature behaviour of the biomass materials during the decomposition and char formation stages varies depending on their decomposition behaviours. The pine and sycamore have similar behaviour over these stages. Both of them show a drop in the loss factor starting from 220 °C up to around 380 °C due to the depolymerisation and devolatilisation of the major biomass constituents. This can be linked to the large weight loss over this range as shown in Figure 5-1. Starting from around 400 °C, the loss factor of pine and sycamore starts to increase steadily with temperature which is an indication of entering the char formation stage. The loss factor at 912 MHz during the char formation stage is greater than that at 2.47 GHz as shown in Figure 5-6 which suggests that the dominant loss mechanism during this stage is the conductive loss.

Wheat straw has a close dielectric-temperature behaviour to that of pine and sycamore. However, the transformations happen earlier in the case of wheat straw as can be seen in Figure 5-5. The transformations in the case of pine bark after the drying stage happen with slower rate of change and over a wider temperature range with the char formation stage starting at higher temperature compared to the other biomass materials as can be seen in Figure 5-5.

The dielectric-temperature behaviour of the seaweed was found to be significantly different from that of the lignocellulosic biomass. Unlike the other biomass materials, the loss factor of the seaweed increases again after the end of the drying stage starting from around 140 °C reaching a peak at around 240 °C. This increase in the loss factor at this temperature can be potentially explained by that some ions from the minerals content of the seaweed are dissolved in the decomposition products, including pyrolysis water from dehydration reactions, in their liquid state before evaporation. Again, this hypothesis can be supported by the dielectric behaviour at different frequencies as displayed in Figure 5-6(e) which shows that

the loss factor at 912 MHz over this range is higher than that at 2.47 GHz. Above 240 °C the loss factor of the seaweed drops again due to the evaporation of the decomposition products. The char formation stage for seaweed starts earlier than the other biomass materials at around 300 °C. As displayed in Figure 5-6(e) during the charring stage, the loss factor at 912 MHz is higher than that at 2.47 GHz.

5.5 Processing Options for Microwave Pyrolysis

As discussed in Sections 3.5 and 3.6, one of the main challenges facing microwave pyrolysis is the heating heterogeneity which can lead to thermal runaway with the char formation. The heating heterogeneity is mainly because of the nature of the standing waves inside the applicator which create areas of high electric field intensity and others of low electric field intensity. As shown earlier in Section 5.4, the loss factor of the biomass materials reaches a minimum value in the range between 300 °C and 400 °C. This minimum value is followed by a sharp increase in the loss factor due to the char formation, and this is what causes the thermal runaway during microwave heating. Figure 5-7 shows that, for the woody biomass, the operating temperature should fall in the range between 350 °C and 400 °C, which can secure around 70 % to 80 % weight loss. Increasing the temperature more than 400 °C would lead to falling into the steadily increased loss factor area with no much gain in terms of the weight loss.

Any microwave pyrolysis process for it to be reliable and scalable needs to be able to provide homogenous heating and be able to control the temperature of the process. It needs to be able to control the char deposition in the system for continuous processing.

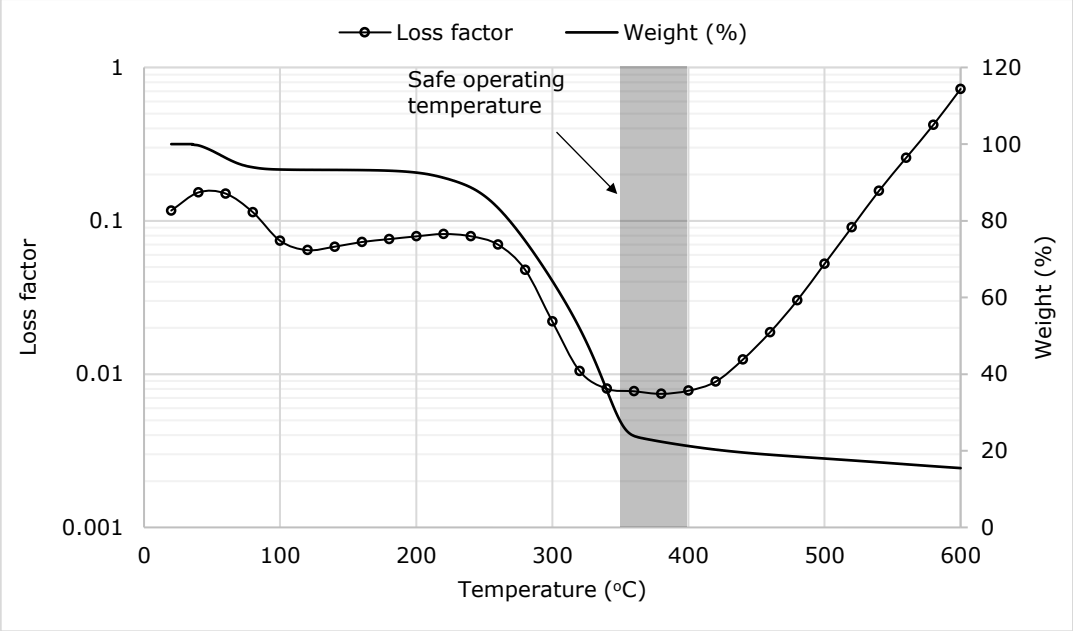

Figure 5-7: Dielectric loss factor of sycamore at 2.47 GHz and 0.5 g·cm^{-3} packing density together with the weight loss as functions of temperature.

Among the existing fast pyrolysis technologies, the fluidised bed technology is the most suitable to achieve these requirements. The fluidised bed technology is more flexible in terms of the heating methods compared to the other technologies as discussed in Section 2.2. The fluidised bed process is one of the most well-established technologies for biomass pyrolysis at industrial scale.

Microwave heating in fluidised bed systems has been used previously for several applications including drying (Goksu et al., 2005; Souraki et al., 2009), chemical vapour deposition (CVD) processes (Gerdes et al., 2006; Willert-Porada et al., 2014) and metal ore processing (Tranquilla and Kruesi, 1999; Tranquilla, 2000). However, there are no published studies on the use of microwave fluidised bed for biomass pyrolysis.

During fluidisation, the particles move freely within the bed supported by the fluidising gas. This movement of the particles provides a form of pneumatic agitation which can improve the heating uniformity in the bed during microwave heating as the particles would be continuously traveling between the heating zones.

If a cold fluidising gas is used, the gas velocity can be used to control the bed temperature at a certain power density. The bed temperature should be adjusted to achieve the highest weight loss without slipping into the thermal runaway zone as explained by Figure 5-7.

Fluidisation also provides a form of particle segregation based on their size and density allowing for continuous removal of the product if they have different size and/or density to those of the feed. In the case of biomass pyrolysis, the formed char particles have lower weight than the feed because of the weight loss through decomposition during pyrolysis. This can help in controlling the char deposition in the system.

The details of the proposed microwave fluidised bed process for biomass pyrolysis will be discussed in the following two chapters. The next Chapter is dedicated to studying the fluidisation behaviour of different biomass materials and the other steps of the process design.

5.6 Conclusions

This chapter was focused on the characterisation of various biomass materials as possible candidates for microwave pyrolysis. The biomass materials involved in this study include pine, sycamore, pine bark, wheat straw and seaweed. These materials were chosen because of their abundance, low economic value, and suitability for pyrolysis. The characterisation involved mainly thermogravimetric analysis and dielectric properties measurement.

The thermogravimetric analysis over the range of pyrolysis temperature showed different decomposition behaviour for the different biomass materials which was related to variations in their chemical composition. The transformations from room temperature to 600 ^{o}C were divided into three main stages: drying, decomposition, and char formation. Pine and sycamore showed close behaviour including a two-stage decomposition in the range between 200 ^{o}C and 400 ^{o}C corresponding to the

depolymerisation of the hemicellulose and cellulose respectively. The wheat straw showed an early one-stage decomposition ending at a temperature lower than that of the woody biomass which was attributed to the high minerals content of the wheat straw. The pine bark decomposition was found to happen slowly over a wider temperature range compared to the other biomass material because of its high lignin content. The seaweed showed largely different decomposition behaviour than the other biomass materials. This is because it does not have similar lignocellulosic structure, and also because of its high minerals content.

The dielectric properties of the biomass materials were studied at different packing densities. The packing density was correlated to both the dielectric constant and the loss factor through quadratic functions with a cofficeint of determination, R^2, greater than 99 % in all the cases indicating a strong relationship.

High-temperature dielectric measurements showed significant variations in the dielectric properties of the biomass material with temperature in the range between 20 ^{o}C and 600 ^{o}C. These variations were linked to the thermogravimetric analysis and the physical and chemical transformations happening during the heating. It was found that the loss factor of the biomass materials reaches a minimum value in the range between 300 ^{o}C and 400 ^{o}C. This minimum value is followed by a sharp increase in the loss factor due to the char formation, and this is what causes the thermal runaway during the microwave heating.

A microwave fluidised bed process was proposed as an attempt to overcome the heating heterogeneity and thermal runaway challenges, and to develop a reliable and scalable microwave pyrolysis process. The fluidised bed technology is one of the well-established technologies for biomass pyrolysis at a commercial scale. The microwave heating technique has been used previously with the fluidised bed technology for diffetent applications including materials drying, chemical vapour deposition (CVD) processes, and metal ore processing. However, there are no published studies on the use of microwave fluidised bed for biomass pyrolysis.

The fluidisation can improve the heating homogeneity through the continuous movement of the particles within the bed. Furthermore, The fluidising gas could be utilised to control the bed temperature and avoid slipping into the increasing loss factor area above 400 ^{o}C. Also, the fluidisation allows for particle segregation based on their size and density. This can be used to control the char deposition in the system during pyrolysis and could allow for continous processing.

The fluidisation behaviour of different biomass materials of different particle sizes will be studied in the next chapter which will also include the steps of the process design.

6 MICROWAVE PYROLYSIS IN A FLUIDISED BED: PROCESS DESIGN

6.1 Introduction

The aim of the work reported in this Chapter is to develop a microwave fluidised bed process for biomass pyrolysis as an attempt to overcome the heating heterogeneity challenge associated with microwave pyrolysis as discussed in Chapter 5. Fluidisation provides a form of pneumatic agitation which can improve the heating homogeneity through the continuous movement of the particles between the heating zones. Furthermore, the fluidising gas could be used to control the bed temperature and the solid deposition in the system. Based on the dielectric behaviour and the thermogravimetric analysis reported in Chapter 5, an optimum operating temperature for the microwave pyrolysis of woody biomass was suggested to fall in a range between 350 ^{o}C and 400 ^{o}C.

There are several published studies on microwave heating in fluidised bed systems in the areas of drying (Goksu et al., 2005; Souraki et al., 2009), chemical vapour deposition (CVD) processes (Gerdes et al., 2006; Willert-Porada et al., 2014), and metal ore processing (Tranquilla and Kruesi, 1999; Tranquilla, 2000).

Gerdes et al. (2006) studied the production of electronic-grade silicon using the CVD* process at around 600 ^{o}C in a microwave fluidised bed reactor (MW-FBR). They showed that microwave heating improves the product quality by enhancing the heterogeneous nucleation which takes place on the solid surface. This was attributed to that microwave heating allows for selectively heating of the solid keeping the surrounding gas at a lower temperature which limits the unwanted homogeneous nucleation in the gas phase. The fluidisation allowed for obtaining a well-defined particle size. The particle size of the product, which is larger than that

* Chemical vapour deposition (CVD) is a chemical process during which a reactive gas mixture is deposited on the surface of a solid to improve its quality (Gerdes et al., 2006).

of the feed (seed), was controlled by adjusting the gas velocity to allow the product (grown seeds) to settle at the bottom of the reactor when they reach the required size (Gerdes et al., 2006). The similarities between this CVD process and biomass pyrolysis is that both of them favour heating in a cold environment to avoid unwanted side reactions, and that fluidisation can be used to control the product deposition in the system based on its size and/or density.

The microwave fluidised bed process has also been suggested for metal ore processing (Tranquilla and Kruesi, 1999; Tranquilla, 2000). Tranquilla and Kruesi (1999) proposed a microwave fluidised bed reactor for the oxidation of pyritic ores. The use of the fluidized bed helps in controlling the oxygen supply to the reactor which governs the rate of the reaction (exothermic) and hence the reaction temperature. The microwave energy is used to initiate the chemical reaction and compensate for the heat losses (Tranquilla and Kruesi, 1999).

Tranquilla (2000) proposed a microwave fluidised bed reactor with a tapered section for processing metal ores and concentrates. The use of the tapered section (small diameter at the bottom) was to reduce the reflected power from the reaction zone and improve the electric field distribution in the process.

Microwave fluidised bed has also been used in drying of agriculture and food products (Goksu et al., 2005; Souraki et al., 2009; Khoshtaghaza et al., 2015). The majority of the studies in this area used a hybrid heating system combining the microwave heating with a hot fluidising gas. Microwave offers rapid drying while fluidisation provide a form of agitation which improves the heating uniformity (Zhang et al., 2006).

It is to be noted here that there are no published studies on the use of microwave fluidised bed for biomass pyrolysis. Even in the published work in the above mentioned areas, there is a lack of details about the process and cavity design.

In the present study, a systematic approach will be followed for the process design taking into account the pyrolysis process requirements, the microwave-material interactions and the fluidisation behaviour of the biomass material.

The fluidisation behaviour of the biomass particles will be studied initially, and the minimum fluidisation velocities will be determined. This will be followed by energy balance calculations to estimate the power requirement. Electromagnetic simulations will be then performed to support the microwave cavity design.

6.2 Fluidisation of Biomass Particles

6.2.1 Background

The development of the fluidised bed processes was initiated during the 1920's and their uses were focused mainly on catalytic cracking in the petroleum industry and for coal combustion for power generation (Richardson et al., 2002; Fouilland et al., 2010). During the past few decades, their use has been extended to cover other applications including combustion, gasification and pyrolysis of biomass (Fouilland et al., 2010). The major merits that fluidised bed systems can offer include: high fluid-solid contact area which enhances the heat and mass transfer, good mixing characteristics due to the continuous movement of the particles within the bed, and the segregation of the particles according to their size and/or density (Richardson et al., 2002; Cui and Grace, 2007; Fouilland et al., 2010). However, one of the main drawbacks of the fluidised bed systems is their limitation with regards to the particle shape and size as will be discussed later in this section.

The theoretical background behind fluidisation can be understood by studying the forces acting on the particle. When a fluid flows upwards through a bed of solid particles, the fluid pressure drops due to the frictional forces. This pressure drop (ΔP) increases when the fluid velocity is increased up to a point where the frictional forces equal the weight of the particles. Increasing the fluid velocity beyond this point leads to the separation of the particles from each other allowing them to be

freely supported in the fluid. The fluid velocity at this point is called the minimum fluidisation velocity. Further increase in the fluid velocity results in more bed expansion until it reaches a state of an upward particle flow. The velocity at this point is called the terminal falling velocity (Pell and Dunson, 1997; Richardson et al., 2002). Figure 6-1 illustrates the relationship between the pressure drop (ΔP) within the bed and the superficial gas velocity (u) over the fixed bed and fluidised bed ranges. Figure 6-2 shows a typical bed transition from a fixed-bed through fluidised-bed to particle transport.

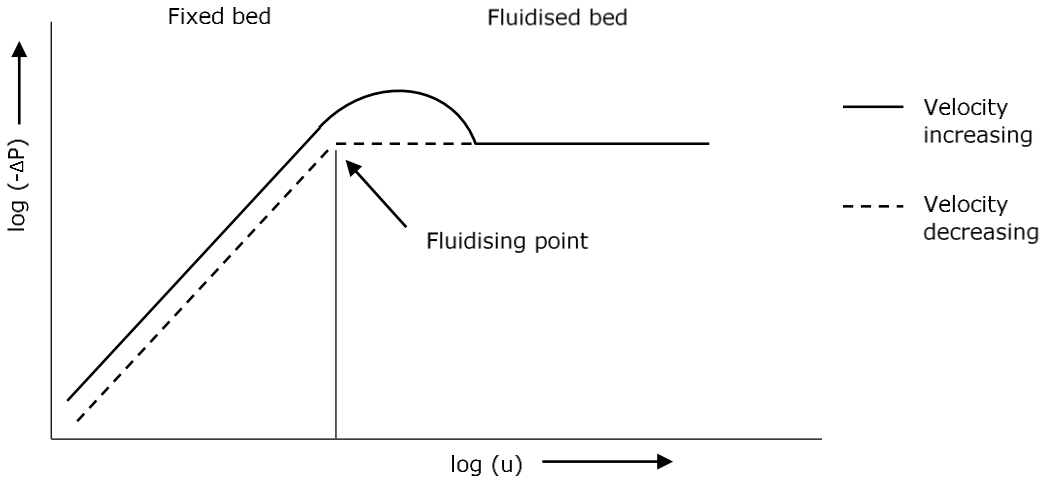

Figure 6-1: Typical relationship between the pressure drop (ΔP) and velocity (u) during the transition from fixed bed to fluidised bed. Adopted from (Richardson et al., 2002).

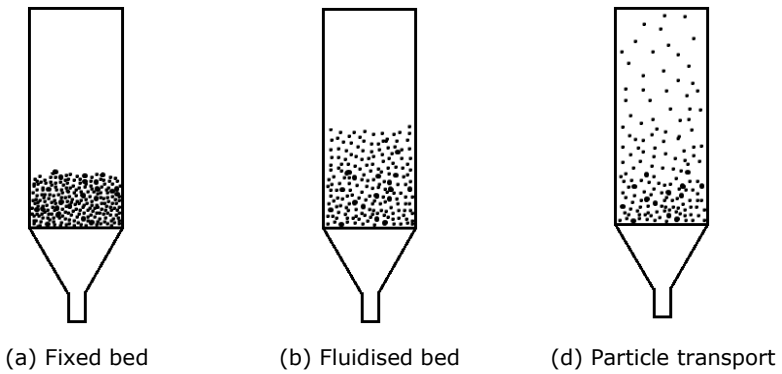

Figure 6-2: Transition from fixed bed to the particle transport

The above-described behaviour is the most uniform form of fluidisation and it is associated mostly with the liquid-solid systems and not common in gas-solid

systems where more complicated behaviours may take place (Richardson et al., 2002).

One of the most seminal studies on the fluidisation behaviour of gas-solid systems is the work published by Geldart (1973). Geldart classified the fluidisation behaviour of solid particles into four groups according to their size and density as shown in Figure 6-3 (Geldart, 1973; Richardson et al., 2002):

- Group A: characterised by particulate expansion over a wide range of gas velocities. Bubbling starts at a velocity higher than the minimum fluidisation velocity. This group is associated with materials of relatively small particle size and/or low particle density (less than 1.4 $g \cdot cm^{-3}$). This is the most homogenous form of fluidisation among the four groups.
- Group B: bubbling starts at velocities less than the minimum fluidisation velocity. This group includes most of the materials with mean particle size of 40 to 500 μm and particle density larger than 1.4 $g \cdot cm^{-3}$.
- Group C: associated with very fine particles. Fluidising materials within this group is difficult because the particles stick to each other and the gas flows upwards through channels. Mechanical stirring or addition of powders could be used to aid the fluidisation.
- Group D: associated with large particle size and/or high-density particles. Unlike Group B materials, the bubbles rise at a velocity lower than the gas velocity. Materials in this group can form a spouting bed where most of the gas flows through the middle of the column with a downwards movement of the particles near the wall.

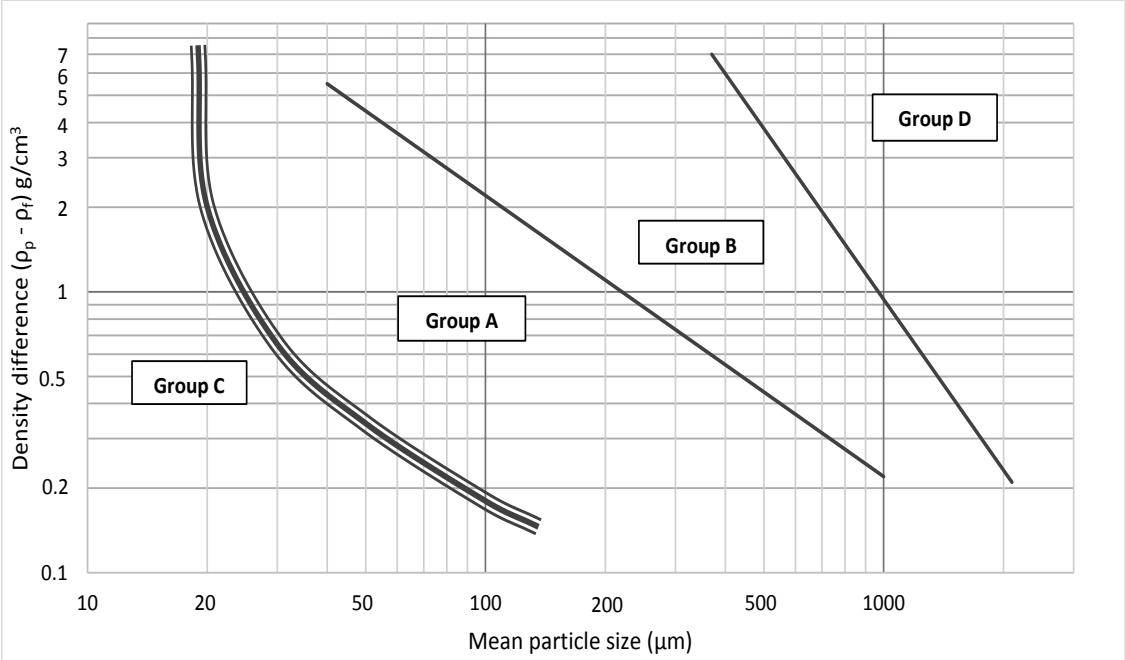

Figure 6-3: Geldart classification diagram for air fluidisation at ambient conditions; Adopted from (Geldart, 1973).

It is not only the size and density of the particle that determine the fluidisation behaviour. The shape of the particle has a significant influence on its fluidisation behaviour. The particle *sphericity* is frequently used as a measure of its shape. It is defined as the surface area of a sphere having the same volume as the particle divided by the volume of the particle itself. The sphericity of a perfect sphere is, therefore, 1. The lower the particle's sphericity, the more complex and less predictable its fluidization behaviour (Reina et al., 2000; Richardson et al., 2002; Cui and Grace, 2007).

Knowledge of the minimum fluidisation (u_{mf}) velocity is fundamental for designing a fluidised bed for any application. The minimum fluidisation velocity could be determined experimentally in a small-scale column or theoretically using an appropriate correlation. One of the most widely used correlations for estimating the minimum fluidisation velocity is Wen and Yu correlation which assumes a relationship between the particle shape and the porosity at the minimum fluidisation velocity (Wen and Yu, 1966; Richardson et al., 2002; Rao et al., 2010):

$$u_{mf} = \left(\frac{\mu}{d_p \rho_f}\right)\left[33.65 \times \left(\sqrt{1 + 6.18 \times 10^{-5} Ga} - 1\right)\right] \quad 6\text{-}1$$

Where Ga is Galileo number and it is given by $Ga = d_p^3 \rho_f (\rho_p - \rho_f) g/\mu^2$; ρ_f and μ are the fluid density (kg·m^{-3}) and viscosity (Pa·s) respectively; ρ_p and d_p are the particle density (kg·m^{-3}) and mean diameter (m) respectively.

Biomass particles, in general, have extremely irregular shapes (long, thin and fibrous) leading to a complex fluidisation behaviour that is difficult to predict (Cui and Grace, 2007). Biomass particles tend to stick to each other and agglomerate when they flow. This is why they are usually mixed with a second inert solid material such as silica sand, aluminium oxide and calcite to improve the fluidisation behaviour (R. Rao and Ram. Bheemarasetti, 2001; Paudel and Feng, 2013). As a consequence, most previous work on the fluidisation behaviour of biomass materials studied them as a mixture with another inert solid (Cui and Grace, 2007; Jia et al., 2015).

Abdullah et al. (2003) studied the minimum fluidization velocity for various biomass residues of different sizes and densities. They found that sawdust, coconut shell, and peanut shell, which were theoretically classified as Geldart Group B particles have good bubbling fluidisation behaviour. The palm fibre which was theoretically classified as Group A particles showed channelling behaviour which was related to their highly irregular shape and low density.

Reina et al. (2000) studied the fluidisation behaviour of different types of wood. They showed that homogeneous fluidisation could be achieved with hardwood particles and for softwood particles, plugging/slugging behaviour was observed. This was related to the low density and the fibrous structure of the softwood particles.

Jia et al. (2015) used a vibrating fluidised bed with a pulsed gas flow in order to improve the fluidisation behaviour of biomass materials. They investigated the

fluidisation of Douglas fir and pine particles which are softwoods as well as switchgrass. It was found that at pulsation frequencies above 3 Hz, the slugging could be stopped and regular bubbling behaviour could be achieved. The vibration was found to improve the fluidisation by breaking up agglomerating particles.

Liu et al. (2014) studied the drying of sawdust particles in a fluidised bed system. They used a gas distributor with 30° vertically inclined orifices to improve the fluidisation and achieve a good solid circulation. They observed changes in the bed fluidisation behaviour with time during the drying process due to the reduction in the moisture content. The reduction in the moisture content was found to improve the fluidisation behaviour which was attributed to the weakening of the capillary forces between the particles due to the removal of the surface water.

It was difficult to find a general correlation that could estimate the minimum fluidisation of biomass particles accurately. Even the Wen and Yu correlation (Wen and Yu, 1966) which is widely used for a broad range of materials was found to give highly inaccurate estimates for the minimum fluidisation velocity of biomass particles as shown by Reina et al. (2000).

It was, therefore, necessary for the present study to run cold experiments to investigate the fluidisation behaviour and determine the minimum fluidisation velocity of the biomass materials involved in this study as a step towards the full design of the microwave fluidised bed process.

Among the biomass materials which were characterised in Chapter 5, pine, sycamore and seaweed were selected to be taken forward for the fluidisation experiments and later for the microwave pyrolysis. Pine and sycamore were chosen, because as mentioned in Section 4.1, wood is the most extensively studied type of biomass materials for pyrolysis due to its ability to produce more consistent and repeatable results compared to the other biomass materials. It was, therefore, important to include wood materials in this study as they provide a comparison

platform for the newly developed process. Previous studies on the fluidisation of biomass particles showed that softwoods have significantly different fluidisation behaviour to hardwoods, and this is why both pine and sycamore were included for the fluidisation investigations. Seaweed was included because of its unique socio-economic advantages including its abundance and lower need for land and fresh water compared to terrestrial biomass as discussed in Section 4.1 placing it as an important candidate for large-scale biofuels production.

6.2.2 Cold Fluidisation Experiments

The fluidisation behaviour and the minimum fluidisation velocity of pine, sycamore and seaweed of different particle size were studied. Description of the experiemntal setup and methods followed are detailed in Section 4.3. The results of the cold fluidisation experiments are summarised in Table 6-1.

The theoretical Geldart's classifications for the particles based on Figure 6-3 was found to be Group A for the small particles, Group B for the intermediate size particles, and Group D for the large particles as listed in Table 6-1. However, the experimental observations indicated different behaviour for most of the particle size groups, as can be seen in the same table. Figure 6-4 shows examples of different kinds of flow behaviour observed during the fluidisation experiments including bubbling, channelling, slugging and turbulent fluidisation.

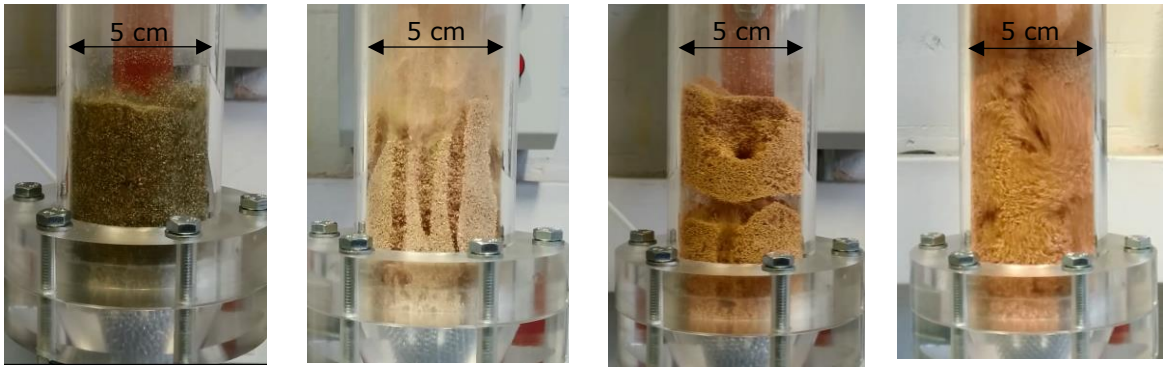

(a) Bubbling	(b) Channelling	(c) Slugging	(d) Turbulent fluidisation
(Seaweed 212 - 425µm)	(Sycamore 212 - 425µm)	(Pine 212 - 425µm)	(Pine 425 - 600 µm)

Figure 6-4: Different kinds of bed behaviour observed during the fluidisation experiments of the biomass particles

Table 6-1: Experimental and theoretical results of the fluidisation behaviour and minimum fluidisation velocity for seaweed, sycamore and pine of different particle size.

Material	Particle size group (μm)	Geldert classification		u_{mf} (m·s^{-1})		
		Experimental	Theoretical [a]	Experimental [b]	Theoretical [c]	Error (%)[d]
Seaweed	45 – 212	B	A	0.017	0.013	25.5
	212 – 425	B	B	0.13	0.09	31.5
	425 – 600	B	B	0.21	0.21	0
	600 – 850	B	B	0.38	0.37	3.1
	850 - 1180	C/B	D	0.64	0.58	8.3
	1180 - 1700	C/B	D	0.81	0.85	5.6
	1700 - 2360	-	D	-	1.15	-
Sycamore	45 – 212	C	A	0.06	0.004	93.0
	212 – 425	C	B	0.30	0.05	83.3
	425 – 600	C	B	0.42	0.12	71.0
	600 – 850	B	B	0.47	0.23	51.7
	850 - 1180	B	B/D	0.59	0.38	36.7
	1180 - 1700	B/D	D	0.72	0.58	19.9
	1700 - 2360	D	D	0.81	0.81	0
Pine	45 – 212	C	A	0.14	0.003	97.5
	212 – 425	C	A	0.34	0.04	89.3
	425 – 600	C	B	0.47	0.09	80.4
	600 – 850	C	B	0.55	0.17	69.0
	850 - 1180	C	B	0.76	0.29	61.7
	1180 - 1700	C	D	0.85	0.46	45.4
	1700 - 2360	-	D	-	0.66	-

[a] The classification is based on Figure 6-3 using the average particle size. The particle density was estimated using Mercury Porosimetery as explained in Appendix B.
[b] Three repeats were made. The accuracy of the measurements was within the accuracy of the flowmeters which were: ±1.0 L·min^{-1} (±0.0085 m·s^{-1}) for velocities less than 0.25 m·s^{-1} and ±5.0 L·min^{-1} (±0.042 m·s^{-1}) for velocities between 0.25 m·s^{-1} and 0.85 m·s^{-1}.
[c] The theoretical u_{mf} was calculated using Wen and Yu correlation.
[d] This is percentage error in the u_{mf} obtained from Wen and Yu correlation relative to the experimental values.

The experiments showed that the fluidisation behaviour of the seaweed groups in the range between 45 μm and 850 μm is homogeneous bubbling and could therefore be classified as Geldart Group B. The larger particle size groups of the seaweed in the range between 850 μm and 1700 μm showed the development of small channels before fluidisation. The minimum fluidisation velocity in these cases was significantly higher compared to the smaller particle size groups, and their fluidisation behaviour was closer to that of Geldart Group C particles which can

possibly be explained by the shape of the seaweed blades. As shown in Figure 6-5, the seaweed blades are long and thin with a thickness of less than 0.5 mm*. Therefore, the particles of size close to the blade thickness would have a more regular shape (higher sphericity) and therefore more homogeneous fluidisation behaviour. The larger particle would have a disc-like shape with low sphericity leading to more complex fluidisation behaviour.

Figure 6-5: Dry seaweed blades.

In the case of the woody biomass, all the pine particle size groups and the smaller groups of sycamore (less than 600 μm) exhibited channelling behaviour similar to that shown in Figure 6-4(b) during fluidisation. The channels started to appear at low gas velocities, depending on the particle size, becoming larger with the increase in the gas velocity. In some cases, when increasing the gas velocity, multiple slugs/layers of the bed material were observed. The gas in these cases flows through one large channel as shown in Figure 6-4 (c). The slugging behaviour appeared more frequently with the pine particles.

The behaviour of pine and the smaller particle size groups of sycamore are similar to that of Geldart Group C particles. However, Group C is usually associated with very fine particles in which London-van der Waals attractive forces are great enough to keep the particles tied together strongly (Richardson et al., 2002). In the case of the woody biomass materials, it is their irregular shape (long and branched) that

* The blade's thickness was measured using an electronic digital calliper (SPI® 13-610-1) which has an accuracy of 0.01mm. After 20 different readings at different places, the blade thickness was estimated at 0.35±0.09mm.

ties the particles together. Figure 6-6 shows images of samples from the studied biomass particles taken using an optical microscope (Nikon® Eclipse LV100ND) connected to a computer with a software (NIS-Elements 4.1) for processing and storing the images. The biomass particles for imaging were placed in glass plate. Figure 6-6 shows that woody biomass particles have highly irregular shapes compared to seaweed, and that pine particles are more fibrous than the sycamore particles. This also explains why pine particles fluidise at velocities much higher than sycamore with the same particle size group as can be seen in Table 6-1.

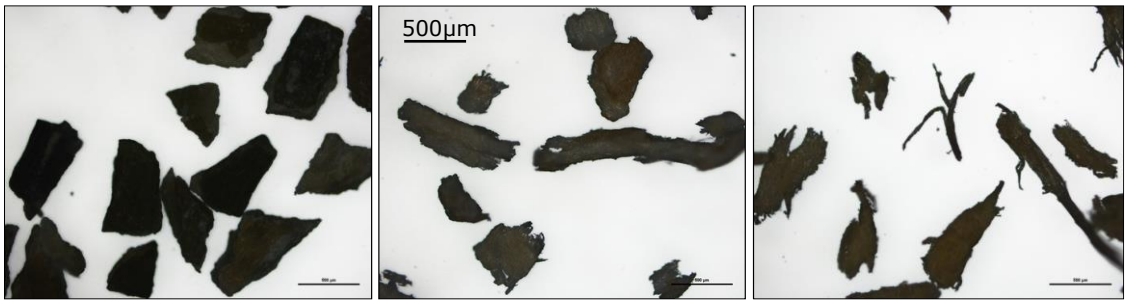

Figure 6-6: Optical images for the shape of the biomass particles.

Fluidisation in the cases of channelling/slugging could not be achieved without disengaging the particles from each other. Two different methods were applied to reach a fluidisation state and to estimate the minimum fluidisation velocity: (a) starting with a high gas velocity, high enough to separate the particles from each other, then reducing the velocity down to a minimum value at which the particles are still fluidised; (b) pouring the biomass particles slowly from the top of the column after introducing the gas. Both methods gave similar values for the minimum fluidisation velocity. However, the observed behaviour was turbulent fluidisation and the minimum fluidisation velocity was found to be significantly higher compared to the theoretical values as shown in Table 6-1.

Increasing the particle size of the woody biomass was found to improve the fluidisation behaviour due to the reduction in the effect of the particles binding forces compared to their weight. It was mentioned earlier in this section that, in

general, fine particles which are classified as Geldart's Group C, tend to stick to each other (agglomerate) during fluidisation because that London-van der Waals attractive forces are great compared to their weight. In the case of biomass particles, their highly irregular shape (long and branched) increases the binding forces between the particles. By increasing the particle size, the effect of both type of binding forces is reduced relative to the weight of the particle resulting in more homogenous fluidisation. It was also found that larger woody biomass particles obtained from the shredded have more regular and less branched (fibrous) shape. Figure 6-7 shows the shape of the biomass particles in the range 1180 to 1700 μm which are less branched (fibrous) compared to the 212 – 425 μm shown in Figure 6-6.

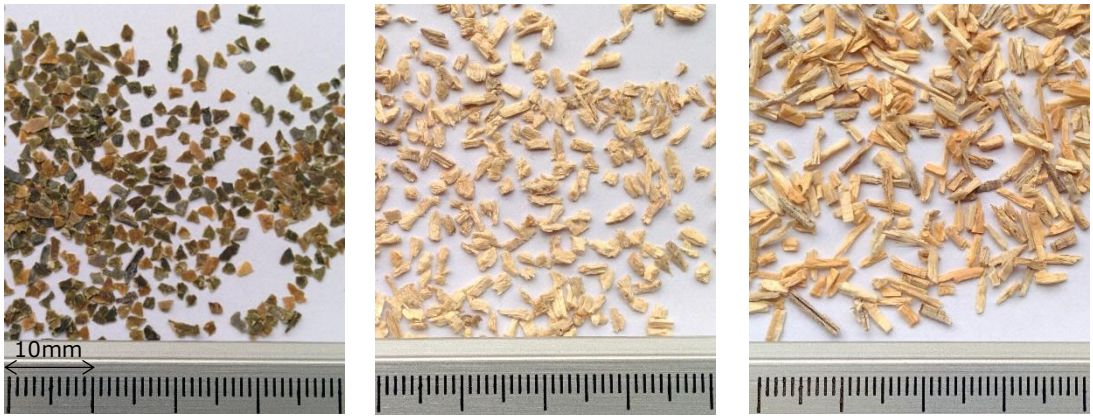

(a) Seaweed 1180-1700 μm (b) Sycamore 1180-1700 μm (c) Pine 1180-1700 μm

Figure 6-7: Particle shape for the three biomass materials with a particle size of 1180 – 1700 μm.

The improvement in the fluidisation caused by increasing the particle size can be seen in the reduction of the difference between the theoretical and experimental u_{mf} for the larger particles as displayed in Table 6-1. This improvement in the fluidisation with the particle size can also be seen for the sycamore particles larger than 600 μm which showed bubbling fluidisation rather than channelling following Geldart's Group B behaviour. However, sycamore particles of a size larger than 1180 μm can be classified as Geldart Group D particles. Large bubbles were observed at the middle of the column with the particles flowing downwards near to the wall.

The fluidisation of a wider range of particle sizes was also investigated. Initially, a particle size range of 45 - 850 μm was used. The particle size distribution of the particles in this range can be found in Appendix A. However, it was observed that a considerable amount of fine particles were transported with the fluidising gas at the minimum fluidisation velocity. This suggests that at the minimum fluidisation velocity of the bulk bed, some of the finer particles had reached their terminal falling velocity. Therefore, a 212 – 850 μm range was used which eliminated particles entrainment at the minimum fluidisation velocity. The minimum fluidisation velocities of the three biomass materials of particle size 212 – 850 μm are listed in Table 6-2. The same table also shows the minimum fluidisation velocity for char particles which were prepared by heating 212 – 850 μm particles in an electric oven. The particle size distribution of the produced char particles is shown in Appendix A.

Table 6-2: The minimum fluidisation velocity of 212 - 850μm biomass particles and biomass char obtained from the same particles size range.

Material	Mean particle size (μm) [a]	Density ($g \cdot cm^{-3}$) [b]	Minimum fluidisation velocity ($m \cdot s^{-1}$) [c]
Seaweed	554	1.60	0.21
Seaweed char	494	0.31	0.14
Pine	531	0.66	0.47
Pine char	415	0.60	0.38
Sycamore	598	0.90	0.38
Sycamore char	505	0.52	0.21

[a] Obtained from the particle size distribution as can be seen in Appendix A.
[b] Obtained using the Mercury Porosimetry as can be seen in Appendix B.
[c] The accuracy of the flowmeter is ±5.0 $L \cdot min^{-1}$ (±0.042 $m \cdot s^{-1}$).

It can be seen from Table 6-2 that the char particles for the three biomass materials have u_{mf} values smaller than those of the raw biomass. This is related to the reduction in the particle size and density after pyrolysis as indicated in Table 6-2. This drop in the u_{mf} after pyrolysis suggests that the formed char would tend to rise to the top of the column. The gas velocity can, therefore, be used to control the char deposition in the system during biomass pyrolysis. For continuous processing, the gas velocity can be set at a value higher than the terminal settling velocity of the char particles and lower than that of the feed particle. This would allow for the

continuous removal of the formed char particles through entrainment while keeping the heavier unpyrolysed particles fluidising in the bed.

6.2.3 Summary of the Fluidisation Behaviour of Biomass Materials

The fluidisation behaviour of pine, sycamore and seaweed particles was studied as one of the steps towards designing a microwave fluidised bed process for biomass pyrolysis. For the range of the particle size involved in this study (45 – 2360 μm) the following can be concluded:

- The majority of the particle size groups showed different behaviour to those predicted from their theoretical Geldart classification which was attributed to their irregular shape.
- The seaweed particles up to 850 μm showed homogeneous bubbling behaviour similar to that of Geldart Group B particles. Small channels were observed prior to fluidisation in the larger particles of seaweed which was related to a reduction in sphericity.
- The pine and particle groups of sycamore up to 600 μm showed Geldart Group C behaviour including channelling and slugging. This was related to the fibrous structure of the woody biomass which encourages agglomeration. Fluidisation in these cases was achieved at relatively high velocities leading to turbulent fluidisation. Increasing the particle size was found to improve the fluidisation by eliminating the channeling and slugging behaviour. Sycamore particles larger than 600 μm demonstrated homogenous bubbling (Geldart Group B) with no channelling.
- It was shown that raw biomass particles have greater minimum fluidisation velocities compared to char prepared using similar particle size feed. This was related to a drop in the particle's size and density after pyrolysis. During processing, this would lead to particle segregation and could be used to control the char deposition and residence time in the bed.

For the next stages of the process design, including the energy requirement calculations and the microwave cavity design. Sycamore will be used as the base for the design. A woody biomass was chosen because of the suitability of wood to provide a comparison platform for the newly developed process as discussed earlier in this Chapter. Sycamore was chosen over pine mainly because it showed better fluidisation behaviour as in all the studied particle size, pine showed more complex behaviour including channelling and slugging. The minimum fluidisation velocity for pine was also greater than sycamore for the similar particle size groups. Sycamore showed more homogeneous behaviour especially for the particle groups in the range 600 μm to 1700 μm which showed bubbling fluidisation as that of Geldart Group B. Sycamore would therefore allow for wider range of particle size and gas velocity to be studied during the pyrolysis experiments compared to pine. Although, the following steps of the process design will be based on sycamore, pine and seaweed will also be included in the pyrolysis experiments in the developed process.

6.3 Energy Requirement for the Microwave Fluidised Bed Process

After studying the fluidisation behaviour of the biomass particles and determining their minimum fluidisation velocities, the following step was to estimate the energy and power requirement for the pyrolysis in the microwave fluidised bed system.

As discussed in Section 2.1, there is a disagreement in the literature on the enthalpy for pyrolysis of biomass materials. The enthalpy for pyrolysis is the sum of the enthalpy required to heat the biomass material up to the pyrolysis temperature (sensible enthalpy) and that required to achieve the pyrolysis reactions (reaction enthalpy). The enthalpy for pyrolysis in this study was determined experimentally. Energy balance calculations were then performed to estimate the energy required to achieve the pyrolysis in the fluidised bed system by taking into account the heat losses to the fluidising gas.

6.3.1 Enthalpy for Pyrolysis

Figure 6-8 shows the heat flow and the weight loss during pyrolysis of sycamore particles which was obtained from the DSC-TGA measurements as detailed in Section 4.4.1. It can be seen that the pyrolysis process is, in general, endothermic. The heat flow decreases with temperature up to around 200 °C. Above 300 °C the heat flow starts to increase rapidly with temperature. This increase in heat flow can be regarded to the depolymerisation of the biomass constituents which can be explained by the large mass loss in the TGA curve over the same range. The heat flow decreases again between 370 °C and 400 °C which indicates the end of the endothermic depolymerisation reactions. Another increase in the heat flow can be seen above 400°C which corresponds to the rearrangement reactions and char formation.

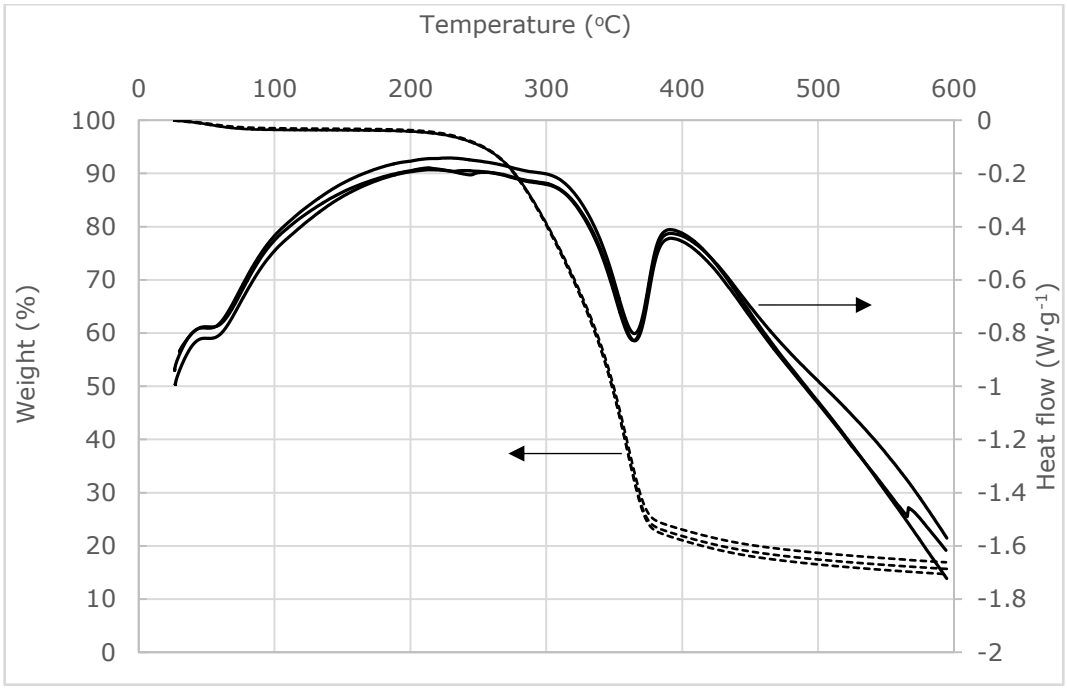

Figure 6-8: Heat flow and weight loss from three sycamore samples using a DSC-TGA.

The enthalpy for pyrolysis was determined by integrating the heat flow curve over the pyrolysis temperature range using Equation 4-7. The results are listed in Table 6-3 which shows the enthalpy for pyrolysis at different temperatures. The majority of the previous studies, as discussed in Section 2.1, report the enthalpy

for pyrolysis at 500 °C. However, it was shown in Section 5.5 that for microwave pyrolysis, the operating temperature should be in the range between 350 °C and 400 °C. It can be seen from Table 6-3 that the enthalpy for pyrolysis for sycamore at 400 °C is 0.88±0.07 kJ·g^{-1}.

Table 6-3: Enthalpy for pyrolysis for dry sycamore as a function of temperature. The results are from three repeats, and the standard uncertainty is indicated.

Temperature (°C)	350	400	450	500
Enthalpy (kJ·g^{-1})	0.71 ± 0.06	0.88 ± 0.07	1.04 ± 0.09	1.28 ± 0.11

6.3.2 Power Density Requirement

The specific heat capacity was determined as a function of temperature from the heat flow using Equation 4-8. Figure 6-9 shows the change in the specific heat capacity of sycamore as a function of temperature which accounts for the sensible heat and the heat of reaction. The relationship between the specific heat capacity of sycamore and temperature was represented by a third-order polynomial as displayed in Figure 6-9 to be used for the energy balance calculations.

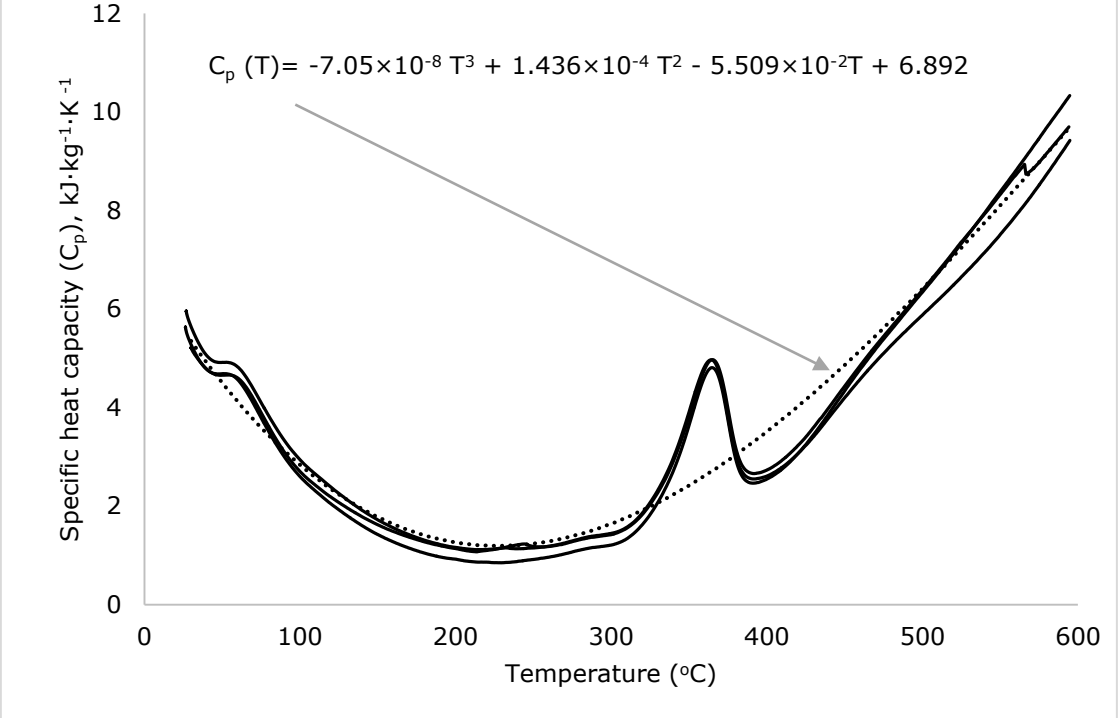

Figure 6-9: Specific heat capacity of sycamore as a function of temperature calculated from the heat flow results shown in Figure 6-8.

Energy balnce calculations were performed to estimate the power density and energy input requirements for microwave pyrolysis in the fluidised bes system. The mathematical models, assumptions, and the computing methods are detailed in Section 4.4.2. Figure 6-10 shows the rise in the bed temperature with time at different values of applied power density which was calculated using Equation 4-11. It can be seen that the bed temperature increases sharply during the first few seconds of heating before it slows down and reaches a point where no significant increase in the temperature with time due to the reached equilibrium between the input power and the heat loss. As can be seen from Figure 6-10, that the minimum power density required to reach 400 °C and 500 °C are 54 MW·m^{-3} and 68 MW·m^{-3} respectively. About 20 seconds is required to reach 400 °C under 54 MW·m^{-3} which corresponds to 4.85 kJ·g^{-1} specific energy.

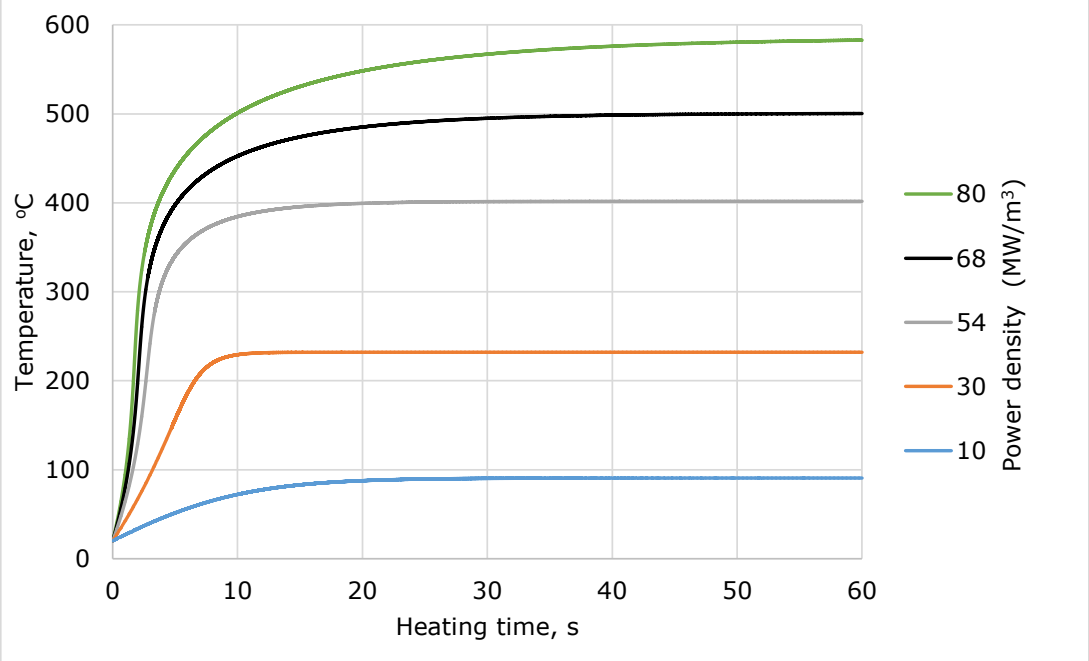

Figure 6-10: Bed temperature as a function power loss density and time for sycamore of 600µm particle size and gas velocity of 0.38 m·s^{-1}.

Table 6-4 shows that increasing the power density leads to reduction in the specific energy required for the pyrolysis. This is mainly because of the reduction in the

heating time as can be seen form Figure 6-10 leading to drop in the heat loss to the fluidising gas.

Table 6-4: The specific energy required to achieve pyrolysis in the fluidised bed process using 600 µm sycamore with a fluidising gas flowing at 0.38 m/s.

Power density ($MW \cdot m^{-3}$)	54	68	70	80	90	100
Specific energy ($kJ \cdot g^{-1}$) at 400 °C	4.85	1.46	1.40	1.22	1.13	1.07
Specific energy ($kJ \cdot g^{-1}$) at 500 °C	-	14.65	6.53	3.31	2.60	2.27

Figure 6-11 shows the temperature gradient inside a single particle calculated using Equations 4-12, 4-13 and 4-14. It shows that for the 600 µm sycamore particle, the temperature at the centre of the particle is 21 °C higher than that of its surface.

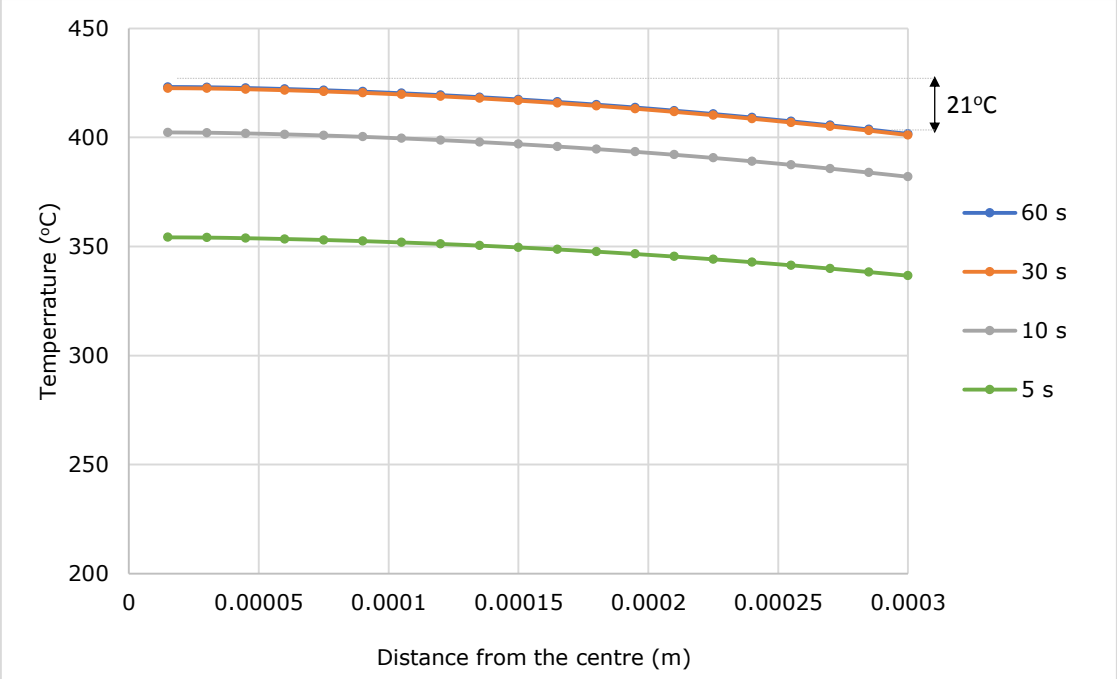

Figure 6-11: Temperature gradient with time in a 600 µm sycamore particle at 54 $MW \cdot m^{-3}$ power loss density and 0.38 $m \cdot s^{-1}$ gas velocity

Increasing the particle size increases the temperature difference between the centre and the surface of the particle. Figure 6-12 shows that for 1.5 mm sycamore particle, the temperature difference is around 70 °C. Increasing the particle size also reduces the power density required to reach certain temperature. As indicated in Figure 6-12, 28 $MW \cdot m^{-3}$ is required to reach a surface temperature of 400 °C for

the 1.5 mm particle compared to 54 MW·m^{-3} for the 600 µm particle. This reduction in power requirement with particle size is related to the smaller surface area for the larger particles leading to lower heat loss to the fluidising gas.

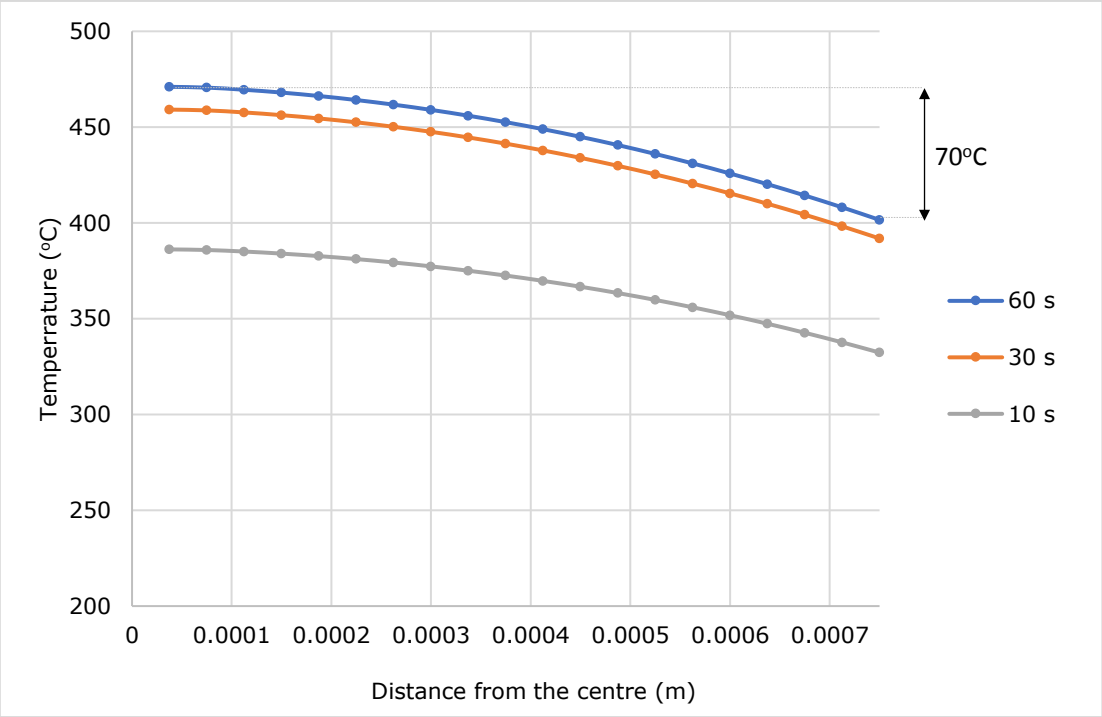

Figure 6-12: Temperature gradient with time in a 1500 µm sycamore particle at 28 MW·m^{-3} power loss density and 0.38 m·s^{-1} gas velocity.

However, larger particles require higher gas velocity to fluidise leading to increased heat loss to the gas. Based on Equations 4-12 to 4-14, increasing the gas velocity to 0.58 m·s^{-1} for the 1.5 mm increases the minimum power density required to reach 400 °C to 48 MW·m^{-3}. It also increases the temperature gradient inside the particle to 120 °C.

It is clear from Figure 6-11 and Figure 6-12 that the temperature gradient within the particle under microwave heating is opposite to that of conventional heating in which heat is transferred from the surface to the centre. The direction of the temperature gradient in the conventional heating techniques has previously been believed to cause deteriorations in the oil yield and quality by stimulating fragmentation and secondary cracking reactions on the hot surface resulting in

lighter products and non-condensable gases (Fouilland et al., 2010; Collard and Blin, 2014). This is the reason why the vapour residence time has to be very short when using a conventional heating technique. Microwave heating, on the other hand, can provide colder particle surface which preserves the oil yield and quality by limiting the secondary cracking reactions.

The maximum temperature gradient would happen at the bottom of the fluidised bed near to the distributor where the gas temperature is at its lowest value, while the minimum gradient is reached when the gas reaches a thermal equilibrium with the particles.

6.3.3 Summary of the Energy Requirement Calculations

After studying the fluidisation behaviour of the biomass particles and determining their minimum fluidisation velocities, the energy and power density requirement were calculated. Firstly, the enthalpy for pyrolysis was determined from the heat flow to the biomass samples using differential scanning calorimetry. The enthalpy for pyrolysis does not include the heat losses. Therefore, energy balance calculations were performed to estimate the power density and the energy requirement in the fluidised bed system including the heat loss to the fluidising gas. It was found that the minimum power density required for the pyrolysis of 600 μm sycamore particles at 400 ^{o}C is 54 MW·m^{-3}. The specific energy corresponding to this power density was found to be 4.85 kJ·g^{-1}. It was shown that increasing the power density leads to a reduction in the specific energy. Only 1.07 kJ·g^{-1} is required when 100 MW·m^{-3} power density is applied which is close to the 0.88 kJ·g^{-1} enthalpy for pyrolysis determined using the DSC at 400 ^{o}C.

The temperature gradient inside the particle was studied by solving the heat transfer equations iteratively over space and time. It was found that the temperature at the centre of a 600 μm sycamore particle is 21 ^{o}C higher than its surface at 54 MW·m^{-3} power density and 0.38 m·s^{-1} gas velocity. Increasing the particle size was shown to increase the temperature difference between the centre and the surface of the

particle. Increasing the particle size was also found to reduce the power density required to reach a surface temperature of 400 ^{o}C.

This temperature gradient which is opposite in direction to that of conventional heating techniques can improve the product quality by limiting the secondary cracking reactions at the surface of the particle as the surface would always have a lower temperature than the centre.

It is to be mentioned here that the bed temperature near the distributor will be lower than that at the top of the bed. This is because that fluidising gas is to be fed into the bed, which is being held at approximately 400 ^{o}C, at room temperature. Thus, the temperature gradient inside a particle at the bottom of the bed would, therefore, be greater than that at the top of the column if the absorbed power density is uniform across the bed.

6.4 Design of the Applicator for the Microwave Fluidised Bed Process

So far, the fluidisation behaviour of the biomass particles have been studied, and the minimum power density requirement to achieve pyrolysis has been estimated. The next step was to design the applicator for heating the biomass particles in the fluidised bed.

The first step in the applicator design is to choose the type of the applicator. As discussed in Section 3.4, there are three main classes of applicators: travelling waves, near-field and resonant applicators. Resonant applicators (or cavities) are the most commonly used types of applicators for microwave heating applications as they allow for intensifying the electric fields inside the cavity for a given power. Resonant cavities can be single-mode or multimode. Each type has its advantages and disadvantages as discussed in Section 3.4. Single-mode cavities have the advantage of the well-defined electric field which allows for placing the material under processing in locations of highest field intensity (Mehdizadeh, 2015). However, one of the great disadvantages of single mode cavities for the current

application is that their dimensions are limited by the half wavelength of the applied wave. This limits the size of the sample to be treated and also increases the possibility of electric breakdown in the area surrounding the reactor due to the presence of a narrow gap and/or edges which create areas of higher electric field intensity. Multimode cavities, on the other hand, have larger dimensions and, therefore, larger spaces between the reactor and the walls of the cavity compared to the single-mode type cavities reducing the risks of electric breakdown. One of the weaknesses of multimode cavities, in general, is that unlike single mode cavities, the electric field is not well defined in space and its distribution is dependent on the size and dielectric properties of the load which could vary during the biomass pyrolysis process as well as the dimensions of the applicator. However, this weakness can be overcome in the present case through the movement of the particles between the hot and cold spot within the bed even if these cold and hot spots change locations during processing.

Electromagnetic simulations using COMSOL Multiphysics® v4.4 were performed to investigate the design of the multimode cavity for the present application. COMSOL is computer code which applies the finite element method to give numerical solutions for physical quantities. The RF (Radio Frequency) Module in COMSOL has been used widely for modelling the electromagnetic field distribution in the microwave heating applicators based on Maxwell's equations, and estimating the power loss within the workload.

Several studies have shown good agreement between the results obtained using COMSOL modelling and those obtained experimentally for processes involving microwave heating. However, one of the main disadvantages of COMSOL, and the finite element methods in general, is that it requires large memory space and long processing time to give accurate results (Salvi et al., 2011).

Salvi et al. (2011) modelled the microwave heating of a continuously flowing fluid in a cylindrical cavity at 915 MHz using the RF Module in COMSOL. They compared

the modelling results with experimental results for two different fluids; tap water and carboxymethyl cellulose (CMC). They found that COMSOL model predicted the power loss in the fluid with only 6% and 2% error for the tap water and CMC respectively.

Salema and Afzal (2015) studied the microwave pyrolysis of empty fruit bunch (EFB) pellets in a modified domestic multimode cavity both experimentally and numerically using COMSOL. They showed good agreement between modelling and experimental results for predicting the location of the hot-spots.

In many of the previous studies, the RF Module in COMSOL is coupled with other modules such as the Heat Transfer Module which allows for estimating the temperature profile within the workload (Salvi et al., 2010; Salvi et al., 2011; Salema and Afzal, 2015; Ferrari-John et al., 2016).

In present study, the RF Module in COMSOL was used to simulate the 3D distribution of the electric field inside the cavity and within the load, and to determine the power loss density within the load for various cavity dimensions. Fluid dynamics and heat transfer were not included in the simulation in this study.

6.4.1 Model Setup

The simulations were solved using the *Electromagnetic Waves Frequency Domain* physics interface which is found in COMSOL under the RF Module. The governing equation of the electric field wave is given by:

$$\nabla \times {\mu_r}^{-1}(\nabla \times E) - k_o^2\left(\varepsilon_r - \frac{j\sigma}{\omega\varepsilon_o}\right)E = 0 \qquad 6\text{-}2$$

Where

μ_r is the relative permeability of the material (for biomass $\mu_r = 1$);

E is the electric field strength which is a vector;

k_0 is the wave number which is given by $k_0 = \omega/c_o$, where ω is the wave angular frequency (rad·s^{-1}) and c_o is the speed of light in vacuum (3×10^8 m·s^{-1})

ε_r is the relative permittivity of the material;

σ is the electric conductivity of the material, S·m^{-1};

j is the $\sqrt{-1}$;

ε_o is the permittivity of free space (8.854×10^{-12} F·m^{-1}).

The power loss density (absorbed microwave power by the material) is determined through Equation 3.2 which was discussed in Chapter 3.

The model was solved at 2.45 GHz frequency. As stated in Section 5.3, sycamore of 212 – 850 μm particle size was used as the basis for the design. Therefore, the parameters listed in Table 4-2 were used for the simulation. It is to be noted that the fluidised bed was simulated as a bulk solid using the bulk density of the bed at the minimum fluidisation velocity. The model was built and solved following the steps below.

6.4.1.1 Simulation geometry

The general geometry used for the simulation is shown in Figure 6-13 which is mainly a quartz column (reactor) with a gas distributor inside a rectangular metallic box. The quartz reactor is surrounded by a metallic tube all the way outside the cavity. Quartz was chosen because of its good dielectric and thermal properties for the present case. It has a loss factor less than 0.001 at 2.45 GHz (Meredith, 1998). It has a typical operating temperature of around 1000 °C. The inner and outer diameter of the column were 0.05 and 0.06 m respectively. The inner diameter of the metallic tube surrounding the column was assumed to have the same value as the outer diameter of the quartz column. This is lower than the critical cut-off

diameter*; the diameter above which microwave power would propagate through the tube (Meredith, 1998). The length of the column was set at 0.6 m. Based on the fluidisation experiments this length is enough for the bed expansion and disengagement.

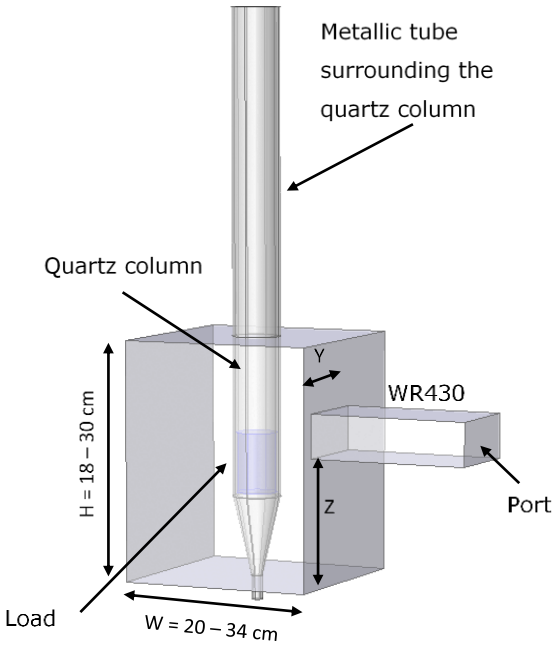

Figure 6-13: Geometry used to simulate the fluidised bed process in a multimode cavity.

6.4.1.2 Materials

The materials involved in the simulation were the biomass material, quartz, and air. The walls of the cavity and the waveguide were assumed to be perfect conductors. The complex permittivity of the biomass material was determined from the quadratic functions which were developed in Section 4.4 for the relationship between both parts of the permittivity and the packing density. The relationships for sycamore were as follows:

$$\varepsilon' = 0.69\rho^2 + 1.376\rho + 1; \qquad \varepsilon'' = 0.117\rho^2 + 0.197\rho$$

* The cut-off radius, a, for the lower-order mode (TE_{11}) through circular choke is $a = \lambda_0/(3.413\sqrt{\varepsilon'})$. Where λ_0 is the free-space wavelength, ε' is the dielectric constant of the medium. At 2.45 GHz frequency and air medium, a = 0.0375 m.

Where ρ is the packing density in g·cm^{-3}. Substituting the bed bulk density of sycamore at the minimum fluidisation velocity which is 0.24 g·cm^{-3} as displayed in Table 4-2 gives a permittivity of: $\varepsilon = 1.37 - 0.055j$.

The space above the bed and that outside the reactor was assumed to be air. The COMSOL library permittivities for air and quartz were used which are 1.0 and 4.2 respectively.

6.4.1.3 Boundary conditions

A *port* boundary condition was added to feed the microwave power into the system. The port is a rectangular TE_{10} placed at the start of a standard WR430 waveguide as indicated in Figure 6-13. The microwave power input through the port was set at 6 kW. The obtained power loss density will be compared to the minimum power density required for the pyrolysis which is 54 kW·m^{-3}. A pe*rfect conductor* boundary condition was also added to the model to simulate the internal walls of the waveguide, the cavity and the metallic tube.

6.4.1.4 Mesh

The finite element method divides the model into small and geometrically simple elements. The accuracy of the solution is affected by the resolution of the mesh. Fine mesh size improves the computational accuracy but increases the solving time and memory requirement. For the current model, the mesh type selected was *physics controlled mesh* and an *extremely fine* element size was selected. This generated 248,251 to 412,739 tetrahedral elements depending on the dimensions of the cavity in each case. The simulation was run on an Intel workstation with eight Dual Core 2.5 GHz Xeon processors, 192 GB RAM (Random Access Memory), with a Microsoft Windows 7, 64 bit operating system. With these memory and processing capabilities, the time needed to solve each case was 4 to 8 minutes.

6.4.1.5 Study

There are many parameters related to the cavity dimensions, load position and microwave power feed position needed to be optimised. In order to limit the number of the variables, some practical choices/assumptions were made as follows:

- The cavity depth (D) equals the width (W)
- The column is at the centre of the cavity.
- The waveguide is attached to the side of the cavity, and not at the top or the bottom.
- The tapered section below the gas distributor is 10 cm long, and all of it is inside the cavity.

This leaves four variables: the cavity height (H); the cavity width (W); the waveguide Y position; and the waveguide Z position. These variables were defined as parameters in the simulation to allow them to be changed during the simulations through the *parametric sweep* function. The parametric sweep function in COMSOL instructs the software to change the value of a parameter within a specified range and solve for each of these values instead of changing it manually. The function allows for more than one parameter to be changed, and the simulation is then solved for all the combinations of the specified parameters. The cavity width, W, was set to vary from 20 to 34 cm at steps of 2.0 cm which covers a number of cavity modes* slightly less than three to more than four. As the load is placed at the centre of the cavity, two modes would create an area of a low electric field within the load. The cavity height, H, was changed from 18 to 30 cm with step changes of 2.0 cm. The lower limit is determined by the height from the bottom of the tapered section to the top of the load. The waveguide Z position was changed to cover all the cavity height while the Y position was changed to cover only half of

* The term "modes" refers to the number of the half-wavelengths generated by the reflection of the waves by the walls inside the cavity. The number of modes could be estimated by dividing the cavity length by the guide half-wavelengths, $\lambda_g/2$.

the depth due to the symmetry. Step changes of 2 cm were used for both Y and Z positions.

The aim was to run the simulations for a range of cavity dimensions and waveguide positions to find the optimum values that minimise the loaded cavity Q-factor (maximise the percentage absorbed power) while providing uniform heating.

6.4.2 Simulation Results

Changing the variables mentioned in model setup section over the specified ranges resulted into more than 2500 simulation cases. Two main criteria were used for comparison and selection: the fraction of the absorbed power (a measure for the Q-factor) and the heating homogeneity. The cases were filtered first based on the absorbed power by excluding all the cases that had less than 80% absorbed power. Then for the cases with similar dimensions and electric field distributions, the case with the highest percent absorbed power was selected. This allowed the number of cases required to be reduced to 30. The heating homogeneity was then used as the criteria to filter the remaining cases. This was achieved by comparing the electric field intensity and the power loss density on a slice passing through the centre of the cavity and the bed, and also the projection of the power loss density. The projection of the power density was obtained by integrating the power loss density over the bed height using the General Projection operator which is a predefined function in COMSOL.

Figure 6-14 displays the simulation results from selected cases showing the electric field distribution and the power loss density. These cases give an example of how the selection based on the heating homogeneity was made. As can be seen in Figure 6-14, different cavity dimensions lead to different results in terms of electric field distribution and therefore the power loss density.

(a) H = 240, W = 240, z = 100, y = 35.1

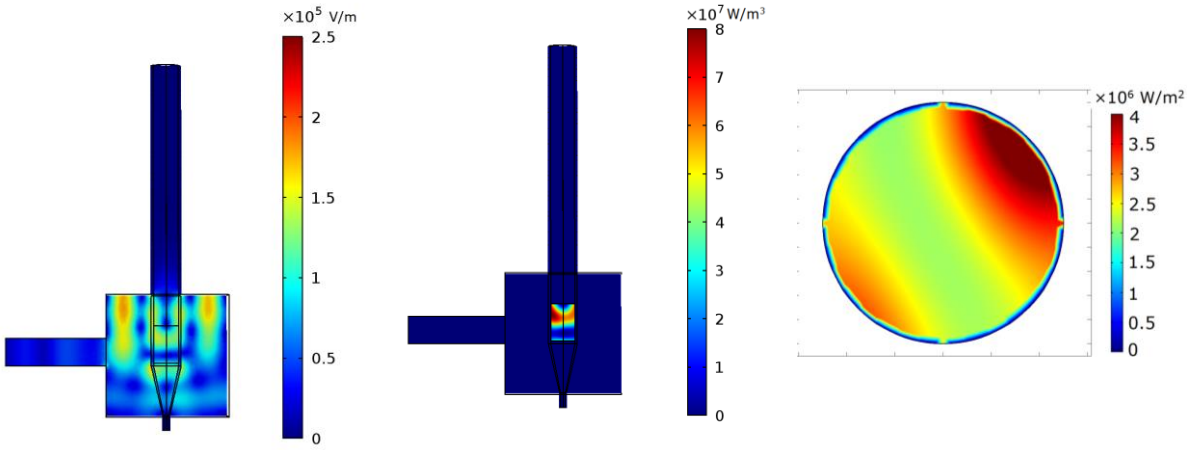

(b) H = 260, W = 200, z = 12.5, y = 72.5

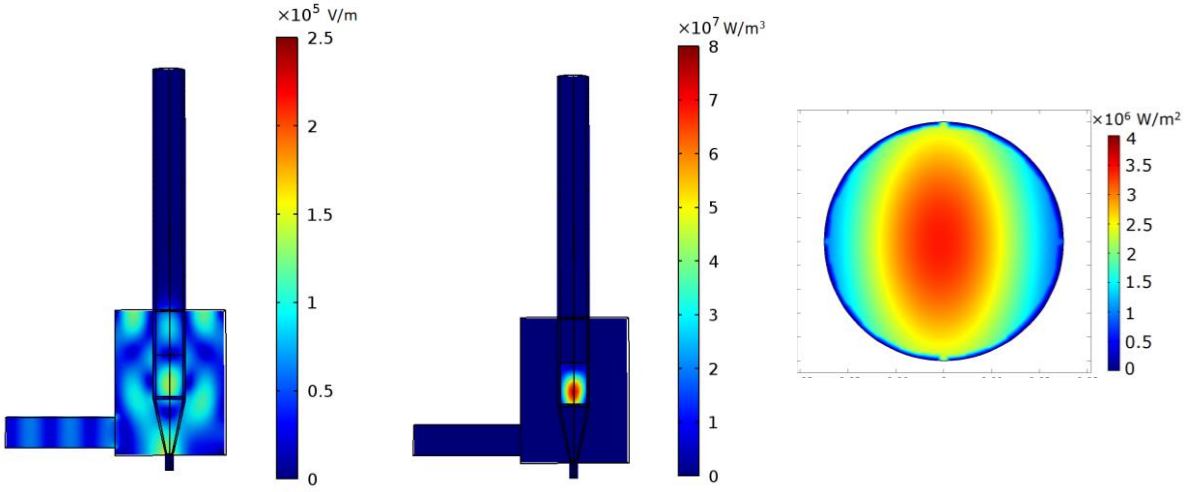

(c) H = 300, W = 240, z = 162.5, y = 20.1

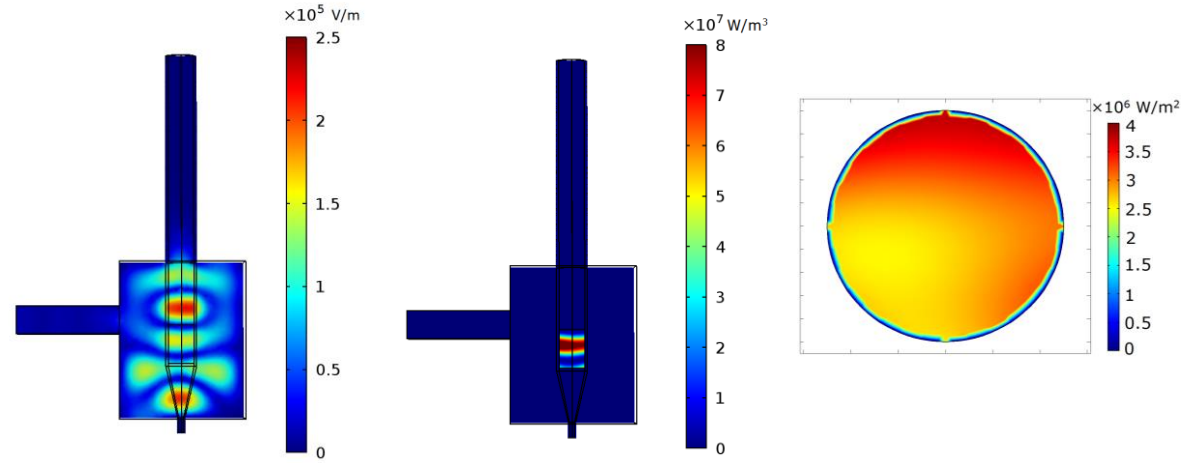

Figure 6-14: Simulation results for selected cases showing electric field intensity (left); power loss density (centre) and projection of the power loss density (right). The dimensions are in millimetres.

It can be seen also from Figure 6-14 that there are always areas of high electric field intensity and others of low field intensity throughout the cavity and within the load. For the present case, achieving uniformity within the load in the radial direction was more important than in the axial direction of the bed. This is because fluidisation provides better mixing in the axial direction. Among the three cases shown in Figure 6-14, Case (c) gives the best homogeneity in the radial direction which can be seen in the projected power loss density in Figure 6-14 (c).

Case (c) has the following values: H = 300, W = 240, y = 20.1 and z = 162.5 with all dimensions in millimetres. The percent absorbed power for this case is 97 % (S_{11} = -15 dB). As can be seen from Figure 6-14 (c), the applied 6 kW power input creates a hot zone at the top half of the bed with power loss density greater than 54 $MW \cdot m^{-3}$ which is the minimum required to achieve pyrolysis at 400^{o}C. Case (c) was, therefore, chosen for the design.

It is important to mention here that chosen case, which is represented by Figure 6-14 (c), has some weaknesses that need to be highlighted. One of these weaknesses comes from the fact that the simulations were performed based on dielectric properties at room temperature. The electric field distribution and power loss density will change when the dielectric properties of the load change during the heating. However, the movement of the particles between the areas of high and low electric field intensity within the bed during their fluidisation can possibly mitigate the effect of any shift in the hotspots.

Another possible challenge is that thermal runaway can occur when char starts to form in the space above the bed, particularly where there is a high electric field intensity as can be seen in Figure 6-14 (c). However, the process can potentially mitigate this issue through three actions: (a) the continuous agitation of the particles by fluidisation; (b) the change in the electric field distribution during the heating with the changes in dielectric properties; and (c) the gas flow could provide enough particle-to-fluid heat transfer to limit the particle temperature at the

hotspots. In addition to these self-mitigations the gas velocity could be increased which would increase the particle-to-fluid heat transfer and limit the maximum achievable particle temperature. However, increasing the gas velocity would increase the heat losses. These weaknesses and challenges will be investigated during the experiments in the developed microwave fluidised bed process.

Figure 6-15 shows a schematic diagram for the proposed microwave fluidised bed process based on the cavity design represented by Figure 6-14 (c). The process consists of a microwave supply and transmission system, a fluidised bed reactor inside a multimode cavity with dimentions based on Figure 6-14 (c), and a condensation system.

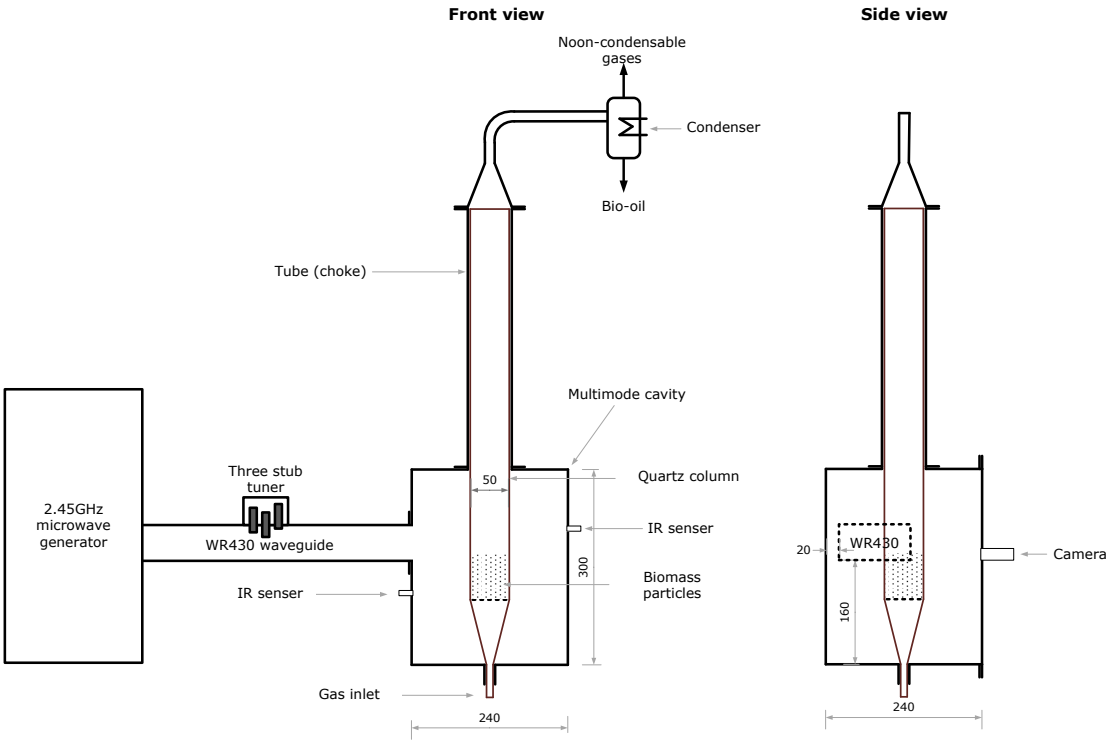

Figure 6-15: A schematic diagram of the developed microwave fluidised bed process. All the dimensions are in millimetres.

The microwave power is provided by a 2.45 GHz generator and transmitted to the cavity through rectangular WR430 waveguides. The waveguide is made of aluminium while the cavity is made of stainless steel 304. Aluminium is the most commonly used material for making microwave waveguides and cavities because of

its high conductivity and low skin depth. Stainless steel was used for the cavity because it provides greater mechanical strength than Aluminium for supporting the fluidised bed column and its contents.

The details of the monitoring and measurement devices, condensation system, and the experimental setup and procedure are discussed in the following Chapter.

6.5 Conclusions

As an attempt to overcome the heating heterogeneity challenge in microwave pyrolysis, a microwave fluidised bed was designed. A systematic approach was followed for the process design taking into account the pyrolysis process requirements, the microwave-material interactions and the fluidisation behaviour of the biomass particles.

Fluidisation experiments were run for biomass materials of different particle sizes in order to study their fluidisation behaviour and to determine their minimum fluidisation velocities. It was found that woody biomass particles have complex fluidisation behaviour due to their irregular shape. Fluidisation was achieved at relatively high velocities with a turbulent behaviour. It was shown that the raw biomass particles have greater values of minimum fluidisation velocity (u_{mf}) compared to char prepared using similar particle size. During processing, this would lead to particle segregation and could be used to control the char deposition and residence time in the bed.

The minimum power density requirement was determined after estimating the enthalpy for pyrolysis using Deferential Scanning Calorimetry (DSC), and then the heat loss to the fluidising gas was included though energy balance calculations. The minimum power density required to reach 400 ^{o}C was found to be 54 MW·m^{-3}.

Electromagnetic simulations were performed to investigate the cavity design. A multimode cavity was chosen based on the lower Q-factor and the heating

homogeneity. However, this design has some possible challenges from a practical standpoint which will be investigated during the experimental studies on the developed process.

7 PYROLYSIS EXPERIMENTS IN A MICROWAVE FLUIDISED BED

7.1 Introduction

The aim of the work reported in this chapter is to operate the microwave fluidised bed process which was developed following the steps discussed in Chapter 6, and run batch pyrolysis experiments to investigate the effect of different processing parameters on the product yield. The effect of the energy input, particle size and the gas velocity on the product yield was studied. The bulk properties of the produced bio-oil were measured and compared to the standard specifications for pyrolysis liquid biofuels. Description of the experiemntal setup and methods for microwave pyrolyis in the developed fluidised bed are detailed in Section 4.5.

7.2 Impedance Matching

The simulation results which were discussed in Section 6.4 as part of the steps of the process deign, suggest that the load would absorb around 97 % of the microwave power input (S_{11} = -15 dB). This was based on several assumptions including dielectric properties at room temperature, homogeneous fluidisation, and a constant generator frequency of 2.45 GHz. However, the dielectric properties do change during heating. Also, any shift in the generator frequency can change the electric field distribution inside the cavity and would, therefore, affect the absorbed microwave power. Figure 7-1 shows the range of frequency measured by the automatic tuner during heating at 5 kW incident power. It can be seen that the frequency fluctuates between 2.466 and 2.473 GHz, and the most dominant frequency is 2.467 GHz. This dominant frequency was used as the basis for the cold matching.

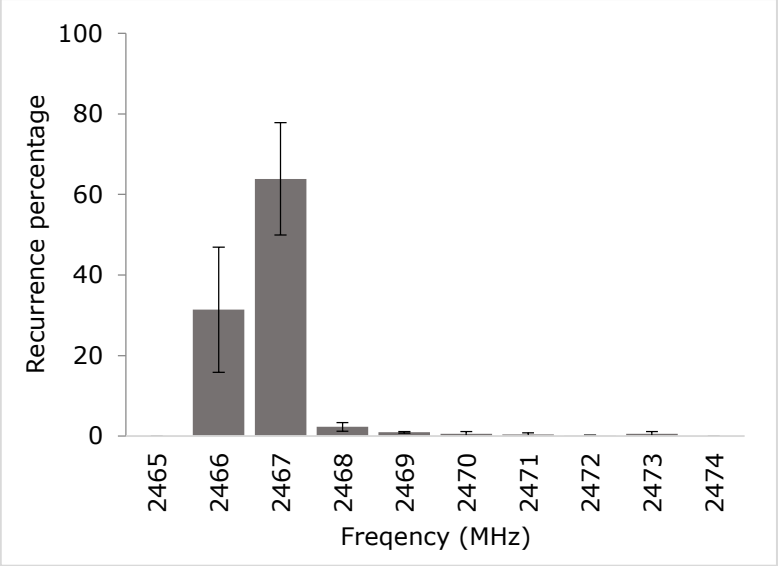

Figure 7-1: Typical frequency distribution at 5kW incident power. The shown results are the average of five runs. The error bars represent the standard uncertainty. The recurrence percentage for each frequency was calculated by dividing the recurrences by the total measured points at each run.

Figure 7-2 shows the reflection parameter, S_{11}, for the fluidised bed at room temperature as a function of frequency before and after the cold matching. The stubs position from the cold matching were used as initial values at the start of the heating process. However, a significant drop in the absorbed power and an increase in the reflected power was observed as soon as the heating started, which was attributed to the change in the dielectric properties.

As an attempt to improve the matching, a trial and error procedure was followed to identify the stub positions that minimise the reflected power throughout the heating. This was achieved by running single-step automatic tuning when the reflected power starts to increase during heating. The stub positions from the single-step tuning in each run was used as an initial position for the next run. This was repeated until the power profile which is shown in Figure 7-5 was obtained. It is to be noted here that it was chosen to keep the stubs position constant during the pyrolysis experiments to achieve a repeatable heating profile. Automatic tuning or one-step tuning leads to different stubs position each time and, therefore, different heating profiles.

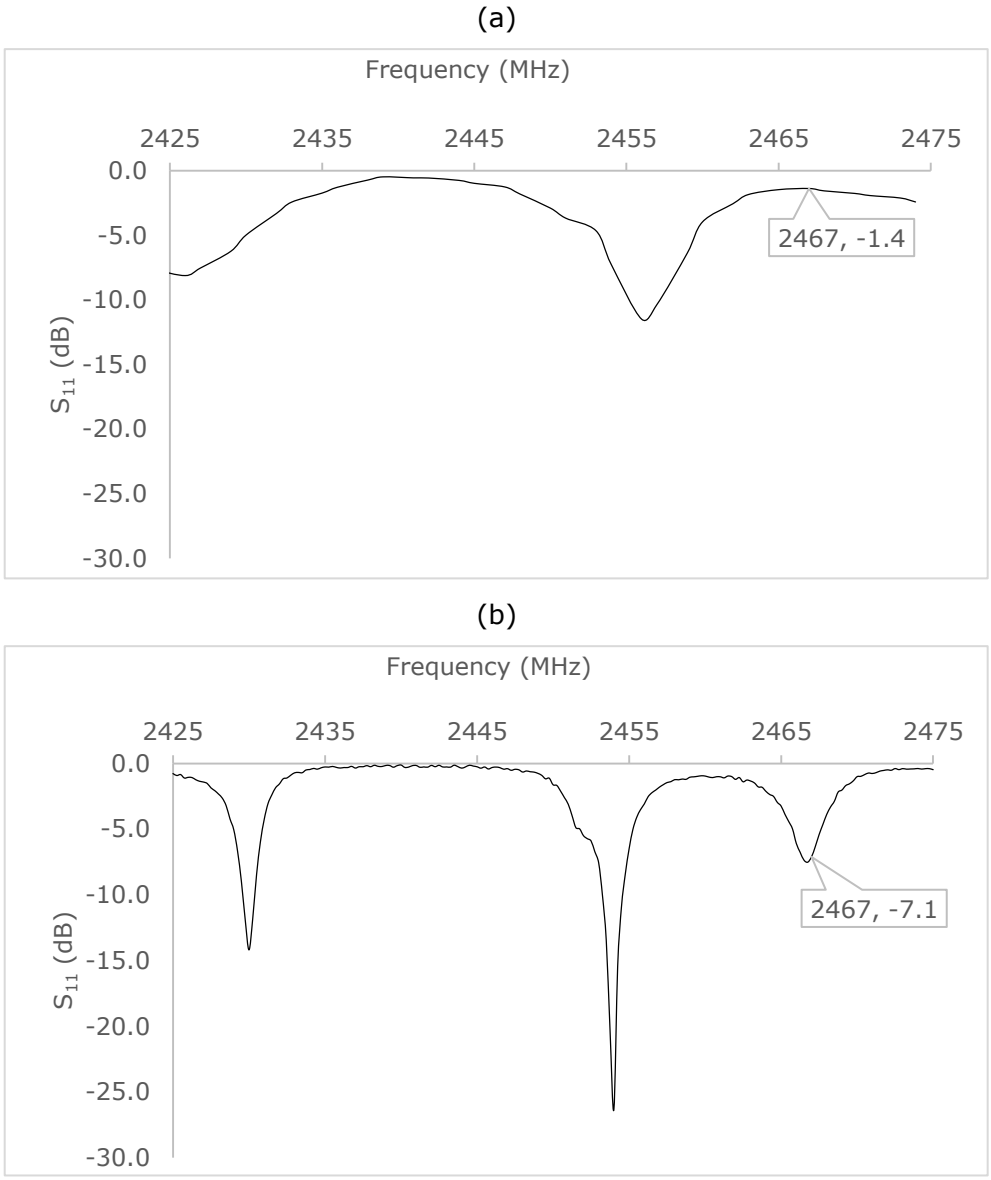

Figure 7-2: The reflection parameter, S_{11}, at different frequencies read by network analyser for 35 g of 212-850 µm sycamore particles fluidised at 0.38 m·s^{-1} nitrogen velocity: (a) Stubs up (unmatched); (b) Cold-matched stubs.

7.3 Preliminary Pyrolysis Experiments

Preliminary microwave pyrolysis experiments were run to identify the boundaries for the processing parameters including the particle size, gas velocity and the bed depth. As a starting point, 35 g of 212 – 850 µm sycamore was used with a fluidising gas velocity of 0.38 m·s^{-1}. These are the values which were used as the basis of the process design.

The minimum fluidisation velocity of the biomass materials involved in this study was determined experimentally at room temperature as shown in Section 6.2. It was shown that the minimum fluidisation of the char particles are lower than that of the raw biomass particles due to the reduction in the particle size and density. Therefore, the gas velocity during the pyrolysis experiments could be set at a value lower than the minimum fluidisation velocity of the raw biomass particles. However, the gas velocity needs to be high enough to induce the fluidisation before the start of char formation at any part of the bed to avoid thermal runaway.

The possibility of thermal runaway could always be decreased by applying higher gas velocities. However, too high a gas velocity would lead to entrainment by the fluidising gas, leaving the biomass unpyrolysed. It is to be noted here that the evolved vapours during the pyrolysis process could affect the fluidisation behaviour and shift the minimum fluidisation velocity as they contribute to the total gas flow through the bed.

From the above discussion, for each particle size group at a certain incident power, the gas velocity should be set between two limiting values. A higher value, above which untreated biomass particles would be entrained by the fluidising gas and the pyrolysis vapours, and a lower value below which the gas velocity is not high enough for the fluidisation to be induced before thermal runaway. These limiting values are higher for larger particles and lower for smaller particles, and they limit the range of particle size that could be used at any power density. Examples of the effect of operating beyond these limiting values are displayed in Figure 7-3.

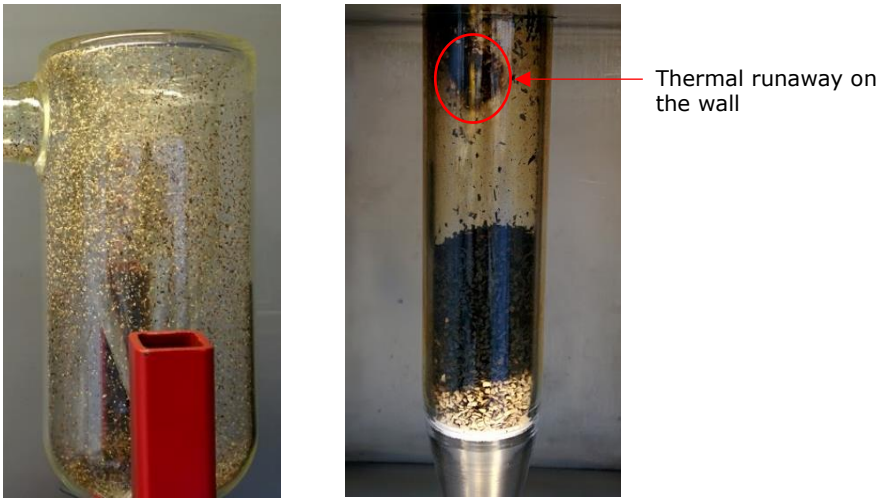

Figure 7-3: Limiting values for the gas velocity: (a) too high velocity leading to entrainment of un-pyrolysed particles to the condensers; (b) too low leading to thermal runaway due to poor mixing (no fluidisation).

The boundaries mentioned above were applied to set the gas velocity for each particle size group. For sycamore, it was found that for the 212 – 850 μm particle size at 5 kW power input, the minimum gas velocity below which thermal runaway takes place was 0.38 $m \cdot s^{-1}$. However, this gas velocity lead also to the entrainment of a significant amount of unpyrolysed particles as shown in Figure 7-3 (a). In order to stop the entrainment of unpyrolysed particles, a narrower particle size range of 0.6 – 0.85 mm was used by filtering out the finer particles.

During the preliminary pyrolysis experiments, thermal runaway occurred at many occasions on the reactor wall even at gas velocities higher than the minimum fluidisation velocity of the raw biomass particles. This was attributed to the condensation of the pyrolysis vapours on the wall above the bed creating a "dirty" zone where some solid particles were stuck to the wall of the column. At the areas of high electric field intensity, these stuck particles are heated very rapidly, leading to thermal runaway as shown in Figure 7-4 (a). To overcome this and to reduce thermal runaway possibilities, the size of the bed was increased by doubling the quantity of the initial raw biomass particles to 70 g. This led to an increase in the bed height during fluidisation shifting that "dirty" zone outside the cavity as shown

in Figure 7-4 (b) where there are no areas of high electric field intensity. The continuous movement of the particles within the bed area acts as a physical sweeper, preventing the particles and condensate from sticking to the wall.

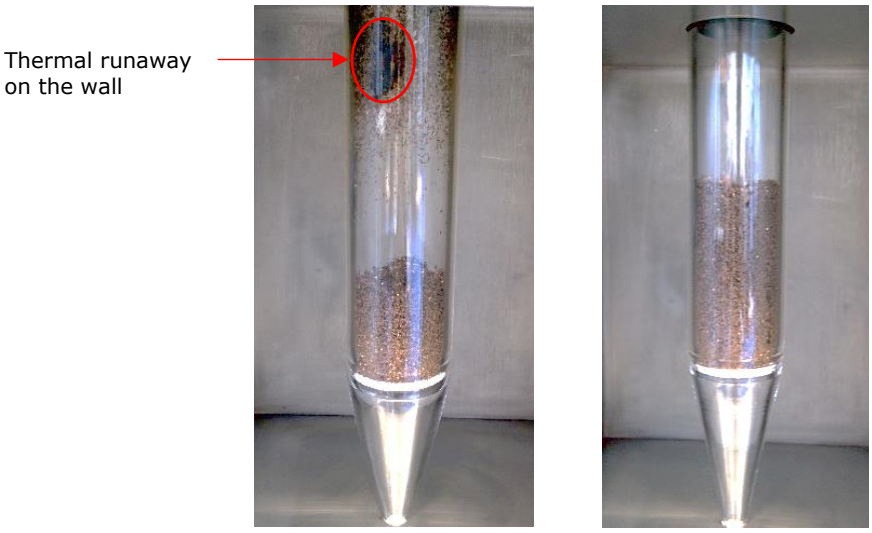

(a) (b)

Figure 7-4: Effect of the bed height on controlling thermal runaway: (a) 35 g raw sycamore particles initially; (b) 70 g raw sycamore particles initially.

7.4 Analysis of the Absorbed Power

The absorbed power profile during the microwave heating can be related to the change in the dielectric properties of the biomass materials with temperature. It was shown in Section 5.4 that the loss factor of biomass materials decreases with temperature until it reaches a minimum value at around 300 °C to 400 °C. Above 400 °C the loss factor increases sharply with temperature due to char formation.

Figure 7-5 shows the change in the absorbed power with time during the microwave pyrolysis at 5 kW incident power and 0.38 $m \cdot s^{-1}$ gas velocity. The displayed results are from five different runs with different heating time, four of them with 1.18 – 1.70 mm particle size and one with 1.70 – 2.36 mm particle size where thermal runaway took place.

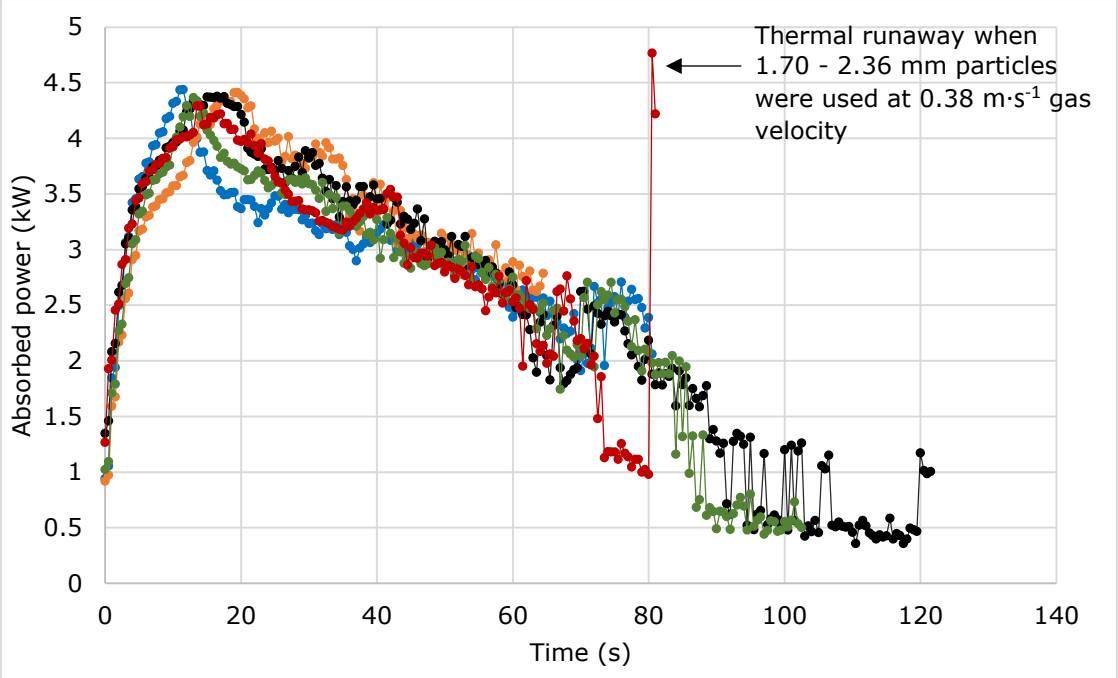

Figure 7-5: Change in the absorbed power during microwave pyrolysis of 70g sycamore of particle size 1.18 – 1.70 mm at 5kW incident power and 0.38 m·s^{-1} gas velocity. Thermal runaway took place when 1.70 – 2.36 mm particles were used as indicated.

The low absorbed power during the first five seconds of the heating could be attributed to the instability in the generator frequency at the start of the heating. After reaching a maximum value, the absorbed power starts to decrease gradually with time until it reaches a minimum value after about 90 seconds. This drop in the absorbed power can be attributed to the drop in the loss factor of the biomass particles with temperature. Another factor which could have a significant contribution towards the drop in the absorbed power is the bed expansion and the increase in the void fraction due to the reduction in the particle size and density. A large fluctuation in the absorbed power can be seen in Figure 7-5 after 60 seconds of the heating, which suggests the process is entering a region of turbulent fluidisation. After about 90 seconds of heating, the absorbed power in the case of the 1.18 – 1.70 mm particles reaches a constant minimum value where an equilibrium is reached between the absorbed power and the heat losses. This equilibrium point is important for controlling the bed temperature to avoid slipping

into the increased loss factor zone above 400 °C where the possibility of thermal runaway increases.

Figure 7-5 also shows the heating profile for a run where thermal runaway took place when the particle size was increased to 1.70 – 2.36 mm for the same gas velocity. As indicated in Figure 7-5, the thermal runaway is accompanied by a sharp increase in the absorbed power.

7.5 Effect of the Processing Parameters on the Product Yield for Sycamore

7.5.1 Effect of particle size

The effect of particle size on the extent of pyrolysis was studied for sycamore particles and the results are listed in Table 7-1. As can be seen in Table 7-1, the solid pyrolysed increases with increasing particle size at a constant energy input.

Table 7-1: Effect of the particle size on the degree of pyrolysis at 3.5 kJ·g^{-1} specific energy

Particle size range	Gas velocity (m·s^{-1})	Solid pyrolysed (%)
0.6 – 0.85 mm	0.38	42.15 ± 2.21
0.85 – 1.18 mm	0.38	53.61 ± 0.62
1.18 – 1.70 mm	0.38	59.08 ± 0.68
1.70 – 2.36 mm	0.59	60.13 ± 0.69

Increasing the particle size decreases the gas-particle contact area leading to a reduction in the heat loss to the fluidising gas. This results in an increase in the temperature at the centre of the particles allowing for more solid to be pyrolysed. The relationship between the particle size and the solid pyrolysed obtained from the batch experiments is in line with the results from the numerical model discussed in Section 6.3. It was shown through numerical modelling that increasing the particle size of the biomass material leads to reduction in the power density needed to reach the pyrolysis temperature, meaning that increasing the particle size at a given

power density would result in an increase in the particle temperature and therefore an increase the degree of pyrolysis.

As can be seen in Table 7-1, there is no significant increase in the solid pyrolysed when the particle size was increased from 1.18 - 1.70 mm to 1.70 - 2.36 mm compared to the changes between the other particle size groups. This can be attributed to the increase in the gas velocity for the 1.70 – 2.36 mm particle size group which required higher gas velocity than the other groups to be pyrolysed without thermal runaway.

The relationship between the particle size and the product yield in conventionally heated fluidised bed systems is different. Previously, Shen et al. (2009) studied the effect of the particle size on the pyrolysis of wood particles in a fluidised bed reactor heated in an electric furnace at 500 ^{o}C using preheated nitrogen as the fluidising gas. They found that the bio-oil yield decreased when the particle size was increased from 0.3 to 1.5 mm. This drop in the yield with the particle size was regarded to the reduction in the heat transfer rate for the larger particles. A similar relationship between oil yield and particle size was reported by other authors (Choi et al., 2012; Montoya et al., 2015).

This difference in the effect of particle size on the product yield between the microwave and conventionally heated fluidised bed systems is mainly because of the difference in the direction of heat transfer. In conventionally heated systems, the heat is transferred from the fluidising gas to the particles. The extent of pyrolysis in this case is improved by reducing the particle size as it increases the specific surface area and, therefore, increases the heat transfer rate to the particles. While in the microwave heated system, where cold fluidising gas is used, the heat is transferred from the biomass particles to the gas. Using larger particles is, therefore, favoured as it reduces the heat losses to the fluidising gas resulting in an improvement in the extent of pyrolysis at a cetrain energy input.

7.5.2 Effect of gas velocity

Figure 7-6 shows the effect of the gas velocity on the degree of pyrolysis for 1.18 - 1.70 mm sycamore particles at 3.5 kJ·g^{-1} specific energy. It can be seen that increasing the gas velocity from 0.38 m·s^{-1} to 0.64 m·s^{-1} results in a limited drop in the solid pyrolysed.

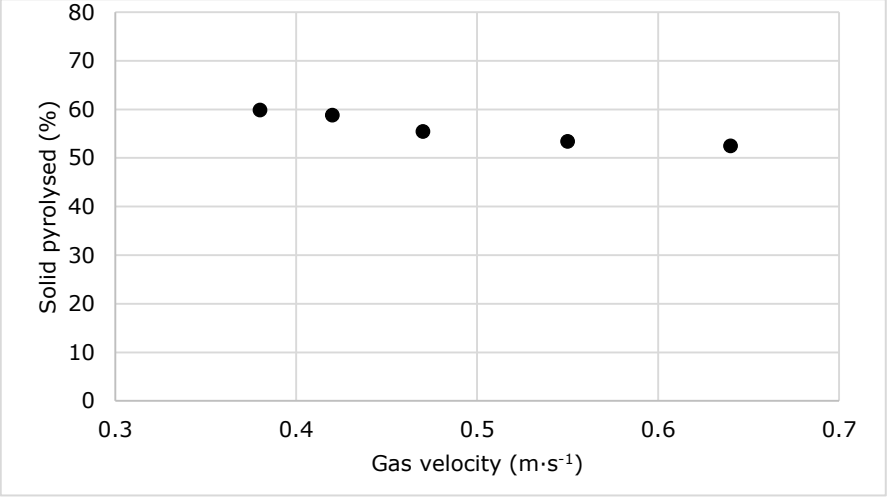

Figure 7-6: Effect of the fluidising gas velocity on the solid pyrolysed for 1.18 – 1.70 mm sycamore particles at 3.5 kJ·g^{-1} specific energy.

The reduction in the solid pyrolysed with the gas velocity was expected because the fluidising gas is fed at room temperature, and increasing the gas velocity increases the heat losses to the fluidising gas. However, it can be seen that only 12 % reduction in the solid pyrolysed for about 68 % increases in the gas velocity.

This limited reduction in the solid pyrolysed compared to the large increase in the gas velocity provides flexibility for using the gas velocity for controlling the other processing parameters including the bed temperature and the solids residence time in the case of continuous processing.

In conventionally heated fluidised bed systems, where the gas is preheated to provide all or part of the energy required for pyrolysis, the relationship between the gas velocity and the product yield is different to that shown in Figure 7-6. Choi et al. (2012) showed that the bio-oil yield in a fluidised bed reactor heated in an electric furnace increases when the preheated gas velocity is increased up to a certain value

beyond which the oil yield starts to decrease. The initial increase in the product yield with the gas velocity was explained by the improvement in the heat transfer rate due to the better mixing provided by the faster-moving bubbles. The following reduction in the bio-oil yield at higher gas velocities was attributed to the formation of large bubbles (slugging) leading to poorer heat transfer. The explanation provided by Choi et al. (2012) for the deterioration in the heat transfer at high gas velocities could be used understand the limited drop in the solid pyrolysed with increasing the gas velocity in the present study especially at higher gas velocities as can be seen in Figure 7-6.

7.5.3 Effect of energy input

The effect of the specific energy input on the degree of pyrolysis was studied for various particle size groups of sycamore. Figure 7-7 shows that the solid pyrolysed increases steadily with the specific energy up to nearly 70 % depending on the particle size.

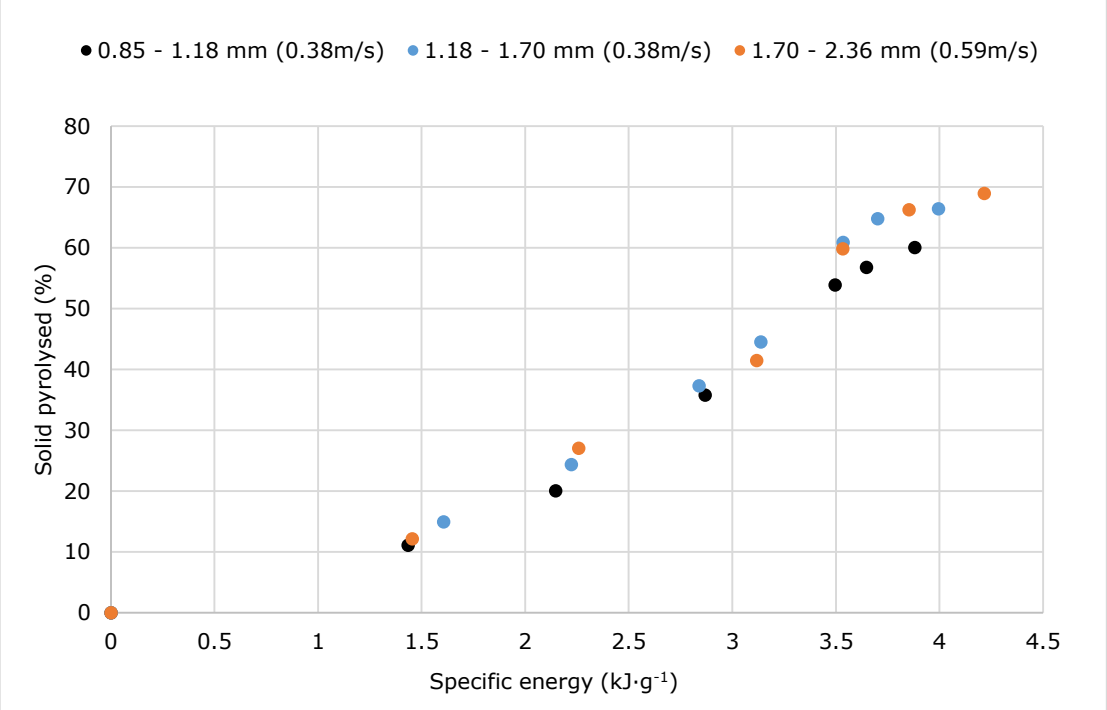

Figure 7-7: Increase in the degree of pyrolysis with the specific energy for sycamore of different particle size at 5 kW incident power. The gas velocity is indicated between brackets.

The extent to which the solid pyrolysed increases with the specific energy is restricted by the drop in the absorber power as shown in Figure 7-5 which was explained by the reduction in the loss factor of the particle and the increase in the bed porosity.

Figure 7-7 shows that around 3.5 to 4.2 $kJ \cdot g^{-1}$ energy input is needed to achieve 60 to 70 % solid pyrolysis. Previously, Robinson et al. (2015) showed that the energy required to reach the same degree of pyrolysis in a microwave heated fixed bed reactor is around 2.2 to 2.5 $kJ \cdot g^{-1}$.

The high specific energy in the fluidised bed system compared to the fixed bed system is mainly because of the heat loss to the fluidising gas, which is fed at room temperature. It was shown in Section 6.3 that the enthalpy for pyrolysis, which excludes any heat losses, of sycamore at 400 ^{o}C is about 0.88 $kJ \cdot g^{-1}$ (Table 5-4). However, it was shown through the numerical modelling in the same section that the specific energy required to pyrolysis 600 µm sycamore particles in the fluidised bed system can range from 1.07 $kJ \cdot g^{-1}$ to 4.85 $kJ \cdot g^{-1}$ (Table 5-5) depending on the power density. The high specific energy in the fluidised bed system compared to the enthalpy for pyrolysis was attributed to the heat losses to the fluidising gas.

7.6 Pyrolysis Experiments for the Other Biomass Materials

7.6.1 Pine

As discussed earlier in Section 6.2, pine particles are more difficult to fluidise than the sycamore particles due to their highly irregular shape, which results in channelling and/or slugging behaviour at lower gas velocities. The cold fluidisation experiments also showed that pine particles require higher fluidisation velocities compared to sycamore, leading to a very turbulent fluidisation regime.

Due to the complex fluidisation behaviour of the pine particles compared to sycamore, applying the same pyrolysis conditions which were used for sycamore led to thermal runaway on the wall of the column as shown in Figure 7-8.

Figure 7-8: Non-fluidising pine particles leading to thermal runaway; particle size = 1.18-1.70 mm pine; initial mass = 70 g; gas velocity = 0.59 $m \cdot s^{-1}$.

As an attempt to improve the fluidisation behaviour of the pine particles, stop the thermal runaway, and provide repeatable results, modifications were made to the processing parameters as follows:

- Using larger particle size, larger than 1.70 mm. It was shown in Section 6.2 that increasing the size of the pine particles improves its fluidisation behaviour due to the decline in the influence of the particle shape compared to the effect of its size and weight.
- Increasing the gas velocity. This was necessary to fluidise the larger particles which were used.
- Reducing the amount of biomass feed. Pine has a bulk density lower than sycamore and using 50 g pine was found to give nearly the same bed high as 70 g of sycamore. Reducing the bed size was found to improve the stability of the fluidisation.

After these modifications, it was possible to run the pyrolysis experiment for two particle size groups of pine which were 1.70 - 2.36 mm and 2.36 - 3.35 mm with a gas velocity of 0.85 $m \cdot s^{-1}$ in both cases. These conditions allowed for running the pyrolysis experiments in the stable region between the two boundaries of thermal runaway at low gas velocities and particle entrainment and high gas velocity.

Figure 7-9 shows the increase in the degree of pyrolysis with specific energy input for the two studied particle size groups. The solid pyrolysed increases steadily with the specific energy up to a point beyond which no significant increase in the degree of pyrolysis with the specific energy. Similar to sycamore, the extent to which the solid pyrolysed increases with the specific energy is restricted by the drop in the absorbed power as shown in Figure 7-5.

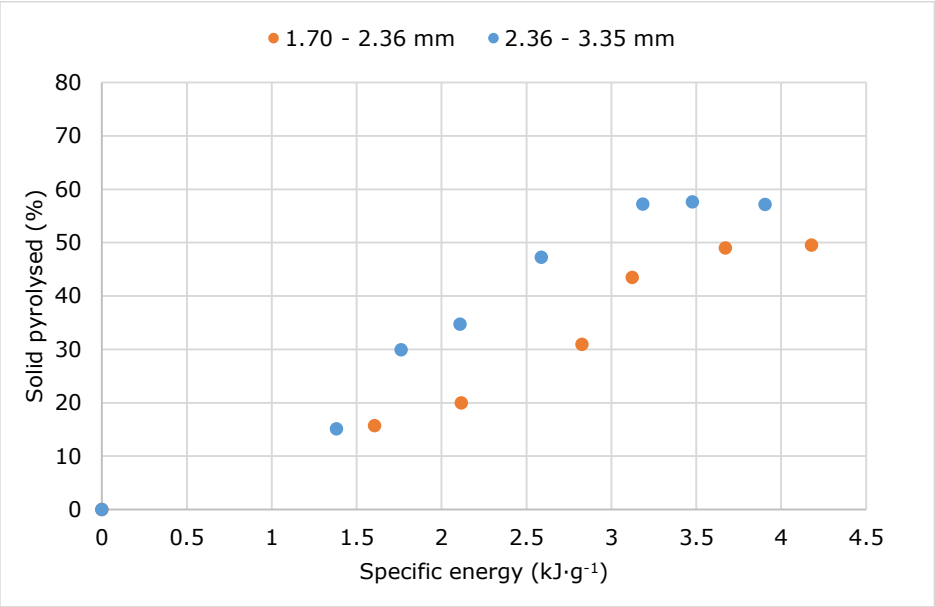

Figure 7-9: Increase in the degree of pyrolysis with the specific energy for pine of different particle size under 5 kW incident power and 0.85 m·s^{-1} gas velocity.

Figure 7-9 shows that, as for sycamore, increasing the particle size increases the degree of pyrolysis. It can be noted that the solid pyrolysed from the pine particles is lower than that obtained from the sycamore at the same specific energy. For example, only 50 % of the 1.70 – 2.36 mm pine is pyrolysed at a specific energy of about 4 kJ·g^{-1}, while over 65 % sycamore of similar particle size was pyrolysed when the same specific energy was applied as shown in Figure 7-7. This lower degree of pyrolysis in the case of pine can be attributed to the higher gas velocity used to fluidise the particles leading to an increase in the heat loss to the gas and, therefore, a decrease in the temperature at the centre of the particle.

7.6.2 Seaweed

The pyrolysis of seaweed in the developed microwave fluidised bed was also investigated. The cold fluidisation experiments discussed in Section 6.2, showed that the seaweed particles have more homogeneous fluidisation behaviour compared to the woody biomass over the studied range of particle size. However, it was much more difficult to limit the thermal runaway in the pyrolysis experiments of the seaweed. Unlike the woody biomass, the thermal runaway in the case of seaweed was because of particles sticking to the walls of the reactor within the fluidisation area as shown in Figure 7-10. Part of the vapours produced during the pyrolysis the seaweed condenses on the wall within the bed allowing the particles to stick to the wall of the reactor. The fluidising particles were not able to sweep the wall and remove the sticking particle in the case of woody biomass because they were strongly bound to the wall. Thermal runaway appeared in the three studied particle size groups of seaweed which were 0.60 – 0.85 mm, 0.85 – 1.18 mm, and 1.18 – 1.70 mm. Even increasing the gas velocity to values where unpyrolysed particles were entrained did not stop the thermal runaway.

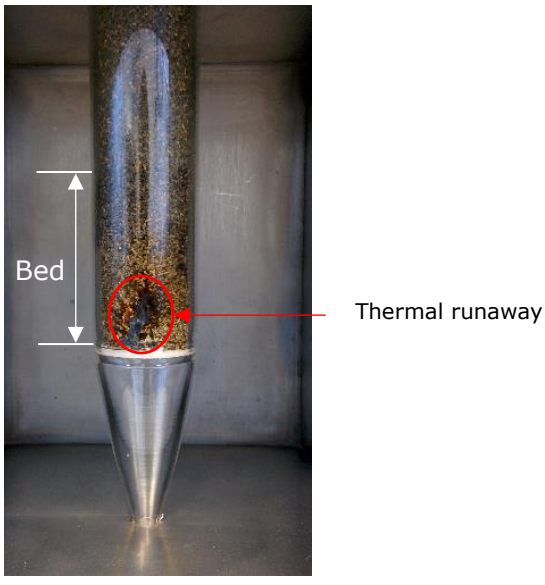

Figure 7-10: Thermal runaway during seaweed pyrolysis due to vapours condensation within the bed leading to seaweed particles sticking to the wall. This case was for 0.85 – 1.18 mm particle size and a gas velocity of 0.68 $m \cdot s^{-1}$.

It was, therefore, difficult to run the pyrolysis experiments successfully for seaweed with the current setup. One of the possible solutions to stop the particles from sticking to the wall is to use a hot fluidising gas. The vapours start condensation within the bed because of the cold environment surrounding the particles, and preheating the gas would help to limit condensation. However, the process design and the experimental setup in the present study did not include the option of preheating the fluidising gas. Future studies should explore this option and investigate the optimum gas temperature that would stop the vapour condensation within the bed and preserve the product quality at the same time.

7.7 Product Quality

The bulk properties of the bio-oil produced from sycamore were measured, and the results are listed in Table 7-2. The same table shows the corresponding values for bio-oil obtained in a conventionally heated fluidised bed process, the ASTM standard specification for pyrolysis liquid biofuels, and standard values for a petroleum-based heavy fuel.

Table 7-2: Bulk properties of bio-oil obtained from sycamore with 60 – 70 % solid pyrolysed. The results are from at least four repeats.

Property	**Measured value**	**Conventional pyrolysis [a]**	**ASTM D7544 [b]**	**HFO [c]**
Water content, wt%	25.06 ± 3.36	23.3	≤30	0.5 (vol%)
Density (20°C), g·cm^{-3}	1.15 ± 0.04	1.20	1.1 – 1.3	>0.876
Viscosity (20°C), cp Kinematic viscosity, mm^2·s^{-1}	23.08 ± 1.98 20.07±1.98 [d]	87.6 73	- ≤125 [e]	- 1.9 – 5.5
Gross calorific value, kJ·g^{-1}	17.5 ± 2.3	16.6	≥15	40 [f]

[a] Bio-oil produced from wood pyrolysis (2.4 % moisture) in a conventionally heated fluidised bed reactor. The data were taken from (Oasmaa et al., 2005)
[b] ASTM standard specification for Grade D and Grade G pyrolysis liquid biofuels.
[c] Heavy Fuel Oil. The values are based on ASTM D396 - 15c specifications for Grades No. 4 (Light) which is a heavy distillate fuel or middle distillate/residual fuel blend used in commercial/industrial burners equipped for this viscosity range with no preheating.
[d] Calculated from the density and viscosity.
[e] Based on measurement at 40 °C. The viscosity in the present study was measured at 20 °C and it is still lower than the value required by the standard.
[f] Typical value for heavy fuel oil (Lehto et al., 2014; Oasmaa et al., 2015).

Table 7-2 shows that all the measured properties are within the limits required by the ASTM standard for pyrolysis liquid biofuels. It also shows that, with the exception of viscosity, the measured bio-oil properties from this study are similar to those obtained from conventionally heated fluidised bed process. It is to be noted that the wood used in the conventionally heated process is pre-dried to 2.4 % while the moisture content of the wood in the present study was 10.6 %. Even with this higher moisture content of the feed, the bio-oil obtained in the present study has a water content similar to that obtained from conventional pyrolysis. The viscosity of the bio-oil obtained from the present study is significantly lower than that from the conventionally heated process.

As shown in Table 7-2 the produced bio-oil fails to meet the standard specifications for heavy fuel oils and, therefore, it cannot be fed to the commercial burners designed for heavy fuel oils. Bio-oil has a higher moisture content and higher viscosity compared to the heavy fuel oils. It also has very low calorific value compared to petroleum-based fuels.

7.8 Discussion and Conclusions

The developed microwave fluidised bed system was operated successfully and used for the pyrolysis of sycamore and pine particles. It was possible with the current system to achieve homogeneous pyrolysis for up to 70 g biomass particles. For each particle size group, the gas velocity was set between two limiting values, a higher value, above which unpyrolysed particles are entrained with the fluidising gas, and a lower value below which thermal runaway takes place before fluidisation. The movement of the particles within the bed acted as a sweeper preventing the solid particles from sticking to the wall of the reactor. However, for the seaweed, a layer of solid particles was formed on the wall of the reactor during pyrolysis due to the condensation of a significant amount of pyrolysis vapours within the bed which led to thermal runaway. The fluidising particles were not able to clean the wall because

that the sticking particles were strongly bound to the wall through the viscous condensed liquid.

It was shown in the study that increasing the particle size of the biomass particles increases the solid pyrolysed at a certain specific energy input. This was attributed to the reduction in the heat losses to the fluidising gas which is caused by the reduction in the specific surface area of the particles. Processing larger biomass particles adds the advantage of reducing the energy costs for crushing the raw feedstock. However, the extent to which the particle size could be increased is restricted by the ability of the particles to fluidise.

The energy consumption in the current microwave fluidised bed system was found to be higher than that obtained previously by Robinson et al. (2015) in a fixed bed reactor which was 2.2 to 2.5 $kJ \cdot g^{-1}$ for 60-70 % solid pyrolysis compared to 3.5 to 4.2 $kJ \cdot g^{-1}$ in the present study. This was attributed to the heat loss to the fluidising gas which was fed at room temperature. The unique advantage of the developed fluidised bed process is that it can process larger feed sizes than the fixed bed system which had failed to control the thermal runaway and provide homogeneous heating for samples size larger than 1.5 cm (around 5 g) as shown by Robinson et al. (2015). The other advantage of the present microwave fluidised bed system is that it is scalable, and the bed temperature and the solid residence time could be controlled by changing the gas velocity.

There is a lack of published data about the energy consumption in the pyrolysis reactor including heat losses in a commercial-scale systems. However, Bridgwater (2012) estimated that the pyrolysis process requires about 15 % of the energy in the biomass feed. Woods have a gross calorific value of about 18 to 20.5 $kJ \cdot g^{-1}$ (Günther et al., 2012). Therefore, based on the 15 % figure, around 2.7 to 3.1 $kJ \cdot g^{-1}$ could be considered an acceptable range of energy consumption for wood pyrolysis. It is clear that that energy consumption in the current microwave fluidised bed system (3.5 to 4.2 $kJ \cdot g^{-1}$ for sycamore) is higher than this range.

However, with some improvements in the process the energy consumption could be significantly reduced. These improvements could include preheating the fluidising gas which would reduce the heat loss to the gas. However, this would increase the capital cost for the heaters. Applying higher power density would also reduce the heating time and, therefore, reduce the heat losses as shown through the theoretical models in Section 6.3. However, increasing the power density and preheating the gas would make it more difficult to control the bed temperature and avoid thermal runaway. Applying higher electric field intensities need to yield higher power densities increases the probability of electric field breakdown within the cavity, which could subsequently damage the reactor.

It is to be noted here that the specific energy presented in this study was based on the absorbed microwave power. However, as shown in Figure 7-5 there is a significant amount of reflected power which vary with time ranging between 10 % and up to around 90 % of the incident power at the late stages of pyrolysis when the loss factor of the bed drops. This large variations in the reflected power are associated with batch processing and could be controlled in the case of continuous processing where the system could be matched based on the steady-state conditions to minimise the reflected power.

Table 7-3 summarises the advantages and limitations of the developed microwave-heated fluidised bed system compared to conventionally-heated fluidised bed process for biomass pyrolysis.

Table 7-3: Summary of the advantages and limitations of microwave heated fluidised bed process compared to conventionally heated process for biomass pyrolysis.

Microwave-heated fluidised bed	**Conventionally-heated fluidised bed**
The current study presented a batch system with only 70 g feed. Needs further research and development to put the technology on track for scaling-up.	Already at commercial scale. Recently, a 10 tonne per day plant has been built in Finland (Oasmaa et al., 2015)
The energy consumption for pyrolysis in the present study was around 3.5 to 4.2 $kJ \cdot g^{-1}$. However, the system can be optimised to minimise energy consumption.	Energy requirement is estimated at around 2.7 – 3.1 $kJ \cdot g^{-1}$ for woody biomass.
Does not require heating medium as the microwave energy is directly absorbed by the biomass material.	Requires a heating medium (hot gas and or hot sand) for heat transfer. This adds capital and operation cost for handling and recirculating this medium in the process.
The gas can be fed at room temperature generating a cold environment around the particle. This limits the unwanted secondary degradation reaction.	The gas has to be at temperature higher than that of the particles to allow for heat transfer. This promotes secondary degradations.
Increasing the particle size improves the degree of pyrolysis. This allows for using larger particles, reducing the energy needed for crushing and preparation.	Smaller particles are needed to improve the heat transfer from the heating source/medium to the particles.

One of the common disadvantages of fluidised bed systems, in general, is the limitations with regards to the particle size and shape. It was shown in the present study that pine particles are more difficult to be pyrolysed compared to sycamore particles mainly because of the highly irregular shape of the softwood. A lower degree of pyrolysis was achieved for pine compared to sycamore due to the high gas velocity needed to fluidise the pine particles. It is clear that with the current setup, it would be even more difficult to process more irregular-shape biomass

particles such as straws. However, adding another inert solid to the system could be used to assist the fluidisation and allow a wider range of particle size and shape to be processed. This inert solid needs to be transparent to the microwaves.

The developed microwave fluidised bed process has shown an ability to overcome many of the challenges associated with microwave pyrolysis of biomass including the improvement in heating uniformity and the ability to control the solid deposition in the process, placing it as a viable candidate for scaling-up. However, it has some weaknesses including its limitation with regards to the shape and size of the biomass material and the difficulty to prevent particles from sticking to the wall during processing which can lead to thermal runaway as shown earlier with the seaweed. Another weakness is the need for high quantity of inert gas for fluidisation which increase the size and duty of the condenser needed for condensing the pyrolysis vapours.

One of the possible ways to overcome these weaknesses is to replace the gas with an inert liquid to provide the inert atmosphere needed for the pyrolysis. The liquid needs to transparent to the microwaves to allow for selectively heating the biomass material.

The liquid system can provide many advantages over the gas-based systems. It can help limit the implications of any thermal runaway that may happen during heating as the liquid can prevent the formed char from sticking to the wall of the reactor. The presence of the liquid can also limit the possibility of electric field breakdown as the electric breakdown voltage of liquids in general is substantially greater than that of gases (Wong and Forster, 1982). The liquid system would require less condensation duty compared to the gas system as the condensation of the pyrolysis vapours can take place within the liquid. The condenser would be needed only for condensation and recycle of any evaporated solvent. The liquid can provide more flexibility in terms of the shape and size of the biomass material as the fluidisation

and flow in liquids is more homogenous and more predictable in the liquids compared to the gases (Richardson et al., 2002).

The following chapter is dedicated for investigating the feasibility of microwave pyrolysis in an inert liquid where the proposed liquid system will be discussed in more details. The feasibility of the system will initially be investigated theoretically including numerical modelling of the heat transfer which will be followed by batch microwave pyrolysis experiments.

8 MICROWAVE PYROLYSIS IN A LIQUID SYSTEM

8.1 Introduction

This chapter investigates the microwave pyrolysis of biomass in a liquid system. The proposed system uses liquid instead of gas to provide the inert atmosphere required for the pyrolysis reaction. The biomass material is to be selectively heated by the microwaves while submerged in the cold liquid. The liquid system can provide many advantages over the gas-based systems. It can help limit the implications of any thermal runaway that may happen during heating as the liquid can prevent the formed char from sticking to the wall of the reactor. The presence of the liquid can also limit the possibility of electric field breakdown as the electric breakdown of liquids in general is substantially greater than that of gases (Wong and Forster, 1982). This would give an extra space for increasing the electric field intensity in the reactor and, therefore, increasing the heating rate. When considering continuous processing, the liquid system would require less condensation duty compared to the gas system as the condensation of the pyrolysis vapours can take place within the liquid. The condenser would be needed only for condensation and recycle of any evaporated solvent.

The liquid used in the process needs to have certain qualities. It should be inert with regards to the pyrolysis reaction. It should also be transparent to the electromagnetic field to allow for selectively heating the biomass material without losing energy for heating its environment. Aliphatic and aromatic hydrocarbons are examples of low loss materials (Metaxas and Meredith, 1983; Robinson et al., 2014) that could be used for the current application. The oxygen content of the bio-oil makes it immiscible with the hydrocarbon liquids (Bridgwater, 2003; Zhang et al., 2007). This allows for separating the produced bio-oil from the inert liquid through decantation. The boiling point of the liquid is an important factor as the bulk temperature of the liquid during processing will be at or below its boiling point. The

liquid temperature will have a significant influence on the temperature on the surface of the biomass material and the heat flow from the biomass material.

The aim of this chapter was to investigate the microwave pyrolysis of biomass in a liquid system through batch pyrolysis experiments. First, the dielectric properties of these liquids and their temperature dependencies were studied. The effect of the particle size, the applied power, and the energy input on the degree of pyrolysis was investigated. The effect of using different hydrocarbon liquids with different boiling points on the degree of pyrolysis was also explored. The degree of pyrolysis and energy consumption obtained from the liquid system were compared with the fluidised bed process. However, before moving to the experimental part, the energy requirement for pyrolysis in the liquid system and the temperature gradient within the particle were studied through numerical modelling of the heat transfer within the system.

8.2 Heat Transfer in the Liquid System

8.2.1 Background

The heat transfer in the microwave pyrolysis of biomass submerged in a liquid can be understood through pool boiling mechanisms. Pool boiling is a type of boiling in which a heating surface is submerged in a relatively large body of stagnant liquid agitated by the motion of the bubbles (Green and Perry, 2007).

Pool boiling is commonly divided into four main boiling regions/regimes according to the heat flux which is a function of the difference between the hot surface temperature and the liquid saturation temperature. These regions/regimes as shown in Figure 8-1 are natural convection, nucleate boiling, transition boiling and film boiling. They are described as follows (Coulson et al., 1999; Green and Perry, 2007):

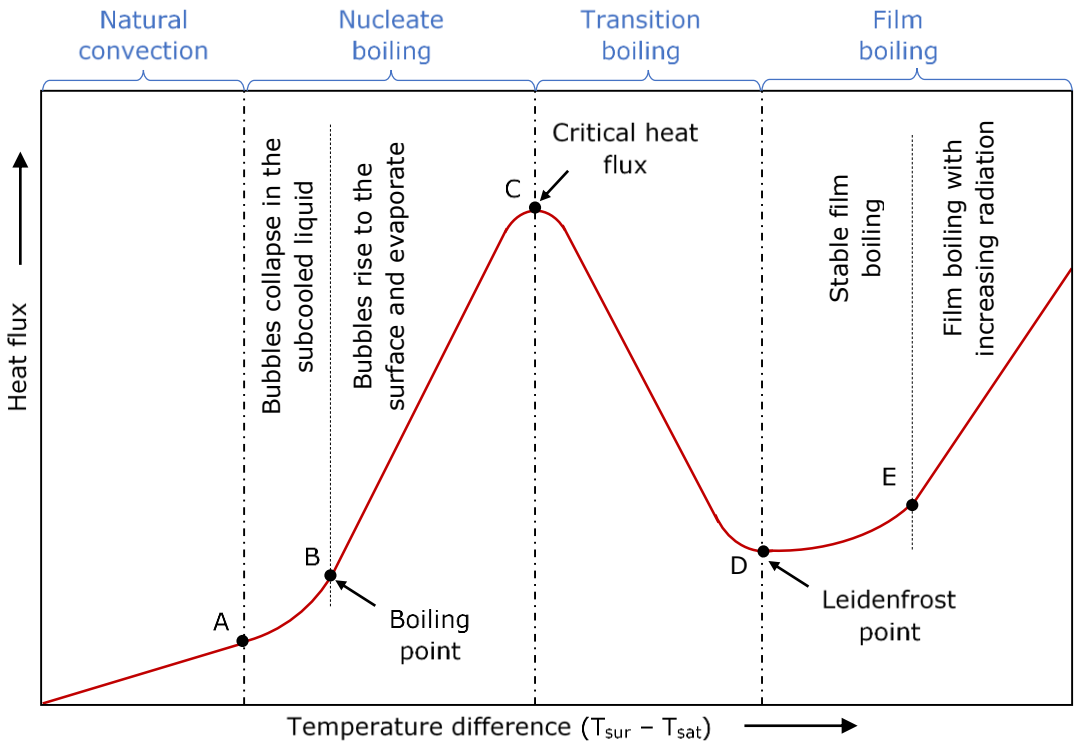

Figure 8-1: Boiling curve over the pool boiling regions/regimes. T_{sur} and T_{sat} are the surface temperature and the liquid saturation temperature respectively. Adopted from (Dhir, 1998; Coulson et al., 1999; Green and Perry, 2007)

1. Natural convection: purely convective heat transfer by the superheated liquid which forms at the interface between the liquid and the hot surface, rising towards the surface. The heat flux in this boiling region increases with the increase in the temperature difference as shown in Figure 8-1.
2. Nucleate boiling: bubbles are formed at the interface between the liquid and the hot surface and rise rapidly. The liquid can be subcooled resulting in a collapse of the bubbles before reaching the surface (line AB in Figure 8-1), or at the saturation temperature resulting in a net vapour evaporation (line BC in Figure 8-1). The heat flux in the nucleate boiling regime increases with the temperature difference until it reaches a maximum point called the critical heat flux or Nukiyama point (point C in Figure 8-1).
3. Transition boiling: this is a transition region between nucleate boiling the film boiling. It is characterised by partial nucleation and the formation of an unstable film at the interface between the hot surface and the liquid. The

heat flux in this region drops with the temperature difference until it reaches a minimum value at the start of the film boiling region called the Leidenfrost point (point D in Figure 8-1).

4. Film boiling: takes place at high values of the temperature difference between the hot surface and the bulk liquid leading to rapid formation of bubbles, creating a film of vapour. This vapour film prevents the liquid from flowing onto the surface causing a substantial reduction in the heat flux. At a very high temperature difference, the heat flux rises again due to the effect of radiative heat transfer.

Among the boiling regions, nucleate boiling is the most favourable boiling regime in industrial reboilers due to its ability to provide high heat transfer rates. However, for the current application, the higher heat transfer rate means greater heat loss from the biomass material to the liquid. From the heat losses point of view, film boiling is the best boiling region for microwave pyrolysis in the liquid system as it provides the minimum heat flux.

8.2.2 Heat transfer Model Setup

Numerical modelling was used to study the heat transfer in the liquid system and estimate the energy requirement and the temperature gradient within the biomass particle. This was achieved by using the same set of equations used for the fluidised bed system (Equations 5.7 to 5.9) which were discussed in Section 6.3.

As in the fluidised bed system, the specific heat capacity of the biomass material in the liquid system was included within the equations as a function of temperature using the same third-order polynomial displayed in Figure 5-13. The main difference between the fluidised bed system and the present liquid system was in estimating the particle-to-fluid heat transfer coefficient.

In the liquid system, the heat transfer coefficient could be estimated from the pool boiling theory discussed earlier in this section. For the heat transfer modelling,

hexane was used as the liquid in which the biomass particles are submerged. However, other hydrocarbon liquids were used in the pyrolysis experiments as will be shown later in Section 8.3. Hexane is a hydrocarbon solvent that meets the requirement for the liquid pyrolysis of having a low loss factor and being immiscible with the pyrolysis oil. It has been used previously for high-pressure liquid-phase catalytic pyrolysis (Klaigaew et al., 2015).

There is a lack of published studies on the pool boiling of hydrocarbons in general. One of the few published studies on the pool boiling of hexane that covers a wide range of temperature is the work reported by Fardad and Ladommatos (1999). They studied the heat flux from a hot surface to hexane up to 300°C surface temperature. They reported a critical heat flux of 724 kW·m^{-2} at around 120 °C and a minimum heat flux (Leidenfrost point) of 32 kW·m^{-2} at around 180 °C as shown in Figure 8-2.

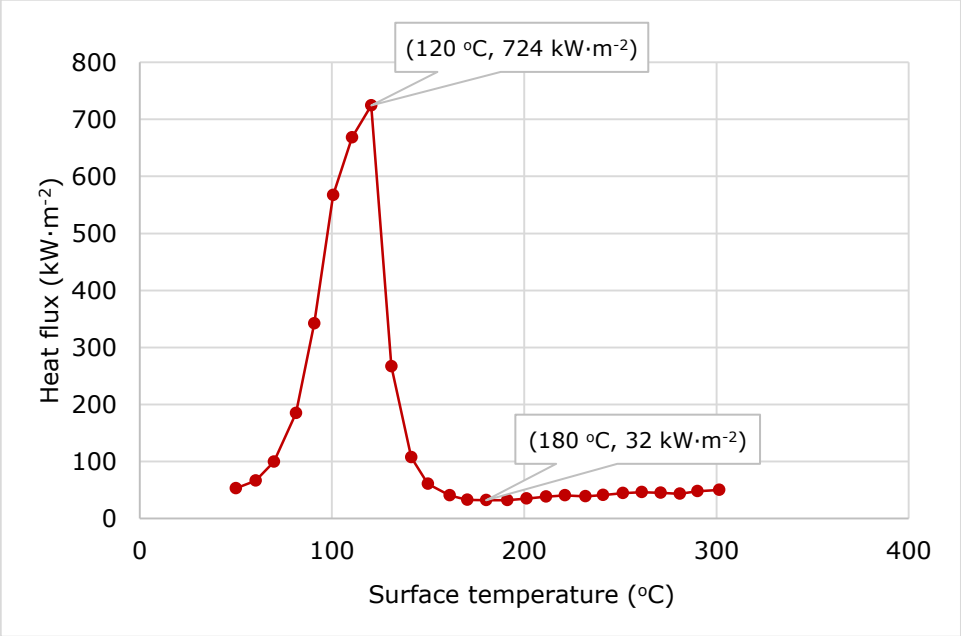

Figure 8-2: Pool boiling curve of hexane. Adopted from (Fardad and Ladommatos, 1999)

The results reported by Fardad and Ladommatos (1999) and displayed in Figure 8-2 were used to estimate the particle-to-fluid heat transfer coefficient for the numerical modelling in the present study as follows:

$$h = \frac{q}{(T_{sur} - T_{sat})} \quad 8\text{-}1$$

Where h is the particle-to-fluid heat transfer coefficient (W·m^{-2}·K^{-1}), q is the heat flux (W·m^{-2}), T_{sur} and T_{sat} are the surface temperature and the liquid saturation temperature respectively.

To solve Equations 5.7 to 5.9 numerically for the liquid system the following assumptions were made:

- The microwave power is absorbed only by the biomass material.
- Homogenous electric field distribution within the biomass material.
- A spherical biomass particle with a constant volume during pyrolysis. The reduction in the particle weight is accounted for in the specific heat capacity calculated from Differential Scanning calorimetry (DSC) measurements, which were based on the initial weight.
- Both the biomass material and the liquid are at 20 ^{o}C before starting the heating. The liquid temperature increases at the same rate as the particle surface temperature until it reaches the liquid saturation temperature. The liquid then remains at its saturation temperature even when the solid surface temperature continues increasing.
- The particle-to-fluid heat transfer coefficient below the liquid saturation temperature is calculated from the minimum Nussult's number, Nu, value for a spherical particle in a stagnant fluid which is given as $Nu = hd_p/k = 2$ (Coulson et al., 1999). Where d_p is the particle diameter and k is the thermal conductivity of the liquid which is 0.126 W·m^{-1}·K^{-1} for hexane (Green and Perry, 2007).
- Above the liquid saturation temperature, the heat transfer coefficient is assumed to increase linearly with the temperature up to the critical heat flux, then decrease linearly with the temperature down to the minimum heat flux (Leidenfrost point). The heat transfer coefficient is then assumed to stay constant throughout the film boiling region.

Similar to the fluidised bed system, the calculations for the power density requirement and the temperature gradient inside the particle were carried out by dividing the particle into 20 control volumes (elements), a core and 19 shells with equal thicknesses as shown in Figure 5-11. The temperature within each of these elements was assumed constant. Equations 5-7 to 5-9 were then solved for each element iteratively with time steps of 0.5 ms adopting the explicit finite difference method reported by Versteeg and Malalasekera (2007). The properties of the biomass materials (sycamore) were the same as those used in the fluidised bed system as listed in Table 5-3.

8.2.3 Heat Transfer Modelling Results

Equations 5-7 to 5-9 were solved to estimate the minimum power density required to reach 400 °C which is the temperature identified for "safe" pyrolysis without slipping into the thermal runaway region as discussed in Section 5.5. Figure 8-3 shows the increase in the temperature at the centre and on the surface of 1.0 mm sycamore particle with the heating time.

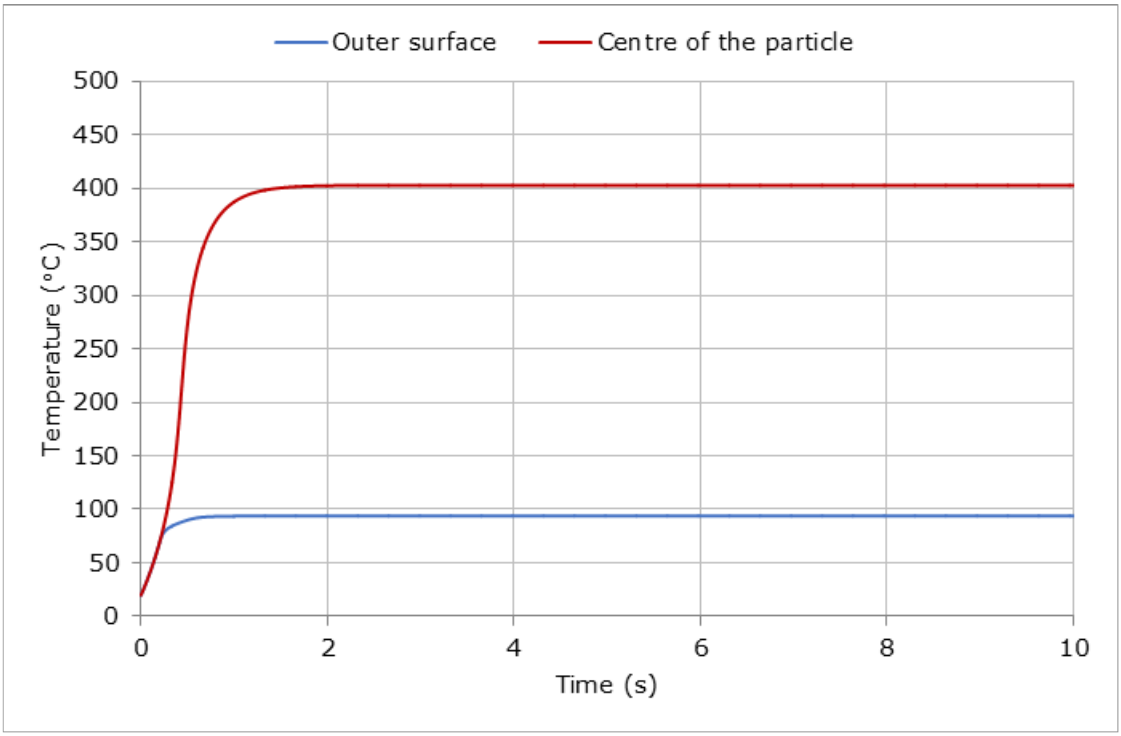

Figure 8-3: Temperature rise at the centre and on the surface of 1 mm sycamore particle at 10.5×10^{8} W·m^{-3} power density.

As can be seen in Figure 8-3, the minimum power density required to reach 400 ^{o}C at the centre of the particle is 10.5×10^{8} W·m^{-3}. Only 1.5 seconds is needed to reach that temperature where an equilibrium is established between the absorbed microwave power and heat loss to the liquid leading to no further increase in the temperature with time. The minimum power density required to reach 400 ^{o}C in the current system is an order of magnitude greater than that required in the fluidised bed system for similar particle size as shown in Section 5.3. This large power density is because of the high rate of heat transfer (loss) to the liquid compared to the gas.

As shown in Figure 8-3, the temperature at the centre of the particle is 310 degrees higher than that of its surface. This large temperature gradient can also be attributed to the high heat transfer coefficient to the liquid resulting in a small temperature gradient at the interface between the solid and the bulk fluid.

Increasing the particle size led to a reduction in the power density requirement. Only 4.4×10^{7} W·m^{-3} power density and 32 seconds were needed to reach 400 ^{o}C at the centre of the particle when a 5.0 mm particle was used. This power density resulted in a specific energy of around 1.61 kJ·g^{-1} compared to 1.75 kJ·g^{-1} in the case of 1.0 mm particle. This reduction in both the power density and specific energy with the increase in the particle size is due to the reduction in the heat loss to the surrounding liquid caused by the reduction in the specific surface area.

Further increase in the particle size leads to further reduction in the power density and specific energy requirement. Figure 8-4 shows that for 10 mm, a power density value as low as 1.4×10^{7} W·m^{-3} can be enough to raise the temperature at the centre of the particle to 400 ^{o}C in 60 seconds. As can be seen in Figure 8-4, increasing the power density results in an increase in the heating rate and, therefore, a reduction in the time required to reach 400 ^{o}C at the centre of the particle.

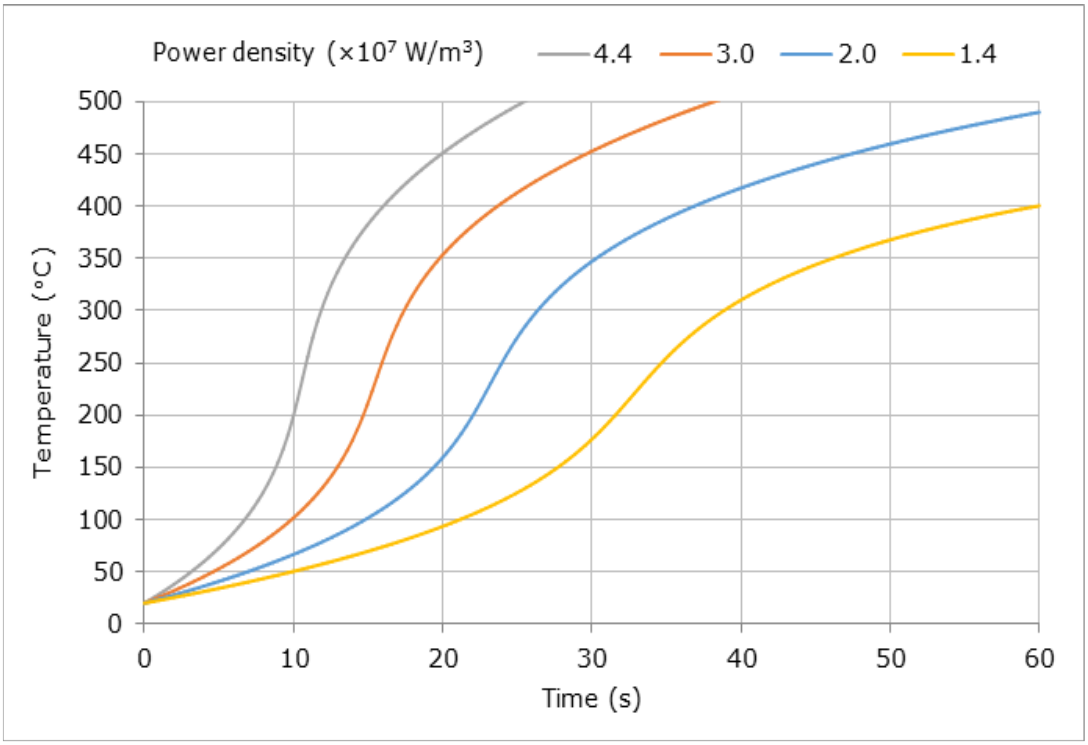

Figure 8-4: Temperature rise at the centre of 10 mm sycamore particle at different power densities.

Increasing the power density also leads to a reduction in the specific energy as shown in Table 8-1. This can be attributed to the reduction in the heat loss to the surrounding fluid by reducing the heating time. Similar relationships were found in the fluidised bed system as discussed in Section 6.3 with differences in the magnitudes with regards to the power density and the heating rate.

Table 8-1: The specific energy required to heat 10mm sycamore particle up to 400°C at the centre as a function of the power density.

Power density ($\times 10^7$ W·m^{-3})	1.4	2.0	3.0	4.4
Heating time (s)	60	37	23.5	16
Specific energy (kJ·g^{-1})	0.933	0.822	0.783	0.782

It can be seen from Table 8-1 that the specific energy required to reach 400 °C at the centre of the particle at 4.4×10^7 W·m^{-3} is only 0.78 kJ·g^{-1}. This value is lower than the enthalpy for pyrolysis at 400 °C which was found to be 0.88 kJ·g^{-1} as shown in Table 6-3 in Section 6.3. The enthalpy for pyrolysis is the minimum energy required to achieve the pyrolysis without taking into account any heat losses. The

reason for obtaining a specific energy lower than the enthalpy of pyrolysis is the large variation in the degree of pyrolysis between the centre of the particle and its surface due to the large temperature gradient. Figure 8-5 shows the change in the temperature gradient inside 10 mm particle with time at 4.4×10^{7} W·m^{-3}. It can be seen from Figure 8-5 that the temperature gradient increases with time until it reaches about 320 °C after 16 seconds. The temperature at the centre reaches 400 °C leaving the surface temperature at around 80 °C, which is far below the pyrolysis temperature. Under these conditions, less than 10 % of the particle volume is at or greater than 400 °C. The degree of pyrolysis over the particle volume could be improved by allowing the material to be heated for a longer time and increasing the temperature at the centre. As displayed in Figure 8-5, after 25 seconds of heating at 4.4×10^{7} W·m^{-3}, the temperature at the centre reaches 500 °C resulting in about 40 % of the particle volume to be at or greater than 400 °C.

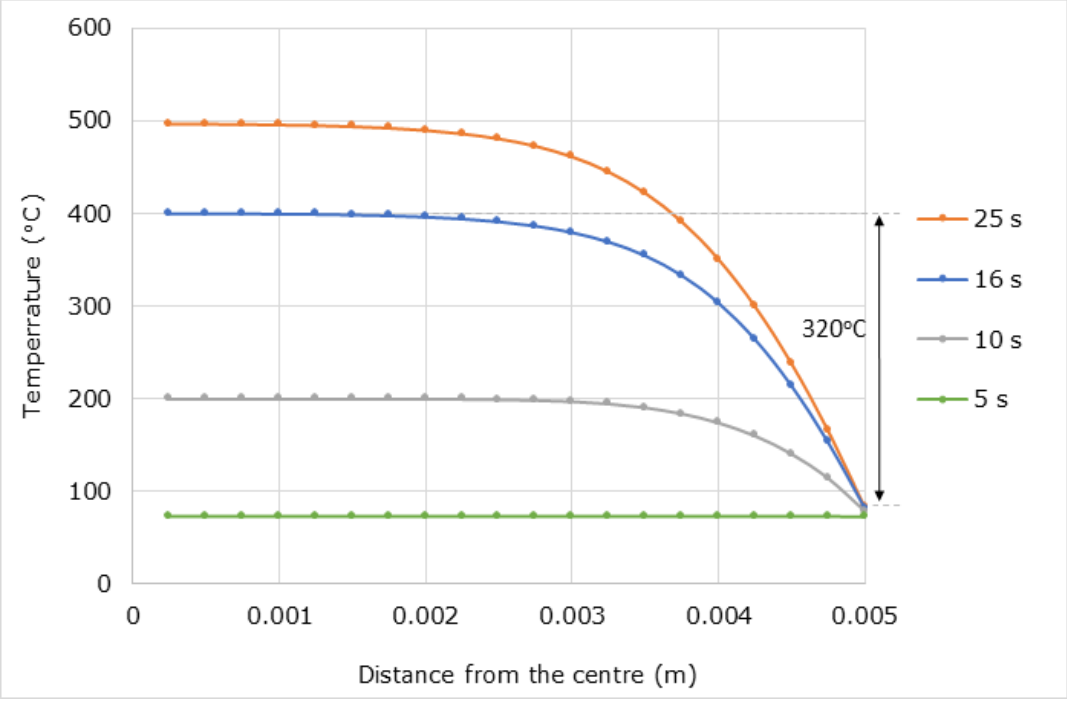

Figure 8-5: Temperature gradient within 10 mm sycamore particle under 4.4×10^{7} W·m^{-3}

Allowing the temperature at the centre of the particle to exceed 400 °C would lead to entering the area of char formation and increasing the possibility of the thermal runaway. However, the effect of the thermal runaway at the centre of the particle

is not as severe as having it on the surface of the particle as the cold surface would act as an insulator containing the char and preventing it from sticking to the walls and damaging the reactor.

It is to be noted here that in all the modelled cases, the temperature on the surface of the biomass particle was always lower than the critical heat flux temperature (Nukiyama point) indicating that the boiling mechanism in these cases is nucleate boiling.

The numerical modelling of the heat transfer showed that pyrolysis in a liquid system is theoretically viable if the biomass solid could be selectively heated by the microwave energy. In the following sections, the microwave pyrolysis of biomass solid submerged in a liquid is investigated experimentally.

8.3 Dielectric Properties of the Solvents

The dielectric properties of the hydrocarbon solvents involved in the microwave pyrolysis experiments were studied. Figure 8-6 shows the dielectric constant and loss factor of the three solvents at 2.47 GHz as functions of temperature. It can be seen that over the studied temperature ranges, the hydrocarbon solvents have a loss factor of less than 0.005, which is greater than the minimum loss factor value of sycamore over the pyrolysis temperature range*. This suggests that the biomass material can be selectively heated when submerged in these solvents. A limited drop in both the dielectric constant and loss factor of the solvents with temperature can be seen in Figure 8-6. This drop can be explained by the reduction in the sample mass during measurement due to evaporation. An average reduction of 5.5 %, 10.1 % and 12.2 % was observed in the volume of the hexane, iso-octane and kerosene respectively after the end of the measurements.

* As shown in Section 5.4, the minimum loss factor value of sycamore at 2.47 GHz and 0.5 $g \cdot cm^{-3}$ density is 0.0075. For the same conditions at room temperature the loss factor of sycamore is 0.117.

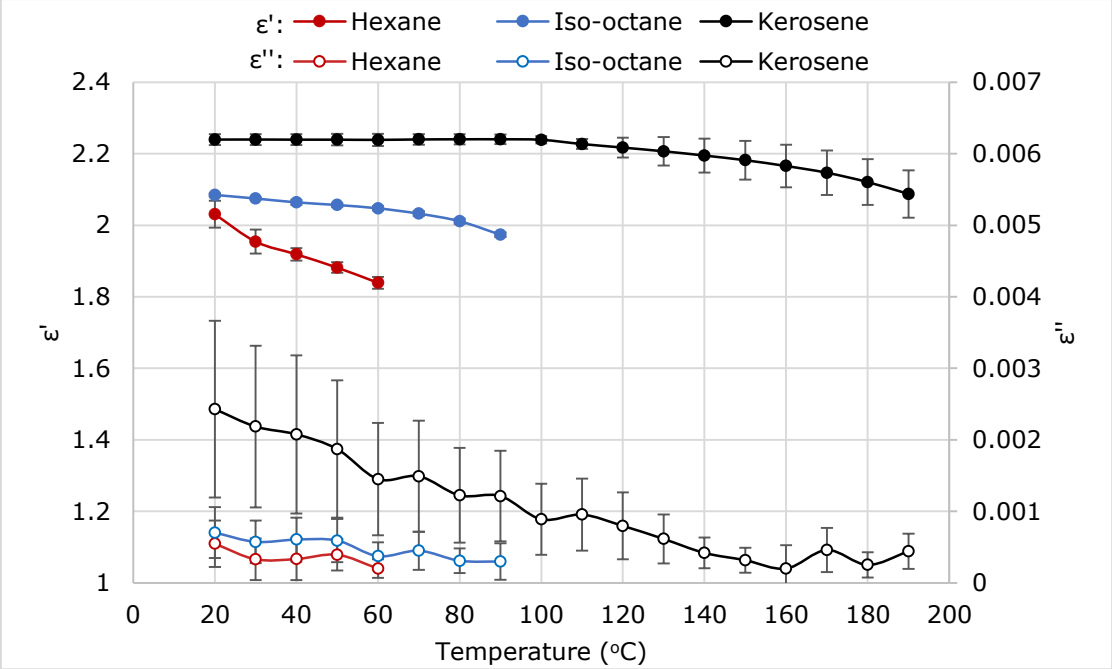

Figure 8-6: The dielectric constant and loss factor of the three solvents involved in this study at 2.47 GHz measured using the cavity perturbation technique. Three repeats were made for each measurement and the standard uncertainty is indicated as error bars.

8.4 Batch Pyrolysis Experiments in the Hydrocarbon Solvents

Description of the experimental setup and methods followed for microwave pyrolysis in hydrocarbon solvents are detailed in Section 4.6. The pyrolysis experiments were first run using hexane and small sycamore blocks of around 1.0 cm size. Figure 8-7 (a) shows the reactor and its contents after microwave heating while Figure 8-7 (b) shows a cross-section cut of the solid blocks after drying them. These results prove that a biomass solid can be selectively heated while submerged in a hydrocarbon liquid and pyrolysis can happen. It is to be noted here that when the biomass blocks are submerged in the solvent, the liquid might seep into the biomass because of its porosity. However, the solvent will start evaporating out as soon as the temperature inside the biomass block reaches the boiling point of the solvent which is much lower than the pyrolysis temperature.

Figure 8-7 (b) shows that there is a significant variation in the degree of pyrolysis between the centre of the block and its surface with char (black in colour) formed at the centre indicating a greater degree of pyrolysis. It was found that the overall

mass loss was only 25 % for 18 kJ·g^{-1} specific energy for the case shown in Figure 8-7. This overall degree of pyrolysis is considerably lower for this level of specific energy when compared to the fluidised bed system which showed 60 to 70 % mass loss for around 3.5 to 4.0 kJ·g^{-1} energy input.

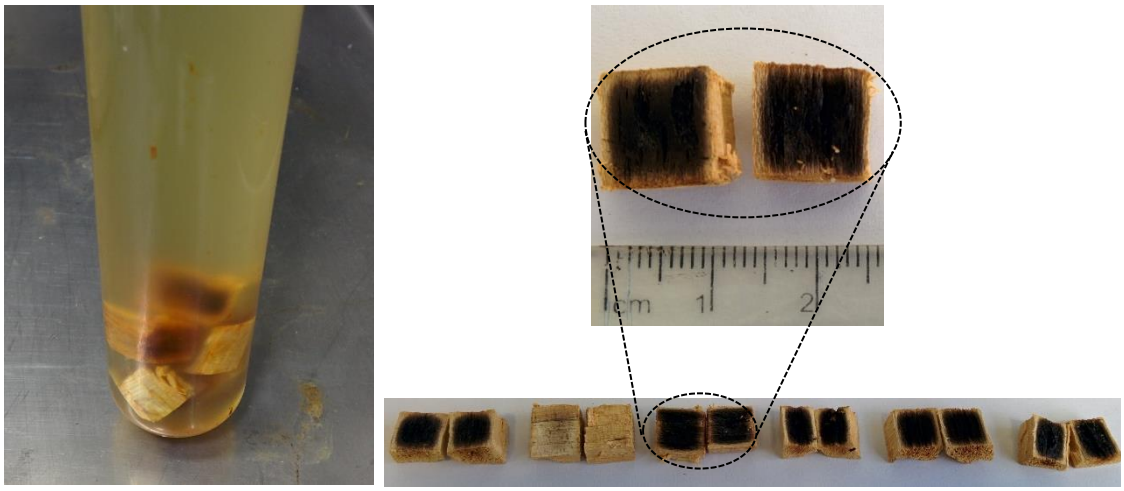

(a) (b)

Figure 8-7: The product after heating 1.0cm sycamore blocks in hexane for 72 seconds with a specific energy of 18 kJ·g^{-1}: (a) the solid product submerged in the liquid inside the reactor, (b) cross-section cut of the dried product.

To improve the degree of pyrolysis and reduce the energy consumption, the biomass particle (block) size was increased. Increasing the block size would reduce the heat loss to the surrounding fluid resulting in an increase in the temperature at the centre at a given energy input as shown through the numerical modelling in Section 8.2. Therefore, single larger blocks with the dimensions of approximately 1.5×1.5×4.0 cm were used. Using such size made the biomass block to float near the surface of the solvent as shown in Figure 8-8 (a). The floating of the biomass block was attributed to the reduction in its bulk density with the increase in its size. Larger sizes have more pores per unit volume contained within the structure reducing the overall bulk density.

To overcome this, a microwave-transparent load/weight was placed on the top of the biomass block to support it at the bottom of the reactor as shown in Figure 8-8 (b). Figure 8-8 (c) shows the reactor contents after the microwave pyrolysis when one large biomass block was used.

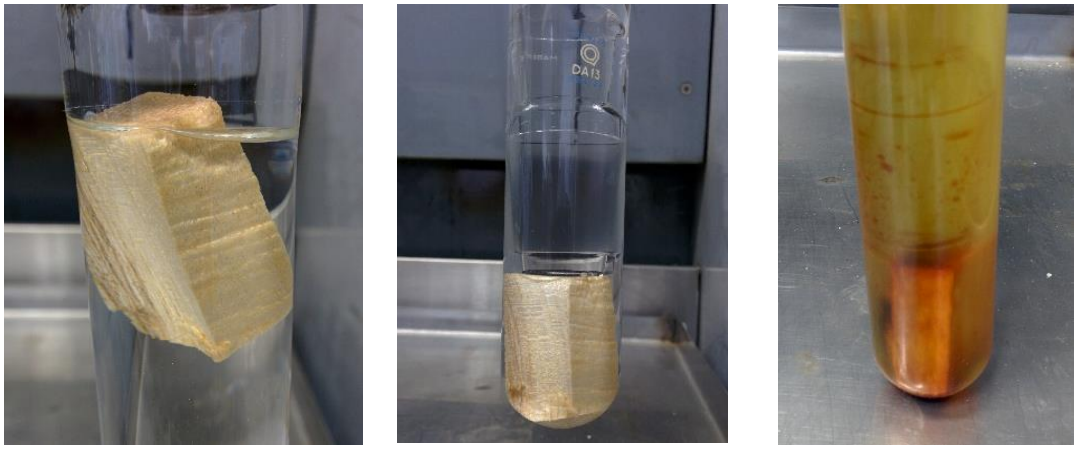

(a) (b) (c)

Figure 8-8: Processing one large block: (a) the sycamore block floating at the top near the liquid surface, (b) the block supported at the bottom of the reactor using a cylindrical hollow glass load, (c) the product after the microwave heating.

Figure 8-9 shows the product after microwave pyrolysis of sycamore block in hexane. Using the larger single block led to an increase in the degree of pyrolysis with a substantial reduction in the energy consumption compared to the smaller 1.0 cm blocks. Only 2.75 $kJ \cdot g^{-1}$ was needed to obtain about 40 % mass loss for the sample displayed in Figure 8-9, compared to 18 $kJ \cdot g^{-1}$ to achieve 25 % mass loss for the 1.0 cm blocks.

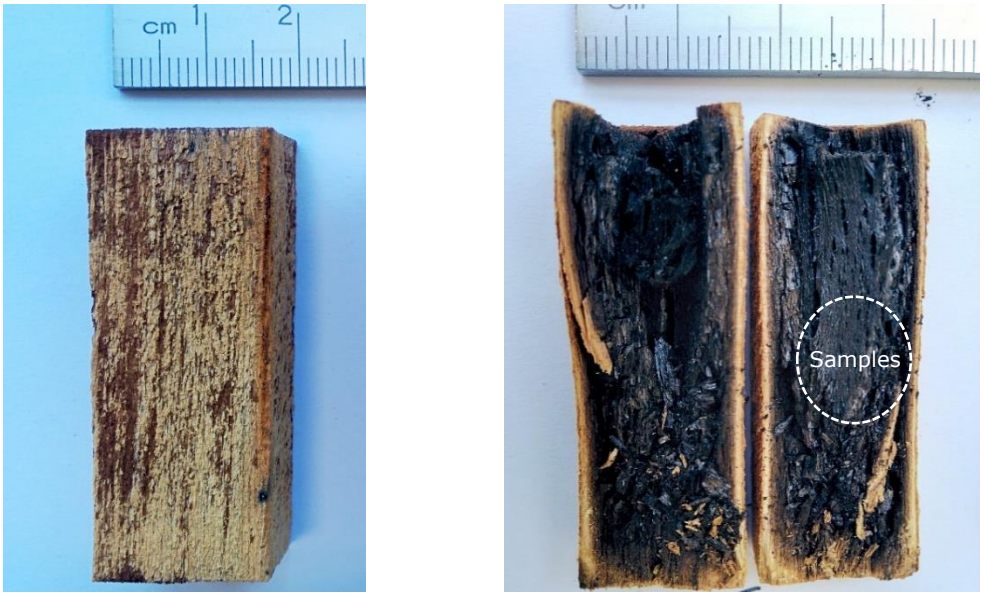

(a) (b)

Figure 8-9: The solid product after microwave pyrolysis in hexane with 2.75 $kJ \cdot g^{-1}$ specific energy at 1.0 kW forwarded power. (a) Dried block, (b) The block cross-section cut. Samples were taken from the centre of the block for TGA analysis as indicated.

Samples from the centre of the block (as indicated in Figure 8-9(b)) and its surface (less than 1.0 mm from the edge) were taken. The samples were analysed using Thermogravimetric Analysis (TGA) to study the variations in the degree of pyrolysis between the centre of the block and its surface. The TGA measurement procedure was the same as described in Section 4.3 with a 10 $^{o}C \cdot min^{-1}$ ramp heating.

Figure 8-10 shows the weight loss as a function of temperature for the samples taken from the processed biomass block as well as a raw biomass sample. It confirms the large variation in the degree of pyrolysis between the centre of the block and its surface.

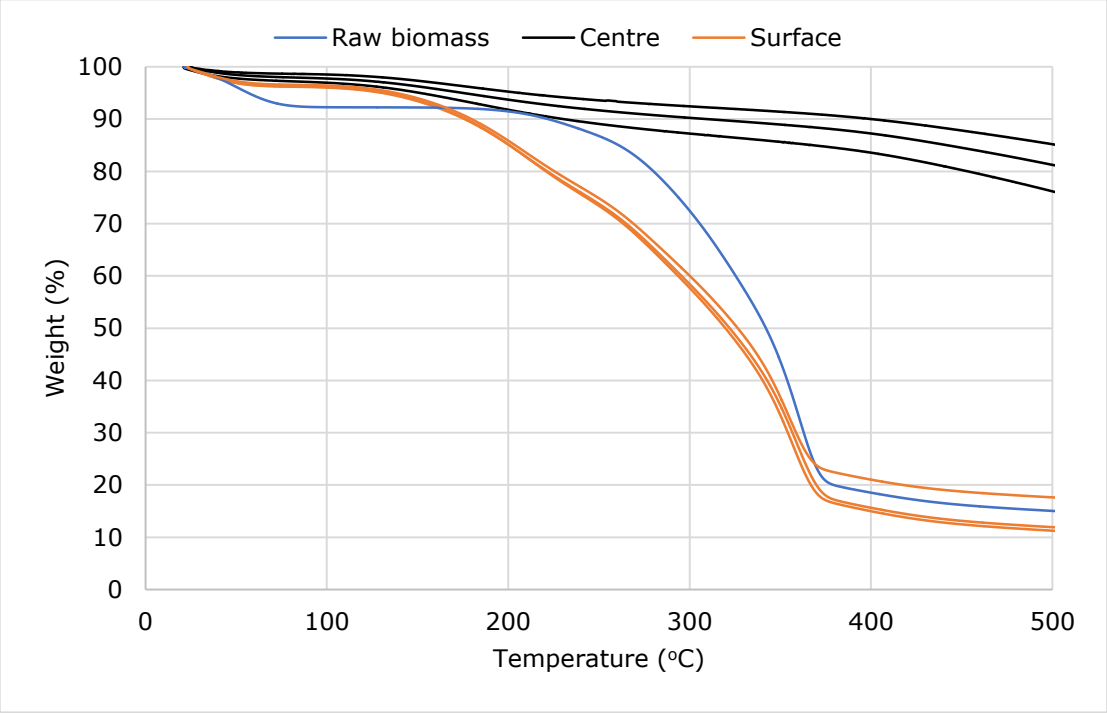

Figure 8-10: The weight loss as a function of temperature for the samples taken from the centre and the surface of the processed sycamore block shown in Figure 8-9 together with an unprocessed sample.

As can be seen in Figure 8-10, the samples from the centre of the block showed very limited weight loss with the increase in temperature up to 500 ^{o}C, indicating that most of the volatile content had already been consumed in the pyrolysis reaction. The samples from the surface of the block showed large weight loss similar to that from the raw sample suggesting that the surface had experienced a limited

degree of pyrolysis. The variation in the degree of pyrolysis can be attributed to the large temperature gradient between the centre of the biomass block and its surface as explained through the numerical modelling discussed in Section 8.2. The microwave power is absorbed by the biomass particle, and not the solvent. Therefore, heat is transferred from the particle to the bulk fluid creating an inter- and intra-particle temperature gradients, with the temperature on the surface of the particle higher than that of the bulk liquid, and lower than that at the centre of the particle.

The effect of the applied power and the energy input on the degree of pyrolysis were studied. Figure 8-11 shows the increase in the degree of pyrolysis with the energy input at different values of applied power.

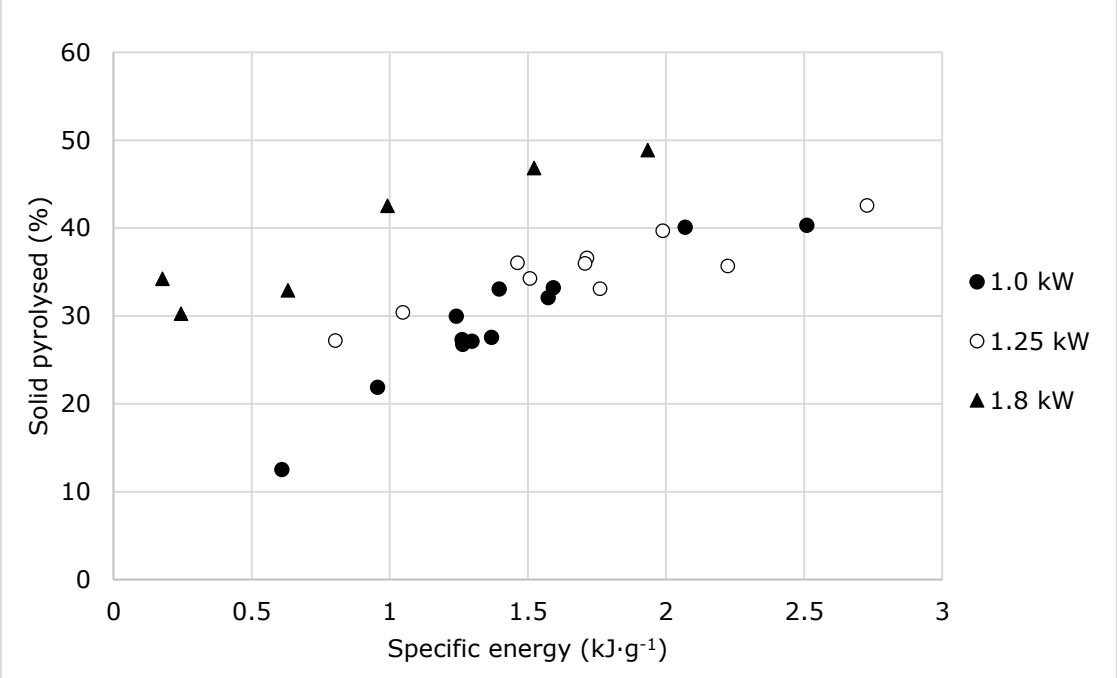

Figure 8-11: Increase in the solid pyrolysed with the specific energy at different values of incident power.

It can be seen from Figure 8-11 that the applied power has a significant effect on the degree of pyrolysis as increasing the applied power leads to an increase in the degree of pyrolysis. This can be seen clearly in the greater degree of pyrolysis in the case of 1.8 kW compared to 1.0 kW and 1.25 kW. With the 1.8 kW applied

power, up to 50 % solid pyrolysed could be achieved at around 1.90 kJ·g^{-1} specific energy while with 1.0 and 1.25 kW power, the degree of pyrolysis is limited to around 40 % to 45 % with up to 2.75 kJ·g^{-1} specific energy as shown in Figure 8-11. The increases in the degree of pyrolysis with the applied power density was discussed through the numerical models in Section 8.2. It was shown that increasing the power density leads to a reduction in the specific energy required to reach a certain temperature. This was attributed to the reduction in the heating time, caused by the higher heating rate, leading to a reduction in the heat loss to the surrounding fluid.

Increasing the energy input beyond 1.9 kJ·g^{-1} at 1.8 kW applied power resulted in the ”explosion” of the biomass block, and some char particles moving from the biomass block to the bulk fluid. This “explosion” happened through the bottom face of the biomass block as shown in Figure 8-12 which indicates that thermal runaway took place on or near the surface of the block at that area.

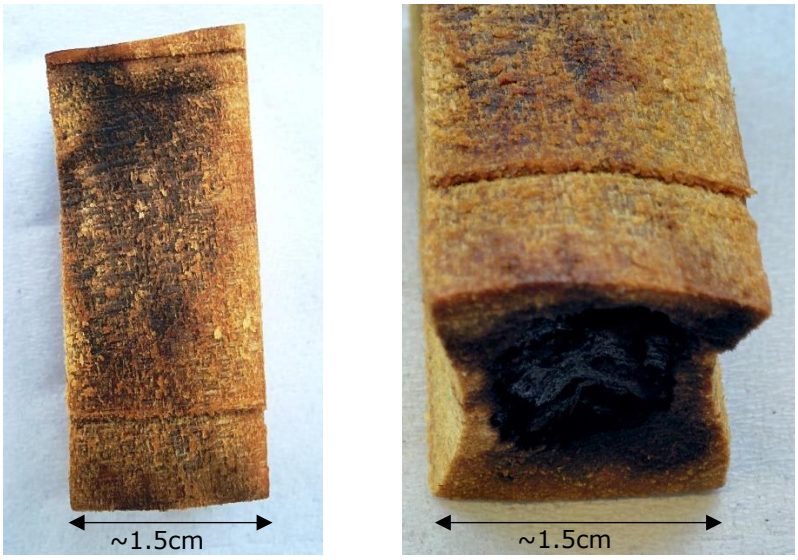

Figure 8-12: Explosion at the base-face of the biomass block after being heated in hexane at 1.8 kW with 2.0 kJ·g^{-1}.

The thermal runaway on the surface could be caused by one of two possible reasons or a combination of them. The first is that the narrow space between the reactor wall and the biomass block prevents the liquid from flowing back to the bottom of

the reactor creating a dry zone of just vapour where the heat transfer coefficient is substantially decreased. The second possible reason for the thermal runaway on the surface is that the minimum heat flux temperature (Leidenfrost point) is reached at the bottom face of the block entering the film boiling regime where the heat flux reaches its minimum. Both explanations results in a significant increase in the heating rate at the surface due to the reduction in the heat transfer to the surrounding fluid.

As mentioned earlier in Section 8.2, the effect of the thermal runaway becomes more severe when it reaches the surface of the particle/block as it may damage the reactor. But, when it happens inside the block, the outer layers act as an insulation containing the char and protecting the reactor wall. However, this insulation layer contributes to the reduction in the overall degree of pyrolysis.

The effect of using different hydrocarbon solvents with a different boiling point on the degree of pyrolysis was studied. Figure 8-13 shows the increase in the degree of pyrolysis with the specific energy at 1.8 kW applied power using different hydrocarbon solvents.

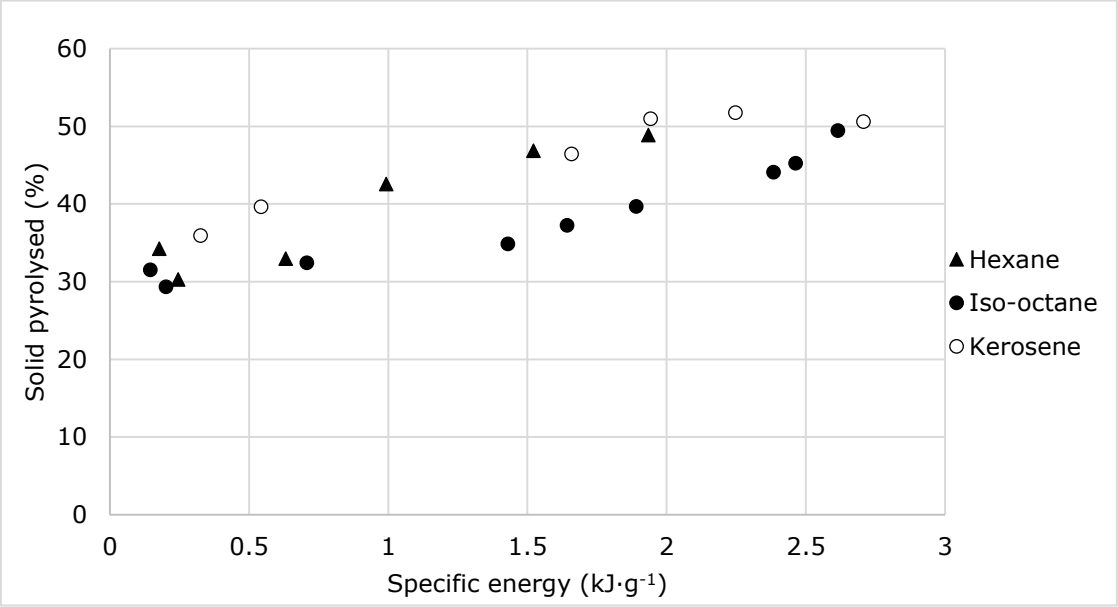

Figure 8-13: Increase in the solid pyrolysed with the energy input for different solvents.

It was found that both iso-octane and kerosene allow for more energy input to be applied before the "explosion" caused by the thermal runaway on the surface takes place. Both solvents can allow for a specific energy of more than 2.5 $kJ \cdot g^{-1}$ at 1.8 kW applied power for the ~1.5×1.5×4 cm sycamore blocks compared to a maximum of 1.9 $kJ \cdot g^{-1}$ for hexane. This is due to the higher boiling points of iso-octane and kerosene compared to hexane as shown in Table 4-4. Their higher boiling points and, therefore, higher Leidenfrost points* give them extra heating time before entering the film boiling region where thermal runaway could take place on the surface.

Comparing the degree of pyrolysis in the liquid system represented by Figure 8-13 to that of the gas-based fluidised bed system represented by Figure 6-9 shows that the degree of pyrolysis in the liquid system is limited to around 50 % while with the fluidised bed system nearly 70 % pyrolysis could be achieved. This limited degree of pyrolysis in the liquid system is mainly due to the large temperature gradient within the biomass particle, resulting in unpyrolysed solid on and near the surface. This is consistent with the numerical modelling in Section 8.2, and the experimental results in Figure 8-9 and Figure 8-10.

However, in the liquid system, pyrolysis up to 50 % could be achieved with much lower energy input compared to the fluidised bed system. Around 2.0 $kJ \cdot g^{-1}$ specific energy is needed to reach 50 % pyrolysis with the liquid system as shown in Figure 8-13 compared to more than 3.0 $kJ \cdot g^{-1}$ needed to achieve the same degree of pyrolysis with the fluidised bed system as shown in Figure 6-9. This is due to the large particle size used in the liquid system, which allowed the centre of the particle to be thermally insulated by the outer layers allowing the temperature at the centre to increase rapidly.

* Mills and Fry (1982) found a linear relationship between the Leidenfrost point and the boiling point of different hydrocarbons.

8.5 Conclusions

In this chapter, the microwave pyrolysis of biomass materials in hydrocarbon liquids was investigated. Numerical modelling was used to study the heat transfer in the liquid system. It was shown that pyrolysis of a biomass solid submerged in a cold liquid is theoretically viable if the biomass can be selectively heated by the microwave energy. The results of the numerical modelling also showed large temperature gradient between the biomass particle and its surface which was attributed to the high heat transfer rate to the surrounding liquid. This large temperature gradient was confirmed by the experimental results.

The dielectric properties of the hydrocarbon liquids involved in the study and their temperature dependencies were studied. It was found that the loss factor of the hexane, iso-octane, and kerosene is lower than 0.005 suggesting that the biomass materials could be selectively heated when submerged in these liquids.

Batch pyrolysis experiments confirmed that the biomass solid can be selectively heated by the microwave energy while being submerged in a hydrocarbon liquid, allowing for the pyrolysis to take place. The biomass particle size was found to have a significant effect on the degree of pyrolysis. It was shown that using a single block of ~1.5×1.5×4 cm gives around 40 % solid pyrolysed with only 2.75 $kJ \cdot g^{-1}$ specific energy at 1.0 kW applied power compared to only 25 % solid pyrolysed with 18 $kJ \cdot g^{-1}$ when multiple 1.0 cm blocks were used. Increasing the applied power was found to improve the degree of pyrolysis with up to 50 % solid pyrolysed was achieved at 1.8 kW incident power. However, it was observed that increasing the applied power leads to thermal runaway on/near the bottom face of the biomass block. The hydrocarbon solvents with a higher boiling point were found to allow for more specific energy before thermal runaway can take place on the surface of the biomass block. This was regarded to the longer time that the solvent with higher boiling point spend before intering the film boiling region.

It was found that the overall degree of pyrolysis obtained using the present liquid system is lower than that obtained from the fluidised bed system discussed in Chapter 7. This was regarded to the large temperature gradient between the centre of the particle/block and its surface in the liquid system leaving a considerable fraction of the outer layer of the block unpyrolysed.

The present liquid system can provide many advantages over the gas-based systems. It can help controlling the thermal runaway as the cold surface acts as an insulator containing the char and preventing it from sticking to the walls and damaging the reactor. The presence of the liquid can also eliminate the possibility of electric breakdown even at high electric field intensity as the electric breakdown voltage in liquid is extremely high compared to gases. When considering continuous processing, the liquid system would require less condensation duty compared to the gas system as the condensation of the pyrolysis vapours can take place within the liquid. The condenser would be needed only for condensing and recycling the evaporated solvent. For a continuous processing system, the liquid inside the reactor could be kept at its boiling point temperature. Part of the liquid would evaporate as soon as it absorb heat from the biomass material equivalent to its latent heat of vaporisation. The condenser would then be needed to compensate for only the latent heat of the liquid. The minimum liquid-to-biomass ratio inside the reactor and the flowrate of the liquid can be calculated based on the applied microwave power density.

Table 8-2 summarises the advantages and limitations of the gas-based and liquid based systems for microwave pyrolysis of biomass.

Future work should consider studying the quality of the bio-oil produced from the liquid system and comparing it to the gas-based microwave pyrolysis systems and the conventionally heated systems. Pyrolysis under continuous liquid flow should also be considered as a step towards scaling up. The multiphase flow behaviour of the liquid and the evaporated vapour needs to be taken into consideration.

Table 8-2: Summary of the advantages and disadvantages of the gas- and liquid-based systems for microwave pyrolysis of biomass.

Gas-based microwave pyrolysis	**Liquid-based microwave Pyrolysis**
Common processing method for pyrolysis. Commercial-scale plants (conventionally heated) are gas-based.	Not common as processing method for pyrolysis. Needs further research and development before scaling-up.
Limitations in terms of particle size and shape in fluidised bed systems, which is the most common processing technology.	Fluidisation and flow in liquids is more homogenous and more predictable compare to gases, allowing wider range of particle size and shape to be processed.
Large volumes of inert gas is needed for fluidisation which lowers the vapour pressure of the pyrolysis vapours in the condenser. Thus, large condenser would be needed.	Condensation of the pyrolysis vapours can happen in bulk inert-liquid. Condensers would be needed only for the recovering and recycling the evaporated inert-liquid.
Electric breakdown (in the form of arcing or plasma) can take place if the electric field intensity reaches 30 kV/cm. This limits the maximum applicable power for large-scale processing.	Electric breakdown voltage in liquids is extremely high compared to gases. Thus, high electric field intensities (and powers) can be applied.
Thermal runaway may damage the processing equipment if char particles produced during pyrolysis stick to the reactor wall during processing.	High temperature gradient within the particle compared to gas-based systems, creating a layer of unpyrolysed solid on the outer surface of the particle containing the char inside. Further, the liquid can help preventing the solid particles from sticking to the reactor walls. However, the high temperature gradient limits the degree of pyrolysis.

9 CONCLUSIONS AND FUTURE WORK

The aim of thesis was to study the interactions between biomass materials and microwave energy over the pyrolysis temperature range, and to develop a reliable and scalable microwave pyrolysis process.

Dielectric properties of selected biomass materials were studied over the pyrolysis temperature range, and their variations with temperature were related to the physical and structural changes during pyrolysis. As an attempt to overcome the challenges associated with microwave pyrolysis of biomass, a microwave fluidised bed process was developed. Batch pyrolysis experiments were carried out to assess the yield and quality of the products obtained from the developed process as well as the energy requirement.

Microwave pyrolysis in a hydrocarbon liquid was investigated as a potential alternative to overcome some of the limitations and weaknesses associated with the gas-based fluidised bed process.

9.1 Materials Characterisation

Different biomass materials were chosen for characterisation as possible candidates for microwave pyrolysis. The biomass materials involved in this study were pine, sycamore, pine bark, wheat straw and seaweed. These materials were chosen because of their abundance, low economic value, and suitability for pyrolysis. The characterisation involved mainly thermogravimetric analysis and dielectric properties measurement.

The thermogravimetric analysis (TGA) over the range of pyrolysis temperature showed different decomposition behaviour for the different biomass materials which was related to variations in their chemical composition.

High-temperature dielectric measurements showed significant variations in the dielectric properties of the biomass material with temperature in the range between 20 ^{o}C and 600 ^{o}C. These variations were linked to the TGA results and the physical

and chemical transformations happening during the heating. It was found that the loss factor of the biomass materials reaches a minimum value in the range between 300 °C and 400 °C. This minimum value is followed by a sharp increase in the loss factor due to the char formation, and this is what causes the thermal runaway during the microwave heating. It was concluded that for the woody biomass, the operating temperature during microwave pyrolysis should be in the range between 350 °C and 400 °C, which can secure around 70 % to 80 % weight loss. Increasing the temperature more than 400 °C would lead to falling into the steadily increased loss factor area with no much gain in terms of the weight loss.

9.2 Microwave Fluidised Bed Process

A microwave fluidised bed process was proposed as an attempt to overcome the challenges associated with microwave pyrolysis of biomass including the heating heterogeneity caused by the nature of the standing waves. A systematic approach was followed for the process design taking into account the pyrolysis process requirements, the microwave-material interactions and the fluidisation behaviour of the biomass particles.

As one of the steps towards designing the microwave fluidised bed process, cold fluidisation experiments were carried out for pine, sycamore and seaweed with different particle size groups in the range between 45 μm and 2.36 mm. This was to study their fluidisation behaviour and to determine their minimum fluidisation velocities. It was found that woody biomass particles have a complex fluidisation behaviour due to their irregular shape. Fluidisation was achieved at relatively high velocities with a turbulent behaviour. It was also found that raw biomass particles have greater minimum fluidisation velocities compared to char prepared using similar particle size feed. This was related to a drop in the particle's size and density after pyrolysis. During processing, this would lead to particle segregation and could be used to control the char deposition and residence time in the bed.

The enthalpy for pyrolysis was determined using differential scanning calorimetry (DSC). It was found that the enthalpy for pyrolysis of sycamore at 400 ^{o}C is about 0.88 kJ·g^{-1}. Energy balance calculations were performed to estimate the power density and the energy requirement in the fluidised bed system including the heat loss to the fluidising gas. It was found that the minimum power density required for the pyrolysis of 600 μm sycamore particles at 400 ^{o}C is 54 MW·m^{-3}. It was also shown that the specific energy required for the pyrolysis of the sycamore particles in the fluidised bed system can range from 1.07 kJ·g^{-1} to 4.85 kJ·g^{-1} depending on the power density.

Electromagnetic simulations were performed to support the cavity design. A multimode cavity was chosen based on the lower Q factor and the heating homogeneity.

The microwave fluidised bed system was built, and batch pyrolysis experiments were carried out to assess the yield and quality of the products obtained from the developed process as well as the energy requirement. It was possible with the developed microwave fluidised bed process to achieve homogeneous pyrolysis for up to 70 g biomass feed. The pyrolysis experiments were carried out for sycamore, pine and seaweed of different particle size groups. For each particle size group, the gas velocity was set between two limiting values, a higher value, above which unpyrolysed particles are entrained with the fluidising gas, and a lower value below which thermal runaway takes place before fluidisation. The movement of the particles within the bed acted as a sweeper preventing the solid particles from sticking to the wall of the reactor. However, for the seaweed, a layer of solid particles was formed on the wall of the reactor during pyrolysis due to the condensation of a significant amount of pyrolysis vapours within the bed which led to thermal runaway. The fluidising particles were not able to clean the wall because that the sticking particles were strongly bound to the wall through the viscous condensed liquid.

It was shown through the pyrolysis experiments that increasing the particle size increases the solid pyrolysed at a certain specific energy input. This was attributed to the reduction in the heat losses to the fluidising gas which is caused by the reduction in the specific surface area of the particles. Processing larger biomass particles adds the advantage of reducing the energy costs for crushing the raw feedstock. However, the extent to which the particle size could be increased is restricted by the ability of the particles to fluidise.

The energy consumption in the developed microwave fluidised bed system was found to be higher than that obtained previously by Robinson et al. (2015) in a fixed bed reactor which was 2.2 to 2.5 $kJ \cdot g^{-1}$ for 60-70 % solid pyrolysis compared to 3.5 to 4.2 $kJ \cdot g^{-1}$ in the present study. This was attributed to the heat loss to the fluidising gas which was fed at room temperature. The unique advantage of the developed fluidised bed process is that it can process larger feed sizes than the fixed bed system which had failed to control the thermal runaway and provide homogeneous heating for samples size larger than 1.5 cm (around 5 g) as shown by Robinson et al. (2015). The other advantage of the present microwave fluidised bed system is that it is scalable, and the bed temperature and the solid residence time could be controlled by changing the gas velocity.

The developed microwave fluidised bed process has shown an ability to overcome many of the challenges associated with microwave pyrolysis of biomass including the improvement in heating uniformity and the ability to control the solid deposition in the process, placing it as a viable candidate for scaling-up. However, it has some weaknesses including its limitation with regards to the shape and size of the biomass material and the difficulty to prevent particles from sticking to the wall during processing which can lead to thermal runaway as shown earlier in the case of seaweed. Another weakness is the need for high quantity of inert gas for fluidisation which increase the size and duty of the condenser needed for condensing the pyrolysis vapours.

Future studies on the microwave fluidised bed system should investigate mixing the biomass feed with another inert microwave-transparent solid such as dry sand to assist the fluidisation and allow for a wider range of particle size and shape to be processed.

Future studies should also investigate the potential improvements in the fluidised bed process to reduce the energy consumption. These improvements could include preheating the fluidising gas which would reduce the heat loss to the gas. Applying higher power density would also reduce the heating time and, therefore, reduce the heat losses. However, increasing the power density and preheating the gas could make it more difficult to control the bed temperature and avoid thermal runaway.

Future work should also consider continuous processing as a step towards scaling up the process. The relationship between the power density, gas velocity and the particle residence time during continuous processing, and their effect on the product yield and energy consumption should be investigated.

9.3 Microwave Pyrolysis in a Liquid System

Microwave pyrolysis in a hydrocarbon liquid was investigated as a potential alternative to overcome some of the limitations and weaknesses linked to the gas-based fluidised bed process.

Numerical modelling was used to investigate the heat transfer in the liquid system. It was shown that pyrolysis of a biomass solid submerged in a cold liquid is theoretically viable if the biomass can be selectively heated by the microwave energy. The results of the numerical modelling also showed large temperature gradient between the centre of the biomass particle and its surface which was attributed to the high heat transfer rate to the surrounding liquid. This large temperature gradient was confirmed by the experimental results as shown in Section 8.4.

Dielectric properties of the hydrocarbon liquids involved in the study and their temperature dependencies were investigated. It was found that the loss factor of the hexane, iso-octane, and kerosene is lower than 0.005 suggesting that the biomass materials could be selectively heated when submerged in these liquids.

Batch pyrolysis experiments confirmed that the biomass solid can be selectively heated by the microwave energy while being submerged in a hydrocarbon liquid, allowing for pyrolysis to take place. The biomass particle size was found to have a significant effect on the degree of pyrolysis. It was shown that using a single block of ~1.5×1.5×4 cm gives around 40 % solid pyrolysed with only 2.75 $kJ \cdot g^{-1}$ specific energy at 1.0 kW applied power compared to only 25 % solid pyrolysed with 18 $kJ \cdot g^{-1}$ when multiple 1.0 cm blocks were used. Increasing the applied power was found to improve the degree of pyrolysis. Up to 50 % solid pyrolysed was achieved at 1.8 kW incident power with only 1.9 $kJ \cdot g^{-1}$ energy input. However, it was observed that increasing the applied power leads to thermal runaway on/near the bottom face of the biomass block. The hydrocarbon solvents with a higher boiling point were found to allow for more specific energy before thermal runaway can take place on the surface of the biomass block. This was regarded to the longer time that the solvent with higher boiling point spend before intering the film boiling region.

It was found that the overall degree of pyrolysis obtained in the liquid system is lower than that obtained from the fluidised bed system. This was regarded to the large temperature gradient between the centre of the particle/block and its surface in the liquid system leaving a considerable fraction of the outer layer of the block unpyrolysed.

The liquid system can provide many advantages over the gas-based systems. It can help controlling the thermal runaway as the cold surface acts as an insulator containing the char and preventing it from sticking to the walls and damaging the reactor. The liquid can also eliminate the possibility of electric breakdown even at high electric field intensity as the electric breakdown voltage in liquids is extremely

high compared to gases. When considering continuous processing, the liquid system would require less condensation duty compared to the gas system as the condensation of the pyrolysis vapours can take place within the liquid. The condenser would be needed only for condensing and recycling the evaporated solvent.

Future work on the microwave pyrolysis in a liquid should investigate the quality of bio-oil produced from the liquid system and compare it to the gas-based microwave pyrolysis systems and conventionally heated systems. Pyrolysis under continuous liquid flow/recycling through fixed and/or fluidised bed should also be considered as a step towards scaling up. The multiphase flow behaviour of the biomass solid, the liquid, and the evaporated vapour needs to be studied.

10 REFERENCES

ABDULLAH, M. Z., HUSAIN, Z. & YIN PONG, S. L. 2003. Analysis of cold flow fluidization test results for various biomass fuels. *Biomass and Bioenergy,* 24**,** 487-494.

ABUBAKAR, Z., SALEMA, A. A. & ANI, F. N. 2013. A new technique to pyrolyse biomass in a microwave system: Effect of stirrer speed. *Bioresource Technology,* 128**,** 578-585.

ALFAAESAR. 2016. *Safety Data Sheet for Kerosene* [Online]. Available: https://www.alfa.com/en/content/msds/british/L14479.pdf [Accessed 26 October 2016].

ALONSO, D. M., WETTSTEIN, S. G. & DUMESIC, J. A. 2012. Bimetallic catalysts for upgrading of biomass to fuels and chemicals. *Chemical Society Reviews,* 41**,** 8075-8098.

ANASTASAKIS, K., ROSS, A. B. & JONES, J. M. 2011. Pyrolysis behaviour of the main carbohydrates of brown macro-algae. *Fuel,* 90**,** 598-607.

ARSHADI, M. & SELLSTEDT, A. 2008. Production of Energy from Biomass. *Introduction to Chemicals from Biomass.* John Wiley & Sons, Ltd.

ATEŞ, F., PÜTÜN, A. E. & PÜTÜN, E. 2006. Pyrolysis of two different biomass samples in a fixed-bed reactor combined with two different catalysts. *Fuel,* 85**,** 1851-1859.

ATSONIOS, K., PANOPOULOS, K. D., BRIDGWATER, A. V. & KAKARAS, E. 2015. Biomass fast pyrolysis energy balance of a 1kg/h test rig. *International journal of thermodynamics,* 18**,** 267-275.

BAE, Y. J., RYU, C., JEON, J.-K., PARK, J., SUH, D. J., SUH, Y.-W., CHANG, D. & PARK, Y.-K. 2011. The characteristics of bio-oil produced from the pyrolysis of three marine macroalgae. *Bioresource Technology,* 102**,** 3512-3520.

BAI, X., KIM, K. H., BROWN, R. C., DALLUGE, E., HUTCHINSON, C., LEE, Y. J. & DALLUGE, D. 2014. Formation of phenolic oligomers during fast pyrolysis of lignin. *Fuel,* 128**,** 170-179.

BENEROSO, D., ALBERO-ORTIZ, A., MONZÓ-CABRERA, J., DÍAZ-MORCILLO, A., ARENILLAS, A. & MENÉNDEZ, J. A. 2016. Dielectric characterization of biodegradable wastes during pyrolysis. *Fuel,* 172**,** 146-152.

BERGO, P., MORAES, I. C. F. & SOBRAL, P. J. D. A. 2012. Effects of moisture content on structural and dielectric properties of cassava starch films. *Starch - Stärke,* 64**,** 835-839.

BJÖRK, H. & RASMUSON, A. 1995. Moisture equilibrium of wood and bark chips in superheated steam. *Fuel,* 74**,** 1887-1890.

BOIS, K. J., HANDJOJO, L. F., BENALLY, A. D., MUBARAK, K. & ZOUGHI, R. 1999a. Dielectric plug-loaded two-port transmission line measurement technique for dielectric property characterization of granular and liquid materials. *Ieee Transactions on Instrumentation and Measurement,* 48**,** 1141-1148.

BOIS, K. J., HANDJOJO, L. F., BENALLY, A. D., MUBARAK, K. & ZOUGHI, R. 1999b. Dielectric plug-loaded two-port transmission line measurement technique for dielectric property characterization of granular and liquid materials. *Instrumentation and Measurement, IEEE Transactions on,* 48**,** 1141-1148.

BORGES, F. C., DU, Z., XIE, Q., TRIERWEILER, J. O., CHENG, Y., WAN, Y., LIU, Y., ZHU, R., LIN, X., CHEN, P. & RUAN, R. 2014. Fast microwave assisted pyrolysis of biomass using microwave absorbent. *Bioresource Technology,* 156**,** 267-274.

BRACE, C. L. 2009. Microwave ablation technology: What every use should know. *Current problems in diagnostic radiology,* 38**,** 61-67.

BRIDGWATER, A. V. 2003. Renewable fuels and chemicals by thermal processing of biomass. *Chemical Engineering Journal,* 91**,** 87-102.

BRIDGWATER, A. V. 2012. Review of fast pyrolysis of biomass and product upgrading. *Biomass and Bioenergy,* 38**,** 68-94.

BRIDGWATER, A. V. & PEACOCKE, G. V. C. 2000. Fast pyrolysis processes for biomass. *Renewable and Sustainable Energy Reviews,* 4**,** 1-73.
BTG-BTL. 2015. *BTG-BTL pyrolysis process* [Online]. Available: http://www.btg-btl.com/en/technology#process [Accessed 14 October 2015].
CHEN, Q., YANG, R., ZHAO, B., LI, Y., WANG, S., WU, H., ZHUO, Y. & CHEN, C. 2014. Investigation of heat of biomass pyrolysis and secondary reactions by simultaneous thermogravimetry and differential scanning calorimetry. *Fuel,* 134**,** 467-476.
CHERUBINI, F. 2010. The biorefinery concept: Using biomass instead of oil for producing energy and chemicals. *Energy Conversion and Management,* 51**,** 1412-1421.
CHOI, H. S., CHOI, Y. S. & PARK, H. C. 2012. Fast pyrolysis characteristics of lignocellulosic biomass with varying reaction conditions. *Renewable Energy,* 42**,** 131-135.
CLARK, D. E. & SUTTON, W. H. 1996. Microwave processing of materials. *Annual Review of Materials Science,* 26**,** 299-331.
CLARK, J. H. & DESWARTE, F. E. I. 2008. The Biorefinery Concept–An Integrated Approach. *Introduction to Chemicals from Biomass.* John Wiley & Sons, Ltd.
CLARK, J. H., LUQUE, R. & MATHARU, A. S. 2012. Green Chemistry, Biofuels, and Biorefinery. *Annual Review of Chemical and Biomolecular Engineering,* 3**,** 183-207.
COLLARD, F.-X. & BLIN, J. 2014. A review on pyrolysis of biomass constituents: Mechanisms and composition of the products obtained from the conversion of cellulose, hemicelluloses and lignin. *Renewable and Sustainable Energy Reviews,* 38**,** 594-608.
CORNELISSEN, T., YPERMAN, J., REGGERS, G., SCHREURS, S. & CARLEER, R. 2008. Flash co-pyrolysis of biomass with polylactic acid. Part 1: Influence on bio-oil yield and heating value. *Fuel,* 87**,** 1031-1041.
COULSON, J. M., RICHARDSON, J. F., BACKHURST, J. R. & HARKER, J. H. 1999. *Coulson and Richardson's Chemical Engineering Volume 1 - Fluid Flow, Heat Transfer and Mass Transfer (6th Edition)*, Elsevier.
CUI, H. & GRACE, J. R. 2007. Fluidization of biomass particles: A review of experimental multiphase flow aspects. *Chemical Engineering Science,* 62**,** 45-55.
DAHMEN, N., DINJUS, E., KOLB, T., ARNOLD, U., LEIBOLD, H. & STAHL, R. 2012. State of the art of the bioliq® process for synthetic biofuels production. *Environmental Progress & Sustainable Energy,* 31**,** 176-181.
DAUGAARD, D. E. & BROWN, R. C. 2003. Enthalpy for Pyrolysis for Several Types of Biomass. *Energy & Fuels,* 17**,** 934-939.
DEAN, E. W. & STARK, D. D. 1920. A Convenient Method for the Determination of Water in Petroleum and Other Organic Emulsions. *Journal of Industrial & Engineering Chemistry,* 12**,** 486-490.
DEFRA 2012. Wood waste: A short review of recent research. Department for Environment, Food and Rural Affairs.
DEFRA 2013. Expermental Statistics: Area of Crops Grown For Bioenergy in England and the UK: 2008 - 2012 *In:* AFFAIRS, D. F. E. F. R. (ed.). UK.
DEFRA 2015. Area of Crops Grown For Bioenergy in England and the UK: 2008 - 2014. Department for Environment, Food and Rural Affairs.
DEMIRBAŞ, A. 2000. Mechanisms of liquefaction and pyrolysis reactions of biomass. *Energy Conversion and Management,* 41**,** 633-646.
DHIR, V. K. 1998. BOILING HEAT TRANSFER. *Annual Review of Fluid Mechanics,* 30**,** 365-401.
DHONDT, G., DE ZUTTER, D. & MARTENS, L. An improved free-space technique modelling for measuring dielectric properties of materials. Antennas and Propagation Society International Symposium, 1996. AP-S. Digest, 21-26 July 1996 1996. 180-183 vol.1.

DI FELICE, R. & GIBILARO, L. G. 2004. Wall effects for the pressure drop in fixed beds. *Chemical Engineering Science,* 59**,** 3037-3040.
DING, T., LI, S., XIE, J., SONG, W., YAO, J. & LIN, W. 2012. Rapid Pyrolysis of Wheat Straw in a Bench-Scale Circulating Fluidized-Bed Downer Reactor. *Chemical Engineering & Technology,* 35**,** 2170-2176.
ENSYN. 2012. *RTP Process* [Online]. Available: http://www.ensyn.com/technology/overview/ [Accessed 13 October 2015].
FAO 2009. Algae-based biofuels: A review of challenges and opportunitites for developing countries. Rome: Food and Agriculture Organization of the United Nations (FAO).
FARDAD, D. & LADOMMATOS, N. 1999. Evaporation of hydrocarbon compounds, including gasoline and diesel fuel, on heated metal surfaces. *Proceedings of the Institution of Mechanical Engineers, Part D: Journal of Automobile Engineering,* 213**,** 625-645.
FERRARI-JOHN, R. S., KATRIB, J., PALADE, P., BATCHELOR, A. R., DODDS, C. & KINGMAN, S. W. 2016. A Tool for Predicting Heating Uniformity in Industrial Radio Frequency Processing. *Food and Bioprocess Technology,* 9**,** 1865-1873.
FOREST-FUELS. 2016. *Fuel Price Comparison* [Online]. Available: http://www.forestfuels.co.uk/about-wood-fuel/fuel-price-comparisons [Accessed 27 September 2016].
FOUILLAND, T., GRACE, J. R. & ELLIS, N. 2010. Recent advances in fluidized bed technology in biomass processes. *Biofuels,* 1**,** 409-433.
FOUST, T. D., IBSEN, K. N., DAYTON, D. C., HESS, J. R. & KENNEY, K. E. 2009. The Biorefinery. *Biomass Recalcitrance.* Blackwell Publishing Ltd.
GABRIEL, C., GABRIEL, S., H. GRANT, E., H. GRANT, E., S. J. HALSTEAD, B. & MICHAEL P. MINGOS, D. 1998. Dielectric parameters relevant to microwave dielectric heating. *Chemical Society Reviews,* 27**,** 213-224.
GARCÍA, R., PIZARRO, C., LAVÍN, A. G. & BUENO, J. L. 2013. Biomass proximate analysis using thermogravimetry. *Bioresource Technology,* 139**,** 1-4.
GELDART, D. 1973. Types of gas fluidization. *Powder Technology,* 7**,** 285-292.
GERDES, T., TAP, R., BAHKE, P. & WILLERT-PORADA, M. 2006. CVD-processes in microwave heated fluidized bed reactors. *Advances in Microwave and radio frequency Processing.* Springer.
GHODGAONKAR, D. K., VARADAN, V. V. & VARADAN, V. K. 1989. A free-space method for measurement of dielectric constants and loss tangents at microwave frequencies. *Instrumentation and Measurement, IEEE Transactions on,* 38**,** 789-793.
GIUDICIANNI, P., CARDONE, G. & RAGUCCI, R. 2013. Cellulose, hemicellulose and lignin slow steam pyrolysis: Thermal decomposition of biomass components mixtures. *Journal of Analytical and Applied Pyrolysis,* 100**,** 213-222.
GOKSU, E. I., SUMNU, G. & ESIN, A. 2005. Effect of microwave on fluidized bed drying of macaroni beads. *Journal of Food Engineering,* 66**,** 463-468.
GÓMEZ-MONEDERO, B., BIMBELA, F., ARAUZO, J., FARIA, J. & RUIZ, M. P. 2015. Pyrolysis of Red Eucalyptus, Camelina Straw, and Wheat Straw in an Ablative Reactor. *Energy & Fuels,* 29**,** 1766-1775.
GREEN, D. W. & PERRY, R. H. 2007. *Perry's Chemical Engineers' Handbook, Eighth Edition*, McGraw-Hill Professional.
GUDE, V., PATIL, P., MARTINEZ-GUERRA, E., DENG, S. & NIRMALAKHANDAN, N. 2013. Microwave energy potential for biodiesel production. *Sustainable Chemical Processes,* 1**,** 1-31.
GÜNTHER, B., GEBAUER, K., BARKOWSKI, R., ROSENTHAL, M. & BUES, C.-T. 2012. Calorific value of selected wood species and wood products. *European Journal of Wood and Wood Products,* 70**,** 755-757.
GUO, M., SONG, W. & BUHAIN, J. 2015. Bioenergy and biofuels: History, status, and perspective. *Renewable and Sustainable Energy Reviews,* 42**,** 712-725.

GUO, W., LIM, C. J., BI, X., SOKHANSANJ, S. & MELIN, S. 2013. Determination of effective thermal conductivity and specific heat capacity of wood pellets. *Fuel,* 103**,** 347-355.
HARDY, G. & GUIRY, M. D. 2003. A Check-list and Atlas of the Seaweeds of Britain and Ireland. London: The British Phycological Society.
HE, F., YI, W. & BAI, X. 2006. Investigation on caloric requirement of biomass pyrolysis using TG–DSC analyzer. *Energy Conversion and Management,* 47**,** 2461-2469.
HENRICH, E., DAHMEN, N., WEIRICH, F., REIMERT, R. & KORNMAYER, C. 2016. Fast pyrolysis of lignocellulosics in a twin screw mixer reactor. *Fuel Processing Technology,* 143**,** 151-161.
HU, Z., MA, X. & CHEN, C. 2012. A study on experimental characteristic of microwave-assisted pyrolysis of microalgae. *Bioresource Technology,* 107**,** 487-493.
HUANG, Y.-F., CHIUEH, P.-T. & LO, S.-L. 2016. A review on microwave pyrolysis of lignocellulosic biomass. *Sustainable Environment Research,* 26**,** 103-109.
IEA 2015. Key World Energy Statistics. Paris, France: International Energy Agency.
IPCC 2013. Climate Change 2013, The Physical Science Basis: Summary for Policymakers. Intergovernmental Panel on Climate Change.
ISIKGOR, F. H. & BECER, C. R. 2015. Lignocellulosic biomass: a sustainable platform for the production of bio-based chemicals and polymers. *Polymer Chemistry,* 6**,** 4497-4559.
JIA, D., CATHARY, O., PENG, J., BI, X., LIM, C. J., SOKHANSANJ, S., LIU, Y., WANG, R. & TSUTSUMI, A. 2015. Fluidization and drying of biomass particles in a vibrating fluidized bed with pulsed gas flow. *Fuel Processing Technology,* 138**,** 471-482.
JONES, D. A., LELYVELD, T. P., MAVROFIDIS, S. D., KINGMAN, S. W. & MILES, N. J. 2002. Microwave heating applications in environmental engineering—a review. *Resources, Conservation and Recycling,* 34**,** 75-90.
KAATZE, U. 1989. Complex permittivity of water as a function of frequency and temperature. *Journal of Chemical & Engineering Data,* 34**,** 371-374.
KATRIB, J., FOLORUNSO, O., DODDS, C., DIMITRAKIS, G. & KINGMAN, S. W. 2015. Improving the design of industrial microwave processing systems through prediction of the dielectric properties of complex multi-layered materials. *Journal of Materials Science,* 50**,** 7591-7599.
KHOSHTAGHAZA, M. H., DARVISHI, H. & MINAEI, S. 2015. Effects of microwave - fluidized bed drying on quality, energy consumption and drying kinetics of soybean kernels. *Journal of Food Science and Technology,* 52**,** 4749-4760.
KITCHEN, H. J., VALLANCE, S. R., KENNEDY, J. L., TAPIA-RUIZ, N., CARASSITI, L., HARRISON, A., WHITTAKER, A. G., DRYSDALE, T. D., KINGMAN, S. W. & GREGORY, D. H. 2014. Modern Microwave Methods in Solid-State Inorganic Materials Chemistry: From Fundamentals to Manufacturing. *Chemical Reviews,* 114**,** 1170-1206.
KLAIGAEW, K., WATTANAPAPHAWONG, P., KHUHAUDOMLAP, N., HINCHIRANAN, N., KUCHONTARA, P., KANGWANSAICHOL, K. & REUBROYCHAROEN, P. 2015. Liquid Phase Pyrolysis of Giant Leucaena Wood to Bio-Oil over NiMo/Al2O3 Catalyst. *Energy Procedia,* 79**,** 492-499.
KOUTINAS, A. A., DU, C., WANG, R. H. & WEBB, C. 2008. Production of Chemicals from Biomass. *Introduction to Chemicals from Biomass.* John Wiley & Sons, Ltd.
LEHTO, J., OASMAA, A., SOLANTAUSTA, Y., KYTÖ, M. & CHIARAMONTI, D. 2014. Review of fuel oil quality and combustion of fast pyrolysis bio-oils from lignocellulosic biomass. *Applied Energy,* 116**,** 178-190.
LESTER, E., KINGMAN, S., DODDS, C. & PATRICK, J. 2006. The potential for rapid coke making using microwave energy. *Fuel,* 85**,** 2057-2063.

LI, L., MA, X., XU, Q. & HU, Z. 2013. Influence of microwave power, metal oxides and metal salts on the pyrolysis of algae. *Bioresource Technology,* 142**,** 469-474.
LIDSTRÖM, P., TIERNEY, J., WATHEY, B. & WESTMAN, J. 2001. Microwave assisted organic synthesis—a review. *Tetrahedron,* 57**,** 9225-9283.
LIN, F., WATERS, C. L., MALLINSON, R. G., LOBBAN, L. L. & BARTLEY, L. E. 2015. Relationships between biomass composition and liquid products formed via pyrolysis. *Frontiers in Energy Research,* 3.
LIU, Y., PENG, J., KANSHA, Y., ISHIZUKA, M., TSUTSUMI, A., JIA, D., BI, X. T., LIM, C. J. & SOKHANSANJ, S. 2014. Novel fluidized bed dryer for biomass drying. *Fuel Processing Technology,* 122**,** 170-175.
LUQUE, R., MENENDEZ, J. A., ARENILLAS, A. & COT, J. 2012. Microwave-assisted pyrolysis of biomass feedstocks: the way forward? *Energy & Environmental Science,* 5**,** 5481-5488.
LY, H. V., KIM, S.-S., CHOI, J. H., WOO, H. C. & KIM, J. 2016. Fast pyrolysis of Saccharina japonica alga in a fixed-bed reactor for bio-oil production. *Energy Conversion and Management,* 122**,** 526-534.
LY, H. V., KIM, S.-S., WOO, H. C., CHOI, J. H., SUH, D. J. & KIM, J. 2015. Fast pyrolysis of macroalga Saccharina japonica in a bubbling fluidized-bed reactor for bio-oil production. *Energy,* 93, Part 2**,** 1436-1446.
MACQUARRIE, D. J., CLARK, J. H. & FITZPATRICK, E. 2012. The microwave pyrolysis of biomass. *Biofuels, Bioproducts and Biorefining,* 6**,** 549-560.
MCKENDRY, P. 2002. Energy production from biomass (part 1): overview of biomass. *Bioresource Technology,* 83**,** 37-46.
MEHDIZADEH, M. 2015. *Microwave/RF Applicators and Probes: for Material Heating, Sensing, and Plasma Generation*, William Andrew.
MEREDITH, R. 1998. *Engineers' Handbook of Industerial Microwave Heating,* London, The Institution of Engineering and Technology.
METAXAS, A. C. & MEREDITH, R. J. 1983. *Industrial microwave heating,* London, Peter Peregrinus Ltd.
METTLER, M. S., VLACHOS, D. G. & DAUENHAUER, P. J. 2012. Top ten fundamental challenges of biomass pyrolysis for biofuels. *Energy & Environmental Science,* 5**,** 7797-7809.
MEULENBROEK, R. & BELD, B. V. D. 2015. Opening of the EMPYRO fast pyrolysis plant, PyNe Newsletter No.37. Birmingham, UK.
MILLS, A. A. & FRY, J. D. 1982. Rate of evaporation of hydrocarbons from a hot surface: Nukiyama and Leidenfrost temperatures. *European Journal of Physics,* 3**,** 152.
MIURA, M., KAGA, H., SAKURAI, A., KAKUCHI, T. & TAKAHASHI, K. 2004. Rapid pyrolysis of wood block by microwave heating. *Journal of Analytical and Applied Pyrolysis,* 71**,** 187-199.
MOHAMED, B. A., KIM, C. S., ELLIS, N. & BI, X. 2016. Microwave-assisted catalytic pyrolysis of switchgrass for improving bio-oil and biochar properties. *Bioresource Technology,* 201**,** 121-132.
MOHAN, D., PITTMAN, C. U. & STEELE, P. H. 2006. Pyrolysis of Wood/Biomass for Bio-oil: A Critical Review. *Energy & Fuels,* 20**,** 848-889.
MONTOYA, J. I., VALDÉS, C., CHEJNE, F., GÓMEZ, C. A., BLANCO, A., MARRUGO, G., OSORIO, J., CASTILLO, E., ARISTÓBULO, J. & ACERO, J. 2015. Bio-oil production from Colombian bagasse by fast pyrolysis in a fluidized bed: An experimental study. *Journal of Analytical and Applied Pyrolysis,* 112**,** 379-387.
MOTASEMI, F. & AFZAL, M. T. 2013. A review on the microwave-assisted pyrolysis technique. *Renewable & Sustainable Energy Reviews,* 28**,** 317-330.
MOTASEMI, F., AFZAL, M. T., SALEMA, A. A., MOURIS, J. & HUTCHEON, R. M. 2014. Microwave dielectric characterization of switchgrass for bioenergy and biofuel. *Fuel,* 124**,** 151-157.

MOTASEMI, F., SALEMA, A. A. & AFZAL, M. T. 2015. Dielectric characterization of corn stover for microwave processing technology. *Fuel Processing Technology,* 131**,** 370-375.
MUKAIDA, K.-I. 1981. Density measurement of small porous particles by mercury porosimetry. *Powder Technology,* 29**,** 99-107.
MUSHTAQ, F., MAT, R. & ANI, F. N. 2014. A review on microwave assisted pyrolysis of coal and biomass for fuel production. *Renewable & Sustainable Energy Reviews,* 39**,** 555-574.
NAKAMURA, E. & FURUICHI, J. 1960. Measurement of Microwave Dielectric Constants of Ferroelectrics Part I. Dielectric Constants of BaTiO3 Single Crystal at 3.3 KMc/s. *Journal of the Physical Society of Japan,* 15**,** 1955-1960.
NELSON, S. O. 1999. Dielectric properties measurement techniques and applications. *Transactions of the American Society of Agricultural Engineers,* 42**,** 523-529.
NELSON, S. O. 2005. Density-permittivity relationships for powdered and granular materials. *Instrumentation and Measurement, IEEE Transactions on,* 54**,** 2033-2040.
NELSON, S. O. 2010. Fundamentals of Dielectric Properties Measurements and Agricultural Applications. *Journal of Microwave Power and Electromagnetic Energy,* 44**,** 98-113.
NELSON, S. O. & BARTLEY, P. G. 1998. Open-ended coaxial-line permittivity measurements on pulverized materials. *Instrumentation and Measurement, IEEE Transactions on,* 47**,** 133-137.
NELSON, S. O. & TRABELSI, S. 2012. Factors Influencing the Dielectric Properties of Agricultural and Food Products. *Journal of Microwave Power and Electromagnetic Energy,* 46**,** 93-107.
NIOSH. 2014. *International Chemical Safety Cards (ICSC): Distillates (Petroleum), Hydrotreated Light* [Online]. The National Institute for Occupational Safety and Health (NIOSH). Available: http://www.cdc.gov/niosh/ipcsneng/neng1379.html [Accessed 11 September 2016].
NPL 2003. A Guide to characterisation of dielectric materials at RF and microwave frequencies. London: National Physical Laboratory and the Institute of Measurement and Control.
OASMAA, A., PEACOCKE, C., GUST, S., MEIER, D. & MCLELLAN, R. 2005. Norms and Standards for Pyrolysis Liquids. End-User Requirements and Specifications. *Energy & Fuels,* 19**,** 2155-2163.
OASMAA, A., VAN DE BELD, B., SAARI, P., ELLIOTT, D. C. & SOLANTAUSTA, Y. 2015. Norms, Standards, and Legislation for Fast Pyrolysis Bio-oils from Lignocellulosic Biomass. *Energy & Fuels,* 29**,** 2471-2484.
ONAY, O. 2007. Fast and catalytic pyrolysis of pistacia khinjuk seed in a well-swept fixed bed reactor. *Fuel,* 86**,** 1452-1460.
ÖZBAY, N., PÜTÜN, A. E. & PÜTÜN, E. 2001. Structural analysis of bio-oils from pyrolysis and steam pyrolysis of cottonseed cake. *Journal of Analytical and Applied Pyrolysis,* 60**,** 89-101.
PARIKKA, M. 2004. Global biomass fuel resources. *Biomass and Bioenergy,* 27**,** 613-620.
PATWARDHAN, P. R., DALLUGE, D. L., SHANKS, B. H. & BROWN, R. C. 2011. Distinguishing primary and secondary reactions of cellulose pyrolysis. *Bioresource Technology,* 102**,** 5265-5269.
PAUDEL, B. & FENG, Z.-G. 2013. Prediction of minimum fluidization velocity for binary mixtures of biomass and inert particles. *Powder Technology,* 237**,** 134-140.
PELL, M. & DUNSON, J. B. 1997. Gas-Solid Operations and Equipment. *In:* PERRY, R. H., GREEN, D. W. & MALONEY, J. O. (eds.) *Perry's Chemical Engineers' Handbook.* Seventh ed. USA: McGraw-Hill Companies, Inc.

PIANROJ, Y., JUMRAT, S., WERAPUN, W., KARRILA, S. & TONGURAI, C. 2016. Scaled-up reactor for microwave induced pyrolysis of oil palm shell. *Chemical Engineering and Processing: Process Intensification,* 106**,** 42-49.
R. RAO, T. & RAM. BHEEMARASETTI, J. V. 2001. Minimum fluidization velocities of mixtures of biomass and sands. *Energy,* 26**,** 633-644.
RAO, A., CURTIS, J. S., HANCOCK, B. C. & WASSGREN, C. 2010. The effect of column diameter and bed height on minimum fluidization velocity. *AIChE Journal,* 56**,** 2304-2311.
RATTANADECHO, P. & MAKUL, N. 2016. Microwave-Assisted Drying: A Review of the State-of-the-Art. *Drying Technology,* 34**,** 1-38.
READER, H. C. 2006. Understanding Microwave Heating Systems: A Perspective on State-of-the-Art. *In:* WILLERT-PORADA, M. (ed.) *Advances in Microwave and Radio Frequency Processing.* Springer Berlin Heidelberg.
REINA, J., VELO, E. & PUIGJANER, L. 2000. Predicting the minimum fluidization velocity of polydisperse mixtures of scrap-wood particles. *Powder Technology,* 111**,** 245-251.
REMYA, N. & LIN, J.-G. 2011. Current status of microwave application in wastewater treatment—A review. *Chemical Engineering Journal,* 166**,** 797-813.
RICHARDSON, J. F., HARKER, J. H. & BACKHURST, J. R. 2002. CHAPTER 6 - Fluidisation. *In:* BACKHURST, J. F. R. H. H. R. (ed.) *Chemical Engineering (Fifth Edition).* Oxford: Butterworth-Heinemann.
RINGER, M., PUTSCHE, V. & SCAHILL, J. 2006. Large-Scale Pyrolysis Oil. *Assessment*.
ROBINSON, J., BINNER, E., SAEID, A., AL-HARAHSHEH, M. & KINGMAN, S. 2014. Microwave processing of Oil Sands and contribution of clay minerals. *Fuel,* 135**,** 153-161.
ROBINSON, J., DODDS, C., STAVRINIDES, A., KINGMAN, S., KATRIB, J., WU, Z. H., MEDRANO, J. & OVEREND, R. 2015. Microwave Pyrolysis of Biomass: Control of Process Parameters for High Pyrolysis Oil Yields and Enhanced Oil Quality. *Energy & Fuels,* 29**,** 1701-1709.
ROBINSON, J., KINGMAN, S., IRVINE, D., LICENCE, P., SMITH, A., DIMITRAKIS, G., OBERMAYER, D. & KAPPE, C. O. 2010a. Understanding microwave heating effects in single mode type cavities-theory and experiment. *Physical Chemistry Chemical Physics,* 12**,** 4750-4758.
ROBINSON, J. P., KINGMAN, S. W., BARRANCO, R., SNAPE, C. E. & AL-SAYEGH, H. 2010b. Microwave Pyrolysis of Wood Pellets. *Industrial & Engineering Chemistry Research,* 49**,** 459-463.
ROBSON, A. 2000. DynaMotive 2000 Progress Report *In:* BRIDGWATER, T. (ed.) *PyNe Newsletter No. 10.* Birmingham, UK.
ROSS, A. B., ANASTASAKIS, K., KUBACKI, M. & JONES, J. M. 2009. Investigation of the pyrolysis behaviour of brown algae before and after pre-treatment using PY-GC/MS and TGA. *Journal of Analytical and Applied Pyrolysis,* 85**,** 3-10.
ROSS, A. B., JONES, J. M., KUBACKI, M. L. & BRIDGEMAN, T. 2008. Classification of macroalgae as fuel and its thermochemical behaviour. *Bioresource Technology,* 99**,** 6494-6504.
SAIREM. 2015. *The generators* [Online]. Available: http://www.sairem.com/the-generators-44.html [Accessed 19 January 2016].
SAIT, H. H. & SALEMA, A. A. 2015. Microwave dielectric characterization of Saudi Arabian date palm biomass during pyrolysis and at industrial frequencies. *Fuel,* 161**,** 239-247.
SALEMA, A. A. & AFZAL, M. T. 2015. Numerical simulation of heating behaviour in biomass bed and pellets under multimode microwave system. *International Journal of Thermal Sciences,* 91**,** 12-24.
SALEMA, A. A. & ANI, F. N. 2012. Microwave-assisted pyrolysis of oil palm shell biomass using an overhead stirrer. *Journal of Analytical and Applied Pyrolysis,* 96**,** 162-172.

SALEMA, A. A., YEOW, Y. K., ISHAQUE, K., ANI, F. N., AFZAL, M. T. & HASSAN, A. 2013. Dielectric properties and microwave heating of oil palm biomass and biochar. *Industrial Crops and Products,* 50**,** 366-374.
SALVI, D., BOLDOR, D., AITA, G. M. & SABLIOV, C. M. 2011. COMSOL Multiphysics model for continuous flow microwave heating of liquids. *Journal of Food Engineering,* 104**,** 422-429.
SALVI, D., BOLDOR, D., ORTEGO, J., AITA, G. M. & SABLIOV, C. M. 2010. Numerical modeling of continuous flow microwave heating: A critical Comparison of COMSOL and ANSYS. *Journal of Microwave Power and Electromagnetic Energy,* 44**,** 187-197.
SCOTT, D. S., MAJERSKI, P., PISKORZ, J. & RADLEIN, D. 1999. A second look at fast pyrolysis of biomass—the RTI process. *Journal of Analytical and Applied Pyrolysis,* 51**,** 23-37.
SCOTT, D. S. & PISKORZ, J. 1982. The flash pyrolysis of aspen-poplar wood. *The Canadian Journal of Chemical Engineering,* 60**,** 666-674.
SCOTT, D. S. & PISKORZ, J. 1984. The continuous flash pyrolysis of biomass. *The Canadian Journal of Chemical Engineering,* 62**,** 404-412.
SCOTT, D. S., PISKORZ, J. & RADLEIN, D. 1985. Liquid products from the continuous flash pyrolysis of biomass. *Industrial & Engineering Chemistry Process Design and Development,* 24**,** 581-588.
SHANG, H., LU, R.-R., SHANG, L. & ZHANG, W.-H. 2015. Effect of additives on the microwave-assisted pyrolysis of sawdust. *Fuel Processing Technology,* 131**,** 167-174.
SHEEN, J. 2005. Study of microwave dielectric properties measurements by various resonance techniques. *Measurement,* 37**,** 123-130.
SHEN, J., WANG, X.-S., GARCIA-PEREZ, M., MOURANT, D., RHODES, M. J. & LI, C.-Z. 2009. Effects of particle size on the fast pyrolysis of oil mallee woody biomass. *Fuel,* 88**,** 1810-1817.
SHRESTHA, B. L., WOOD, H. C. & SOKHANSANJ, S. 2011. Microwave Dielectric Properties of Alfalfa Leaves From 0.3 to 18 GHz. *Instrumentation and Measurement, IEEE Transactions on,* 60**,** 2926-2933.
SIHVOLA, A. 1999. *Electromagnetic Mixing Formulas and Applications*, Institution of Engineering and Technology.
SMETS, K., ADRIAENSENS, P., VANDEWIJNGAARDEN, J., STALS, M., CORNELISSEN, T., SCHREURS, S., CARLEER, R. & YPERMAN, J. 2011. Water content of pyrolysis oil: Comparison between Karl Fischer titration, GC/MS-corrected azeotropic distillation and 1H NMR spectroscopy. *Journal of Analytical and Applied Pyrolysis,* 90**,** 100-105.
SMITH, A. D., LESTER, E., THURECHT, K. J., EL HARFI, J., DIMITRAKIS, G., KINGMAN, S. W., ROBINSON, J. P. & IRVINE, D. J. 2010. Dielectric Properties of Free-Radical Polymerizations: Molecularly Symmetrical Initiators during Thermal Decomposition. *Industrial & Engineering Chemistry Research,* 49**,** 1703-1710.
SOURAKI, B. A., ANDRÉS, A. & MOWLA, D. 2009. Mathematical modeling of microwave-assisted inert medium fluidized bed drying of cylindrical carrot samples. *Chemical Engineering and Processing: Process Intensification,* 48**,** 296-305.
STEFANIDIS, S. D., KALOGIANNIS, K. G., ILIOPOULOU, E. F., MICHAILOF, C. M., PILAVACHI, P. A. & LAPPAS, A. A. 2014. A study of lignocellulosic biomass pyrolysis via the pyrolysis of cellulose, hemicellulose and lignin. *Journal of Analytical and Applied Pyrolysis,* 105**,** 143-150.
SUBHADRA, B. & EDWARDS, M. 2010. An integrated renewable energy park approach for algal biofuel production in United States. *Energy Policy,* 38**,** 4897-4902.
SUN, Y. & CHENG, J. 2002. Hydrolysis of lignocellulosic materials for ethanol production: a review. *Bioresource Technology,* 83**,** 1-11.

TRABELSI, S. & NELSON, S., O. 2003. Free-space measurement of dielectric properties of cereal grain and oilseed at microwave frequencies. *Measurement Science and Technology,* 14**,** 589.
TRANQUILLA, J. M. 2000. Method and apparatus for optimization of energy coupling for microwave treatment of metal ores and concentrates in a microwave fluidized bed reactor. Google Patents.
TRANQUILLA, J. M. & KRUESI, P. R. 1999. Method for the microwave induced oxidation of pyritic ores without the production of sulphur dioxide. Google Patents.
TUHKALA, M., JUUTI, J. & JANTUNEN, H. 2013. Method to characterize dielectric properties of powdery substances. *Journal of Applied Physics,* 114**,** -.
TURLEY, D. B. 2008. The Chemical Value of Biomass. *Introduction to Chemicals from Biomass.* John Wiley & Sons, Ltd.
UN 2015. World Population Prospects: The 2015 Revision, Key Findings and Advance Tables. United Nations, Department of Economic and Social Affairs, Population Division.
VALENTÍN, L., KLUCZEK-TURPEINEN, B., WILLFÖR, S., HEMMING, J., HATAKKA, A., STEFFEN, K. & TUOMELA, M. 2010. Scots pine (Pinus sylvestris) bark composition and degradation by fungi: Potential substrate for bioremediation. *Bioresource Technology,* 101**,** 2203-2209.
VAN DAM, J. E. G., DE KLERK-ENGELS, B., STRUIK, P. C. & RABBINGE, R. 2005. Securing renewable resource supplies for changing market demands in a bio-based economy. *Industrial Crops and Products,* 21**,** 129-144.
VAN DE VELDEN, M., BAEYENS, J., BREMS, A., JANSSENS, B. & DEWIL, R. 2010. Fundamentals, kinetics and endothermicity of the biomass pyrolysis reaction. *Renewable Energy,* 35**,** 232-242.
VARADAN, V. V., HOLLINGER, R. D., GHODGAONKAR, D. K. & VARADAN, V. K. 1991a. Free-space, broadband measurements of high-temperature, complex dielectric properties at microwave frequencies. *Instrumentation and Measurement, IEEE Transactions on,* 40**,** 842-846.
VARADAN, V. V., HOLLINGER, R. D., GHODGAONKAR, D. K. & VARADAN, V. K. 1991b. Free-space, broadband measurements of high-temperature, complex dielectric properties at microwave frequencies. *IEEE Transactions on Instrumentation and Measurement,* 40**,** 842-846.
VENKATESH, M. S. & RAGHAVAN, G. S. V. 2005. An overview of dielectric properties measuring techniques. *Canadian Biosystems Engineering,* 47**,** 7.15-7-30.
VERSTEEG, H. K. & MALALASEKERA, W. 2007. *An introduction to computational fluid dynamics: the finite volume method*, Pearson Education.
WANG, S., JIANG, X. M., WANG, Q., JI, H. S., WU, L. F., WANG, J. F. & XU, S. N. 2013a. Research of specific heat capacities of three large seaweed biomass. *Journal of Thermal Analysis and Calorimetry***,** 1-7.
WANG, S., RU, B., LIN, H. & SUN, W. 2015. Pyrolysis behaviors of four O-acetyl-preserved hemicelluloses isolated from hardwoods and softwoods. *Fuel,* 150**,** 243-251.
WANG, S., WANG, Q., JIANG, X., HAN, X. & JI, H. 2013b. Compositional analysis of bio-oil derived from pyrolysis of seaweed. *Energy Conversion and Management,* 68**,** 273-280.
WEN, C. Y. & YU, Y. H. 1966. A generalized method for predicting the minimum fluidization velocity. *AIChE Journal,* 12**,** 610-612.
WILLERT-PORADA, M., ROSIN, A., SCHMIDT, A., GERDES, T. & ADAM, M. Analysis of microwave heating in a fluidized bed reactor. 2014 IEEE MTT-S International Microwave Symposium (IMS2014), 2014. IEEE, 1-4.
WONG, P. P. & FORSTER, E. O. 1982. The Dynamics of Electrical Breakdown in Liquid Hydrocarbons. *IEEE Transactions on Electrical Insulation,* EI-17**,** 203-220.

YANG, H., KUDO, S., KUO, H.-P., NORINAGA, K., MORI, A., MAŠEK, O. & HAYASHI, J.-I. 2013. Estimation of Enthalpy of Bio-Oil Vapor and Heat Required for Pyrolysis of Biomass. *Energy & Fuels,* 27**,** 2675-2686.
YANG, H., YAN, R., CHEN, H., LEE, D. H. & ZHENG, C. 2007. Characteristics of hemicellulose, cellulose and lignin pyrolysis. *Fuel,* 86**,** 1781-1788.
YANG, H., YAN, R., CHEN, H., ZHENG, C., LEE, D. H. & LIANG, D. T. 2006. In-Depth Investigation of Biomass Pyrolysis Based on Three Major Components: Hemicellulose, Cellulose and Lignin. *Energy & Fuels,* 20**,** 388-393.
YANIK, J., STAHL, R., TROEGER, N. & SINAG, A. 2013. Pyrolysis of algal biomass. *Journal of Analytical and Applied Pyrolysis,* 103**,** 134-141.
YIN, C. 2012. Microwave-assisted pyrolysis of biomass for liquid biofuels production. *Bioresource Technology,* 120**,** 273-284.
YU, V. B., RYBAKOV, K. I. & SEMENOV, V. E. 2001. High-temperature microwave processing of materials. *Journal of Physics D: Applied Physics,* 34**,** R55.
ZHANG, J., CHOI, Y. S., YOO, C. G., KIM, T. H., BROWN, R. C. & SHANKS, B. H. 2015. Cellulose–Hemicellulose and Cellulose–Lignin Interactions during Fast Pyrolysis. *ACS Sustainable Chemistry & Engineering,* 3**,** 293-301.
ZHANG, M., TANG, J., MUJUMDAR, A. S. & WANG, S. 2006. Trends in microwave-related drying of fruits and vegetables. *Trends in Food Science & Technology,* 17**,** 524-534.
ZHANG, Q., CHANG, J., WANG, T. & XU, Y. 2007. Review of biomass pyrolysis oil properties and upgrading research. *Energy Conversion and Management,* 48**,** 87-92.

11 APPENDICES

11.1 Appendix A: Particle Size Distribution

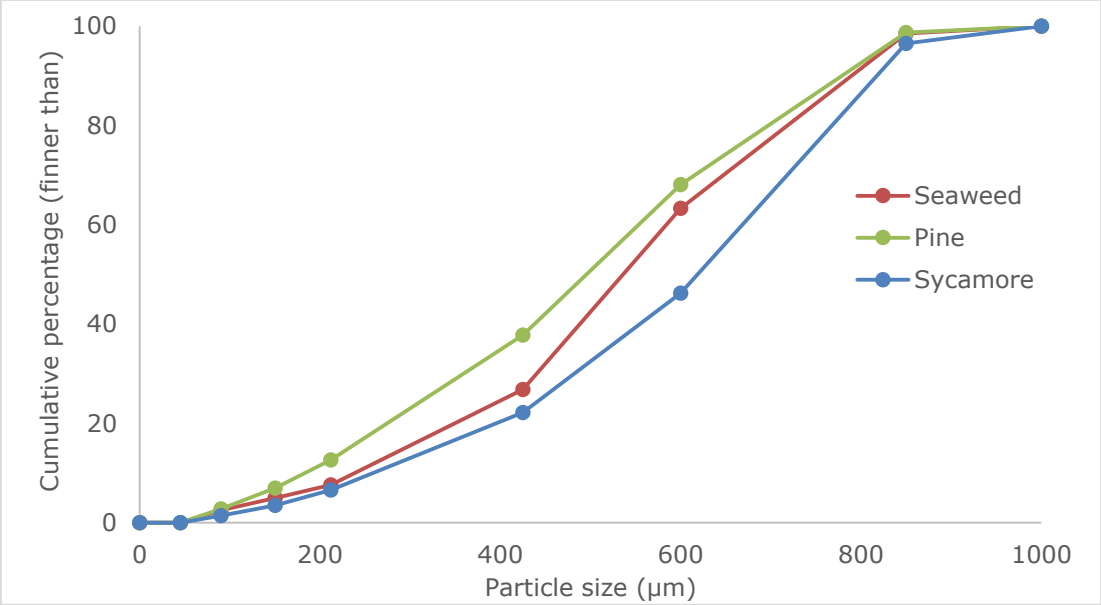

Figure A-1: Particle size distribution of the biomass materials after crushing them in a shredder using 0.75 mm shredder mesh.

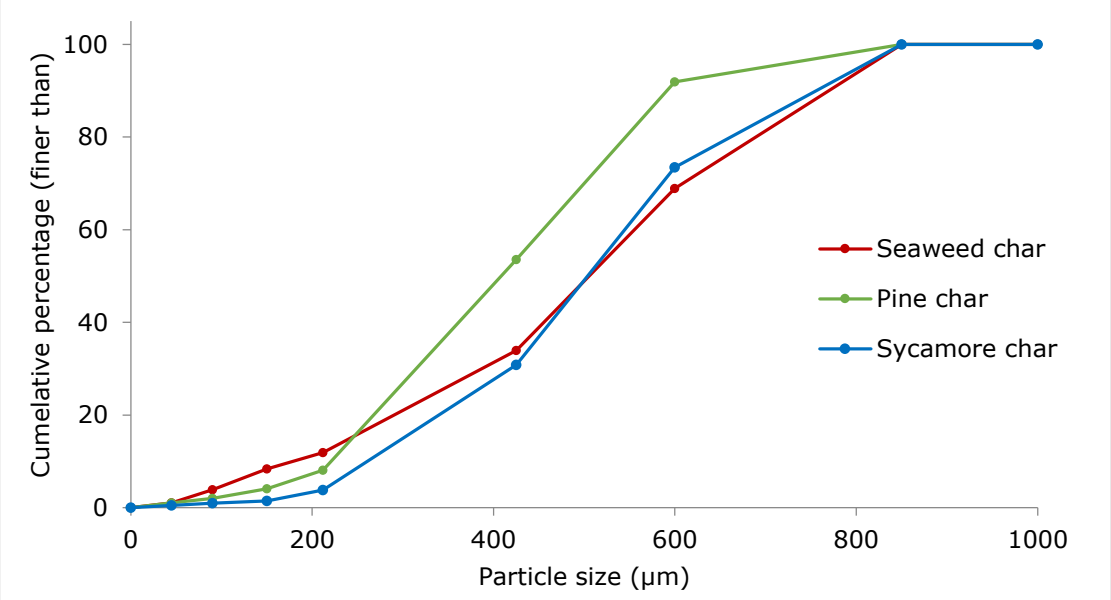

Figure A-2: Particle size distribution of char particles after pyrolysis of particles with the size distribution shown in Figure A-1.

11.2 Appendix B: Mercury Porosimetery Results

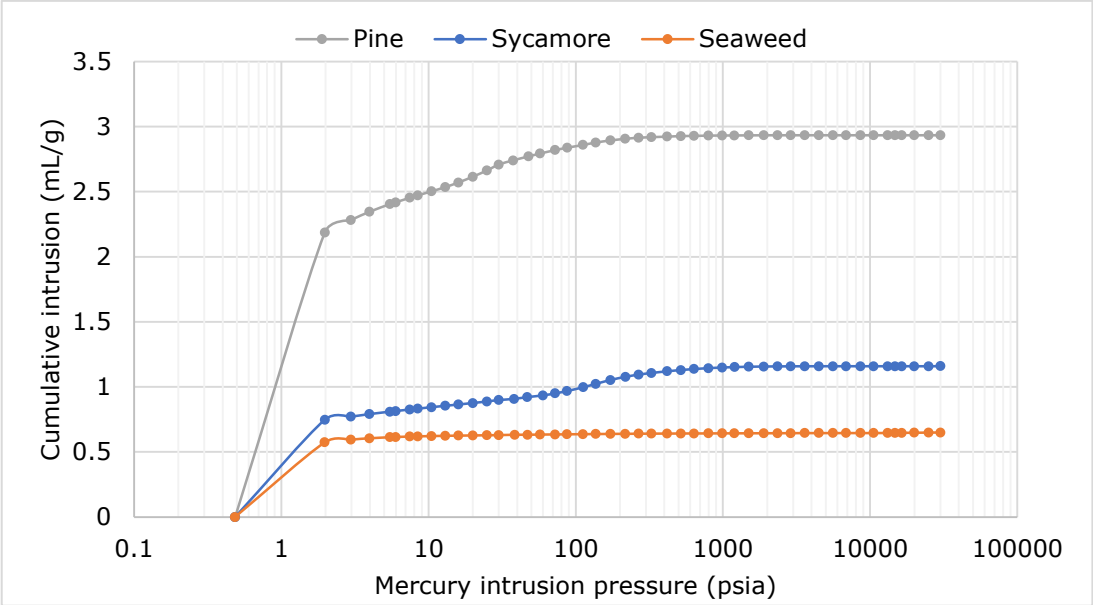

Figure B-1: Mercury intrusion results for the biomass particle of the size 212 – 850 µm.

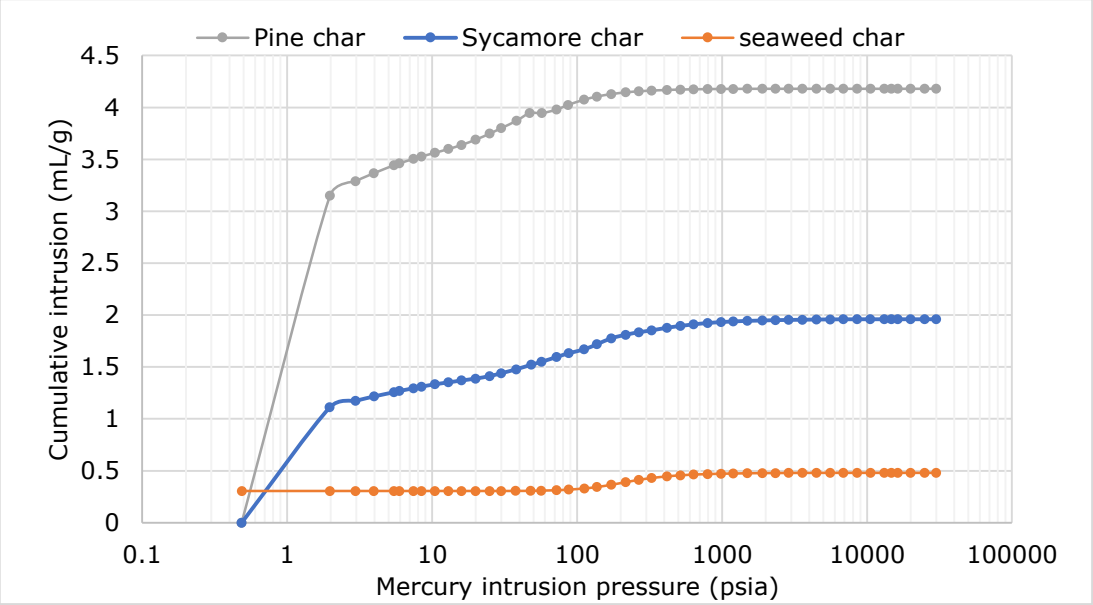

Figure B-2: Mercury intrusion results for the char produced from biomass of particle size 212 – 850 µm.

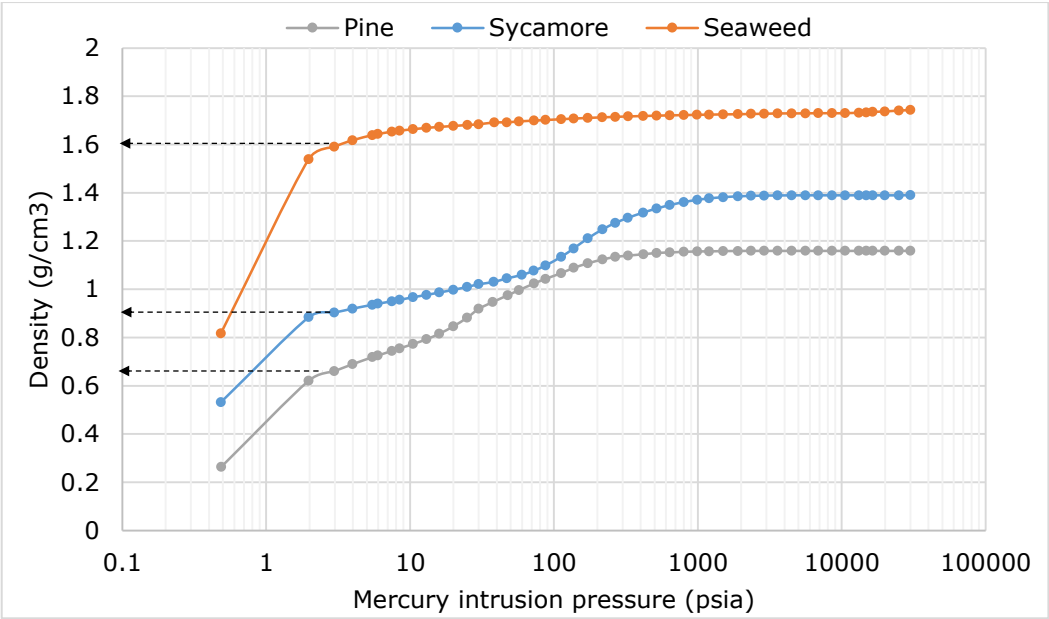

Figure B-3: Density of the biomass particle determined using the Mercury Porosimetery technique. The densities were calculated from the mercury intrusion volume at each intrusion pressure following the method reported by Mukaida (1981).

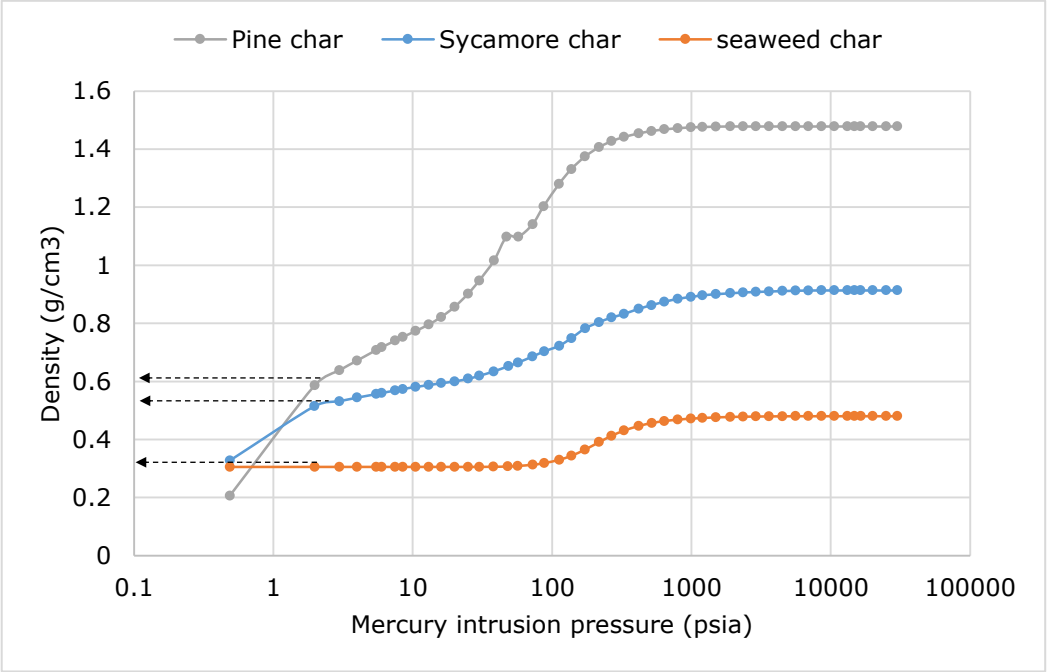

Figure B-4: Density of the char particles determined using the Mercury Porosimetery technique. The densities were calculated from the mercury intrusion volume at each intrusion pressure following the method reported by Mukaida (1981).

11.3 Appendix C: Numerical Models for the Heat Transfer in the Fluidised Bed System

The temperature gradient within the particle was studied by dividing the spherical particle into 20 control volumes (elements); a core and 19 shells with equal thicknesses as explained in Figure A-7. The assumptions listed in Section 5.3 were applied. The temperature within each of these elements is assumed constant.

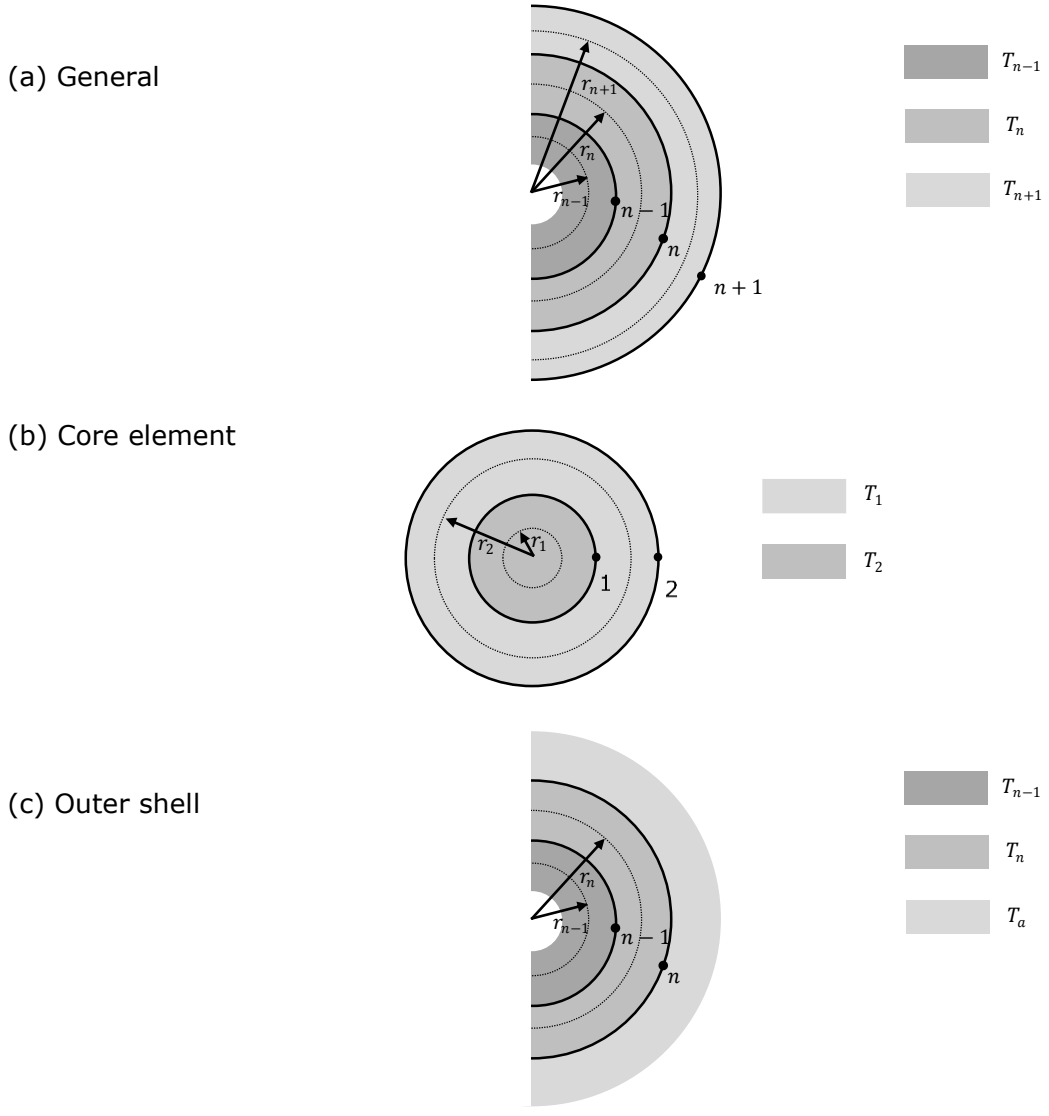

Figure C-1: Control volumes (elements) used for estimating the temperature gradient within a particle during the microwave pyrolysis in a fluidised bed process.

The heat conduction, Q, through a spherical shell with an inner diameter, r_1, and an outer dimeter, r_2, is given as (Coulson et al., 1999):

$$Q = \frac{4\pi k(T_2 - T_1)}{\frac{1}{r_2} - \frac{1}{r_1}} \qquad \text{C-1}$$

At each element, the increase in the element's thermal state is the sum of the absorbed microwave power by the element and the heat transferred from the previous element minus the heat transferred to the next element.

The heat transfer equations were solved at each element iteratively in both space and time. Adopting the explicit finite difference method reported by Versteeg and Malalasekera (2007) in which the temperature from the previous time step is used to calculate the heat transfer between element at the new time step. A general equation for calculating the temperature at each element can be written as follows:

$$m.cp\frac{(T_n - T_n^0)}{\Delta t} = P + \frac{4\pi k(T_n^0 - T_{n-1}^0)}{\frac{1}{r'_n} - \frac{1}{r'_{n-1}}} - \frac{4\pi k(T_{n+1}^0 - T_n^0)}{\frac{1}{r'_{n+1}} - \frac{1}{r'_n}} \qquad \text{C-2}$$

Where:

m is the mass of biomass particles per unit volume, g/ m^3;

cp the specific heat capacity of the biomass particle, J/g.^{o}C.;

T_n and T_n^0 are the temperature of the n^{th} element at time t (in seconds) and $(t - \Delta t)$ respectively, ^{o}C;

P is the absorbed microwave power per unit volume, W/m^3;

r'_n is the average of the inner and the outer diameter of the n^{th} element, m;

k is the thermal conductivity of biomass, W/m.^{o}C;

The left-hand side of Equation C-2 refers to the change in the thermal state of the nth element. The first term in the right-hand side refers to the microwave power absorbed by the nth element. The second term in the right-hand side refers to the heat transferred between the n-1th element and the nth element. The third term in

the right-hand side refers to the heat transferred between the n^{th} element and the $n+1^{th}$ element.

For the core element, the heat is exchanged with only one side which is the outer shell. Therefore, after eliminating the second term of the right-hand side, Equation C-2 could be reduced to:

$$m.cp\frac{(T_1 - T_1^0)}{\Delta t} = P - \frac{4\pi k(T_2^0 - T_1^0)}{\frac{1}{r'_2} - \frac{1}{r'_1}} \qquad \text{C-3}$$

For the outer shell, the heat is exchanged with the previous shell and the surrounding fluid instead of an outer shell. Therefore, Equation C-2 is replaced by:

$$m.cp\frac{(T_n - T_n^0)}{\Delta t} = P + \frac{4\pi k(T_n^0 - T_{n-1}^0)}{\frac{1}{r'_n} - \frac{1}{r'_{n-1}}} - h.S(T_n^0 - T_a) \qquad \text{C-4}$$

Where:

h is the particle-to-fluid heat transfer coefficient, W/m^2.^{o}C;

S is the surface area of the particles per unit volume, m^2/m^3;

T_a is the temperature of the surrounding fluid, ^{o}C.

The third term of Equation C-4 refers to the heat transferred between the outer element (shell) of the particle and the surrounding fluid.

Rearranging Equations C-2, C-3 and C-4 gives:

The general equation:

$$T_n = T_n^0 + \frac{\Delta t}{m.cp}\left[P + \frac{4\pi k(T_n^0 - T_{n-1}^0)}{\frac{1}{r'_n} - \frac{1}{r'_{n-1}}} - \frac{4\pi k(T_{n+1}^0 - T_n^0)}{\frac{1}{r'_{n+1}} - \frac{1}{r'_n}}\right] \qquad \text{C-5}$$

For the core element:

$$T_1 = T_1^0 + \frac{\Delta t}{m.Cp}\left[P - \frac{4\pi k(T_2^0 - T_1^0)}{\frac{1}{r'_2} - \frac{1}{r'_1}}\right] \qquad \text{C-6}$$

For the outer shell:

$$T_n = T_n^0 + \frac{\Delta t}{m.Cp}\left[P + \frac{4\pi k(T_n^0 - T_{n-1}^0)}{\frac{1}{r'_n} - \frac{1}{r'_{n-1}}} - h.S(T_n^0 - T_a)\right] \quad \text{C-7}$$

Equations 8-1,4-13 and 4-14 were solved iteratively with time steps of 0.5 ms. The calculations were carried out using Microsoft Excel® 2013 spreadsheets.

11.4 Appendix D: Calculations for Inerting the Fluidised Bed Column for Pyrolysis

Base on the British Standards (CEN/TR 15281:2006), the following equation can be used for the flow-through inerting calculations:

$$C_f = C_i + \frac{(C_o - C_i)}{EXP(\frac{Q \times t}{V})} \quad \text{D-1}$$

Where:

C_f = oxygen content after flow purging

C_i = oxygen content of inert gas which is 0% for the nitrogen feed

C_o = initial oxygen content which is 21% for fresh air

Q = inert gas flow-rate. Nitrogen was used with a minimum flowrate of 40 L/min

t = time required for purging. At least 10 second was allowed

V = system volume. The volume of the fluidised bed column is ~1.24 L

It can be seen from Figure D-1 that after 10 seconds, the oxygen concentration in the bed falls to less than 0.1% at 40 L/min nitrogen flow.

The same method was used to calculate the time needed to inert the cavity in the liquid system discussed in Chapter 7.

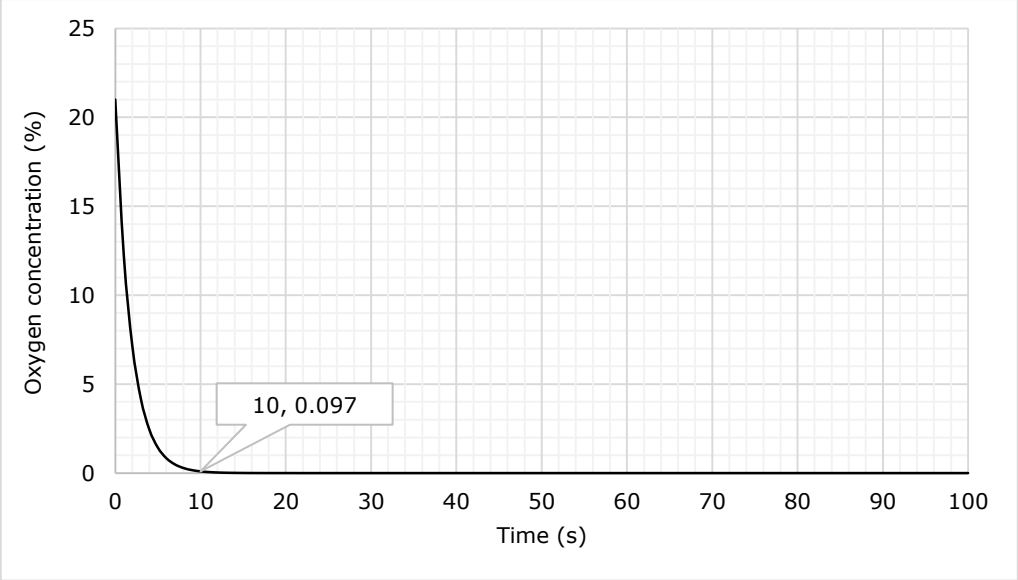

Figure D-1: The oxygen concentration as a function of time inside the fluidised bed column when a nitrogen flowing at 40L/min is fed to the system.

11.5 Appendix E: Error and Uncertainty

11.5.1 Standard Uncertainty

The standard uncertainty, $u_i(x)$, of an n measurement repeats of a quantity, x, is the standard deviation of the results, and it is calculated by the following formula:

$$u_i(x) = \sqrt{\frac{\sum_{j=1}^{n}(x_j - \bar{x})^2}{n-1}} \qquad \text{E-1}$$

Where $\bar{x}$ is the average of measurement results of the quantity, x.

In this thesis, the uncertainty intervals (error bars in graphs) were based on the standard uncertainty. The results of repeated measurements were, therefore, represented as: $x \pm u_i(x)$. The standard uncertainty provides a level of confidence of approximately 68%.

11.5.2 Relative Standard Uncertainty

The relative standard uncertainty, $u_r(x)$, is the standard uncertainty divided by the average value:

$$u_r(x) = \frac{u_i(x)}{\bar{x}} \qquad \text{E-2}$$